Sheffield Hallam University

Ground reaction force estimation to assess football player movement on hybrid turfs

D'ANDREA, Francesca

Available from the Sheffield Hallam University Research Archive (SHURA) at:

http://shura.shu.ac.uk/28899/

A Sheffield Hallam University thesis

This thesis is protected by copyright which belongs to the author.

The content must not be changed in any way or sold commercially in any format or medium without the formal permission of the author.

When referring to this work, full bibliographic details including the author, title, awarding institution and date of the thesis must be given.

Please visit http://shura.shu.ac.uk/28899/ and http://shura.shu.ac.uk/information.html for further details about copyright and re-use permissions.

Ground Reaction Force Estimation to Assess Football Player Movement on Hybrid Turfs

Francesca d'Andrea

A thesis submitted in partial fulfilment of the requirements of
Sheffield Hallam University
for the degree of Doctor of Philosophy

Collaborating Organisation: adidas

December, 2020

Candidate Declaration

I hereby declare that:

1. I have not been enrolled for another award of the University, or other academic or professional organisation, whilst undertaking my research degree.

2. None of the material contained in the thesis has been used in any other submission for an academic award.

3. I am aware of and understand the University's policy on plagiarism and certify that this thesis is my own work. The use of all published or other sources of material consulted have been properly and fully acknowledged.

4. The work undertaken towards the thesis has been conducted in accordance with the SHU Principles of Integrity in Research and the SHU Research Ethics Policy.

5. The word count of the thesis is 43500.

Name	Francesca d'Andrea
Award	PhD
Date of Submission	December, 2020
Faculty	Health and Wellbeing
Director of Studies	Dr Marcus Dunn

Abstract

The majority of elite level football teams around the world play and train on hybrid turf pitches. However, relatively little is known about hybrid turf surfaces' mechanical properties and effect on player movement.
Surfaces' mechanical properties and construction characteristics may influence shoe-surface interaction. For this reason, to evaluate players' performance, it is fundamental to keep into consideration also the mechanical properties of the specific sport surface where the movements are performed. Through a secondary analysis of the Labosport ScorePlay™ dataset, the mechanical properties ranges of hybrid turfs were identified and compared with those of natural grass surfaces. The results showed that hybrid turfs are less compliant than natural grass, and that stitch-based hybrid turf surface systems are the most consistent surfaces, since their mechanical properties show less variability, and they are less affected by weather and usage, however, these surface system presents higher rotational traction compared to the other construction types.
An inertial measurement unit (IMU) based method was developed in order to estimate three-dimensional ground reaction forces (GRFs) and contact times in the field during high-intensity football-specific movements representative of a real game scenario. The method was developed to assess football player movement performance and it is based on the measurements of eight IMUs and the consideration of two mechanical phenomena: the collision of the lower limb with the surface and the motion of the remainder of the body mass throughout the stance phase.
This method was used in the field to evaluate the effect of two hybrid turf surfaces of different construction, a stitched-based (SISgrass) and a reinforced rootzone (Fibrelastic), and two shoes, with differences in outsole rigidity and stud shape, on player movement. Twenty male participants (age: 23.1 ± 3.7 years; mass: 77.5 ± 7.9 kg; stature: 1.81 ± 0.04 m) of different football experience levels (9 competitive, 10 recreational and 1 not competing in official leagues) completed an agility course for each shoe-surface condition. The course was designed in order to involve accelerations, decelerations, anticipated and unpredicted changes of direction. The results of this study suggested that cylindrical studs provide higher traction during straight acceleration compared to prismatic studs, especially on the SISgrass surface. In addition, the outcomes showed that players' movements are the result of a complex interaction between surface, shoe, participant, task and environment, rather than specific shoe or surface effects.
To the best of the author's knowledge, this thesis represents the first collection of data on hybrid turf surfaces' mechanical properties and on the evaluation of their effect on player movement in the field. In addition, the method developed to estimate in-field 3D GRFs during high-intensity movements provides the possibility to characterise different shoes or surfaces in a variety of field-based sport activities.

Acknowledgements

There are several people I would like to thank for their assistance, support and guidance throughout this research project. First of all, I would like to thank my supervisors Dr Marcus Dunn, Dr Ben Heller and Prof David James for all your time, the continued support, advice and knowledge provided over the last three years that helped me achieving this work and improving as a researcher. This gratitude extends to all members of the Sports Engineering Research Group at Sheffield Hallam University, in particular to Dr John Hart for the design of the sensor mount frame.

I am grateful to adidas for the sponsorship of this project. In particular, I would like to thank Harald Koerger, Patrick Henning-Bortmes, Heiko Schlarb and Karsten Westphal. Also thank you to Marc Lamka for the help during the first data collection and to both Marc and Steven, without you it would have not been possible to reach a good cohort of participants for my final study.

Furthermore, I would like to thank Labosport for sharing their Scoreplay dataset and allowing me to borrow the AA test device for six weeks of testing in Germany. These mechanical test data provided important information for this work. Also thanks to David Rigby and Tom for teaching me how to use the mechanical test devices.

Apart from the people directly involved with the research, I would like to thank all my friends, both those I known for years and all the great people I met during this PhD journey. Thank you for all the laughs, chats, coffee breaks and for letting me know I can always count on your support. A huge thank goes to Linda and Ben for making me feel part of a family during these months of COVID-19 pandemic.

Finally, but most importantly, thanks to my family. Thanks to my brother and my grandma for being always supportive and believing in me, and especially to my parents for all your love and support, without you I would not be the person I am now and I would have not been able to get where I am.

Contents

1 Introduction **1**

1.1 Surface characteristics 1

1.1.1 Natural grass surface 1

1.1.2 Artificial turf surface 3

1.1.3 Hybrid turf surface 4

1.2 Shoe characteristics 5

1.3 Motivation for the research 7

1.4 Aim and objectives 8

2 Literature review **9**

2.1 Football players' movements 9

2.2 Shoe-surface interaction 10

2.2.1 Compliance 10

2.2.2 Traction 11

2.3 Shoe-surface interaction measurements 13

2.3.1 Mechanical tests 13

2.3.1.1 Drop tests 13

2.3.1.2 Translational and rotational tests to assess the effect of footwear outsole design 14

2.3.1.3 Translational and rotational tests to assess the effect of surfaces 16

2.3.1.4 Tests to assess surfaces' mechanical properties over a season 17

2.3.1.5 Mechanical test limitations 18

2.3.1.6 Summary of mechanical tests 20

2.3.2 Biomechanical tests 20

2.3.2.1 Tests to assess the effect of shoes 21

2.3.2.2 Tests to assess the effect of surfaces 23

2.3.2.3 Mechanically available and utilised traction 24

2.3.2.4 Other biomechanical tests of football-specific movements . . . 28
2.3.3 Subjective-sensory tests . . . 29
2.4 Inertial measurement unit sensors . . . 30
2.4.1 Ground reaction force estimation based on biomechanical models 32
2.4.1.1 Non locomotive tasks . . . 32
2.4.1.2 Locomotive tasks . . . 33
2.4.1.3 High intensity and sport-specific movements . . . 35
2.4.1.4 Estimating ground reaction forces for football-specific movements . . . 36
2.4.1.5 Estimating ground reaction forces from other mechanical models . . . 38
2.4.2 Ground reaction force estimation using machine learning . . . 41
2.5 Chapter summary . . . 43

3 Mechanical properties of surfaces: testing methods and characterisation of hybrid turf surfaces 46
3.1 Introduction . . . 46
3.1.1 Testing devices and protocol . . . 47
3.1.1.1 Artificial Athlete (AA) device . . . 47
3.1.1.2 Advanced Artificial Athlete (AAA) device . . . 49
3.1.1.3 Rotational traction test device . . . 52
3.1.1.4 Moisture meter . . . 53
3.2 Aim and objectives . . . 53
3.3 Methods . . . 54
3.3.1 Labosport ScorePlay and surfaces included in the database . . . 54
3.3.2 Statistical analysis . . . 54
3.4 Results . . . 55
3.5 Discussion . . . 59
3.6 Conclusion . . . 62

4 Use of inertial measurement units to estimate ground reaction forces during a football-related movement 64
4.1 Introduction . . . 64
4.2 Aim and objectives . . . 65
4.3 Methods . . . 65
4.3.1 Participants . . . 65
4.3.2 Experimental set-up . . . 66
4.3.3 Protocol . . . 67
4.3.4 Data processing . . . 70

4.3.4.1 Conversion of the inertial measurement units' raw accelerations into the global system 70
4.3.4.2 Filtering 71
4.3.4.3 Ground reaction force estimation 75
4.3.5 Statistical analysis 77
4.4 Results 77
4.5 Discussion 83
4.6 Conclusion 86

5 Use of inertial measurement units to estimate ground reaction forces during football-specific movements 87
5.1 Introduction 87
5.2 Aim and objectives 88
5.3 Methods 88
5.3.1 Participants 88
5.3.2 Experimental set-up 88
5.3.2.1 Foot segment 91
5.3.2.2 Shank segment 92
5.3.2.3 Thigh segment 92
5.3.2.4 LPT segment 93
5.3.2.5 HAT segment 93
5.3.3 Protocol 95
5.3.4 Data processing 97
5.3.4.1 Conversion of the inertial measurement units' raw accelerations into the global system 97
5.3.4.2 Ground reaction force estimation 101
5.3.5 Statistical analysis 105
5.4 Results 105
5.5 Discussion 120
5.6 Conclusion 127

6 Effect of football hybrid turf surfaces on players' performance and traction perception 128
6.1 Introduction 128
6.2 Aim and objectives 129
6.3 Methods 129
6.3.1 Participants 129
6.3.2 Experimental set-up 129
6.3.2.1 Environment 129
6.3.2.2 Surfaces 129

6.3.2.3 Shoes 130
6.3.2.4 Devices 131
6.3.2.5 Agility course 132
6.3.3 Protocol 134
6.3.3.1 Surface mechanical tests 134
6.3.3.2 Biomechanical tests 134
6.3.3.3 Subjective-sensory data tests 136
6.3.4 Data processing 137
6.3.4.1 Surface mechanical tests 137
6.3.4.2 Biomechanical tests 137
6.3.5 Statistical analysis 141
6.3.5.1 Surface mechanical tests 141
6.3.5.2 Biomechanical tests 141
6.3.5.3 Subjective-sensory data tests 142
6.3.5.4 Relationship between biomechanical and subjective-sensory data 142
6.4 Results 143
6.4.1 Surface mechanical tests 143
6.4.2 Biomechanical tests 145
6.4.2.1 Performance time 145
6.4.2.2 Ground reaction force loading characteristics and contact time during the acceleration task 146
6.4.2.3 Ground reaction force loading characteristics and contact time during the deceleration task 149
6.4.2.4 Ground reaction force loading characteristics and contact time during the change of direction task 153
6.4.3 Subjective-sensory data tests 156
6.4.4 Relationship between biomechanical and subjective-sensory data 157
6.5 Discussion 161
6.5.1 Surface mechanical tests 161
6.5.2 Biomechanical tests 163
6.5.3 Subjective-sensory data tests 166
6.5.4 Relationship between mechanical, biomechanical and subjective-sensory data 167
6.5.5 Summary of the findings 169
6.6 Conclusion 171

7 Conclusion **173**
7.1 Summary of the research 173

7.2 Limitations of the research 176
7.3 Future work 177

References **178**

Appendix A Sensor selection **192**

Appendix B A pilot study to define the sensor attachment method **195**
B.1 Introduction 195
B.2 Aim and objectives 195
B.3 Methods 196
B.3.1 Participants 196
B.3.2 Experimental setup 196
B.3.2.1 HAT segment 196
B.3.2.2 LPT segment 196
B.3.2.3 Thigh segment 197
B.3.2.4 Shank segment 198
B.3.2.5 Foot segment 199
B.3.3 Protocol 200
B.3.4 Data processing 200
B.4 Results 200
B.4.1 HAT segment 200
B.4.2 LPT segment 202
B.4.3 Thigh segment 203
B.4.4 Shank segment 207
B.4.5 Foot segment 208
B.5 Discussion 209
B.5.1 HAT segment 209
B.5.2 LPT segment 209
B.5.3 Thigh segment 209
B.5.4 Shank segment 210
B.5.5 Foot segment 210
B.6 Conclusion 210

List of Figures

1.1 Natural grass surfaces composition. 2
1.2 Artificial turf surfaces. 3
1.3 Hybrid turfs. 4
1.4 Football boots history. 6

2.1 Energy input, returned and lost in a sport surface. 11
2.2 Example of forces applied during an athletic manoeuvre. 12
2.3 Alignment of stud with respect to shoe outsole and surface. 14
2.4 Example of translational and rotational traction test setup. 14
2.5 Rotational traction test results for bladed and studded shoes. 15
2.6 Rotational traction test results for 5 surfaces under dry and wet conditions. 16
2.7 Roll, pitch and yaw angles between shoe and surface. 19
2.8 Device designed by Grund et al. 19
2.9 Examples of biomechanical tests. 21
2.10 Rouch et al. test setup. 24
2.11 Effect of mechanical available traction on GRF, utilised traction and lean angle. 25
2.12 Movements over the force platform. 26
2.13 Force platform. 30
2.14 Example of IMU with global and local systems. 31
2.15 Multi-link trunk models. 32
2.16 Comparison of measured and estimated GRF by Gurchiek et al. 35
2.17 Raised cosine bell curve. 39
2.18 Estimated vertical GRF curve profile in comparison to force platform measurements for different foot-strike patterns, running speeds and lower limb mass percentages. 40

3.1 Example of Laboport ScorePlay™ testing system results. 47
3.2 Artificial Athlete Berlin. 48
3.3 Artificial Athlete Stuttgart. 49
3.4 Advanced Artificial Athlete. 50

3.5 Example of curve representing the falling mass acceleration over time. 51
3.6 Example of curve representing the falling mass velocity over time. . . . 51
3.7 Rotational traction test device and studs' configuration. 52
3.8 Moisture meter. 53
3.9 Comparison of rotational traction and moisture content between hybrid turf surfaces and natural grass; data from Labosport ScorePlay™ dataset. 55
3.10 Comparison of shock absorption, vertical deformation and energy restitution between hybrid turf surfaces and natural grass; data from Labosport ScorePlay™ dataset. 56

4.1 iSen IMU sensor with its dimension. 66
4.2 IMU sensors' attachment locations. 66
4.3 Markers' locations. 67
4.4 Schematic of a test movement over time with left foot contact over the force platform. 68
4.5 Example of LSJ task with left foot contact on the force platform. 69
4.6 Shoes used during the test. 69
4.7 IMU local and global coordinate systems. 70
4.8 IMUs' local coordinate systems, IMU global NED system and laboratory global system. 71
4.9 Example of PSD calculated for each IMU global acceleration during one trial. 72
4.10 Example of PSD calculated for each segment CoM acceleration during one trial. 73
4.11 Example of the comparison between global acceleration calculated from the markers' trajectories and from the IMU for the midPSIS location after filtering. 74
4.12 Foot vertical global acceleration calculated from the markers' trajectories and from the IMU before and after synchronisation. 75
4.13 Body segments. 76
4.14 Good and bad examples of measured and estimated vertical GRF. . . . 78
4.15 Good and bad examples of measured and estimated medio-lateral GRF. 79
4.16 Magnetic field measured by each sensor compared to the Earth's magnetic field. 80
4.17 Effect of the magnetometer interference on the GRF estimation. The second stance phase of a trial is reported as example. 81
4.18 Shanks and feet accelerations recorded by IMUs and derived from the markers' trajectories. The second stance phase of a trial is reported as example. 82

4.19 Example of different oscillatory responses on the medio-lateral GRF estimation. 85

5.1 Sensor mount technical drawings. 89
5.2 Back and front view of the body landmarks. 90
5.3 Sensors' attachment locations. 91
5.4 Foot sensor attachment method. 91
5.5 Shank sensor attachment method. 92
5.6 Thigh sensor attachment method. 93
5.7 LPT sensor attachment method. 93
5.8 HAT CoM and endpoints. 94
5.9 HAT sensor attachment method. 95
5.10 Movements performed. 96
5.11 Example of coordinate system calculated with the non optimal estimator and sensor local coordinate system. 98
5.12 Coordinate systems of IMUs, motion capture and force platforms with respect to the final global coordinate system, defined in accordance with the movements analysed. 99
5.13 Example of magnetic interference effect during a 90° change of direction trial. 100
5.14 Example of stance phase identification. 102
5.15 Example of the steps of the GRF estimation process. 103
5.16 Best measured and estimated GRF curve profiles for each movement analysed. 106
5.17 Representative measured and estimated GRF curve profiles for each movement analysed. 107
5.18 Resultant GRF curve RMSE distribution for each sub-task. 108
5.19 Resultant GRF curve profile and FLoA for 45° and 90° change of direction tasks. 109
5.20 Resultant GRF curve profile and FLoA for 180° change of direction task. 110
5.21 Resultant GRF curve profile and FLoA for the acceleration steps. 111
5.22 Accelerometer range limit, comparison between markers and IMUs' accelerations. 118
5.23 Example of the IMU sample frequency limitation. 118
5.24 Comparison of 3D GRF measured from the force platform, and estimated from inertial, and optical motion captures. 119

6.1 Hybrid turf surfaces with the artificial component highlighted. 130
6.2 adidas shoes used during the test. 130
6.3 Sensors' location and attachment methods. 131

6.4 Agility course schematic representation. 132
6.5 Different views of the agility course set-up. 133
6.6 AA set-up for shock absorption and vertical deformation measurements. 134
6.7 Photos of two change of direction tasks. 135
6.8 Reference systems in the agility course. 138
6.9 Course schematic with the steps necessary to complete the course. . . . 139
6.10 GRFs estimated for one participant for each condition. 140
6.11 Course schematic with the steps necessary to complete the course and the stance phases corresponding to each group of movements highlighted. 142
6.12 Course schematic with the first step of acceleration and the individual changes of direction highlighted. 143
6.13 Comparison of shock absorption, vertical deformation, rotational traction and moisture content between hybrid turf and natural grass surfaces used in match play and the surface tested in the current work. . . 144

A.1 IMU analysed. 193

B.1 Trunk attachment methods. 196
B.2 LPT attachment methods. 197
B.3 Thigh attachment methods. 198
B.4 Shank attachment methods. 199
B.5 Foot attachment methods. 199
B.6 HAT attachment method comparison. 201
B.7 LPT attachment method comparison. 202
B.8 Thigh attachment method 1 and 2 comparison. 203
B.9 Thigh attachment method 3 and 4 comparison. 204
B.10 Thigh attachment method 5 and 6 comparison. 205
B.11 Thigh attachment method 4 and 6 comparison. 206
B.12 Shank attachment method comparison. 207
B.13 Foot attachment method comparison. 208

List of Tables

1.1 Example of football boot groups. 7

2.1 The 'Bloomfield Movement Classification' behaviours and modifiers. . . 10
2.2 Summary of characteristics influencing shoe-surface mechanical interaction. 20
2.3 RMSE, impulse, impact peak and loading rate errors of the resultant GRF estimated from fifteen segmental accelerations for different tasks by Verheul et al. 37
2.4 Summary of the studies using IMU sensors to estimate GRF. 45

3.1 Laboport ScorePlay™ testing criteria. 47
3.2 Mean ± standard deviations for shock absorption, vertical deformation, energy restitution, rotational traction and moisture content of hybrid turf surfaces and natural grass surfaces; data from Labosport ScorePlay™ dataset. 57
3.3 Mann-Whitney's U statistics for shock absorption, vertical deformation, energy restitution, rotational traction and moisture content of hybrid turf and natural grass surfaces; data from Labosport ScorePlay™ dataset. 58
3.4 Pearson's correlation coefficient between the shoe-surface performance variables and moisture content, and respective *p*-values; data from Labosport ScorePlay™ dataset. 58

4.1 Cut-off frequencies related to each sensor and axis. 74
4.2 Body segments with their mass percentages. 76
4.3 RMSE, nRMSE and RelErr for estimated vertical and medio-lateral GRF components for each stance phase. 77
4.4 RMSE and RelErr comparison between this study and previous research for estimated vertical and medio-lateral GRF components. 83

5.1 Body segment inertia parameters, defined by Zatsiorsky-Seluyanov. . . 90
5.2 Sub-tasks considered for each task. 102
5.3 RMSE, impulse, impact peak, loading rate and active peak errors of the resultant GRF estimated for each sub-task. 113

5.4 RMSE, impulse, impact peak, loading rate and active peak errors of the horizontal GRF component estimated for each sub-task. 114
5.5 RMSE, impulse, impact peak, loading rate and active peak errors of the vertical GRF component estimated for each sub-task. 115
5.6 RMSE and impulse errors of the antero-posterior GRF component estimated for each sub-task. 116
5.7 RMSE and impulse errors of the medio-lateral GRF component estimated for each sub-task. 116
5.8 Spearman's rank correlation coefficient for impulse and active peak force.117
5.9 Spearman's rank correlation coefficient for impact peak force and loading rate. 117
5.10 RMSE and RelErr comparison between this study and previous research for estimated vertical and horizontal GRF components. 122
5.11 Comparison between the results obtained in this study with those of Verheul et al. for GRF curve profile, impulse and impact peak force errors in the resultant direction for acceleration, deceleration and change of direction tasks. 123

6.1 Mean value calculated for each mechanical property for each surface. . 143
6.2 Performance time reported as mean ± standard deviations for each shoe-surface condition and two-way ANOVA test *p*-value results with Cohen's *d* effect sizes. 145
6.3 Best performance times for each participant and shoe-surface combination; and two-way ANOVA test *p*-values and Cohen's *d* effect sizes. . . . 145
6.4 Between participants active peak force, impulse, and contact time mean ± standard deviation for each shoe-surface condition and variable for the acceleration task. 146
6.5 Between participants active peak force, impulse, and contact time two-way ANOVA test results for the acceleration task. 146
6.6 Within participant mean ± standard deviation for each shoe-surface condition vertical active peak force from the acceleration task, and two-way ANOVA test results. 147
6.7 Within participant mean ± standard deviation for each shoe-surface condition horizontal active peak force from the acceleration task, and two-way ANOVA test results. 147
6.8 Within participant mean ± standard deviation for each shoe-surface condition vertical impulse from the acceleration task, and two-way ANOVA test results. 148

6.9 Within participant mean ± standard deviation for each shoe-surface condition horizontal impulse from the acceleration task, and two-way ANOVA test results. 148
6.10 Within participant mean ± standard deviation for each shoe-surface condition contact time from the acceleration task, and two-way ANOVA test results. 149
6.11 Between participants active peak force, impulse, and contact time mean ± standard deviation for each shoe-surface condition and variable for the deceleration task. 149
6.12 Between participants active peak force, impulse, and contact time two-way ANOVA test results for the deceleration task. 150
6.13 Within participant mean ± standard deviation for each shoe-surface condition vertical active peak force from the deceleration task, and two-way ANOVA test results. 150
6.14 Within participant mean ± standard deviation for each shoe-surface condition horizontal active peak force from the deceleration task, and two-way ANOVA test results. 151
6.15 Within participant mean ± standard deviation for each shoe-surface condition vertical impulse from the deceleration task, and two-way ANOVA test results. 151
6.16 Within participant mean ± standard deviation for each shoe-surface condition horizontal impulse from the deceleration task, and two-way ANOVA test results. 152
6.17 Within participant mean ± standard deviation for each shoe-surface condition contact time from the deceleration task, and two-way ANOVA test results. 152
6.18 Between participants active peak force, impulse, and contact time mean ± standard deviation for each shoe-surface condition and variable for the change of direction task. 153
6.19 Between participants active peak force, impulse, and contact time two-way ANOVA test results for the change of direction task. 153
6.20 Within participant mean ± standard deviation for each shoe-surface condition vertical active peak force from the change of direction task, and two-way ANOVA test results. 154
6.21 Within participant mean ± standard deviation for each shoe-surface condition horizontal active peak force from the change of direction task, and two-way ANOVA test results. 154

6.22 Within participant mean ± standard deviation for each shoe-surface condition vertical impulse from the change of direction task, and two-way ANOVA test results. 155
6.23 Within participant mean ± standard deviation for each shoe-surface condition horizontal impulse from the change of direction task, and two-way ANOVA test results. 155
6.24 Within participant mean ± standard deviation for each shoe-surface condition contact time from the change of direction task, and two-way ANOVA test results. 156
6.25 Questionnaire results reported as mean ± standard deviations. 156
6.26 Questionnaire two-way ANOVA *p*-values results and Cohen's *d* effect sizes.157
6.27 Spearman's rank correlation coefficient between performance time and traction perception or time perception for each participant. 157
6.28 Spearman's rank correlation coefficient between estimated vertical active peak force and traction perception for the first step of acceleration and change of direction manoeuvres. 158
6.29 Spearman's rank correlation coefficient between estimated horizontal active peak force and traction perception for the first step of acceleration and change of direction manoeuvres. 159
6.30 Spearman's rank correlation coefficient between estimated vertical impulse and traction perception for the first step of acceleration and change of direction manoeuvres. 159
6.31 Spearman's rank correlation coefficient between estimated horizontal impulse and traction perception for the first step of acceleration and change of direction manoeuvres. 160
6.32 Spearman's rank correlation coefficient between estimated contact time and traction perception for the first step of acceleration and change of direction manoeuvres. 160

Nomenclature

3D	Three-dimensional
AA	Artificial Athlete
AAA	Advanced Artificial Athlete
ACL	Anterior Cruciate Ligament
ACR	Acromion
AJC	Ankle Joint Centre
ASIS	Anterior Superior Iliac Spine
BW	Body Weight
C7	Seventh Cervical Vertebra
CoM	Centre of Mass
CoP	Centre of Pressure
EJC	Elbow Joint Centre
ER	Energy Restitution
FIFA	Fédération Internationale de Football Association
FLoA	Functional Limits of Agreement
GRF	Ground Reaction Force
GRI	Ground Reaction Impulse
HAT	Head-Arm-Trunk
HEEL	Heel
HJC	Hip Joint Centre
ICC	Intraclass Correlation Coefficient
IMU	Inertial Measurement Unit
KJC	Knee Joint Centre

L4	Fourth Lumbar Vertebra
L5	Fifth Lumbar Vertebra
LLT	Lower Limb Trunk
LPT	Lower Part Trunk
LSJ	Lateral Skater Jump
MET3	Third Metacarpale
MIDH	Mid-point between Hip Joint Centres
midPSIS	Mid-point between Posterior Superior Iliac Spines
MPT	Middle Part Trunk
NED	North-East-Down
nRMSE	Normalised Root Mean Square Error
OMPH	Omphalion
PSD	Power Spectral Density
RelErr	Relative Error
RMSE	Root Mean Square Error
SA	Shock Absorption
SJC	Shoulder Joint Centre
SPHY	Sphyrion
SUPR	Suprasternale
T2	Second Thoracic Vertebra
T4	Fourth Thoracic Vertebra
TIB	Tibiale
TTIP	Toe Tip
UEFA	Union of European Football Associations
VAS	Visual Analogue Scale
VD	Vertical Deformation
VERT	Vertex
WJC	Wrist Joint Centre
XYPH	Xyphion

Chapter 1

Introduction

Football is the world's most played sport [1], with 265 million players (male and female) registered worldwide in 2006 [2]. Over recent years, football has become a more powerful and faster game, characterised by explosive starts, quick sprints and rapid changes in direction [3]. Players have become more athletic [1], playing surfaces have evolved and research into footwear design has progressed in order to assist players enhancing performance and reducing injury risk.

1.1 Surface characteristics

Research has been focused on improving playing surfaces in order to provide firm footing, adequate resiliency on impact, resistance to tearing and compacting effects during play, and good drainage [4].

1.1.1 Natural grass surface

Natural grass pitches consist of a living grass plant anchored, via its root structure, to a soil matrix below. The grass plant and the underlying soil influence the pitch performance and its interactions with players and balls. Soil matrices consist of solid rigid particles in contact with each other, and a pore space filled with different percentages of air and water [5]. The solid particles are characterised by varying percentages of silt, clay and sand (Fig. 1.1), which determine the mechanical properties of soil, such as load bearing, traction, impact absorption and elastic recovery [6].

Native soils, on which traditional fields have been developed, have a high silt and clay content, which provides high root zone stability, but very low drainage and ease of compaction during use [4, 7]. An increase in moisture content results in a decrease of the surface playability, due to poorer mechanical properties, with the turf presenting extensive damage, such as loss of grass cover and tears [8]. At the other end, sand-

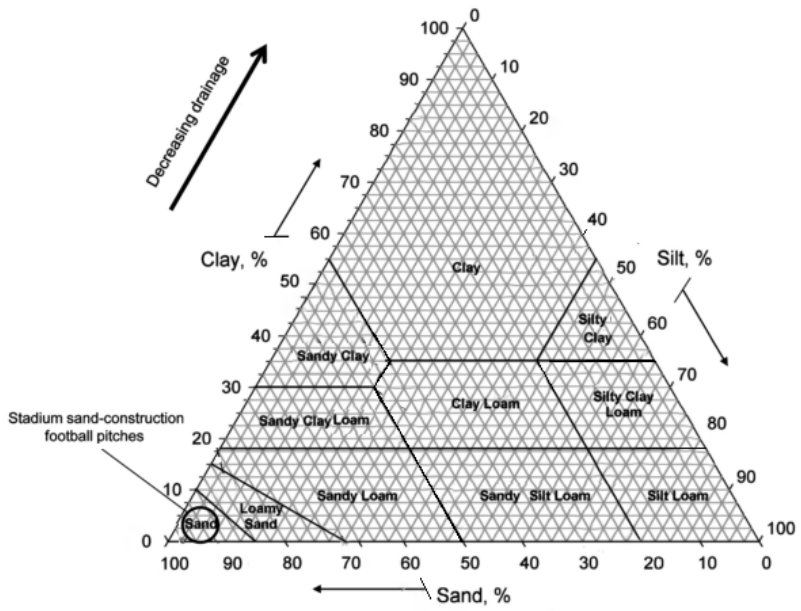

Figure 1.1: Natural grass surfaces composition [6].

based soils resist compaction, have far superior drainage capabilities [4] and higher shear strength, for these reasons they became the sub-soil of choice; however, they lack of root zone stability and require more intensive maintenance practices like watering and nutrient delivery [4, 9].

The grass plant reinforces the soil, so a good coverage increases the stability of the upper soil [9]. Grass mowing height in football is between 20 and 35 mm; lower cut heights increase ball roll distance and speed, however, if too low the grass plant can be stressed and the root depth decrease, which results in lower shear strength and traction. Surface performance in terms of tolerance to shade and close mowing, and resistance to disease, drought and wear is influenced also by grass species, which could be divided into warm and cool season grasses. The former presents higher heat and drought tolerance than the latter. The use of a single grass species provides uniform grass-ball interaction and colour, but increases the soil stress and the maintenance costs [6]. In many areas of the world, it is not possible to maintain a warm season grass during the whole year, since with low temperature it becomes dormant and is not able to recover from divots; therefore, the warm season grass usually needs to be over-seeded with the cool season grass during winter.

A natural grass pitch needs sufficient water, air, light and nutrients to grow and recover from wear; and its performance is influenced by its structural characteristics, its response to wear, and weather conditions [10].

1.1.2 Artificial turf surface

In order to overcome the sensitivity to frequent use and cold climate of natural grass pitches, football on artificial turf has been introduced and developed over the years, encountering high commercial success and becoming common in many European countries [11].

The first use of artificial turf for athletic fields was at the Houston Astrodome Baseball Arena (Texas, United States) in 1966 [12]. Initially, artificial turf pitches were installed only for American football and baseball, whereas a few years later they were also used to host association football games. This first generation of artificial turf (Fig. 1.2a) consisted of a concrete bottom layer covered with a short pile carpet, made of nylon fibres, featuring no infill [12]. At the end of 1970s, the second generation artificial turf (Fig. 1.2b) made of polypropylene fibres was developed. The fibres were twice as long as previously used (20 − 25 mm) and were tufted into strands, spaced wider apart than before. The bulk of installations were sand-filled surfaces to provide stability and some control of ball bounce. Early investigations [14] reported that the first and second generation of artificial turf showed differences in ball bounce and roll compared to natural grass; and that players found these surfaces more difficult to start, turn and stop, and experienced skin burns after falls and sliding tackles. These observations prevented the first two generations of artificial turf from being used regularly as match play surfaces [15].

The third-generation of artificial turf (Fig. 1.2c) was developed in 1998. It consists of polyethylene fibres, which are softer and longer (40 − 65 mm in length) than those of

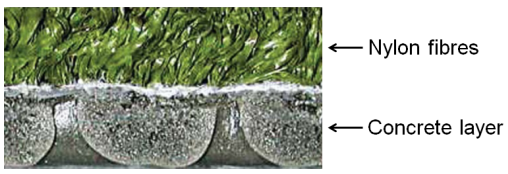

(a) First generation [12].

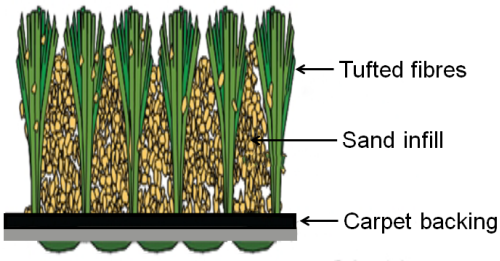

(b) Second generation [12].

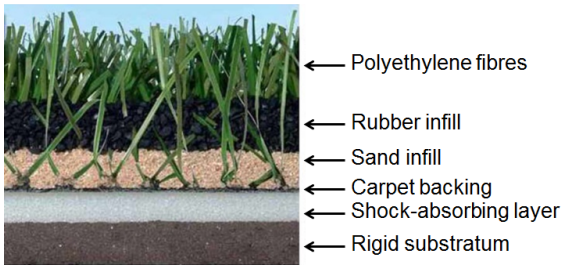

(c) Third generation [13].

Figure 1.2: Artificial turf surfaces.

the first and second generations, and a 40 mm layer of rubber and sand infill, instead of pure sand. Some systems also utilise a shock-absorbing layer underneath the turf for added safety [12]. Compared to natural grass, artificial turf surfaces require no light or irrigation, lower maintenance, and have higher wear resistance, which facilitates the extension of time for play, regardless of the weather. Thus, third-generation artificial turfs are widely used on athletic and recreational fields. However, these pitches are often criticised because of their high initial costs, high abrasiveness when athletes fall on the surface, high temperatures recorded in summer periods that can exceed 93°C, their unpleasant rubber odour, and the concerns related to the use of rubber crumb, which is a micro-plastic pollution and potential carcinogen [16, 17].

Artificial turf surfaces present significant quality differences between the various systems available, as a consequence in 2004 the Fédération Internationale de Football Association (FIFA) introduced a Quality Programme for Football Turf [18] in order to sanction the use of these pitches if they do not satisfy playing performance, safety, durability and quality requirements. Since then, a number of international matches and tournaments have been played on third-generation artificial pitches, such as FIFA women's 2015 World Cup, FIFA World Cup and UEFA EURO qualifiers [18].

1.1.3 Hybrid turf surface

Hybrid turf pitches have been introduced in an attempt to combine the feel, look and comfort of natural grass with the resilience and resistance to tearing, divots and adverse climatic conditions of artificial turf. A hybrid turf is a natural grass pitch reinforced with synthetic elements. These surfaces, depending on their construction, could be divided into three groups: reinforced rootzone, stitched-based and carpet-based hybrid turf systems.

Reinforced rootzone turf systems (Fig. 1.3a) are 100% natural grass pitches with synthetic elements, usually polypropylene or elastane fibres, added to the sand-based rootzone profile of the natural turf in order to provide reinforcement. Some providers

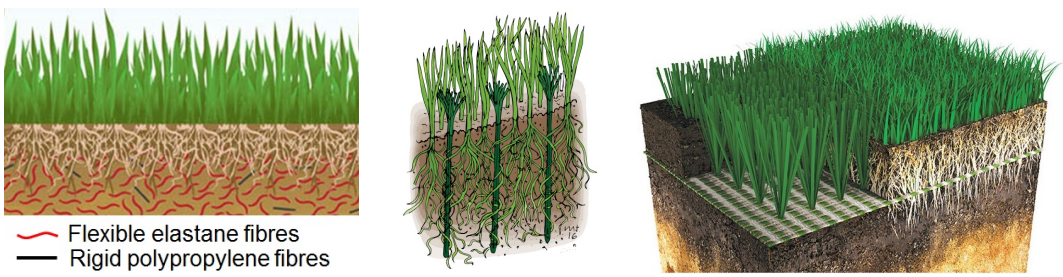

(a) Reinforced rootzone [19]. **(b)** Stitched-based [20]. **(c)** Carpet-based [21].

Figure 1.3: Hybrid turfs.

add granulated cork to the rootzone in order to increase surface shock absorption and energy restitution. Stitched-based hybrid turf surfaces (Fig. 1.3b) are characterised by polyethylene or polypropylene fibres inserted 200 mm deep into the sand-based rootzone and placed at 2 cm intervals or wider gaps. Natural grass roots, anchoring to the artificial fibres, grow deeper within the system and increase the stability and strength of the surface. Approximately 2 cm of artificial fibres are left above the ground level, leaving a surface with a 100% natural grass look. In carpet-based hybrid turf surfaces (Fig. 1.3c), the natural grass grows up and through a mat or backing on which artificial fibres are tufted into. The natural grass roots anchor to the synthetic carpet and the ground underneath it.

Initially, the evolution and use of hybrid turf pitches was limited to the United Kingdom. One of the first surfaces installed was a reinforced rootzone system at Oldham Athletic Stadium (Greater Manchester, UK), whilst in 1992 the first stitched-based hybrid turf was installed at Huddersfield Town Football Club (Huddersfield, UK). In recent years, hybrid turf surfaces have been developed and installed around the world, becoming the dominant surface for the major professional leagues, especially in the Union of European Football Associations (UEFA) regions.

1.2 Shoe characteristics

Footwear provides the interface between surface and player, and is fundamental to performance, comfort and protection of the foot during kicking. In the early days of football, players wore heavy, hard leather work boots (Fig. 1.4a), which covered the ankles and often included a metal toe-cap and metal studs or tacks. The boots weighed 500 g and double this weight in wet weather conditions. The growth of football in South America, where the pitches were drier, leaded to lighter and more flexible boots, moving the focus of footwear design from protection to performance enhancement. Adi Dassler, founder of adidas, designed the first boot with interchangeable screw-in studs (Fig. 1.4b) in order to adapt the footwear to different weather conditions. This boot was designed for the West Germany national team to wear at the 1954 World Cup in Switzerland. The Germans won the final in heavy rain weather condition against the favourite Hungarian team, after replacing the regular length studs with longer ones into their boots, which allowed an increase in traction. These boots included also other significant improvements: lighter weight (380 g), a narrower last, a lower cut upper, a more flexible outsole, and the hard toe cap was removed to improve ball control. After this event, in the 1960s the high-ankle boots were replaced by lower cut designs (Fig. 1.4c) and the focus moved at reducing weight and increasing movability; moreover, improvements to synthetic materials led to more durable and lighter

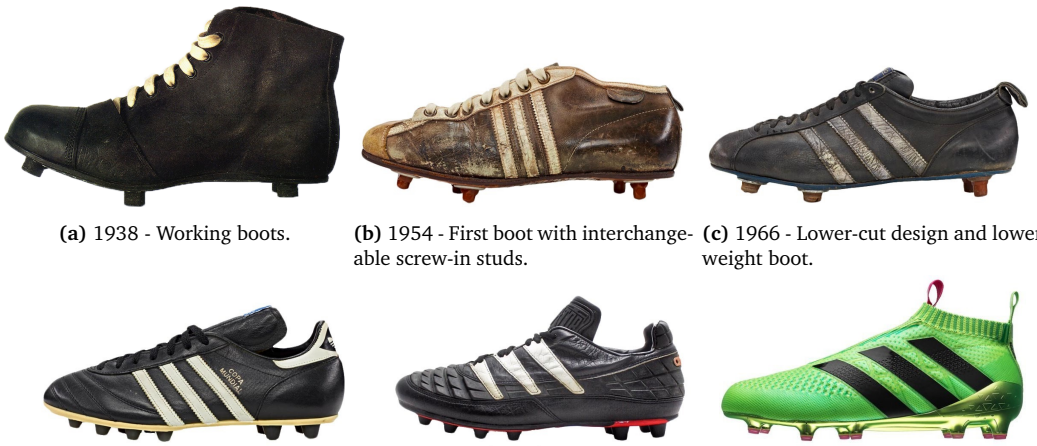

(a) 1938 - Working boots.

(b) 1954 - First boot with interchangeable screw-in studs.

(c) 1966 - Lower-cut design and lower weight boot.

(d) 1982 - First Copa Mundial boot.

(e) 1994 - First Predator boot.

(f) 2015 - First laceless boot.

Figure 1.4: Football boots history.

weight boots (200 g). In 1979, adidas released the Copa Mundial (Fig. 1.4d), which featured an extra leather support around the heel and a shorter 12 studs design to suit the hard Spanish pitches of the 1982 World Cup; this boot remains the highest-selling football shoe of all times. The Copa Mundial was followed by the release of adidas Predator (Fig. 1.4e) in 1994, where part of the leather was replaced with rubber to increase ball control. Nowadays, manufacturers introduced laceless boots (Fig. 1.4f) and alternative materials to produce even lighter footwear, and the best world players have boots specifically designed for themselves.

Currently, footwear manufacturers offer different football boots options, typically based on a leather construction, cut below the ankles and with the outsole both thin, to provide flexibility, and hard, to provide a firm surface to attach the studs. The studs can be moulded as part of the boot or detachable, and they can vary in number, distribution, length and geometry. Long studs ensure a deeper penetration into a soft ground surface, providing the desired amount of traction and avoiding slipping, but they do not penetrate enough into a hard surface, leading to pressure areas on the foot, a decrease in foot stability and total whole-body balance with subsequent slippage [15]. An increase in the number of studs on the outsole, increases the possibility for the muddy soil to stick to the outsole and, therefore, the risk to slip [15]. The different studs' geometries include cylindrical, conical, prismatic and bladed shapes.

Depending on the outsole configuration, football boots could be classified into five groups: turf, artificial grass, hard ground, firm ground and soft ground designs. An example of these groups and their characteristics is reported in table 1.1. When playing on hybrid turf surfaces, players use football shoes with stud configurations designed for natural grass, since football shoes specific for these surfaces have not been designed yet.

Table 1.1: Example of football boot groups.

Outsole	Boot model	Suitable surface	Studs' material	Studs' number	Studs' size [mm]
	Turf	Artificial turf	Rubber	>55	6 – 7
	Artificial grass	Artificial turf	Plastic	21	8 – 10
	Hard ground	Hard and icy natural grass	Plastic	14	10 – 12
	Firm ground	Natural grass in good and dry condition	Plastic	12	10 – 12
	Soft ground	Wet and muddy natural grass	Aluminium	6	13 – 16

1.3 Motivation for the research

The evolution of playing surfaces and development of new footwear are the results of research efforts focused on increasing athletic performance and minimising the risk of injury. Nowadays, the majority of top league stadiums around the world use hybrid turf surfaces, however, despite their popularity in the professional game, relatively little is known about hybrid turfs' mechanical properties and their effect on player movement. Moreover, football shoes are typically designed for natural grass and shoes specific for hybrid turfs have not been designed yet.

The knowledge of the interaction between shoes and surfaces, and the evaluation of its effect on player movement are fundamental to reduce injury and improve athletic performance. Shoe-surface interaction could be quantified through mechanical and biomechanical measurements. Mechanical tests are highly reliable and able to describe the material properties of surface sample tested, but they do not consider realistic player loading on the surface and athletes' adaptation to different shoe-surface conditions. Whereas, biomechanical tests are typically conducted in a scenario not representative of the real game environment.

This programme of research is sponsored by adidas AG, who would like to better understand player movement on hybrid turf surfaces and be able to assess it in a real scenario, in order to gain new knowledge and insights to develop new surface specific footwear. High intensity movements, characterised by explosive starts, quick sprints and rapid changes of direction, are the player movement of interest, since they are the most crucial moments during match play and the most critical in relation to performance and injury risk. To conclude, the lack of knowledge on hybrid turf surfaces and the potential to develop a new method to assess their effect on player movement provide the motivations for this programme of research.

1.4 Aim and objectives

The aim of this programme of research is to evaluate the effect of football boots and hybrid turfs used in match play on in-field shoe-surface interaction, to aid understanding of player movement performance.

To achieve this, the following objectives have been identified:

1. characterise the mechanical properties of hybrid turfs regularly used for elite level match play;
2. develop a method to evaluate in-field biomechanical shoe-surface interaction;
3. validate the developed method for football-related and football-specific movements;
4. use the validated method to assess in-field shoe-surface interaction for different boots and hybrid turfs;
5. assess the relationship between in-field shoe-surface interaction, player movement performance and player movement perception.

Chapter 2

Literature review

2.1 Football players' movements

Movements observed during football games can be classified using the Bloomfield Movement Classification [22] (Table 2.1), which provides details of direction, intensity, tuning/swerving and on the ball activities. Bloomfield et al. [23] used this method to analyse the movements of 55 players during the 2003-2004 English Premier League season. 40.6% of the game was spent performing purposeful movements, including low intensity activities; the mean duration of each movement was 13.1 ± 3.2 s and the mean time between them was 20.4 ± 5.3 s. The authors observed a high frequency of turns with a mean of approximately 600 turns between 0° and 90° during a match play, compared to a mean of approximately 100 between 90° and 180°, and 10 for greater angles.

High and very high intensity movements contribute only to $5.6 \pm 2.1\%$ of the total match time [23], however these actions are the most crucial moments of the game, since they contribute directly to win the ball possession, score a goal or prevent one. High-speed actions can be classified as actions requiring acceleration, maximal speed or agility, which are relatively independent attributes in professional football players [24]. Agility is defined as the ability to change direction, start and stop quickly in response to a sport-specific stimulus.

The knowledge of football movements is crucial in the development of new surfaces and footwear, as well as in their interaction, which should be evaluated especially during high or very high intensity movements.

Table 2.1: The 'Bloomfield Movement Classification' behaviours and modifiers [22].

BEHAVIOURS (Modifiers in parenthesis)	MODIFIERS
1.TIMED **Motion** Sprint (A+B), Run (A+B), Shuffle (A+B), Skip (A+B), Jog (A+B), Walk (A), Stand still, Slow down (A+B), Jump (C), Land, Dive (D), Slide (D), Fall, Get up (B) **Initial channel** Start of observation	**(A) Direction** Forwards, Forwards diagonally right/left, Sideways right/left, Backwards, Backwards diagonally right/left, Arc forwards left to right/right to left, Arc backwards left to right/right to left, Arc Sideways right/left **(B) Intensity** Low, Medium, High, Very high **(C) Jump** Vertical, Forwards, Backwards, Sideways (E)
2. INSTANTANEOUS (NON-TIMED) **Other movement** Stop (B), Swerve (E), Impact (F+B) **Turns** 0°-90°(E) 90°-180°(E) 180°-270°(E) 270°-360°(E) >360°(E) **On the ball activity** Receive (G), Pass (H+I), Shoot (H+I), Dribble (J+K), Tackle, Trick, Other	**(D) Dive** Feet first, head first **(E) Turn** Right/Left **(F) Type** Push, Pull, Pushed, Pulled, Other **(G) Control** Right/Left foot, Head, Chest, Thigh, Other **(H) Pass/Shoot** Long air, Short air, Long ground, Short ground, Other **(I) How** Right/Left foot, Header, Backheel Overhead, Other **(J) Dribble** Start, End **(K) Touches** Start, 1-3, 4-6, 7-10, >10

2.2 Shoe-surface interaction

With the increase in football boot models and surfaces available on the market, it is important to understand the shoe-surface interaction in order to increase athletic performance and reduce injury risk. Research efforts have been focused at traction and compliance, which can describe this interaction [25].

2.2.1 Compliance

A surface deforms under the load of an athlete moving on it, and the amount of energy developed by the athlete to move is transferred to the surface. When the athlete leaves the surface, part of this energy is returned and its magnitude is relevant only if

it is large enough to have an influence on athletic performance. The amount of energy returned depends on time-dependent properties of the materials, by which the surface is comprised, and the capability of the surface to return energy at the right location, since the point where the athlete leaves the surface is usually different to the location of the first contact [26].

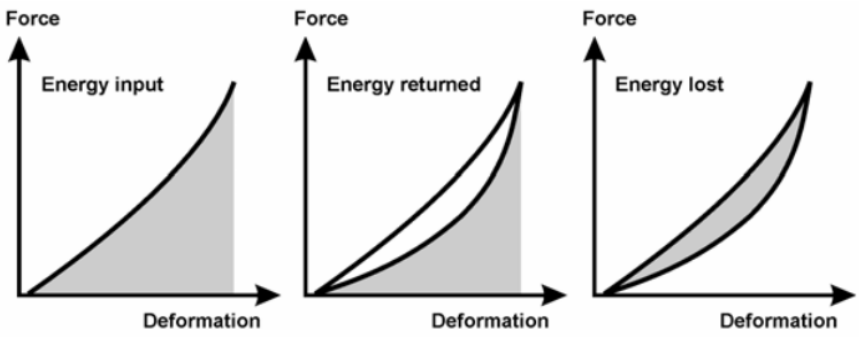

Figure 2.1: Energy input, returned and lost in a sport surface. In each case, the grey region represents the magnitude of the energy [26].

The amount a material will deform when placed under a given force is defined by compliance, the inverse of stiffness. The main variables used to quantify surface compliance are: shock absorption, vertical deformation and energy restitution. Shock absorption or force reduction is the surface ability to reduce impact forces when loaded by an athlete, and it is influenced by the amount of surface vertical deformation, which is the surface ability to deform under load. If shock absorption and vertical deformation are too low, an athlete would experience high deceleration and impact forces, which would expose him/her to injury. Whereas, too high shock absorption and vertical deformation result in high foot instability, with consequent risk of injury, and an higher amount of energy being wasted, which increases fatigue and reduces athletic performance [25, 27].

2.2.2 Traction

Friction is defined as the resistance to relative motion between two surfaces in sliding contact. A sufficient frictional force between footwear and playing surface is important for sport performance. The coefficient of friction describes the ratio of frictional and normal forces; it is a material-dependant constant, independent of time, velocity and contact pressure and follows the classical Amontons-Coulomb laws of friction. However, these laws are not enough to describe complex interactions, such as those between shoes and surfaces [28]. Thus, the term traction, instead of friction, was proposed [29] to describe the propulsive or braking force generated on the sport surface by an athlete to achieve a chosen manoeuvre [5].

The resistance to motion can be described by two types of traction. Translational traction determines how much horizontal force is necessary to cause the shoe to move over the surface, it is always parallel to the stationary surface and is directed opposite to the motion of the moving object [5]. Rotational traction determines how much force must be applied as a moment of force to cause the shoe to pivot on the surface [30]. Translational traction is commonly quantified using a traction coefficient, defined as the ratio between shear and normal forces (Fig. 2.2). However, shoe-surface interaction is not a simple material constant and varies with time, normal load, pressure, contact area and sliding velocity [28, 29], therefore, the use of a traction coefficient is a limit. The absolute value and the time history of vertical and horizontal force components have been suggested as the parameters to evaluate, in order to understand the mechanics of shoe-surface interaction [31, 32]. Rotational traction is not characterised by a coefficient, but it is described by the peak moment of rotation with respect to the vertical axis through the instantaneous centre of rotation [30, 33] (Fig. 2.2).

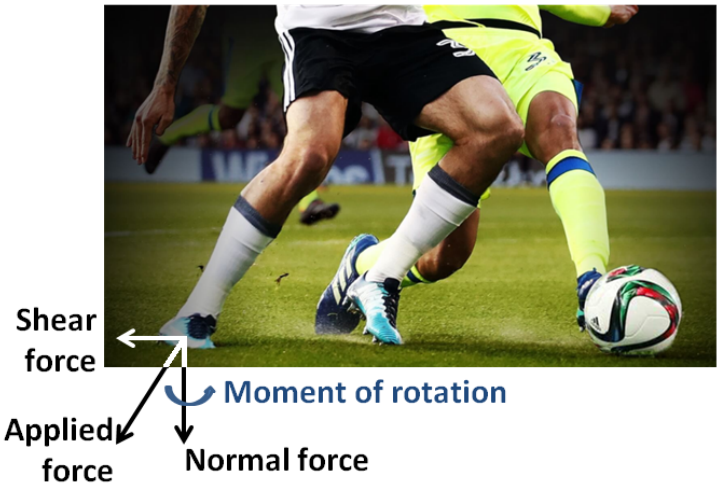

Figure 2.2: Example of forces applied during an athletic manoeuvre.

Football movements are characterised by high acceleration starts, quick sprints and rapid changes in direction [3], during which athletes require that the shoe does not slip on the surface along the horizontal force's direction or stick to the surface preventing relative rotation of the foot on it. In the evaluation of football movements, it is important to keep into consideration both translational and rotational traction, some studies [30, 34] suggest that the first is the critical element in performance on sport surfaces and the latter is the critical element in injury prevention. Some researchers [35, 36] reported that excessive rotational traction prevents the shoe from moving freely during twists, pivots and cuts, resulting in foot fixation, while the structures above the foot continue to rotate. This leads to the development of high forces and moments in the knee and ankle joints [34, 37], which increase the ligaments' injury risk [38]. Low translational traction can lead to a slip or slide of the shoe, and,

as a consequence, a decrease in performance or it can result in overstretch or tear injuries [39].

The desired level of traction between a shoe and a playing surface should lie in an optimum range that provides adequate slip resistance for dynamic movements without producing excessive resistance to rotation.

2.3 Shoe-surface interaction measurements

To characterise and quantify shoe-surface interaction, mechanical, biomechanical and subjective-sensory tests have been used [40].

2.3.1 Mechanical tests

Mechanical test procedures used in the assessment of shoe-surface interaction can be classified as drop, translational or rotational tests.

2.3.1.1 Drop tests

Drop tests are used to mechanically assess the compliance of a playing surface [32]. As previously stated (Sec. 2.2.1), compliance is measured by two main variables: shock absorption and vertical deformation. These variables can be quantified by devices such as the Artificial Athlete (AA) or Advanced Artificial Athlete (AAA).

Drop tests are used also to assess stud penetration into a surface. Keshvari et al. [41] demonstrated that the amount of stud penetration into a surface is related to studs' cross sectional area, whereas no relationship was found with the studs' shape investigated through a change in their perimeter. On the contrary, Dé and James [42] found a significant relationship, with greater perimeters resulting in higher negative acceleration rates, suggesting that a lower penetration is more likely to occur. The difference between these two studies is in the dropping height, 20 cm for the former and 60 cm for the latter, suggesting that the test results may be dependent on the drop height. Moreover, these tests investigate the stud penetration in case of normal impact with the studs penetrating perpendicularly the surface (Fig. 2.3b), which is not representative of players' movements. When athletes contact the surface through their shoes, the studs are not perpendicularly aligned with the surface (Fig. 2.3c), resulting in higher penetration resistance [43]. Therefore, the study of stud penetration into a surface and the relationship with studs' cross sectional area, perimeter or shape should be investigated at impact angles representative of players' loading conditions.

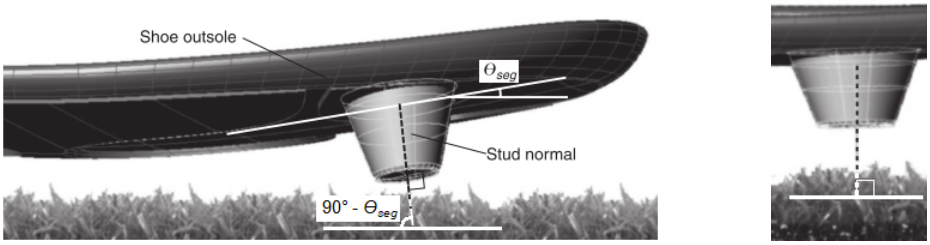

(a) Alignment of stud normal with respect to shoe outsole.

(b) Optimum penetration of stud when stud normal is perpendicular to ground for a normal impact.

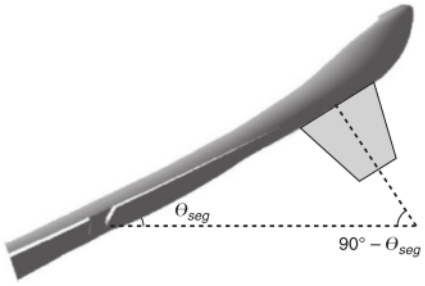

(c) Alignment of stud to surface in traditional shoes.

Figure 2.3: Alignment of stud with respect to shoe outsole and surface [43].

2.3.1.2 Translational and rotational tests to assess the effect of footwear outsole design

Translational tests measure the resistance to motion through the coefficient of traction; these tests are performed by pulling a plate with a standard material or a football boot mounted on a test foot across a surface (Fig. 2.4a). Rotational tests are used to assess the moment required to rotate a plate, equipped with a standard material or a football boot mounted on a test foot, when in contact with a surface (Fig. 2.4b).

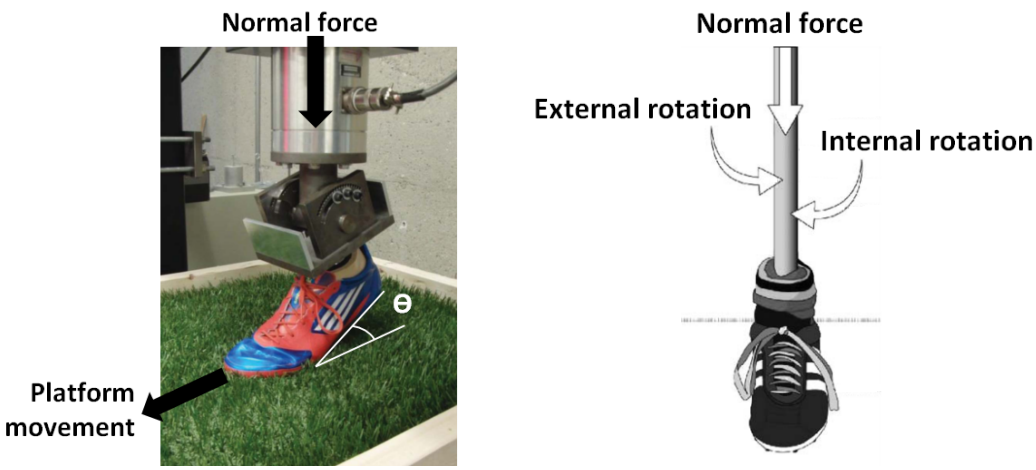

(a) Translational traction test setup with test foot equipped with shoe. θ is the plantar-flexion angle [25].

(b) Rotational traction test setup with test foot equipped with shoe [44].

Figure 2.4: Example of translational and rotational traction test setup.

Stud penetration and effective cross sectional area, defined as the stud's total sectional area penetrated into the surface, have been shown to affect translational and rotational traction. On natural grass, an increase in translation traction was found as the effective cross sectional area of the studs increased, whereas no relationship was found on artificial turf, probably because of the surface infill movement during penetration [45]. Regarding rotational traction, the peak moment of rotation increases with the studs' length both on natural grass [46] and artificial turf [47].

The relationship of stud shape with traction has been widely analysed, especially the comparison between bladed and studded football boots, since the former has been criticised as a factor responsible of the increased amount of injuries [48]. Some studies found no significant differences between studded and bladed boots in rotational traction tests, either rotating the shoe externally or internally, or applying the load on the entire sole in contact with the surface or only on the forefoot [49–51]. During translational traction tests, higher traction values were measured for bladed studs (2.08), but not significantly different compared to those obtained for regular circular studs from hard and soft ground design boots (1.53 and 1.96, respectively) [52]. Another study [44] considered bladed and studded shoes on five different football surfaces, for a total of ten shoe-surface combinations, and found significant higher moment of rotation associated with blades compared to studs only on natural grass and on a 2 years old artificial turf with infill, whereas no significant differences were found for a hybrid turf surface, an artificial turf without infill and a 6 years old artificial turf with infill (Fig. 2.5a). Moreover, the authors found significantly higher torques for external rotation compared to internal rotation for bladed shoes (Fig. 2.5b).

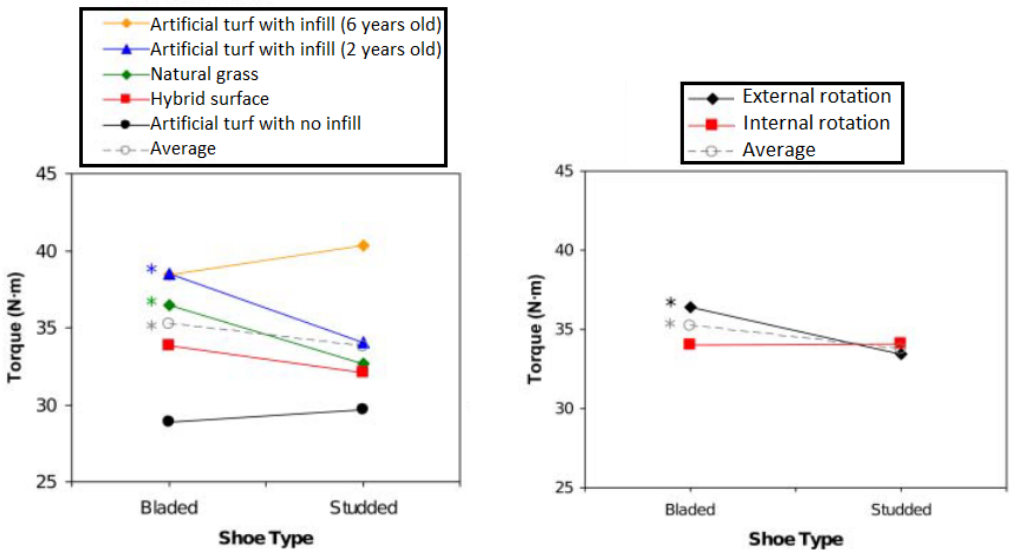

(a) Bladed and studded shoes interaction with 5 different football surfaces [44].

(b) Bladed and studded shoes interaction with external or internal rotation direction [44].

Figure 2.5: Rotational traction test results for bladed and studded shoes obtained by Smeets et al. [44].

These results highlight how footwear and surface can act together to influence the traction measurements. Therefore, the analysis of traction generated by different shoe outsole designs should be considered in association to specific surfaces; and traction measured with different shoes on a single surface should not be generalised, but considered as specific to that shoe-surface interaction.

2.3.1.3 Translational and rotational tests to assess the effect of surfaces

Contrasting results have been found comparing the moment of rotation between different surfaces. Villwock et al. [50] reported significantly higher rotational moment on artificial turf compared to natural grass (115.1 Nm and 89.5 Nm, respectively), with the latter showing higher moments on sand-based soil compared to native soil (95.9 Nm and 83.1 Nm, respectively). Galbusera et al. [49] found the same results when the load was applied with support on the forefoot only (49.8 Nm and 38.3 Nm for artificial turf and natural grass, respectively), but opposite results (45.0 Nm and 68.2 Nm for artificial turf and natural grass, respectively) when considering the same loading configuration used by Villwock et al. [50], with the force applied on the entire shoe sole in contact with the surface.

Smeets et al. [44] measured the moment of rotation on a natural grass surface, a stitched-based hybrid turf, two artificial turf with infill (2 and 6 years old) and one without infill, applying the load on the entire shoe outsole. The artificial turf without infill presented the lowest value of moment of rotation; whereas the oldest artificial turf with infill showed the highest values, significantly greater than those measured on the natural grass and the hybrid turf, which values were similar. However, when the same test was repeated under wet condition, the only surface that was minimally influenced was the hybrid turf, thus the authors concluded that the stitched-based hybrid turf was the most consistent surface tested for moisture content changes (Fig. 2.6). This study highlights how the surface traction not only varies between natural grass, artificial and hybrid turf surfaces, but it is dependent also on the surface construction (e.g. presence of infill), surface's age, and moisture content.

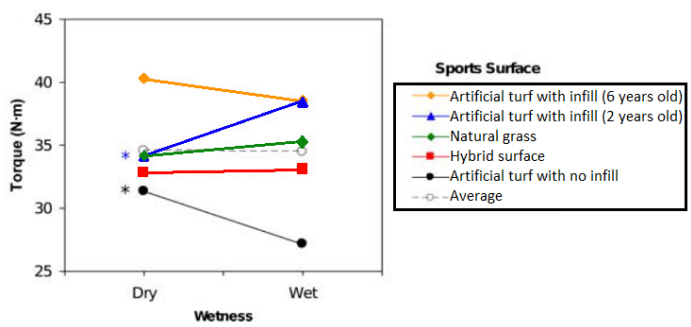

Figure 2.6: Smeets et al. [44] rotational traction test results for 5 surfaces under dry and wet conditions.

The contrasting results and large differences in the measured moment of rotation obtained in these studies may be explained by the differences in the experimental set-up and loading conditions. In the studies from Villvock et al. [50] and Galbusera et al. [49], a vertical load of 1000 N was applied, however, the former authors applied a rotation rate of 180°s^{-1} and the latter of 45°s^{-1}, which may explain the contrasting results. Another factor that could be responsible for the differences in the results may be the turfs' ages; the former study considered a 5 and a 7 years old artificial turfs, whereas the latter prepared the surfaces specifically for the mechanical test presented. Moreover, Villvock et al. [50] conducted their measurement on site, where the movement of the infill components may be different compared to that of small portions of the same surface. Finally, Smeets et al. [44] applied vertical loads of 200, 300 and 400 N on the entire shoe sole and the rotation was applied manually by different operators at rotation rates not specified, with the possibility of variability introduced by the operators' input. Consistent experimental set-ups and loading characteristics should be used throughout different studies to compare the effect of each surface on rotational traction; and information regarding the infill construction properties, age and moisture content should always be included in the presentation of the results.

2.3.1.4 Tests to assess surfaces' mechanical properties over a season

Mechanical test were conducted in the field to assess changes in surfaces' mechanical characteristics over a season due to the amount of usage and variation of grass species. Wannop et al. [53] tested a natural grass surface and an artificial turf both at the beginning and end of a season. At the beginning of the period analysed, both surfaces were very consistent, showing uniform traction values regardless of the specific location of the pitch; however, their condition significantly changed with the season progression, and rotational traction was much more affected than translational traction. The authors found smaller changes on the artificial turf, which are due to the movement of the infill material during use, compared to the natural grass surface. However, they stated that the changes on the artificial turf, even if smaller, expose athletes to a higher risk of injury, since the surface appears consistent; whereas on the natural grass the damaged areas are visible, so the athletes could adjust their movements.

Caple et al. [54] compared the changes in energy absorption, shear and penetration resistance over a season between six surfaces: four native soil natural grass surfaces, a reinforced rootzone hybrid turf and a stitched-based hybrid turf. The authors showed that the hybrid turfs have lower energy absorption and are more consistent over a season compared to natural grass surfaces. A comparison between the two hybrid turfs revealed similar values of energy absorption over a season, but differences in their shear and penetration resistance. The stitched-based turf was found more consistent

than the reinforced rootzone one, although the authors believe that the latter is more influenced by external factors that reduce the grass cover and, as a consequence, the surface strength.

Thomson et al. [46] tested a sand-based soil natural grass pitch over a season, on which the grass type changed from warm-season grass, to warm-season grass over-seeded with cool-season grass, to predominantly cool-season grass. The results of this study show that the surfaces' properties could vary over a season also in relationship to a change in grass species, since higher values of translational traction were measured on the warm-season grass (2.5 compared to 1.9 for cool-season grass), and lower rotational traction values on the cool-season grass (36.3 Nm compared to 47.4 Nm for warm-season grass and 42.8 Nm for warm-season grass over-seeded with cool-season grass).

These studies showed how surfaces' characteristics, such as construction and grass species, may affect the surfaces' mechanical properties. Moreover, they highlight how the surfaces' mechanical properties could vary during the season, due to the amount of usage, temperature and weather conditions.

2.3.1.5 Mechanical test limitations

Mechanical tests of rotational and translational traction present some limitations, in particular because they do not reflect the real scenario, where athletes are involved.

The majority of the mechanical tests are conducted as a rotational test by applying on a test foot a load of less than one body weight; however, when an athlete loads a surface, this exerts forces, defined as ground reaction forces (GRF), which are 2.5 to 3 times the body weight [55]. The load is applied to the test foot, on which is usually mounted a football boot, either with the full outsole or only the forefoot in contact with the surface, and the load is directed normally to the surface (Fig. 2.4). Driscoll et al. [56, 57] observed that during a sprint movement only the forefoot studs come into contact with the surface with an initial pitch angle of -16°, yaw angle of -25° and roll angle small enough to be considered negligible (Fig. 2.7); whereas, during a side-cut movement the shoe form a flatter angle with the surface, although still on the medial side and externally rotated, with angles of 4.9°, 24.9° and 6.3° for pitch, yaw and roll, respectively. These data suggest that the forces are directed at an oblique angle, rather than normally to the surface, and all the ankle joint angles must be considered. A possible solution to this problem is provided by Grund et al. [51], who designed a mechanical test device (Fig. 2.8) able to replicate the full range of motion of the ankle joint in order to secure realistic positioning of the tibia with reference to the boot and the playing surface, and to direct the applied forces and torques along the axis of the

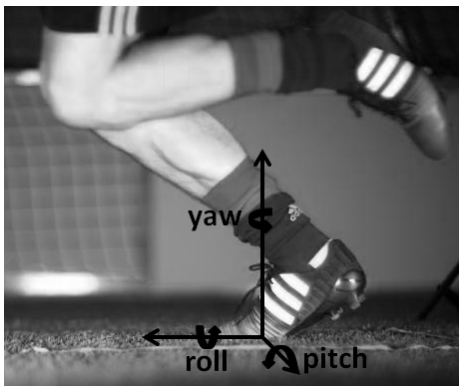

Figure 2.7: Roll, pitch and yaw angles between shoe and surface.

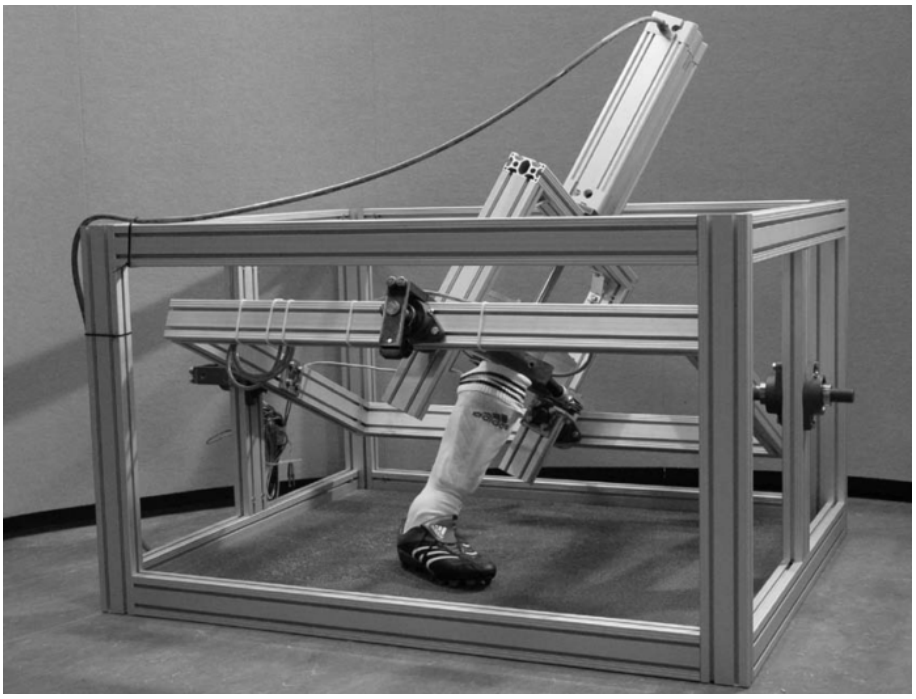

Figure 2.8: Device designed by Grund et al. [51].

lower leg.

Another limitation is related to the use of a football boot, since the shoe upper could deform and the sole rotate under the artificial foot, affecting the results. The use of only the shoe outsole attached directly to the measuring device could represent a solution to this problem [50].

The analysis of shoe translation and rotation relative to the surface during biomechanical tests, revealed that, during sprint and change of direction movements, the shoe displacement relative to the surface ranges between 8 and 14 mm [56–58], where 30 mm is hypothesised as the translational distance that humans are able to perceive as a slip [59]; and on average the shoe rotation ranges between 6° and 12° [56, 57, 60] at speeds of 170°s^{-1} for sprint movement and 60°s^{-1} for changes of direction [56, 57].

However, the peak moment of rotation measured during rotational traction tests is recorded at an angle of about 40° [47], which is not reached during biomechanical tests. The initial and linear rotational stiffnesses, defined as the rate at which the torque is developed under rotation, measured between 0° – 2° and 2° – 10° of rotation respectively, have been suggested by Livesay et al. [61] as more sensitive indicators of shoe-surface interaction during rotational traction tests, since the variation of rotational stiffness was found to be greater than the variation of the peak moment of rotation across ten shoe-surface combinations; moreover, these values would fall inside the range measured during biomechanical tests.

2.3.1.6 Summary of mechanical tests

The previous sections highlight the difficulties in the use of mechanical tests to evaluate shoe-surface interaction representative of human movement, to compare the results and generalise the findings, due to the amount of variables that may have an effect. Four main parameters were found to influence the interaction: surface, shoe, environment and experimental set-up. In table 2.2, for each one of these parameters, some of the possible variables identified in the previous sections that may affect shoe-surface interaction are reported.

Table 2.2: Summary of characteristics influencing shoe-surface mechanical interaction. NG = natural grass. AT = artificial turf. HT = hybrid turf.

Surface	Shoe	Environment	Experimental set-up
Construction type	Studs' shape	Moisture content	Vertical load
Infill (AT)	Studs' number	Humidity	Amount of rotation
Fibres (AT, HT)	Studs' perimeter	Temperature	Rotational rate
Soil matrix components (NG)	Studs' cross sectional area	Maintenance	Translational speed
Grass species (NG, HT)		Usage	Contact area
Age			Direction of rotation
			Sample size

In the analysis of surfaces' mechanical characteristics, it is fundamental to understand these parameters and their influence on shoe-surface interaction, in order to provide representative results.

2.3.2 Biomechanical tests

A number of studies used biomechanical tests to analyse the effect of different footwear and surfaces on players' performance. These studies considered different movements, such as sprint acceleration, changes of direction and a variety of agility courses, of which some examples are reported in figure 2.9.

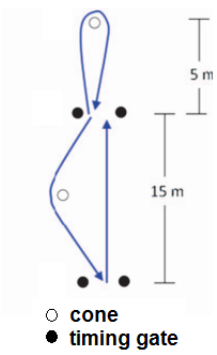

(a) Agility course [62].

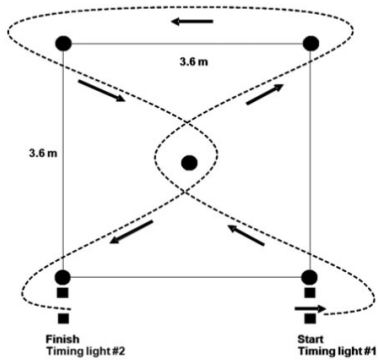

(b) Agility course [63].

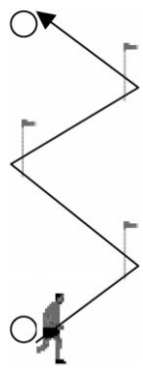

(c) Zig-zag run [24].

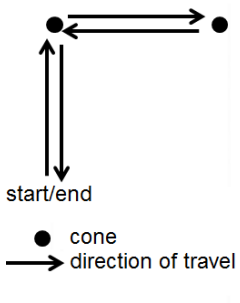

(d) L-agility course.

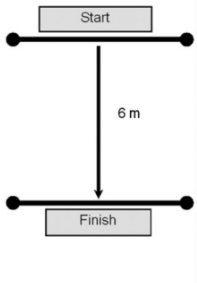

(e) Straight acceleration [64].

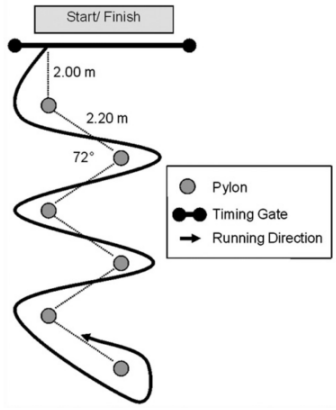

(f) Slalom course [64].

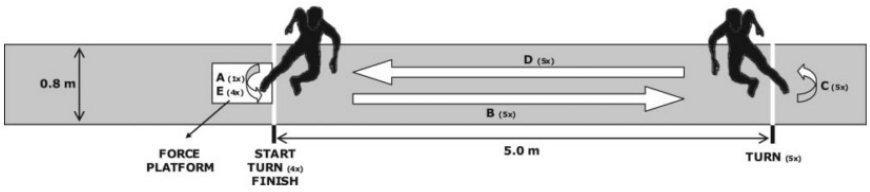

(g) Shuttle run test [65].

Figure 2.9: Examples of biomechanical tests.

2.3.2.1 Tests to assess the effect of shoes

Three main properties of footwear have been linked to performance: shoe mass, forefoot bending stiffness and outsole traction.

Two studies [63, 66] evaluate the effect of shoe mass on running time performance to complete fast and short agility courses (Fig. 2.9b and Fig. 2.9f). Sterzing et al. [66] considered shoe masses of 200 g and 270 g, whereas, Worobets and Wannop [63] compared shoe masses of 331, 414 and 497 g. An alteration of 35−40% of shoe mass was found to not affect running time performance, however the authors did not evaluate the effect of shoe mass on running economy, which could play an important role during a 90 minute game. Fuller et al. [67] suggested that only a mass per shoe pair greater than a threshold value of 440 g affects running economy, since any weight disadvantage below this value may be balanced by other beneficial factors, such as

shoe cushioning, stiffness and comfort. However, this threshold value was set based on treadmill running, therefore the effect of shoe masses on running economy should be evaluated for football turfs, where parameters, such as surface compliance, may lead to different results.

Bending stiffness was shown to slightly influence performance, with increases of 50% related to an improvement of 1% and 1.7% for sprint and change of direction tasks (Fig. 2.9b), respectively [63].

Sterzing et al. [66], in a series of eight studies conducted between 2002 and 2007, analysed the effect of outsole traction on the running time performance on an artificial turf surface, by changing studs' type, geometry and length. The reduction of studs' length to half of their original size and their removal from the outsole, resulted in significantly slower times during acceleration (Fig. 2.9e) and a slalom course (Fig. 2.9f), in particular stud removal resulted in 26% slower running times. Studs' type and geometry were found to affect performance time on an artificial turf surface during a slalom course (Fig. 2.9f), with bladed studs allowing faster times than elliptic studs, whereas no significant differences were recorded during sprint acceleration (Fig. 2.9e). The effect of shoe studs' design was evaluated also relative to different weather conditions. Bladed studs revealed better performance compared to elliptic studs when completing an agility course on icy/snow natural grass surface [66]. No differences were noticed between soft, firm, hard and artificial ground designs between wet or dry artificial turf [65, 66], whereas slower running times and lower traction were associated with a turf outsole design while completing an agility course (Fig. 2.9g) during wet conditions [65].

In addition to performance time, also kinetic variables have been analysed to evaluate the effect of shoe outsole on performance. No significant differences between footwear were found during cutting [68] and 90° land-to-cut [69] movements performed on an artificial turf surface, whereas a significantly lower peak medial GRF was observed for a natural grass shoe design compared to both artificial turf and non-studded footwear (1.1, 1.3, 1.4 BW, respectively) during a 180° turn [69].

The results obtained in these studies show that performance can be improved through different studs' type and geometries, however, each shoe outsole is designed to provide the optimal level of traction when moving on a specific surface condition, therefore these results should not be considered as absolute, but as a response to the specific interaction with the surface analysed. For example, a soft ground outsole is designed for natural grass wet surfaces, which present different characteristics to wet artificial turf, and, therefore, a difference in performance time between dry and wet natural grass fields would be expected, despite no differences on dry or wet artificial turf were

found. Moreover, different results were found between sprint acceleration and agility courses, suggesting that the optimal level of traction may differ between tasks and, therefore, it is important to analyse shoe properties' effects on performance during different movements.

2.3.2.2 Tests to assess the effect of surfaces

Some biomechanical tests have been conducted in order to evaluate differences in performance between different surfaces. No main differences were found between natural grass and artificial turf surfaces in sprint performance [62, 70], whereas faster times were recorded on artificial turf compared to natural grass during agility courses (Fig. 2.9a, 2.9d and 2.9f), including change of direction tasks [62, 70, 71]. In section 2.3.1.6, it was suggested that shoe-surface interaction is specific to each condition, therefore, performance time during biomechanical tests should be analysed in relation with the shoes used by the participants and the mechanical properties of the surfaces analysed.

Two studies [27, 72] evaluating the relationship between surfaces' mechanical properties and running time performances during agility courses were found in the literature. Sanchez-Sanchez et al. [27] evaluated the performance time during a 40 m sprint with a 180° turn after 20 m on four different artificial turf surfaces, characterised by different values of rotational traction and shock absorption. The authors found faster performance times associated with surfaces having rotational traction values inside the required band, and that the shock absorption did not affect performance time, except in case of excessively rigid surfaces (i.e. very low shock absorption), on which slower times were recorded. On the other hand, Nunome et al. [72] found that higher shock absorption is related to slower performance times during a zig-zag run (Fig. 2.9c). Only the authors of the latter study specified that the same shoes were used between all the participants, this suggests that the contradictory results between the two studies may be associated with the specific shoe-surface interaction with the presence of shoes' characteristics able to balance unfavourable surfaces' mechanical properties. Therefore, the evaluation of performance time in association with a specific surface's mechanical property should be evaluated, removing the shoe variability.

Despite the performance related to natural grass or artificial turf having been widely analysed, hybrid turfs have rarely been investigated. To the best of the author's knowledge, the only study looking at athletes' biomechanics on hybrid turfs in comparison to natural grass and artificial turf is a study from Rouch et al. [73]. The authors built a reinforced rootzone turf, together with natural grass and artificial turf, inside a greenhouse over force platforms, and analysed sprinting and side step cutting performance (Fig. 2.10). No significant difference in speed was found between the surfaces

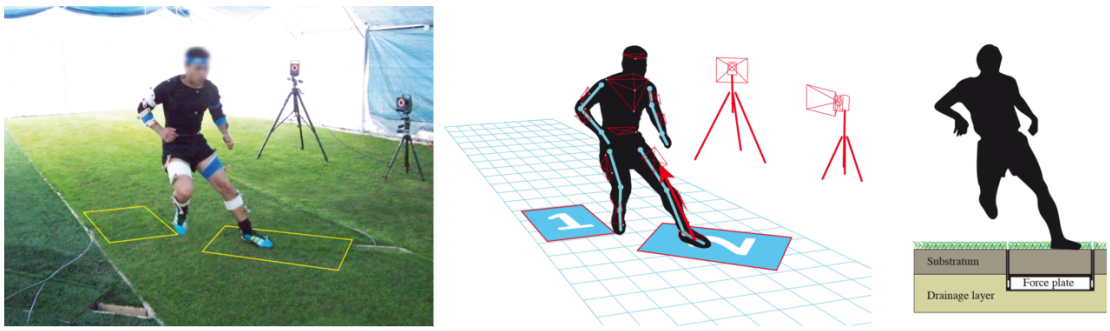

Figure 2.10: Rouch et al. test setup [73].

whereas higher values of weight acceptance phase time during the first cutting step was observed for the artificial turf, with the hybrid turf and natural grass surfaces showing similar results. The authors measured also the peak values of knee valgus and internal rotation moments, which are considered to increase the anterior cruciate ligament (ACL) injury risk. They concluded that the artificial turf is the less safe surface, because the knee moments are significantly higher, whereas the hybrid turf surface analysed had the lowest values. This study had only one surface for each construction type, with no details of the specific artificial turf construction. As reported in section 2.3.1.3, artificial turf surfaces' mechanical properties may be very different depending on characteristics such as the infill and the surface's age, therefore, the results of this study could not be generalised to all artificial turfs.

2.3.2.3 Mechanically available and utilised traction

The direct comparison of mechanical and biomechanical data of traction properties revealed that they do not reflect each other [64, 74]. Fong, Hong, and Li [75] explained the difference between these test methods by reporting that mechanical measurements allow the quantification of mechanically available traction, which describes the material properties of the two surfaces in contact associated with their ability to resist relative sliding; whereas biomechanical measurements quantify utilised traction, which is the actual force ratio occurring between the footwear and the playing surface during athletic movements.

Different authors evaluated the relationship between mechanically available and utilised traction, by altering the coefficient of traction between shoe and surface, through the attachment of different materials to the outsole of basketball [63, 76] or bowling shoes, or the application of various amounts of wax to the floor [77]. Pedroza et al. [77] analysed the time to complete a change of direction task, involving two 135° cutting movements, and the GRFs exerted during it, while the subjects wore shoes with coefficient of traction ranging from 0.3 to 0.7; the authors found that increasing the coefficient of traction up to 0.5 resulted in improved performance, recorded

as shorter completion time and higher peak force, whilst values above 0.5 did not lead to improved performance. Worobets et al. [63] analysed three conditions with coefficients of traction of 0.8, 1.0 and 1.2. The authors found that increasing the coefficient from 0.8 to 1.0 resulted in time performance improvements of 10% during sprint and 30% during an agility course (Fig. 2.9b); whereas a traction increase from 1.0 to 1.2 was associated with no advances in sprint performance and only a 4% improvement during cutting manoeuvres. Luo and Stephanyshyn [76] analysed the effect of four shoe conditions, with coefficient of traction of 0.2, 0.5, 0.8 and 1.1, on a maximum-effort curved sprint performance. The authors found that coefficient of traction increases from 0.2, to 0.5 and 0.8 have a significant effect on curved sprint performance, associated with greater lean angle, greater horizontal GRF and shorter ground contact times, whereas small or no increases in average vertical GRF were observed. For coefficient of traction increases from 0.8 to 1.1, no performance improvements were observed (Fig. 2.11).

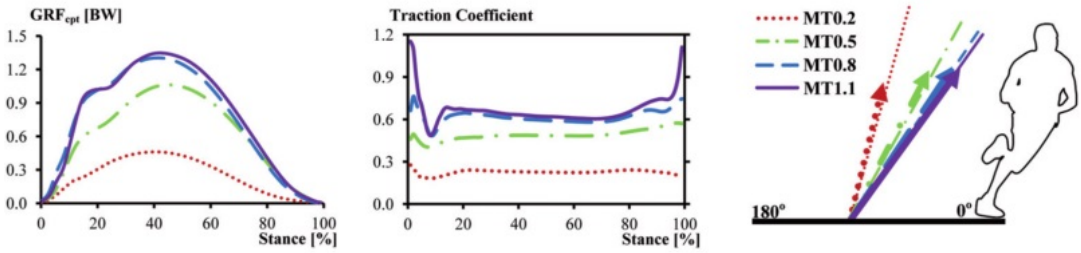

(a) Average GRF over normalised stance phase.

(b) Averaged utilised traction over normalised stance phase.

(c) Averaged lean angle (line) and averaged GRF (arrow) over the stance phase. MT is the mechanically available traction coefficient.

Figure 2.11: Effect of mechanical available traction on GRF, utilised traction and lean angle [78].

These findings show that increasing mechanical available traction can influence performance until a threshold is reached, after which factors other than traction seem to limit the performance improvement. The results suggest that the threshold is specific to each movement, with straight and curved sprinting performance improvements associated with greater thresholds compared to changes of direction.

Other authors evaluated the relationship between mechanically available and utilised traction specifically for football, by considering different football footwear and surfaces. Schrier et al. [25] analysed performance time and utilised traction during a sprint acceleration and a 180° turning movement (Fig. 2.12a and Fig. 2.12c, respectively) performed by participants wearing football indoor shoe or firm ground boots, on laboratory or artificial turf surfaces. The mechanical available tractions were equal to 1.0, 1.2 and 1.7 for indoor shoe on laboratory floor, indoor shoe on artificial turf and firm ground boot on artificial turf, respectively. During the comparison between the surfaces, while participants wore the football indoor shoes, faster running times

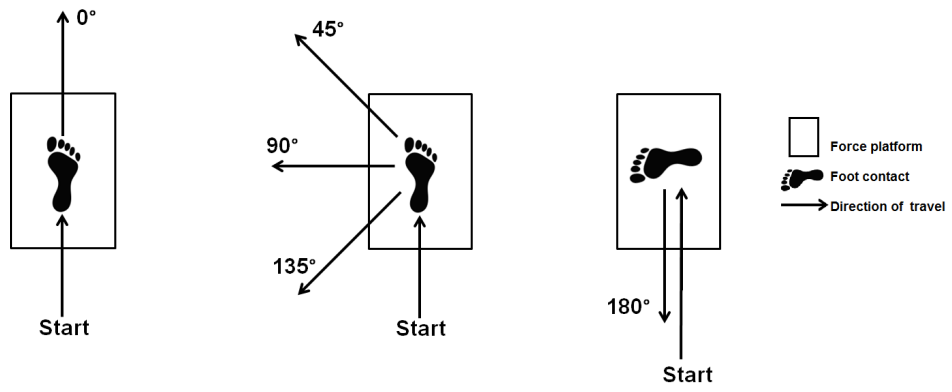

(a) Straight acceleration.

(b) Cutting movements of different angles on the left, planting the right foot on the force platform.

(c) Turning movement.

Figure 2.12: Movements over the force platform.

on the artificial turf surface (1.08 s vs 1.04 s) and significantly greater peak utilised traction on the laboratory floor (1.11 vs 0.83) were observed during sprint acceleration; no significant differences were noticed during a turning movement (performance time of 2.67 s vs 2.68 s; utilised traction of 0.93 vs 1.05, for artificial turf and laboratory floor, respectively). When comparing the different footwear on the artificial turf, there was no difference in performance time (1.04 s vs 1.04 s) and utilised traction (0.83 and 0.87 for the indoor shoe and studded boot, respectively) during the sprint acceleration, whereas a significant decrease in time (2.67 s vs 2.56 s) and increase in peak utilised traction (0.93 vs 1.09) were observed with the football boot during the turning movement. The same results, when comparing different football boots on an artificial turf, were obtained by Sterzing et al. [79], who found no differences in the kinetic variables in the acceleration performance (Fig. 2.12a), but observed higher shear forces and faster times during a 45° cut (Fig. 2.12b) and a turning movement (Fig. 2.12c) performed for shoes with shorter studs.

Schrier et al. [25] concluded that traction has a significant effect on turning movement, by allowing athletes to apply higher horizontal forces to brake efficiently and accelerate in the new direction more rapidly, but it does not have a significant effect during sprint acceleration. Compliance appears to improve performance where traction is not a limiting factor, such as during sprint acceleration. However, in the previous section (Sec. 2.3.2.2), two studies were reported where differences in running time performance in association with different values of compliance were found also to complete agility courses. This suggests that compliance may improve performance during different tasks for ranges specific to each movement, highlighting the importance of the measurement of surfaces' mechanical properties in association with biomechanical tests.

The results obtained by Schrier et al. [25] suggest that changes of direction performance improvements are associated with mechanical available traction thresholds greater than sprint acceleration, since significant differences were found for the former task when mechanical available traction increased from 1.2 and 1.7, whereas differences were found between traction values of 1.0 and 1.2 for the latter task. Differently from Schrier et al. [25], who found no differences in change of direction performance for mechanical available traction increasing from 1.0 to 1.2, Worobets et al. [63] found an improvement of 30% in performance time when considered the same traction values. These coefficients were obtained by using a football indoor shoe on the laboratory floor or on an artificial turf for the former study and by changing the shoe outsole material and performing the movement on a laboratory floor for the latter. This highlights that the traction thresholds associated with performance improvements vary not only between the movement analysed, but they depend also on the surface where these movements are performed, where other factors, such as compliance, may play a role.

The data from Schrier et al. [25] show how biomechanical utilised traction may differ considerably from mechanical available traction. The analysis of athletes' kinematics and kinetics showed how players adapt their movements prior to and during change of direction tasks in response to different traction conditions. Dowling et al. [80] evaluated players' movement during a 30° change of direction task on two surfaces with coefficients of friction equal to 0.38 and 0.87, and found lower knee flexion angle and moment, higher knee valgus moment and greater medial distance of the centre of mass (CoM) from the support limb associated with the high friction surface. Müller et al. [81] found that players exhibited a less powerful approach and more cautious movement behaviour to perform a 135° cutting movement (Fig. 2.12b) on an artificial turf surface with non-studded shoes compared to artificial turf, firm ground and soft ground football boots design, by reducing the horizontal GRF prior to the movement and turning with a more vertical alignment of the distal segments relative to the surface, even if the approaching velocity was the same as the higher traction conditions; despite these adaptations, players were still subjected to an increased medio-lateral foot translation during turning. The authors found a more cautious approach also in case of too high traction condition, in fact they found significantly lower peak shear forces and lower coefficient of traction during cutting movements and slower running performance time during both slalom (Fig. 2.9f) and straight acceleration (Fig. 2.9e) when participants wore the soft ground boot design. The use of this boot on the artificial turf, considered in this study, was related to reduced medio-lateral foot translation and increased ankle moments, suggesting that the use of this boot could cause foot fixation, rather than foot instability due to the studs not penetrating enough into the surface.

These studies highlight that mechanically available and utilised traction measurements should not be evaluated without assessing also athletes' kinematics and perception of traction, which are fundamental to understand movements adaptations related to unsuitable traction conditions.

2.3.2.4 Other biomechanical tests of football-specific movements

The analysis of kinetic and kinematic variables showed that faster change of direction time performance is related to significantly shorter ground contact time, greater horizontal peak force, lower vertical impact force and greater medial distance of the CoM from the centre of pressure (CoP) [82, 83]. When comparing the stance phase of the cutting or turning step with the step preceding it, an even distribution over the two steps is revealed during a 45° cut [84], whereas a greater horizontal peak force on the step prior the change of direction is observed during 90° cut [84] and 180° turn [82] movements. Greater braking force applied on the steps prior to turning means that the CoM velocity is reduced and the body can rotate and align into the new intended direction more effectively, this results in shorter contact times on the pivoting step, quicker application of the force into the new direction and a faster exit from the change of direction. Whereas, the application of force in a more vertical direction and not decelerating predominantly on the penultimate step could result in longer time spent slowing down with subsequent longer ground contact times and slower change of direction performance [82, 84, 85].

During a game situation, changes of direction are usually unanticipated and occur as a sudden reaction to external stimulus, such as avoiding another player or following the bounce of the ball [86]. For this reason, it is important to evaluate the performance of cutting manoeuvres considering the reaction to specific stimuli. Besier et al. [86] showed a decrease in performance and increase in knee joint external moments during unanticipated conditions compared to preplanned manoeuvres. The authors explained these results as due to the lower amount of time that athletes have to implement appropriate postural adjustment strategies, such as a change in foot placement on the ground and varying amounts of trunk lean toward the new direction of travel. An increase of trunk lean has been associated with higher knee abduction moment and risk of ACL injury [87].

In the previous section (Sec. 2.3.2.3), it was reported that biomechanical utilised traction may differ considerably from mechanically available traction, due to potential movements mechanisms of the athletes in response to the specific traction conditions. Therefore, kinematics should be evaluated in association with kinetics, however, the results of the studies presented in this section, highlight that the analysis of these variables only during the change of direction step may be a limit. Movement adaptations

are recorded during the steps prior changes of direction and may be different between preplanned and unpredicted tasks, with consequences in performance. Studies evaluating shoe-surface interaction effect on players' performance during football-specific tasks should consider not only the change of direction step but also those prior to it, and include the analysis of unpredicted movements.

2.3.3 Subjective-sensory tests

Despite a relationship between mechanical and biomechanical data of traction properties exists, they do not exactly reflect each other, because the latter are influenced by players' adaptation in response to different shoe-surface conditions [15, 64, 86], as has been reported in the previous sections (Sec. 2.3.2.3 and 2.3.2.4). For this reason, it is important to understand also the players' perceptions of traction in association to the quantitative data collected during biomechanical tests, in order to better evaluate shoe-surface interactions.

Subjective-sensory data have been collected about the perception of performance, surface properties and shoe-surface interaction, and to directly compare natural grass and artificial turf surfaces. The overall responses about the surface comparison revealed that players perceive artificial turf to be harder, faster, more abrasive, have less grip and thinner grass compared to natural grass [88]. The perception about faster running time performance on artificial turf confirms the findings reported previously (Sec. 2.3.2.2), where faster times were recorded on artificial turf compared to natural grass during agility courses [62, 70, 71]. Moreover, running time performance association with players' perception of faster times has been found in different studies [64, 66, 79]. A comparison between players' perception and surface rotational traction, energy restitution and shock absorption, showed that the latter is the only parameter to significantly influence players' perception, with lower shock absorption values reported as the higher comfort situation [27].

Morio et al. [89, 90] studied the relationship of traction perception with static and dynamic friction during a forward cutting manoeuvre performed over a force platform with different shoe and surface conditions. Static and dynamic traction coefficients were calculated over the stance phase of the change of direction step, with the former defined as the maximum value in the early 50 ms of the stance phase, and the latter as the mean during 100 ms of the mid-stance phase. The authors found significant correlation for both coefficients with traction perception. However, the authors suggested that the static traction coefficient is more relevant than the dynamic one to investigate the grip perception of sports footwear, since the former is dependent only on the shoe-surface contact; whereas, during the dynamic phase the foot can be con-

trolled, becoming a foot-shoe-surface interface. As stated in section 2.2.2, the use of a traction coefficient is a limit; therefore, the traction perception relationship with the shear forces during the impact and mid-stance phases should have been evaluated. Moreover, this study considered a single task, whereas, the results of biomechanical tests highlight that traction is dependent on the movement analysed; therefore, the relationship between static and dynamic traction coefficients with traction perception may be different for other movements, especially for sprint acceleration and faster changes of direction.

2.4 Inertial measurement unit sensors

GRFs are of interest to understand the mechanics of shoe-surface interactions and their consequences for athletic performance. The gold standard technique for GRF measurement are force platforms. The use of these devices is limited due to their fixed position and small area on the ground of a laboratory, on which participants must place their foot in order to obtain a successful measurement, which could result in movement adaptations not representative of the specific task analysed; and, due to their high costs, most laboratories are equipped with only one or two platforms, making the measurement of successive steps impossible. On the contrary, the possibility to measure GRFs in the field through a body-worn measurement system, rather than on a fixed position, will match more closely the movements recorded in a real game environment, allowing the incorporation of the protocol in a normal training session, the measurement on surfaces on which players train and play regularly, and a larger testing area, thus athletes do not need to alter their movements to target a specific region [43].

The increasing accuracy, small size, low weight, portability and relatively low cost of inertial measurement unit (IMU) sensors have been proposed as an alternative for in-field motion analysis. An IMU is an integrated electronic device that contains tri-axis accelerometer, magnetometer and gyroscope, which measure the sum of gravity and

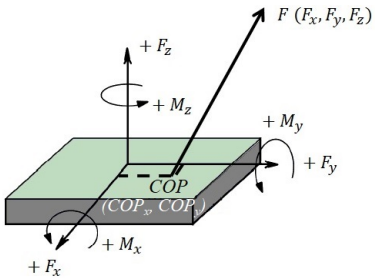

Figure 2.13: Force platform. F is the GRF and F_x, F_y, F_z its components. M_x, M_y, M_z are the moments of rotations measured respect each axis. CoP_x and CoP_y are the CoP components along the x and y axes.

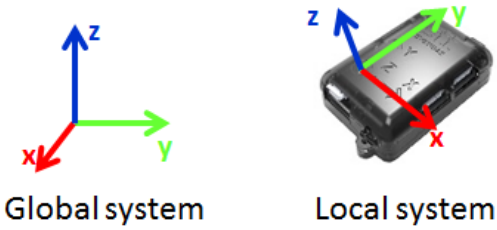

Figure 2.14: Example of IMU with global and local systems.

inertial linear accelerations, the Earth's magnetic field vector components and the angular velocities, respectively. The signals of the three integrated devices are measured along their three orthogonal axes or, in other words, in the sensor local orientation system, and they can be used to obtain information about the sensor orientation in a global reference system (Fig. 2.14).

The device orientation can be determined with respect to a global reference system by gyroscope integration, however, the orientation estimation error grows over time, since this technique suffers from gyroscope bias drift. To overcome this problem the measurement of the three sensors can be combined through sensor fusion algorithms, which use the direction of the gravity vector to determine the vertical axis and the direction of the Earth's magnetic north for heading estimation. The most common sensor fusion techniques are extended Kalman filter and complementary filter. The former uses a statistical description of the state of the system under analysis, by modelling the noise as a Gaussian distribution, to estimate the orientation; whereas the latter uses the frequency domain analysis to filter the sensor's noisy measurements and fuse the filtered signals together to obtain the orientation estimation. However, these approaches are still subject to errors, in particular due to the presence of ferromagnetic materials or electrical appliances, which could affect the magnetometer's measurement, especially indoors.

The performance of the two mentioned sensor fusion algorithms have been compared with gyroscope integration by Bergamini et al. [91] for the estimation of the orientation of a sensor during daily-life manual activities and walking. The authors concluded that the performance of the three techniques are similar in the first 20 s of analysis, after which the level of accuracy of sensor fusion is significantly higher; however, they noted how the benefit of sensor fusion could be seen before this threshold for movements where impacts are involved. The two sensor fusion algorithms have similar accuracy [91]; however, the extended Kalman filter has been demonstrated to be the best choice, regardless its higher computational cost and higher complexity, because it is reliable and allows to add further sensory information, such as GPS data, without the need to redesign the estimation filter or change the parameters of the algorithm [92].

IMUs have been primarily used to measure joint angles during different movements, achieving a level of accuracy which ranges between 1° and 5° depending on the specific task [93]. Recently, the possibility of using IMUs to estimate GRFs saw a growing interest in the research community. The literature research showed that GRFs can be estimated with a single IMU or with multiple sensors, either using Newton's second Law of Motion in conjunction with a biomechanical model or a machine learning approach.

2.4.1 Ground reaction force estimation based on biomechanical models

Several authors analysed the accuracy in the estimation of GRFs using Newtonian mechanics from IMU data collected during different tasks of varying intensity, and comparing the forces predicted with those directly measured by a force platform.

2.4.1.1 Non locomotive tasks

GRFs have been estimated using IMUs with a root mean square error (RMSE) smaller than 20 N during non locomotive tasks of low intensity, such as trunk bending exercises [94], sit to stand [95] and squat motion [95, 96]. Faber et al. [94] used 17 IMUs, whereas less sensors have been used by Min et al. [96] and Kodama and Watanabe [95], who applied the devices only to the trunk and one lower limb assuming bilateral symmetry. Kodama and Watanabe [95] compared three body models, which differ in the amount of links the trunk was divided into (Fig. 2.15). The trunk was split into upper, middle and lower trunk using the lower end of the rib and the highest point of the iliac crest as dividing point, with the upper segment including head and arms. No significant differences between a three or two-link trunk model were found, with two-link considered both as the upper and middle-lower trunk division and the upper-middle and lower trunk configuration, whereas the use of the trunk as a single segment led to worse results. Therefore, when different body segments are considered in the estimation of GRFs, the trunk should be divided into two or three links.

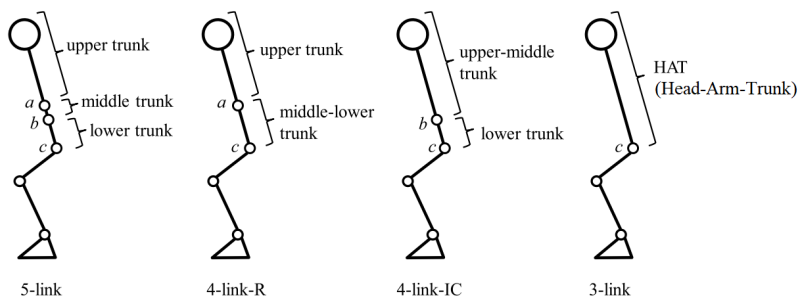

Figure 2.15: Multi-link trunk models [95]. *a*, *b* and *c* are the lower end of the rib, the highest point of the iliac crest and the great trochanter, respectively.

Contrasting results were obtained in the estimation of the vertical GRF during non locomotive tasks of higher intensity, such as vertical jumping [97–100] and plyometrics [101]. Elvin et al. [97] applied two accelerometers to the subjects' tibiae and found a strong correlation between the peak GRF measured by the force platform and the peak acceleration recorded by the accelerometers, concluding that the peak GRF may be estimated with Newton's second Law of Motion. However, the direct comparison between measured and estimated GRF had contrasting results. Howard et al. [98] found percentage differences higher than 30% between the GRF measured by a force platform and the one estimated from an accelerometer attached close to the subject's CoM, concluding that accelerometers can not be used interchangeably with force platforms; whereas, Pouliot-Laforte et al. [99], Setuain et al. [100] and Meyer et al. [101] found correlation coefficients higher than 0.89 between measured and estimated GRFs, even if the error increased with the increase of force magnitude [100, 101]. The difference in the results with the study from Howard et al. [98] may be related to the sample frequency used, 1000 Hz compared to 100 Hz or lower, suggesting that the presence of noise at the higher frequencies might have affected the results, therefore appropriate sample frequency and low-pass filter to estimate GRF from IMUs should be investigated.

Elvin et al. [97] measured peak acceleration values higher than 40g at landing. This suggests that some of these studies results were limited by the accelerometer ranges of ±6 g or ±8 g [99, 101]. These studies showed that the GRFs during non locomotive tasks can be estimated with very high correlation (> 0.90) using only one sensor attached close to the CoM or to the right hip. However, the tasks considered in this section are symmetrical, therefore, the use of only one sensor, especially if attached on the hip may not present high correlation with force platform's measurements when evaluating asymmetrical movements.

2.4.1.2 Locomotive tasks

Ohtaki et al. [102] estimated GRFs during straight walking using three IMU sensors, attached on the distal position of shank and thigh of the right leg and on the sacrum assuming bilateral symmetry. The authors reported values of 0.076 and 0.310 N BW^{-1} as the highest RMSE for horizontal and vertical forces, respectively, between the different walking speeds considered.

Karatsidis et al. [103] used 17 IMUs mounted on different segments through a tight-fitting suit and estimated the GRFs using Newton's equation of motion for the single support phase of walking and a distribution algorithm based on a smooth transition assumption function that uses statistical models based on empirical data for the double support phase. The predicted values were compared with those directly measured

by the force platform and RMSE of 0.039, 0.019, 0.076 N BW^{-1} (corresponding to relative RMSE of 10.2%, 13.8% and 6.2%) were found for antero-posterior, medio-lateral and vertical force components, respectively.

These studies estimated the GRFs both in the vertical and horizontal directions, with the former study reporting lower errors for the shear forces and the latter for the vertical forces. These differences may be related to the estimation of the time of heel contact events, which was predicted with mean errors of 110 ms for the former and of 16 ms for the latter study, suggesting that gait events should be detected using the accelerations recorded at the feet, rather than at the shanks. Moreover, the assumption of bilateral symmetry used by Ohtaki et al. [102] limits the use of this method to walking on straight line and to healthy participants, since injuries or pathologies could result in asymmetrical walking. A reduction in the number of sensors used by Karatsidis et al. [103] should be analysed in order to simplify the methodology and participants' preparation.

The estimation of GRFs during the double support phase of walking represents one of the biggest challenges. Karatsidis et al. [103] used a different approach compared to the single support phase in the attempt to improve the forces prediction, however, higher errors were still obtained, with values up to three times higher compared to the single support phase for the vertical force component. This does not represent a problem during running, where the full stance phase is characterised by single support, however different challenges are expected due to higher impacts at foot strike and higher amount of sensors' oscillations related with faster movements.

A statistical model was considered by Neugebauer et al. [104] to estimate the peak vertical and horizontal GRFs during walking and running. The authors attached a single sensor over the most lateral aspect of the iliac crest of the right hip and used a statistical model based on the assumption that sex, body mass and type of locomotion were good predicting factors. Errors of 8.3% or 106.4 N and 17.8% or 33.2 N were obtained for the peak vertical and horizontal GRFs, respectively. However, they concluded that a more detailed biomechanical model must be considered to provide an accurate representation of the body loads.

Charry et al. [105] and Raper et al. [106] estimated vertical GRF from tibial acceleration using a logarithmic approach during walking and running at different speeds. The results show a constant pattern of measurements compared with the force platform [106] and similar results for both legs [105]. Charry et al. [105] reported a RMSE of 5.8% in the peak vertical GRF estimation on average between speeds and subjects, with higher errors found during walking and sprinting. These studies show that the measurement of tibial accelerations allows to estimate vertical GRF, however,

the sensors attached to the tibiae can not be used in the estimation of the horizontal component of force since the accelerations are not representative of the body's CoM, limiting their use.

2.4.1.3 High intensity and sport-specific movements

Setuain et al. [107] attached a single IMU over the fourth-fifth lumbar vertebrae (L4-L5) region and calculated the step-averaged horizontal and vertical force over a 20 m sprint acceleration to compare the results with the values measured from a force platform. The authors reported relative errors (RelErr) between the estimated and measured forces of $45.3 \pm 55.0\%$ and $7.3 \pm 8.0\%$ for horizontal and vertical force, respectively.

Gurchiek et al. [108] analysed the ability of a single IMU sensor to estimate GRF during a standing sprint start and a 45° change of direction. The authors attached the sensor over the sacrum at the mid-point between the posterior superior iliac spines (midPSIS), assumed as the closest point to the subject's CoM, and compared the three components of GRF and the resultant force, both as instantaneous and step-averaged forces, with the values measured by a force platform. The RMSE reported for the step-averaged forces during the sprint start are 37.7 N, 66.3 N, 77.1 N and 73.6 N for anterior, lateral, vertical and resultant force respectively, and 97.5 N, 163.7 N, 54.2 N and 70.2 N for the change of direction task. In figure 2.16, the instantaneous force is reported, showing larger errors in the estimation of the force compared to the step-averaged values, in particular for the forces in the horizontal direction, confirming the worse results found from the step-averaged data.

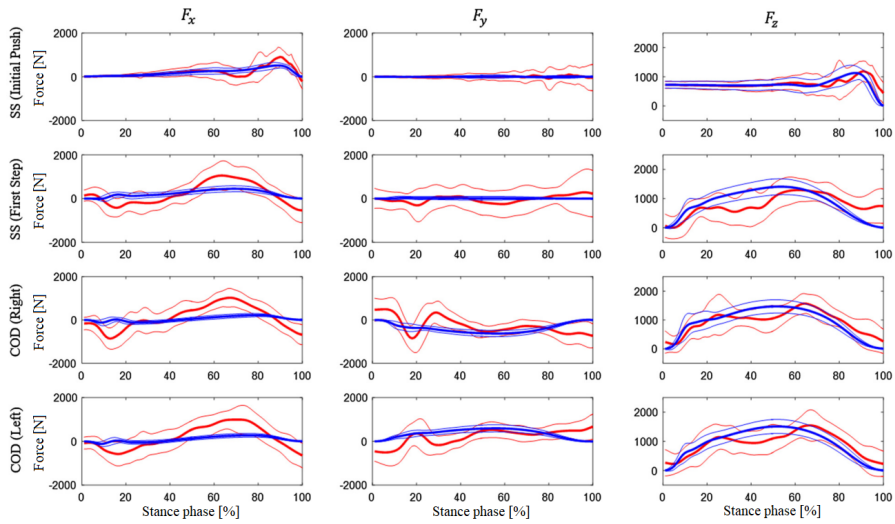

Figure 2.16: Comparison of measured (red line) and estimated (blue line) GRF by Gurchiek et al. [108]. The left, middle and right columns are the results for the antero-posterior, medio-lateral and vertical forces, respectively. The rows are for the initial two-foot push of the start sprint (SS), the first step of the start sprint, right and left change of direction (COD), respectively.

Wundersitz et al. [109] used a tri-axial accelerometer fixed on the centre of the upper back at the level of the second thoracic vertebra (T2) to estimate peak vertical and resultant GRF during straight running and change of direction tasks of different angles (45°, 90° and 180°). Comparing the results with force platform's measurements, the authors observed that the estimation error increased with greater change of direction angle, with the error ranging from 12 to 24%.

A direct comparison between these studies is not possible, since different error calculations were reported. However, the results show that lower accuracy was obtained in the estimation of the forces in the horizontal direction, and the errors increased with the force magnitude. The higher errors obtained for the horizontal direction could be related to the use of a single sensor and its position, since during the movements analysed the subject's CoM could move from the sacral region [108, 109]. The importance of the shear forces was highlighted in section 2.3.2.4, where their relationship with performance improvements were reported, therefore, a multiple-sensor approach should be considered to improve the estimation of shear forces for high-intensity football-specific movements.

Finally, it is worth reporting the use of IMU sensors to estimate GRF during a ski jump by Logar and Munih [110]. The researchers attached six IMUs to the athletes and two on the skis and estimated GRF during take-off through inverse dynamics both in a laboratory simulation on a force platform and outdoor on a ski jumping hill equipped with a force platform at the end of it. RMSE of 65.2 ± 259.0 N and 81.3 ± 184.0 N were obtained for the indoor and outdoor validation, respectively. The comparable results between indoor and outdoor validation highlight the portability of an IMU-based method in the estimation of in-field GRFs; moreover, these studies show the possibility to use an IMU-based method to evaluate performance during a great variety of sport activities.

2.4.1.4 Estimating ground reaction forces for football-specific movements

The use of IMUs to estimate three-dimensional (3D) GRFs through a Newtonian mechanics approach showed promising results, although a single sensor has been shown not to be sufficient to estimate GRFs during high-intensity football-specific tasks, such as straight acceleration and cutting manoeuvres. Therefore, the study conducted by Verheul et al. [111] to investigate if Newton's Second Law of Motion can be used to estimate GRFs for high-intensity tasks and the minimum number of segments required is of great interest.

The authors estimated resultant GRF curve profile and loading characteristics, such as impulse, impact peak and loading rate, applying Newtonian mechanics to body

segments' accelerations. Each segmental acceleration was obtained by double differentiation of the segment's CoM motion, which was calculated from the markers' trajectories measured using a motion capture system. The authors compared the validity of a full-body model, based on fifteen body segments, and models based on a reduced number of segments with the measurements of a force platform. All combinations from a minimum of one to a maximum of fifteen segments were considered. Movements of varying intensity were analysed: second or third step of acceleration; first or second step of deceleration from maximal sprinting to immediate stand-still; 90° cut; and straight-line running at low, moderate and high speed.

Details of the estimation errors obtained by the authors from the full-body model are reported in table 2.3. In general, the authors found that GRF estimation accuracy was dependent on the specific task, with higher accuracy for lower intensity tasks, such as running at low speeds.

Table 2.3: RMSE, impulse, impact peak and loading rate errors of the resultant GRF estimated from fifteen segmental accelerations for different tasks by Verheul et al. [111].

	RMSE		Impulse error		Impact peak error		Loading rate error	
	[N kg^{-1}]	[%]	[N s kg^{-1}]	[%]	[N kg^{-1}]	[%]	[N kg^{-1} s^{-1}]	[%]
Accelerations	2.82±0.7	8.4±14.0	0.25±0.1	9.1±4	3.27±2.8	28.5±33	229±264	33.2±27
Decelerations	5.77±1.8	6.1± 8.8	0.26±0.1	11.1±6	7.68±5.5	15.0± 9	380±404	20.1±16
90° cut	2.67±0.7	3.3± 4.1	0.21±0.1	3.8±2	3.33±2.9	9.8± 8	234±210	24.5±18
Low speed running	1.62±0.4	1.8± 2.0	0.09±0.1	2.3±2	2.22±2.3	13.8±22	173±101	33.0±13
Moderate speed running	2.48±0.6	3.1± 5.7	0.16±0.1	4.6±2	1.96±1.5	9.2± 8	281±174	34.0±14
High speed running	3.26±1.7	4.8± 8.3	0.20±0.1	6.8±7	4.00±4.1	13.1±15	323±326	29.3±19

In order to achieve estimated GRF errors lower than 3 N kg^{-1}, rated as moderate or lower, the authors concluded that a minimum of two and three segments was required for low and moderate speed running, eight segments for cutting movements and eleven for accelerations. For the highest intensity tasks, such as deceleration and high speed running, the authors found high or very high errors ($>$ 3 N kg^{-1}) regardless of the number of segments used. Moreover, they suggested that the trunk segment should be included in all the combinations, being the main contributor due to the highest percentage of body mass; this segment is followed in order of importance by thighs, head, shanks, arms, pelvis and feet.

The results of this study show that high-intensity movements can not be accurately represented from the accelerations of a single segment, suggesting that an IMU-based multiple-sensor approach may improve the GRF estimation obtained in the studies presented in the previous section (Sec. 2.4.1.3). However, an accurate representation for the highest intensity tasks, such as deceleration, may not be possible with Newtonian mechanics.

This study evaluated the validity of estimating GRFs from segmental accelerations by comparing measured and estimated resultant force. However, in section 2.2.2, the importance in the understanding of the single component of force was highlighted. Therefore, the validity of this method should have been evaluated for the vertical and shear forces separately, and the authors should have investigated if the number of segments necessary to obtain moderate or lower errors differs between force components. In addition, in section 2.3.3, a relationship between active peak force with players' perceptions was found, therefore also the accuracy in the estimation of this GRF loading characteristic should be investigated.

2.4.1.5 Estimating ground reaction forces from other mechanical models

Clark et al. [112, 113] found that two mechanical phenomena acting in parallel, the collision of the lower limb with the running surface and the motion of the remainder of the body mass throughout the stance phase, are sufficient to predict the vertical GRF during steady running, regardless of different speed and foot strike conditions. The authors developed a two-mass model by overlapping two individual force-time waveforms, calculated through a raised cosine bell curve function from two impulses, J_1 and J_2. The former impulse results from the vertical deceleration of the lower limb mass m_1 during impact with the running surface, and is determined from the time interval, between touchdown and the vertical velocity of m_1 slowing to zero, and the change in velocity during this time interval. The authors represented J_1 as a finite impulse during the impact interval, since after it the lower limb velocity is relatively constant and, thus, the force negligible. During steady-speed level running, where no net vertical displacement of the CoM over each step and constant speed were assumed, a runner supports an average of one body weight during the step time, where each step is defined by the sum of contact time with vertical GRF and aerial time with zero force. This allows the calculation of the stance-averaged vertical GRF and consequently the total ground reaction impulse (GRI) and impulse J_2, since the total GRI is the sum of the two distinct body segment impulses J_1 and J_2.

The raised cosine bell curve function is defined over a finite time interval of one period as:

$$F(t) = \begin{cases} 0 & \text{for } t < B - C \\ \frac{A}{2}\left[1 + \cos\left(\frac{t-B}{C}\pi\right)\right] & \text{for } B - C \leq t \leq B + C \\ 0 & \text{for } t > B + C \end{cases} \tag{2.1}$$

where A is the peak amplitude, B the centre time of the peak, and C half-width time interval (Fig. 2.17a), when the CoM's displacement is symmetrical during the movement.

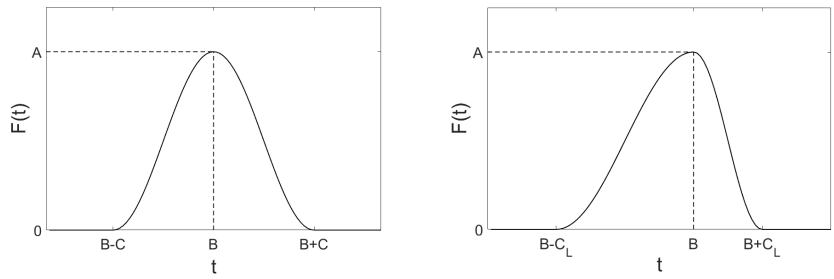

(a) Symmetrical. **(b)** Asymmetrical.

Figure 2.17: Raised cosine bell curve.

In case of asymmetrical impulse profile (Fig. 2.17b), parameters C_L and C_T, leading and trailing half-width time interval, respectively, needs to be included to control the symmetry:

$$F(t) = \begin{cases} 0 & \text{for } t < B - C_L \\ \frac{A}{2}\left[1 + \cos\left(\frac{t-B}{C_L}\pi\right)\right] & \text{for } B - C_L \leq t \leq B \\ \frac{A}{2}\left[1 + \cos\left(\frac{t-B}{C_T}\pi\right)\right] & \text{for } B \leq t \leq B + C_T \\ 0 & \text{for } t > B + C_T \end{cases} \tag{2.2}$$

Clark et al. [113] reported that, because of the simple properties of this function, the peak amplitude can be defined as $A = 2F_{avg}$, where F_{avg} is the average force during the total time interval of the impulse, and the area under the curve is $J = AC$.

Different mass percentages for the lower limb (m_1) were analysed: 1.5%, 8.0% and 16.0% BW, representing the approximate foot mass, a constant arbitrary value and the approximate lower limb mass, respectively. The vertical GRF curve profile in comparison to force platform measurements are represented in figure 2.18 for the different mass percentages, speeds and foot strike considered. The use of the foot or lower limb effective mass percentages resulted in an under or over-prediction of the impact force recorded at the beginning of the stance phase, respectively, with consequent decrease in the overall waveform fit. Whereas, the constant value of 8.0% leaded to the best results regardless the different speed and foot-strike conditions, with a total RMSE of 0.21 ± 0.09 BW when comparing the results with those measured by an instrumented treadmill. Thus, the authors concluded that the use of an effective mass may be unnecessary for accurate modelling and could be mechanically incorrect. It is believed that the use of an arbitrary value, instead of the effective mass, represents a limitation to the generalisability of the model and a different definition should be identified in order to associate the lower limb mass component to a biomechanical explanation. A possible reasoning behind the selection of this constant value may be related to the use of a marker positioned on the ankle to measure the deceleration of the lower limb. This location is not representative of the segment's CoM acceleration.

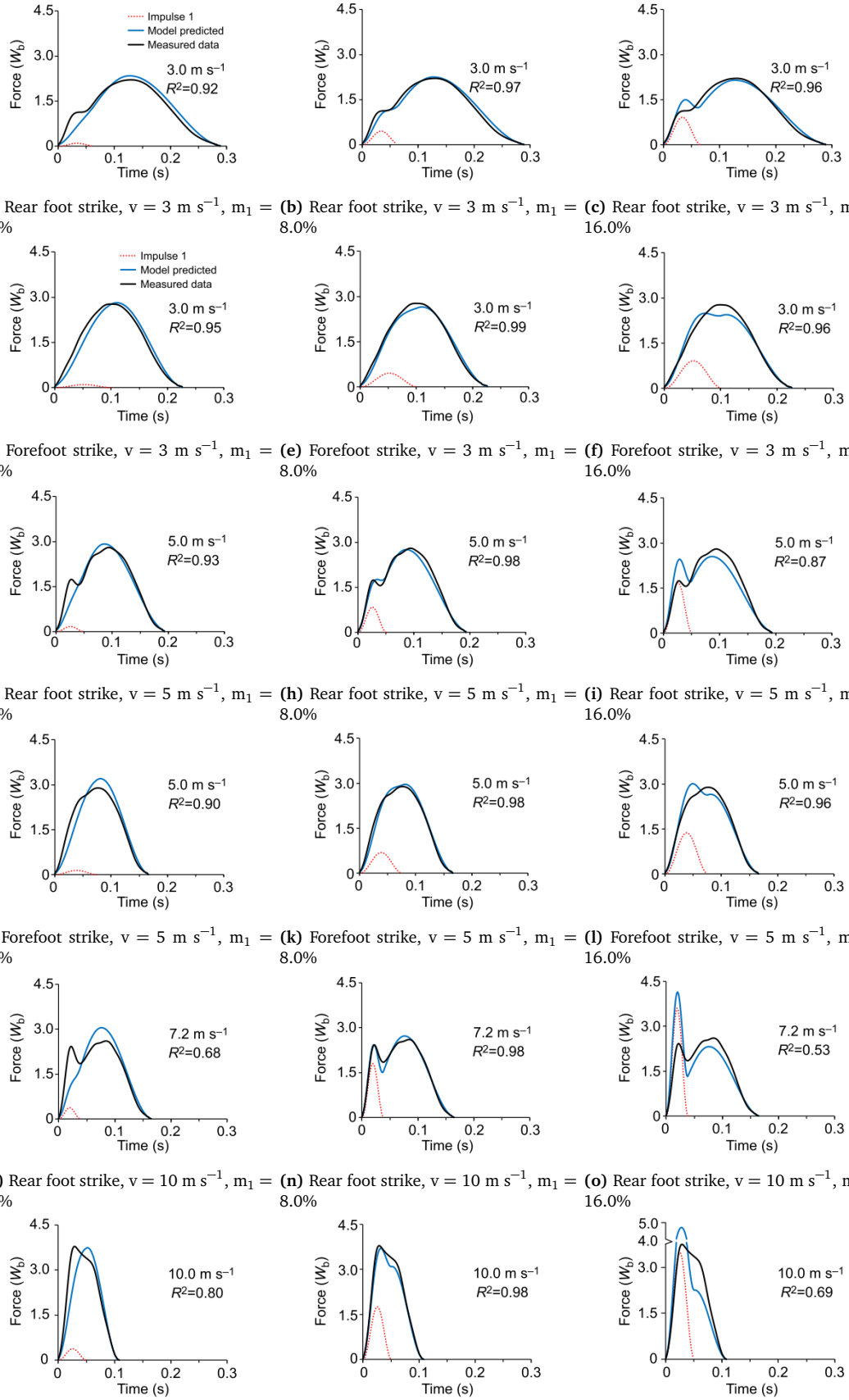

(a) Rear foot strike, v = 3 m s^{-1}, m$_1$ = 1.5% **(b)** Rear foot strike, v = 3 m s^{-1}, m$_1$ = 8.0% **(c)** Rear foot strike, v = 3 m s^{-1}, m$_1$ = 16.0%

(d) Forefoot strike, v = 3 m s^{-1}, m$_1$ = 1.5% **(e)** Forefoot strike, v = 3 m s^{-1}, m$_1$ = 8.0% **(f)** Forefoot strike, v = 3 m s^{-1}, m$_1$ = 16.0%

(g) Rear foot strike, v = 5 m s^{-1}, m$_1$ = 1.5% **(h)** Rear foot strike, v = 5 m s^{-1}, m$_1$ = 8.0% **(i)** Rear foot strike, v = 5 m s^{-1}, m$_1$ = 16.0%

(j) Forefoot strike, v = 5 m s^{-1}, m$_1$ = 1.5% **(k)** Forefoot strike, v = 5 m s^{-1}, m$_1$ = 8.0% **(l)** Forefoot strike, v = 5 m s^{-1}, m$_1$ = 16.0%

(m) Rear foot strike, v = 10 m s^{-1}, m$_1$ = 1.5% **(n)** Rear foot strike, v = 10 m s^{-1}, m$_1$ = 8.0% **(o)** Rear foot strike, v = 10 m s^{-1}, m$_1$ = 16.0%

(p) Forefoot strike, v = 10 m s^{-1}, m$_1$ = 1.5% **(q)** Forefoot strike, v = 10 m s^{-1}, m$_1$ = 8.0% **(r)** Forefoot strike, v = 10 m s^{-1}, m$_1$ = 16.0%

Figure 2.18: Estimated vertical GRF curve profile in comparison to force platform measurements for different foot-strike patterns, running speeds and lower limb mass percentages [113].

The method presented in this study represents a valid alternative to the use of Newton's second Law of Motion in the estimation of the vertical GRF and its use in association with IMUs measurements should be evaluated. Moreover, the validity of this method in the estimation of the horizontal force component, and more dynamic and complex movements, for which assumptions of constant speed and no vertical displacement of the CoM can not be considered, should be investigated.

2.4.2 Ground reaction force estimation using machine learning

The studies reported in the previous section (Sec. 2.4.1) use biomechanical models to assign a percentage of body weight to each segment. However, these percentages are based on anthropometric tables defined from a population sample, introducing a limitation in their use. A different method to determine GRF from IMU data is based on machine learning. This data analysis technique uses computational methods to learn information directly from data given as input and create a model without relying on predetermined equations or anthropometric tables. The model can be subject-specific, when it is trained with data from a single subject and used to predict the forces on the same participant, or an averaged model, when it is built from a pool of different subjects.

Guo et al. [114] used the vertical force measured by pressure insoles to train a model, subsequently used to predict the vertical GRF from the acceleration of a single sensor attached on three different locations during walking. The authors predicted the vertical GRF during a controlled walk with relative RMSE of 3.8%, 4.0% and 4.2% for the sensors attached to L5, seventh cervical vertebra (C7) and forehead, respectively. These errors increase to 5.0%, 5.6% and 6.0% during a free outdoor walk, including not only gait in straight line. Differently from the use of Newtonian mechanics the estimation of the GRFs during double support phase present lower errors compared to the single support phase (e.g. RMSE from the L5 attachment during free outdoor walking equal to 6.4% and 5.8% for single and double support phase, respectively). The best results in all conditions were obtained for the sensor located on L5, suggesting that the accelerations most representative of the body's CoM lead to the best fitting also in case of a machine learning approach.

Miller et al. [115] trained a neural network model using step-averaged resultant tibial acceleration of the dominant leg and vertical GRF measured on an instrumented treadmill. The training data were collected from 34 subjects running at three different speeds on the treadmill and tested on 4 participants with different foot-strike patterns. The results showed that the model was able to predict vertical GRF from tibial acceleration independently of foot strike pattern and running speed with RMSE

of 102.4 N or 0.16 BW. A more complex model was built by Wouda et al. [116]. The authors used 17 IMUs and an instrumented treadmill to train a model based on two concatenated neural networks to estimate vertical GRF for running at different speeds. The first network mapped the orientation of three IMUs placed on pelvis and lower limbs to predict joint angles, which together with the vertical acceleration measured in the global system by the same sensors, are given as input to the second network to estimate the vertical GRF. The authors created both a subject-specific model and an averaged model built on seven subjects and tested on a representative eighth subject. Vertical GRF was estimated with RMSE of 0.29 BW for the averaged model and with RMSE of 0.10 BW for the subject-specific neural network. These studies considered comparable running speeds ranging between 10 and 14 km h^{-1}, and the results highlight the differences in accuracy between a subject-specific model and an averaged one, and, for the latter case, the importance of the amount of data used to train the model, with errors of 0.16 BW for a model trained on 34 participants and 0.29 BW when based on data from 7 subjects.

Finally, a study from Leporace et al. [117] proved that it is possible to predict all three components of GRF from the accelerations measured at the distal and anterior part of the shank by using an artificial neural network trained and controlled with the data from force platform's measurements. The use of neural network to estimate the three component of force could be achieved through a single network with three outputs or three networks with one output each. The authors obtained with the former method errors of 5.4, 4.8, 13.0% in the antero-posterior, vertical and medio-lateral direction, respectively; and errors of 5.2, 4.7, 12.8% for the latter option using a different number of neurons in the hidden layer to obtain the best fit for each model.

This section shows the ability of a neural network approach to predict GRFs independently of the running speed and foot-strike pattern. However, the use of a subject-specific model requires a training phase for each new subject and results in an overfitting; whereas, an averaged model is more generalisable, but its prediction accuracy is limited by the need of a population with large variability. Moreover, these studies modelled neural networks for running at constant speeds on a treadmill, therefore, it is not possible to translate the findings from the laboratory to an applied sport setting. The ability of neural networks in the prediction of GRFs during outdoor over-ground running or higher intensity movements should be investigated.

In comparison to Newtonian mechanics, a machine learning approach is not limited by biomechanical models, however, it is computationally expensive and requires a large amount of data to train the system. Therefore, the use of a method based on physics is considered superior, due to its higher generalisability, with the possibility to be used

between participants and movements without the need for new training.

2.5 Chapter summary

In the last years, football playing surfaces and footwear design evolved significantly in order to assist the player in enhancing performance and to reduce injury risk. For this reason, many top-level football teams play and train on hybrid turf surface pitches, which have been recently introduced in the attempt to combine the advantages of natural grass and artificial turf pitches. Hybrid turfs have been identified as the most consistent surfaces, since their mechanical properties are almost not influenced by moisture content, footwear [44] and use over a season [54]. However, a lack of knowledge regarding more detailed hybrid turfs' mechanical characteristics and their relationship with performance and injury risk has been identified and shoes specific for these surfaces have not been designed yet.

Research efforts to reduce injury and improve athletic performance have been focused at the shoe-surface interaction, which could be quantified through mechanical and biomechanical measurements. Mechanical tests are highly reliable and able to describe the material properties of surface sample tested, but they do not keep into account the athletes' adaptation to different shoe-surface conditions, which results in changes in magnitude and direction of the external forces and players' lower limb kinematics. These adaptations could also be different between individuals and specific movements [32].

Shoe-surface interaction under realistic loads cannot be described through a linear relationship between the vertical and horizontal forces, moreover the absolute magnitudes of the force components are of interest to understand the mechanics of the interaction, and the consequences for athletic performance and injury risk. For this reason, it has been suggested that the use of traction coefficient is a limit, whereas the absolute value and the time history of vertical and horizontal force components need to be considered in the evaluation of shoe-surface interaction [31,32]. In particular, it is important to evaluate shear forces, which, in section 2.3.2.4, have been shown to be the primary contributing factor for the evaluation of footwear traction characteristics, since higher forces in the horizontal direction allow better braking application and more dynamic propulsion during dynamic movements [81–83].

Force platforms are the gold standard for measuring GRF; however, they are expensive, the athletes may adjust their movements to target a specific area and they are difficult to install outside the laboratory under football surfaces, where athletes train and play regularly. IMUs are potential candidates to overcome these limitations and

estimate GRFs in the field.

The analyse of the literature showed that GRFs have been estimated from a single IMU or a multiple-sensor approach, using Newtonian mechanics or machine learning (Table 2.4). The use of a single sensor simplifies participant preparation, data acquisition and analysis, but has lower accuracy, especially in the estimation of the force components in the horizontal direction, compared to a multiple-sensor approach, which gives a better understanding of motion and acceleration of each body segment. The use of Newton's second Law of Motion is used in combination with human models, used to assign a percentage of body weight to each segment, but they represent a limitation being not subject specific. Whereas, the use of machine learning is affected by the chosen input parameters, is computationally expensive and requires a large amount of data to train the system. However, a method based on physics, is believed to be a stronger approach, especially when the aim is to estimate GRFs during football movements, which could be unpredicted, and a machine learning approach would require an amount of data too big to be realistically collect.

To the best of the author's knowledge, only three studies [107–109], highlighted in bold in table 2.4, used IMUs to estimate step-averaged and instantaneous 3D GRFs during football-specific movements. These authors applied Newton's second Law of Motion to the acceleration of a single sensor attached on the subjects' upper or lower back, however, the results highlight the need of an improvement in the estimation of shear forces. Football-specific tasks were analysed also in a study conducted by Verheul et al. [111], who estimated the resultant GRF for dynamic and high intensity movements applying Newton's second Law of Motion to different combinations of fifteen body segment accelerations, which were derived from the markers' trajectories recorded with an optoelectronic motion capture system. The results of this study suggest that the use of a multiple-sensor approach may allow to estimate 3D GRFs during football-specific movements with higher accuracy. In particular, the authors suggested that a minimum of eight segmental accelerations are required for cutting movements and eleven for accelerations.

In conclusion, an IMU-based multiple-sensor approach represents a good candidate to predict 3D GRFs in the field and characterise different shoes and surfaces, therefore, a method based on this approach will be investigated in order to address the research question of this programme of research.

Table 2.4: Summary of the studies using IMU sensors to estimate GRF. AP = antero-posterior. ML = medio-lateral. The references reported in bold will be used as comparison throughout this thesis.

Study	Number of sensors	Movement	Method	Reported RMSE or other inaccuracy measures		
				F_V	F_H	F_R
Faber et al. [94]	17	Trunk bending	Biomechanical model	18 N	16 N	
Min et al. [96]	3	Squat	Biomechanical model	11 N		
Kodama and Watanabe [95]	5	Squat Sit to stand	Biomechanical model	17 N	15 N	
Elvin et al. [97]	2	Vertical jump	Correlation	R^2=0.748		
Howard et al. [98]	1	Countermovement jump Drop jump	Biomechanical model			35.8% 53.6%
Pouliot-Laforte et al. [99]	1	Countermovement jump	Biomechanical model	31%, R=0.96		
Setuain et al. [100]	1	Countermovement jump	Biomechanical model	19%, R=0.93		
Meyer et al. [101]	1	Drop jump	Biomechanical model	R=0.89		
Ohtaki et al. [102]	3	Walking	Biomechanical model	0.31 N BW^{-1}	0.076 N BW^{-1}	
Karatsidis et al. [103]	17	Walking	Biomechanical model	0.076 N BW^{-1} (6.2%)	AP: 0.039 N BW^{-1} (10.2%) ML: 0.019 N BW^{-1} (13.8%)	
Neugebauer et al. [104]	1	Walking Running	Statistical model	106.4 N (8.3%)	33.2 N (17.8%)	
Charry et al. [105]	2	Walking Running	Biomechanical model	151 N (6.1%)		
Raper et al. [106]	1	Walking Running	Biomechanical model	16.04%, ICC=0.886		
Setuain et al. [107]	**1**	**Sprint**	**Biomechanical model**	7.3 ± 8.0%	45.3 ± 55.0%	
Gurchiek et al. [108]	**1**	**Sprint acceleration** **Change of direction**	**Biomechanical model**	**77.1 N** **54.2 N**	**AP: 37.7 N, ML: 66.3 N** **AP: 97.5 N, ML: 163.7 N**	**73.6 N** **70.2 N**
Wundersitz et al. [109]	**1**	**Sprint** **Change of direction**	**Biomechanical model**	**16.2%** **19.7%**		**16.4%** **23.0%**
Logar and Munih [110]	10	Ski jumping indoor validation Ski jumping outdoor validation	Biomechanical model and inverse dynamics			65.2±259 N (9.7±14%) 81.3±184 N (6.1±14%)
Guo et al. [114]	1	Walking	Machine learning: subject-specific model	5.0%		
Miller et al. [115]	1	Running	Machine learning: averaged model	102.4 N (0.16 BW)		
Wouda et al. [116]	3	Running	Machine learning: averaged model Machine learning: subject-specific model	0.29 BW 0.10 BW		
Leporace et al. [117]	1	Walking	Machine learning: averaged model	4.7%	AP: 5.2%, ML: 12.8%	

Chapter 3

Mechanical properties of surfaces: testing methods and characterisation of hybrid turf surfaces

3.1 Introduction

In section 2.3.1.3, it was reported how surfaces' mechanical properties and construction characteristics may influence shoe-surface interaction. For this reason, to evaluate players' performance, it is fundamental to keep into consideration also the mechanical properties of the specific sport surface where the movements are performed. However, a lack of knowledge regarding hybrid turf surfaces' mechanical characteristics was highlighted.

The FIFA Handbook for test methods [118] describes the devices and procedures used to verify that artificial turf properties fall inside the required bands defined in the FIFA Quality Programme, in order to satisfy quality, performance and safety standards. These methods have been used also to assess the quality of natural grass and hybrid turf pitches by Labosport Ltd., an international testing laboratory and consultancy organisation specialised in sports surfaces. As part of their ScorePlay^{TM} testing system (Fig. 3.1), Labosport tested a wide range of sport surfaces, through a combination of surface performance, construction and agronomy testing (Table 3.1) to assess the properties of each venue analysed [119].

The aim of this programme of research is to understand the effect of hybrid turf surfaces on players' movements, therefore, only the surfaces' mechanical properties related to shoe-surface performance (Table 3.1) were considered for a secondary analysis. To these testing criteria, moisture content was added, due to its effect on surface's mechanical properties, as reported in section 2.3.1.3.

Table 3.1: Laboport ScorePlay™ testing criteria.

Performance	Construction	Agronomy
Shoe-surface performance Shock absorption Vertical deformation Energy restitution Rotational resistance	Surface regularity Infiltration rate Moisture content Moisture at core base	Ground cover Thatch depth Effective root depth Weed content Ground compaction Sward height Sward colour Colour uniformity Soil health Insect pests and diseases
Ball-surface performance Ball roll Ball rebound height		

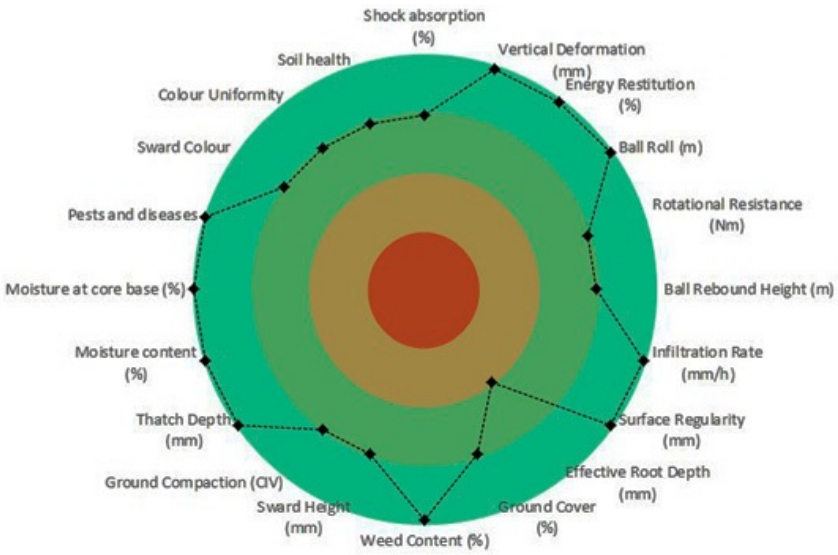

Figure 3.1: Example of Laboport ScorePlay™ testing system results [119]. Higher scores or better results correspond with the outer part of the circle (darker green colour).

3.1.1 Testing devices and protocol

The mechanical properties related to shoes-surface performance are measured through three portable devices. AA and AAA are the devices used to assess surface compliance, by measuring shock absorption, vertical deformation and energy restitution; and a rotational traction device is used to measure rotational traction. A moisture meter is used for the moisture content.

3.1.1.1 Artificial Athlete (AA) device

The AA device is the method used from the 1970s to measure compliance and, nowadays, it is the only method included in the European Standards. Since it needs to be configured in two different ways in order to assess shock absorption or vertical deformation, it is known with two different names: AA Berlin or AA Stuttgart, respectively.

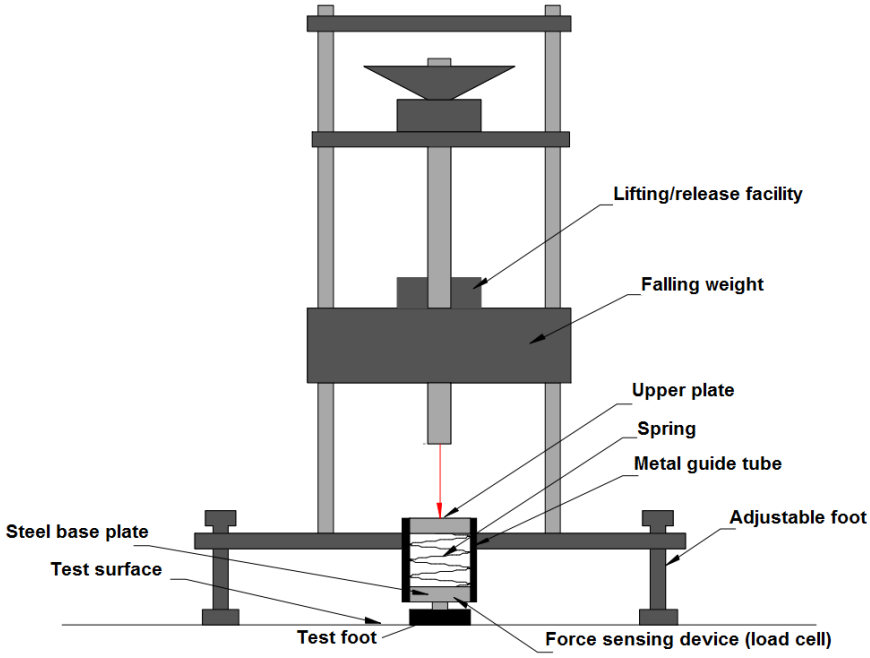

Figure 3.2: Artificial Athlete Berlin [120].

The AA Berlin (Fig. 3.2) drops a 20 kg mass from a standardised 55 mm height over a spring with stiffness of 2000 N mm^{-1}, which is positioned over a test foot with a spherical base that lies on the surface of interest. The frame of the device comprises a guide for the falling mass and three supporting legs. The measuring device is a force transducer placed in the test foot and measures the impact force time history.

The peak force recorded (F_{max}) is compared to a reference impact force value (F_{ref}) measured on a rigid concrete floor, in order to calculate the surface shock absorption (SA) through the following formula:

$$SA = \left(1 - \frac{F_{max}}{F_{ref}}\right) \cdot 100 \tag{3.1}$$

The AA Stuttgart (Fig. 3.3) drops a 20 kg mass from a standardised 120 mm height over a spring with 40 N mm^{-1} stiffness positioned over a test foot with a flat base that lies on the surface of interest. Two strain gauges are mounted on both sides of the test foot perpendicularly to the surface on a structure independent to the main frame. The strain gauges measure the maximum surface deformation (D_{max}), whilst the maximum force (F_{max}) recorded during the test is measured by the force transducer placed in the test foot. From these values the vertical deformation (VD) is calculated as:

$$VD = \frac{1500N}{F_{max}} \cdot D_{max} \tag{3.2}$$

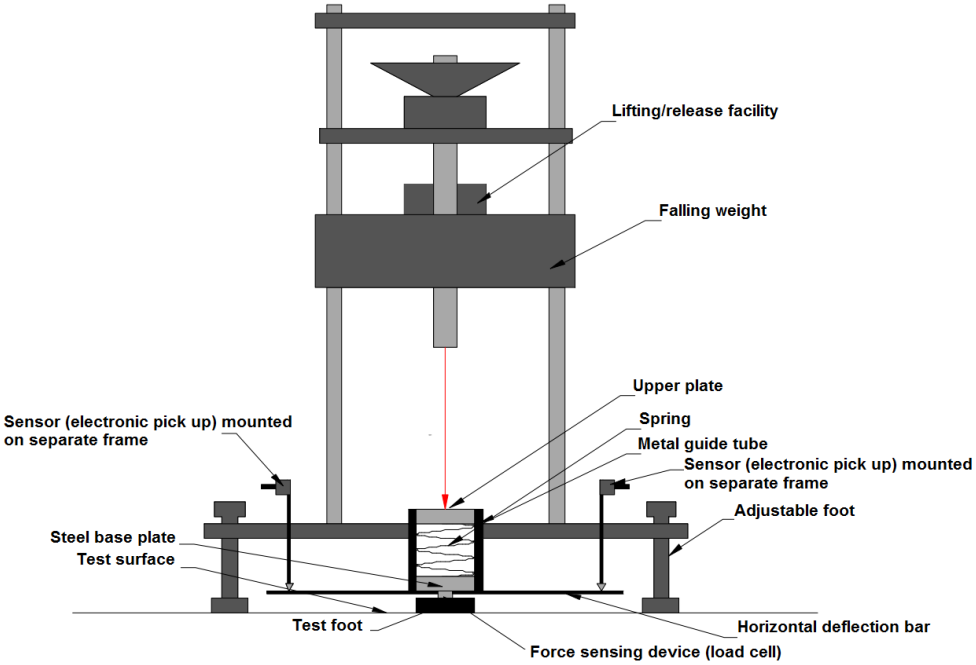

Figure 3.3: Artificial Athlete Stuttgart [120].

The measurement of shock absorption and vertical deformation on a full size pitch requires three drops on each of nineteen locations; whereas for the reference surface, the protocol requires eleven impacts on one location [118]. Each drop starts when the electric magnet, to which the mass is attached, allows it to fall. The resting time between impacts is 60 ± 5 s, in order to allow the surface to relax after the removal of the mass. Within the first 10 s after impact the dropping height needs to be checked and the mass re-attached to the magnet. During the vertical deformation test, the mass rebounds on the spring, therefore it must be caught before the results would be altered by the occurrence of a second impact; moreover, during the resting time it is necessary to check that the voltmeter readings of the two strain gauges do not differ of more than 0.5 V and ranges between 3 and 4.5 V. The reference impact force value is the mean of the peak force measured between the second and eleventh impact on the concrete floor, whereas the resulting values for shock absorption and vertical deformation are calculated as the mean of the second and third impacts for each location.

3.1.1.2 Advanced Artificial Athlete (AAA) device

The AAA device (Fig. 3.4) was introduced in 2004 as an alternative to the AA, and since 2012 it is the only method included in the FIFA Handbook for test methods [118]. This device is a simplified version of the AA, requiring a single configuration to measure shock absorption and vertical deformation at the same time.

A 20 kg dropping mass is released from an height of 55 mm over the surface, and

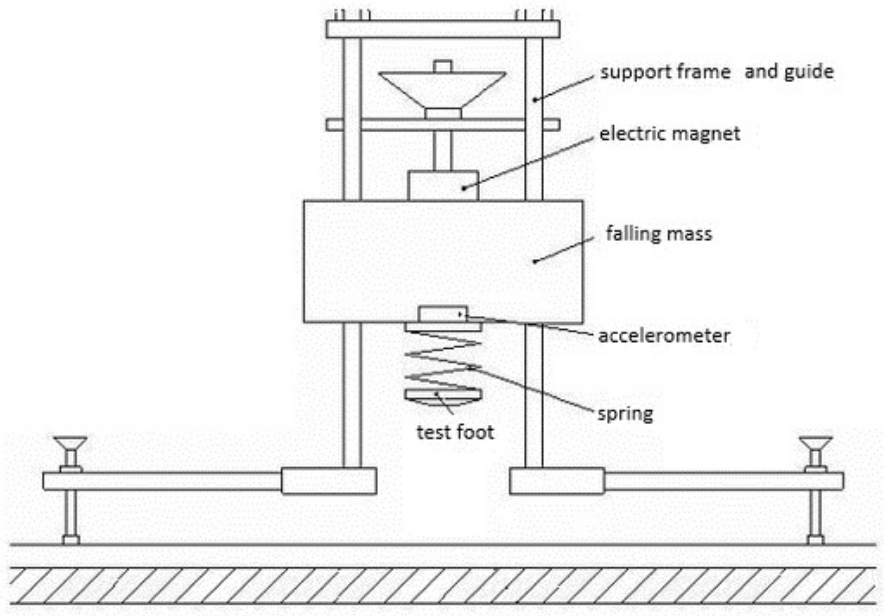

Figure 3.4: Advanced Artificial Athlete [118].

includes a 2000 N mm^{-1} stiff spring, a test foot, and an accelerometer to record the impact on the surface of interest. The maximum force recorded is calculated as:

$$F_{max} = mg(1 + G_{max}) \tag{3.3}$$

where m is the dropping mass, g the acceleration of gravity and G_{max} the peak acceleration during impact, expressed in units of g (Fig. 3.5). The shock absorption is calculated using equation 3.1, but compared to the AA, the reference force is not measured, but fixed at 6760 N.

The vertical deformation is calculated as:

$$VD = D_{mass} - D_{spring} \tag{3.4}$$

where the displacement of the falling mass (D_{mass}) is calculated by double integration of the acceleration over the contact time $[T_1, T_2]$ of the test foot with the surface:

$$D_{mass} = \int \int_{T_1}^{T_2} gG_{max} dt \tag{3.5}$$

and the displacement of the spring (D_{spring}) as:

$$D_{spring} = \frac{mgG_{max}}{C_{spring}} \tag{3.6}$$

where C_{spring} is the spring constant.

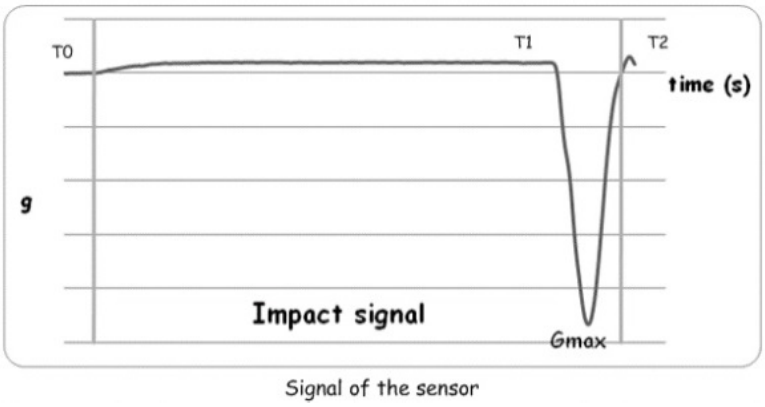

Figure 3.5: Example of curve representing the falling mass acceleration over time, where T_0 is the time when the mass starts to fall, T_1 is the contact time between test foot and surface, G_{max} is the peak acceleration during impact, and T_2 is the time corresponding to the end of the contact phase [118].

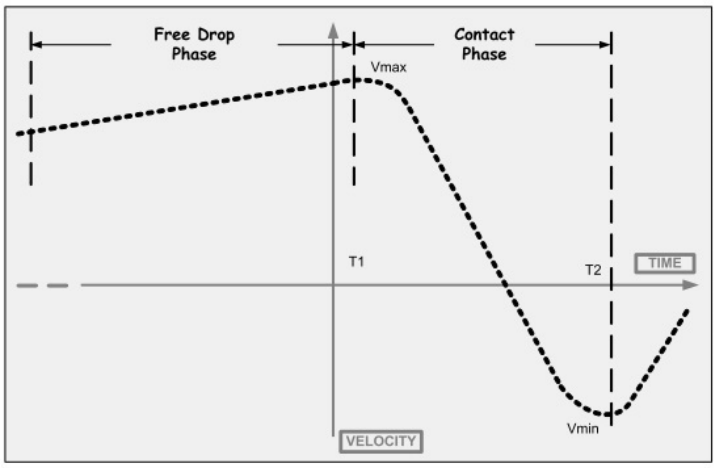

Figure 3.6: Example of curve representing the velocity of the falling mass over time, where T_1 is the contact time between test foot and surface, corresponding with the maximum velocity V_{max} and T_2 is the time of minimum velocity V_{min} after impact [118].

The AAA differently from the AA is also able to calculate the Energy Restitution (ER) through the following formula:

$$ER = \frac{E(T_2)}{E(T_1)} * 100 \tag{3.7}$$

where $E(T_1)$ and $E(T_2)$ are the energy before and after impact, respectively, calculated as:

$$E(T_1) = \frac{1}{2} m V_{max}^2(T) \tag{3.8}$$

$$E(T_2) = \frac{1}{2} m V_{min}^2(T) \tag{3.9}$$

with V_{max} identifying the maximum velocity occurring at the time of contact between test foot and surface (T_1), and V_{min} corresponds to the minimum velocity recorded at the end of the contact phase time (T_2).

The amount of locations to be tested is the same described for the AA device, whereas the resting time between impacts is reduced to 30 ± 5 s, within the first 10 s of which the dropping height needs to be checked and the mass re-attached to the magnet. As for the AA, the resulting values are calculated as the mean of the second and third impacts for each location.

3.1.1.3 Rotational traction test device

The FIFA rotational traction approved device (Fig. 3.7) has a test foot comprising a metal disc with a diameter of 150 mm and six 13 mm long football studs on the bottom of the disc equally spaced at 46 mm from the centre of the disc (Fig. 3.7b). A shaft, onto which weights are added, is attached to the disc and is equipped with lifting handles and a two-handled torque wrench; the former is used by the operator to manually lift the mass and drop it from 60 mm onto the surface, allowing the studs to penetrate it, and the latter is then used to rotate the mass and measure the peak moment of rotation. The mass is rotated of 180° with a speed of rotation of 12 rpm, with the peak moment occurring at about 40° of rotation [47]. The total dropping mass is comprised of studded disc, weights and shaft, for a total weight of 46 kg.

The testing protocol requires five individual measurements, at least 100 mm apart, on six specified test locations. The mean value is reported to the nearest 1 Nm with uncertainty of ±2 Nm.

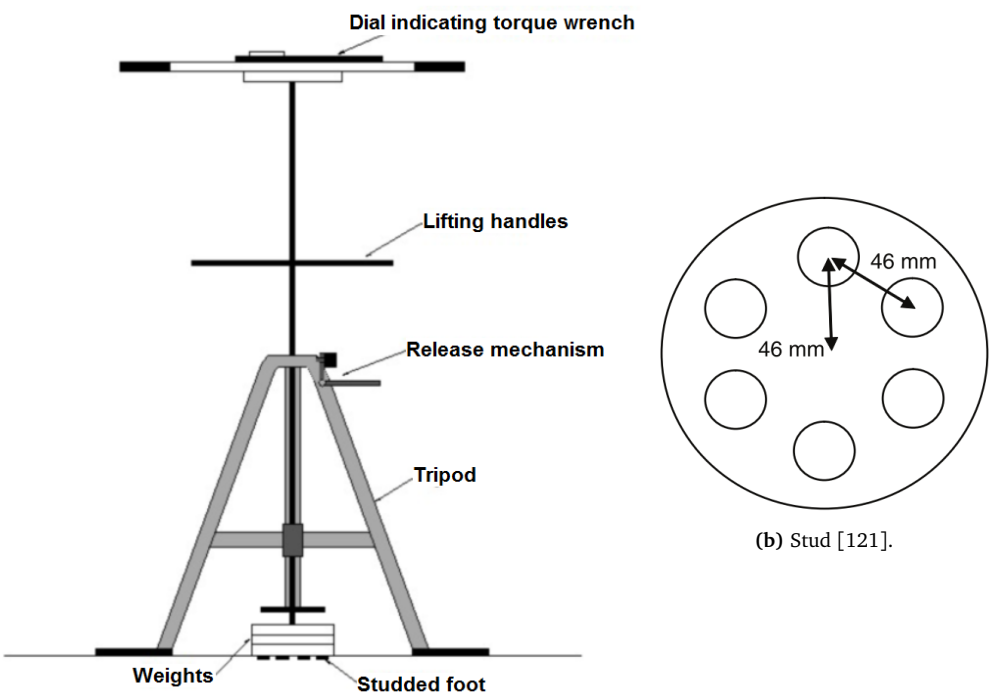

(a) Device [118].

(b) Stud [121].

Figure 3.7: Rotational traction test device and studs' configuration.

3.1.1.4 Moisture meter

The moisture meter used by Labosport is the ThetaProbe HH2 Soil Moisture Meter (Delta-T Devices, Cambridge, UK). It comprises four 50 mm long tines, which are fully inserted into the soil to measure its volumetric water content. This variable, expressed as a percentage, is the ratio between the volume of water present in the soil and the total volume of the sample. It is determined as a response to changes in the apparent dielectric constant of moist soil, which is converted into moisture content through a linearisation table and soil type parameters included in the device software.

Figure 3.8: ThetaProbe HH2 moisture meter (Delta-T Devices, Cambridge, UK).

3.2 Aim and objectives

The aim of this chapter is to characterise the mechanical properties of hybrid surfaces regularly used for elite level match play.

The objectives to achieve this aim are the following:

1. identify prevalence of hybrid turf surface construction type in elite level competitions;
2. compare the surfaces' performance amongst different hybrid turf construction systems and between hybrid turf and natural grass surfaces;
3. define the ranges of the mechanical properties derived from shoe-surface performance testing of the hybrid turf surfaces used in elite competition.

3.3 Methods

3.3.1 Labosport ScorePlay and surfaces included in the database

A secondary analysis of the surfaces' mechanical properties related to shoe-surface performance (Table 3.1) included in Labosport Ltd.'s ScorePlay™ database was performed, following data sharing consent and institutional ethics approval. The database comprises tests conducted between 2015 and January 2019 on a total of 191 different surfaces, located in the following countries: Australia, Canada, China, France, Ireland, Japan, Peru, Singapore, Spain and United Kingdom. These surfaces are community (n=24) and elite level (n=167) football (n=121), rugby (n=68), cricket (n=1) and baseball (n=1) fields, which could be classified into natural grass (n=123) and stitched-based (n=33), carpet-based (n=13) and reinforced rootzone (n=22) hybrid turf surfaces.

3.3.2 Statistical analysis

The mechanical property data of interest measured on hybrid turf and natural grass surfaces by Labosport, as part as their ScorePlay™ dataset, are graphically reported as beeswarm boxplots, in order to represent their ranges and distribution. The properties of interest were not available for all the surfaces included in the dataset. In more detail, a total of 129 surfaces was tested for shock absorption and vertical deformation (28 stitched-based, 12 carpet-based, 20 reinforced rootzone and 69 natural grass), 127 for energy restitution (28 stitched-based, 12 carpet-based, 20 reinforced rootzone and 67 natural grass), 152 for rotational traction (28 stitched-based, 12 carpet-based, 18 reinforced rootzone and 94 natural grass) and 154 for moisture content (27 stitched-based, 13 carpet-based, 16 reinforced rootzone and 98 natural grass).

The differences between each pair of surfaces were quantified through the Mann-Whitney U-test, after Bonferroni correction was performed. U is calculated as:

$$U = W - \frac{N_1(N_1 + 1)}{2} \tag{3.10}$$

where W is the Wilcoxon rank sum and N_1 the size of sample 1. The effect size r_{ES} was estimated from the z-score as:

$$r_{ES} = \frac{z}{\sqrt{N}} \tag{3.11}$$

where N is the sum of the sample sizes of the surfaces compared by z. Pearson's product-moment correlation coefficient (r) was calculated to verify if there is any relationship between the shoe-surface performance variables and the surface moisture

content. A statistical significant level of 0.05 was set for both analyses.

The data processing and statistical analysis were performed with Matlab R2019a (Mathworks, Natick, MA, USA).

3.4 Results

In figure 3.10 and 3.9 the data ranges and distribution of different hybrid turf surfaces and natural grass pitches are presented as beeswarm boxplots for each mechanical property considered. The numeric values of medians are reported on the figure for each surface type.

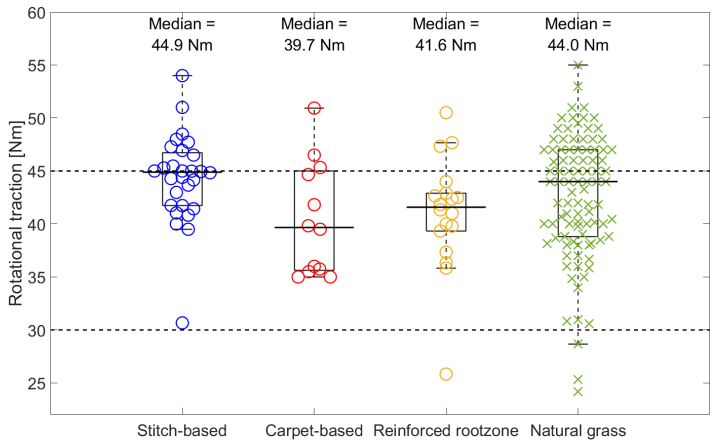

(a) Rotational traction.

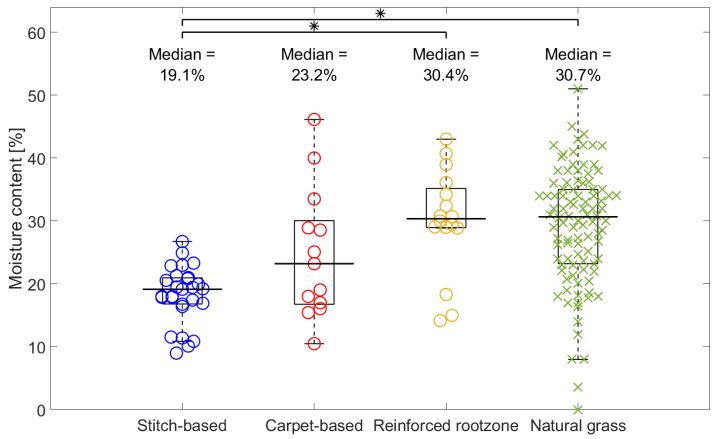

(b) Moisture content.

Figure 3.9: Comparison of rotational traction and moisture content between stitched-based, carpet-based, reinforced rootzone hybrid surface systems and natural grass; data from Labosport ScorePlay^{TM} dataset. Statistical differences are highlighted with an asterisk and the dashed lines represent the limits of the required band for FIFA quality pro artificial turf.

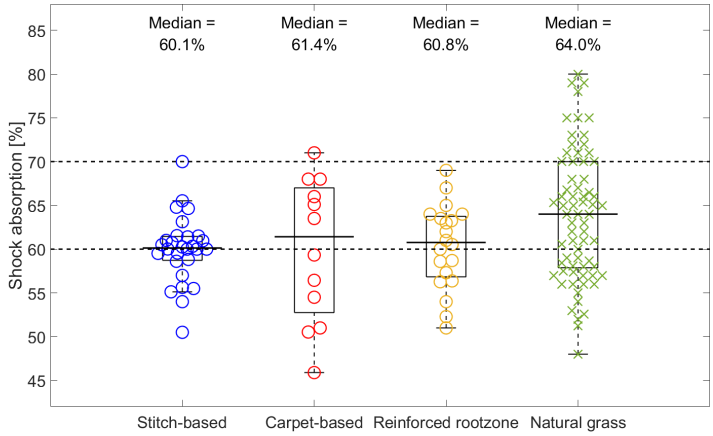

(a) Shock absorption.

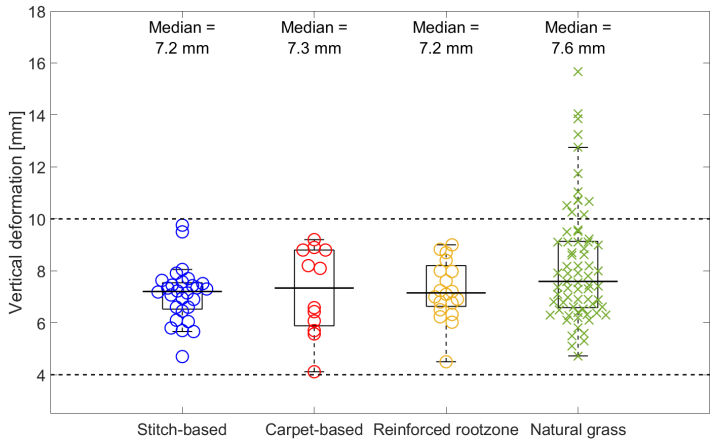

(b) Vertical deformation.

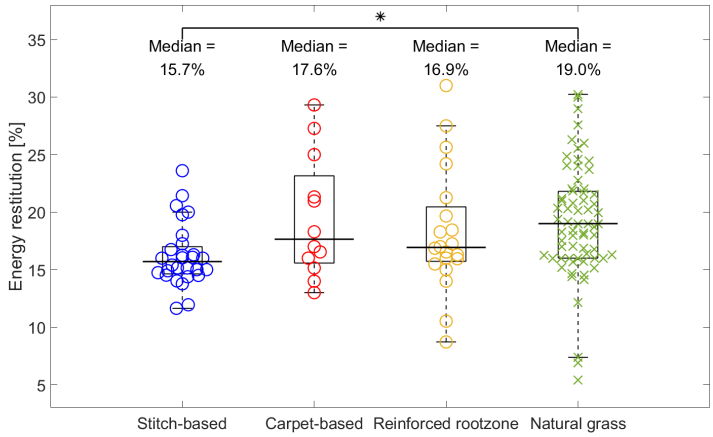

(c) Energy restitution.

Figure 3.10: Comparison of shock absorption, vertical deformation and energy restitution between stitched-based, carpet-based, reinforced rootzone hybrid surface systems and natural grass; data from Labosport ScorePlay^{TM} dataset. Statistical differences are highlighted with an asterisk and the dashed lines represent the limits of the required band for FIFA quality pro artificial turf.

Table 3.2: Mean ± standard deviations for shock absorption, vertical deformation, energy restitution, rotational traction and moisture content of stitched-based, carpet-based, reinforce rootzone hybrid turf surfaces and natural grass pitches; data from Labosport ScorePlay™ dataset.

Surfaces	Shock absorption [%]	Vertical deformation [mm]	Energy restitution [%]	Rotational traction [Nm]	Moisture content [%]
Stitch-based	60.02±3.8	7.09±1.1	16.22±2.7	44.35±4.2	18.29±4.5
Carpet-based	59.94±8.2	7.21±1.7	19.49±5.3	40.49±5.4	24.72±10.4
Reinforced rootzone	60.34±4.8	7.29±1.1	18.28±5.4	41.03±5.4	30.04±8.3
Natural grass	63.80±7.4	8.21±2.3	19.14±4.9	42.56±5.9	29.24±9.3

Table 3.3 reports the Mann-Whitney's U statistic, the corresponding z-score, significance value after Bonferroni correction (p), and effect size (r_{ES}). Between the compliance variables, differences were found only for energy restitution between stitched-based hybrid turf and natural grass surfaces. Lower values were recorded for the former (median = 15.7%) compared to the latter (median = 19.0%), $U = 491\%$, $z = -3.65$, $p = 0.002$, $r_{ES} = -0.374$. No differences were found between pairs of surfaces for rotational traction. Moisture content is significantly different between stitched-based (median = 19.1%) and reinforced rootzone (median = 30.4%) hybrid turf surfaces, $U = 58\%$, $z = -3.96$, $p < 0.001$, $r_{ES} = -0.604$; and between the former and natural grass (median = 30.7%) surfaces, $U = 371\%$, $z = -5.71$, $p < 0.001$, $r_{ES} = -0.511$.

Table 3.4 reports Pearson's r correlation coefficient between each shoe-surface performance mechanical variable and the surface moisture content. A high positive significant correlation ($r > 0.70$ and $p < 0.05$) was found only for the shock absorption measured on carpet-based hybrid turf surfaces.

Table 3.3: Mann-Whitney's U statistics for shock absorption, vertical deformation, energy restitution, rotational traction and moisture content of stitched-based, carpet-based, reinforced rootzone hybrid turf surfaces and natural grass pitches; data from Labosport ScorePlay™ dataset. Statistical significant differences are highlighted with a dagger.

Surfaces		Shock absorption				Vertical deformation				Energy restitution				Rotational traction				Moisture content			
Group 1	Group 2	U [%]	z	p	r_{ES}	U [mm]	z	p	r_{ES}	U [%]	z	p	r_{ES}	U [Nm]	z	p	r_{ES}	U [%]	z	p	r_{ES}
Stitched	Carpet	160.0	-0.22	1.000	-0.035	158.5	-0.27	1.000	-0.042	105.0	-1.84	0.390	-0.292	241.0	2.14	0.194	0.338	121.0	-1.56	0.713	-0.247
Stitched	Reinforced	257.5	-0.46	1.000	-0.066	255.0	-0.51	1.000	-0.074	195.0	-1.77	0.463	-0.255	364.5	2.52	0.070	0.372	58.0	-3.96	<0.001†	-0.604
Stitched	Natural	673.0	-2.33	0.119	-0.237	710.0	-2.03	0.252	-0.207	491.0	-3.65	0.002†	-0.374	1513.5	1.20	1.000	0.109	371.0	-5.71	<0.001†	-0.511
Carpet	Reinforced	125.0	0.18	1.000	0.031	118.0	-0.06	1.000	-0.010	132.5	0.47	1.000	0.083	89.0	-0.78	1.000	-0.143	65.0	-1.69	0.548	-0.314
Carpet	Natural	316.0	-1.30	1.000	-0.144	320.0	-1.24	1.000	-0.138	387.5	-0.19	1.000	-0.022	407.0	-1.56	0.710	-0.152	432.5	-1.87	0.368	-0.178
Reinforced	Natural	501.0	-1.85	0.383	-0.196	556.5	-1.31	1.000	-0.139	563.5	-1.07	1.000	-0.115	702.5	-1.13	1.000	-0.107	813.0	0.23	1.000	0.022

Table 3.4: Pearson's correlation coefficient between the shoe-surface performance variables (shock absorption, vertical deformation, energy restitution and rotational traction) and moisture content, and respective p-values; data from Labosport ScorePlay™ dataset. Statistical significant differences are highlighted with a dagger; high and very high correlations are highlighted in bold.

Surface	Shock absorption		Vertical deformation		Energy restitution		Rotational traction	
	r	p	r	p	r	p	r	p
Stitched-based	0.305	0.168	0.110	0.627	-0.095	0.675	-0.490	0.021†
Carpet-based	**0.719**	**0.008**†	0.685	0.014†	-0.656	0.021†	0.136	0.674
Reinforced rootzone	0.091	0.747	0.380	0.162	0.043	0.880	-0.036	0.907
Natural grass	0.221	0.145	0.355	0.017†	-0.388	0.010†	0.154	0.145

3.5 Discussion

Hybrid turf surfaces are natural grass pitches reinforced with synthetic elements, however even if there is an artificial component, these surfaces do not need to satisfy the same specific requirements for quality, performance and safety reasons, as artificial turf pitches do. Despite this, the use of the same methods described in the FIFA Handbook for test methods [118] allows the evaluation of the mechanical properties of the hybrid turf surfaces tested by Labosport in comparison with the artificial turf requirements, and to ensure that these surfaces do not constitute a more dangerous condition compared to natural grass fields.

FIFA quality pro artificial turf pitches must fall inside the following bands: $60-70\%$ for shock absorption, 4—10 mm for vertical deformation, and 30—45 Nm for rotational traction [122]. The shock absorption median values of all the hybrid turf surfaces fall inside the required band for FIFA quality pro artificial turf; however, the median shock absorption values are close to the lower limit fixed at 60%, with a total of 38% of the surfaces falling below the band lower limit (35.7% stitched-based, 50% carpet-based, 40% reinforced rootzone and 36.2% natural grass). Therefore, 40% of the hybrid turf surfaces and 36.2% of natural grass pitches included in the dataset have lower shock absorption compared to the values considered as safe for FIFA quality pro artificial turf pitches, with these harder shock absorption values ranging from 32.2% and 60%. A harder surface does not respect safety requirements, since it would lead to an increased risk of injury due to high decelerations and impact forces when an athlete come in contact with it. The vertical deformation standard is satisfied by all the hybrid turf surfaces tested, whereas 13 natural grass pitches (18.8%) have higher vertical deformation with values over 10 mm. The statistical analysis showed that hybrid turf surfaces have similar compliance, and only the energy restitution of stitched-based hybrid turfs is significantly different to natural grass surfaces. The analysis of the surfaces' mechanical characteristic ranges (Fig. 3.10a to 3.9b) and standard deviations (Table 3.2) highlighted smaller variability between stitched-based hybrid turfs compared to the other surface types, allowing us to conclude that this represents the most consistent surface. Natural grass is more compliant than the hybrid turf surfaces, especially compared to stitched-based systems, however, it also presents the biggest range, with the presence of higher values of shock absorption and vertical deformation, suggesting that, when athletes ran on them, there is a higher possibility of energy being wasted and, as consequence, performance reduction [25, 27].

The evaluation of rotational traction showed no statistical differences between any pair of surfaces, and that the median values for all the surface types tested fall inside the required band for FIFA quality pro artificial turf pitches. However, even if stitched-

based hybrid turfs and natural grass surfaces do not statistically differ from the other construction types, they present higher median values, with the 35.7% of the stitched-based and 36.2% of natural grass pitches tested by Labosport exceeding the 45 Nm upper limit specified in the FIFA requirement. This results in a higher possibility of foot fixation when athletes perform change of direction tasks on stitched-based hybrid turf surfaces and natural grass fields, with consequent decrease in performance and increase of injury risk [34,37,38]. Moreover, natural grass presents a bigger data range compared to the hybrid turf surfaces, as could be seen from figure 3.9a, suggesting the possibility to find also a surface on which players have a higher risk of slipping when changing direction, which could result in performance reduction and increased risk of injury [39].

In section 2.3.1.3, it was reported that higher moisture content could result in poorer mechanical properties, for this reason the moisture content measurements are outlined in this chapter, in the attempt to evaluate their relationship with the mechanical properties of interest. The moisture content of stitched-based hybrid turf surfaces is significantly lower compared to reinforced rootzone and natural grass surfaces. The study from Smeets et al. [44], reported in section 2.3.1.3, showed how surface rotational traction is dependent on the moisture content, with a stitched-based hybrid turf and a natural grass surface presenting similar values in dry condition, but when tested in a wet scenario only the rotational traction measured on the former surface was almost not influenced. The results obtained in this chapter with similar median values for rotational traction between stitched-based hybrid turf and natural grass, confirm the finding from Smeets et al. [44], assuming that most of the tests were carried out in good dry conditions; however, the rotational traction range of natural grass surfaces present a longer tail towards lower values (Fig. 3.9a), which could suggest a relationship with the bigger range of moisture content data (Fig. 3.9b), assuming some tests were carried out in wet conditions, however, there was not a relationship between the two variables (Table 3.4). To the best of the author's knowledge, there are no studies comparing the moisture content between different hybrid turf construction systems and its influence on the mechanical properties differences. The ranges obtained from the Labosport ScorePlay™ dataset suggest that the stitched-based hybrid turf system is the surface least influenced by the weather conditions.

Only one study [54] was found in the literature comparing the shock absorption over a season between two different hybrid turf surfaces (Sec. 2.3.1.4). The authors found similar results for a stitched-based and a reinforced rootzone surface, even if the former was more consistent and the latter was believed to be more influenced by external factors that reduced the grass cover. The results reported in this chapter confirmed that stitched-based surfaces are the most consistent, and reinforced rootzone pitches

could be more influenced by external parameters, such as higher moisture content (Fig. 3.9b), since it could lead to tears on the surface and, as consequence, less grass cover.

The limitations of this study are related to some useful information missing from the dataset provided by Labosport. Firstly, it was not specified which device was used for the compliance measurements; however, the comparison of the number of surfaces tested for energy restitution with those on which shock absorption and vertical deformation were measured, suggests that only two natural grass surfaces were tested with the AA device, rather than the AAA. Moreover, from the literature review, it is known that mechanical properties could be affected by factors such as maintenance, usage, weather, moisture content and grass species (Sec. 2.3.1.6); however, the database does not include information regarding pitches' age and weather condition at time of testing, as well as the grass species.

In this chapter, the surfaces' mechanical properties related to shoe-surface performance included in Labosport ScorePlay™ database were considered for a secondary analysis. These mechanical properties were evaluated using the devices and procedures described in the FIFA Handbook for test methods [118], however, these tests are not representative of a scenario where athletes are involved. Manoeuvres commonly associated with performance and injury risk, such as deceleration and rapid changes of direction, involve velocity components of the foot in both the horizontal and vertical directions [123], and loads that are 2.5 to 3 times the athlete's body weight [55]. The AA and AAA devices provide measurements only in the vertical direction and consider a vertical load lower than one body weight, whereas a more representative device should include the measurements of shear force and displacement in the horizontal direction. In the literature review (Sec. 2.2.2 and 2.3.2.4), it was highlighted how the possibility of applying higher shear forces allows to brake more efficiently and change direction quicker [82, 84, 85], however, both too high or too low forces could lead to a decrease in performance and increase of injury risk, since the former could result in foot fixation and the latter in a slip or slide of the shoe on the surface [34–39]. An example of a more representative mechanical test device is the one designed by Kent et al. [123], able to combine translational and drop tests by launching a foot form into a playing surface with both vertical and horizontal components of velocity. When the foot form impacts the surface, its motion is arrested only by the interaction of the studs with the surface. By selecting appropriate mass, horizontal speed and drop height, the authors were able to generate a vertical GRF with peak and duration similar to those recorded during biomechanical tests; therefore, the possibility of selecting these input values would allow the evaluation of impacts representative of different football manoeuvres. In addition to the measurement of individual GRF

components as a function of time, it would be beneficial also to measure the horizontal displacement of the test foot; these measurements would provide useful information to understand the mechanics of shoe-surface interaction, and facilitate the comparison with values measured during biomechanical tests giving the possibility of evaluating the impact on performance, injury risk and traction perception.

In the evaluation of football movements, it is important to keep into consideration also the rotational traction, since shoe rotations of angles between 6° and 12° are observed while participants perform sprint accelerations and changes of direction [56, 57, 60], and excessive rotational traction results in an increased risk of injury. However, the rotational traction test device described in the FIFA Handbook for test methods [118] presents two main limitations, it requires to be rotated by the operator, which might be source of variability, and it measures the peak moment of rotation at an angle of about 40° [47], which is not reached during biomechanical tests. A mechanical test device to improve the evaluation of rotational traction should be able to apply representative vertical load and rotational speed with a good level of repeatability and report the measurement of initial and linear rotational stiffnesses, which were suggested as more sensitive indicators of shoe-surface interaction during rotational traction tests by Livesay et al. [61].

To conclude the surfaces' mechanical properties related to shoe-surface performance reported in this chapter are not representative of player movement, therefore, they do not provide an appropriate method of comparison with biomechanical tests. For this reason, the data presented in this chapter were useful to fill the gap of knowledge highlighted in the literature review by identifying the range of mechanical properties of hybrid turfs and compare them with those of natural grass surfaces. These data will be used in chapter 6 only to identify the representativeness, within the context of match play surfaces, of the hybrid turfs where biomechanical tests were carried out, since these test methods could not be used as a comparison with biomechanical test data. Moreover, the aim of this programme of research is to evaluate the effect of hybrid turfs on player movement performance, therefore, the focus in the following chapters will be on the estimation of 3D GRFs rather than the rotational resistance, since some studies [30, 34] suggest that the first is the critical element in performance on sport surfaces and the latter is the critical element in injury prevention.

3.6 Conclusion

The aim of this chapter was to identify the range of mechanical properties of hybrid turfs and compare them with those of natural grass surfaces. The database provided by Labosport, which includes a wide range of sport surfaces tested as part of their

ScorePlay™ testing system, helped to achieve this aim and cover the gap of knowledge regarding hybrid turf surfaces' mechanical properties highlighted in the literature review.

From the data reported in this chapter, it was concluded that stitched-based hybrid construction system is the most consistent surface type tested, since it shows less variability in the ranges of its mechanical properties. This turf system is less affected by weather and usage, and its performance could be more consistent during a season. Even if the rotational traction values of stitched-based hybrid turfs do not statistically differ from the other construction types, their higher median values and high amount of surfaces exceeding the upper limit suggests a higher risk of foot fixation, with consequent possibility of performance reduction and increase of injury risk, during change of direction tasks compared to the other hybrid turf construction systems.

These data will be used in chapter 6 to identify the representativeness, within the context of match play surfaces, of the hybrid turfs on which the data collection was carried out.

Chapter 4

Use of inertial measurement units to estimate ground reaction forces during a football-related movement

4.1 Introduction

In chapter 2, the importance of shoe-surface interaction understanding was outlined, as well as the possibility to evaluate it in the field through GRF estimation. A potential candidate for in-field analysis is represented by IMUs. These devices could be used in a scenario similar to a real game environment without the alteration of athletes' movements, thanks to their smaller size, lower weight, cheaper price and larger testing area compared to the gold standard measurement system, the force platform, which use is limited to the laboratory environment.

GRFs can be estimated from IMUs using Newton's second Law of Motion in conjunction with a biomechanical model or using a machine learning approach. The former is believed to be a stronger approach, since it is assumed that a method based on physics could be applied to any type of movement without specific training data needed, and especially considered that many football movements could be unpredicted, a model based on a machine learning approach would require an amount of training data too big to be realistically collect. To the best of the author's knowledge, only one study [117] used a machine learning approach to predict 3D GRFs during straight walking, which does not involve high accelerations in the horizontal direction (Sec. 2.4.2). Whereas, IMUs have previously been used to estimate step-averaged and instantaneous 3D GRFs during football-specific movements, such as straight-line acceleration and changes of direction (Sec. 2.4.1.3), through the application of Newton's second Law of Motion to the acceleration of a single sensor attached on the subjects' upper (T2) or lower (L4-L5 or midPSIS) back [107–109]. The results of these studies

show good agreement between the estimated and measured vertical GRF, but poor accuracy in the estimation of the shear forces. In addition, the instantaneous forces estimation (Fig. 2.16) was found to have larger errors compared to step-averaged forces [108]. During change of direction manoeuvres, the forces in the horizontal direction are a primary contributing factor for performance improvement and evaluation of footwear traction characteristics, since the possibility for athletes to apply higher shear forces allow them to decelerate more efficiently and perform more rapid changes of direction [81–83] (Sec. 2.3.2). Therefore, shear forces are a critical element in the method validation and their step-averaged and time history estimation requires higher accuracy compared to previous studies.

In this chapter, a multiple-sensor approach is proposed to estimate 3D GRFs. The method is validated during an alternate lateral bounding movement, requiring high medio-lateral accelerations, such as those recorded during high intensity changes of direction in football match play.

4.2 Aim and objectives

The aim of this chapter is to develop a method to estimate 3D GRFs using IMUs.

To achieve this, the following objectives were identified:

1. transform raw acceleration data into a global system;
2. identify segment-specific mass and filter characteristics to allow GRF estimation;
3. validate the proposed method in a football-relevant movement against force platform's measurements.

4.3 Methods

4.3.1 Participants

Twenty-five male participants (age: 24.5 ± 2.9 years; mass: 78.0 ± 6.6 kg; stature: 1.78 ± 0.04 m), with 8.5 UK foot size, free from injuries and with different levels of football experience, volunteered to take part in the study. Participants were classified regarding their football level into competitive (n= 15), recreational (n=6) and not competing in official leagues (n=4) players. The study was approved by Sheffield Hallam University Research Ethics Committee.

4.3.2 Experimental set-up

Eight IMU wireless sensors (STT-IWS iSen, STT System, Spain) were used. Each sensor (Fig. 4.1) measured 56 x 38 x 18 mm, weighed 46 g, and comprised three-axis accelerometer, gyroscope and magnetometer, operating between ± 16 g, ± 2000°s^{-1} and ± 1300 µT, respectively. The selection criteria for these sensors is reported in appendix A.

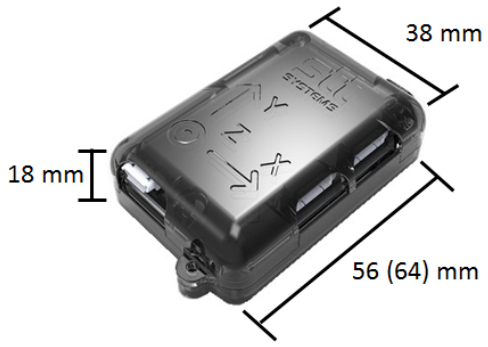

Figure 4.1: iSen IMU sensor with its dimension.

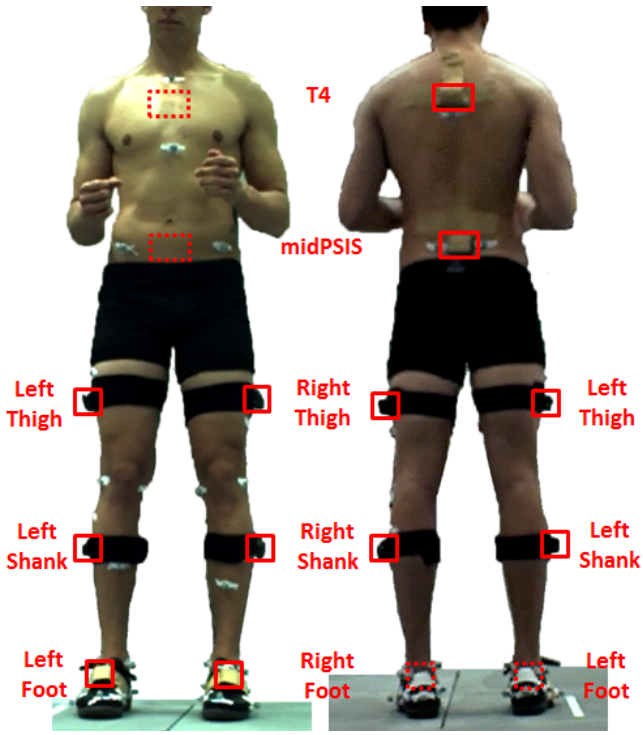

Figure 4.2: IMU sensors' attachment locations, front and back view.

The sensors were affixed to the fourth thoracic vertebra (T4), the midPSIS, on the lateral aspect of thighs and shanks, and on the feet over the shoe laces, as shown in figure 4.2. The sensors were attached to the lower limbs through velcro bands, whereas at the other locations velcro straps and additional tape were used. This study was part of a wider data collection that included a thirty-three marker model (Fig. 4.3). The

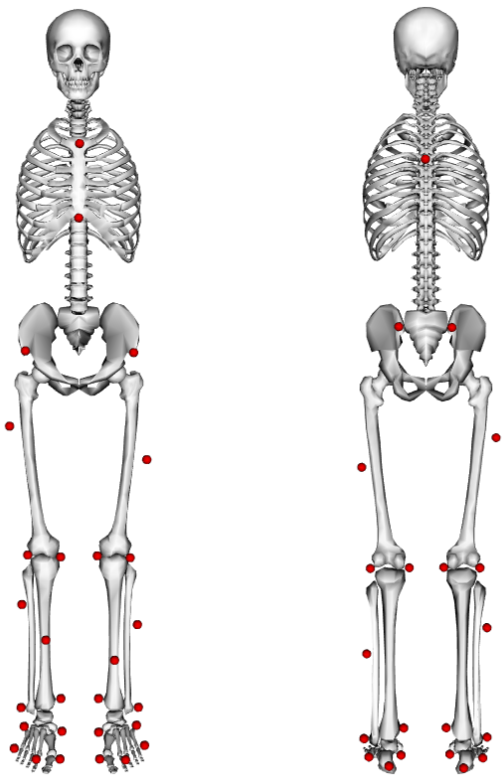

(a) Front view. **(b)** Back view.

Figure 4.3: Markers' locations, front and back view.

presence of the retro-reflective markers limited the IMUs' attachment locations, since the sensors had to be placed on each body segment without modifying the markerset and in order to avoid marker occlusions.

The data were recorded from the IMUs at the maximum selectable sample frequency of 100 Hz and compared to the data of a force platform (Kistler AG, Switzerland), sampling at 1000 Hz. The markers' trajectories were recorded with a sixteen cameras VICON motion analysis system (Oxford Metrics Ltd., Oxford, United Kingdom) sampling at 200 Hz.

4.3.3 Protocol

In chapter 2, it was reported that high intensity movements are the most crucial moments in football and they can be classified as actions requiring acceleration, maximal speed or agility, with the latter defined as the ability to change direction, start and stop quickly in response to a sport-specific stimulus (Sec. 2.1). A typical agility-based movement performed by field athletes in a strength and conditioning training for performance and injury prevention purposes is the lateral skater jump (LSJ) [124]. It is a structured and repeatable movement, performed predominantly on a single plane of motion and it does not require the athlete to respond to an external stimulus, which

would increase inter-individual movement variability; moreover, it involves an increasing distance of medio-lateral jumps with a 180° change of direction, which leads to high medio-lateral accelerations comparable to those recorded during high intensity changes of direction in football match play. Therefore, the LSJ was selected for this study as the test movement in order to focus on the differences between IMU and force platform's measurement while performing a football-relevant movement, reducing the variability between subjects and allowing the evaluation of shear forces similar to those recorded in a real game environment.

Before the test, participants completed a standardised warm-up routine, involving jogging, skip, lounges, side-stepping and sprints; extra time was given for self-selected stretching and to familiarise with the exercise. A three second static trial was recorded, with the participants standing on the force platform in T-pose with the feet kept parallel at a predefined distance.

Five lines were marked on the floor at the following standardised distances from the centre of the force platform: 1.2, 1.4, 1.6, 1.8 and 1.9 m. Participants were instructed to start in a standing position with one foot close to the 1.2 m line mark and perform alternate lateral jumps to and from the force platform, increasing the distance after each jump from it. The movement ended in standing position after a total of four contacts over the force platform with the foot close to the 1.9 m line mark (Fig. 4.4 and 4.5). Participants were asked to keep their arms flexed and close to the torso and to look in front of them where some lines were placed on the floor for reference. They were made aware that it was not important to reach the lines placed on the floor, but to perform the movement as fast as possible with short contact times, trying to increase the jumping distance, in order to keep the movement more laterally than vertically directed and to increase the medio-lateral impact accelerations during the exercise. After familiarisation with the testing procedure, participants were asked to perform six trials of the movement, three on each side in order to have contacts with both the left and right foot over the force platform.

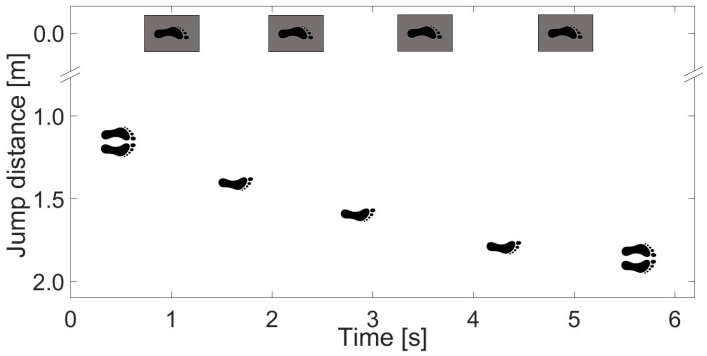

Figure 4.4: Schematic of a test movement over time with left foot contact over the force platform.

(a) Starting position on 1.2 m line mark.

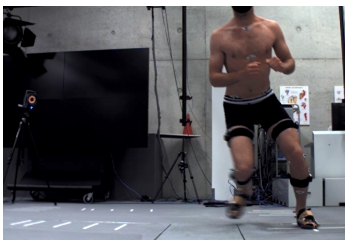

(b) Force platform first contact.

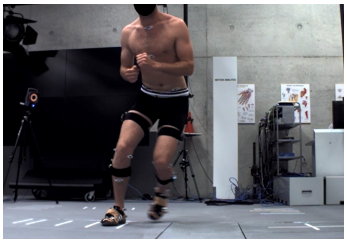

(c) 1.4 m line mark.

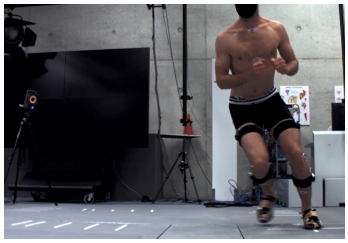

(d) Force platform second contact.

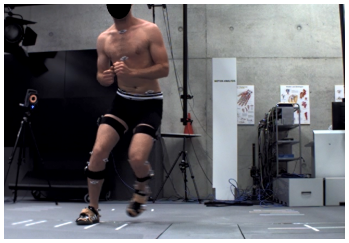

(e) 1.6 m line mark.

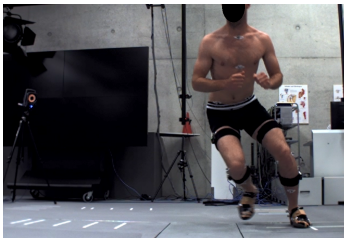

(f) Force platform third contact.

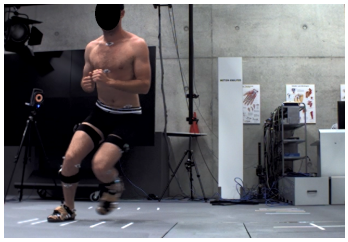

(g) 1.8 m line mark.

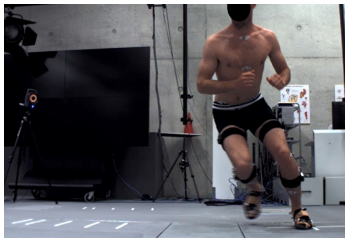

(h) Force platform fourth contact.

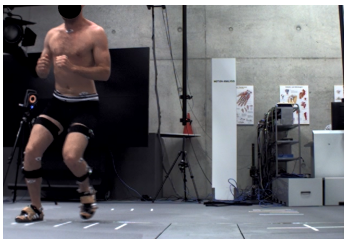

(i) 1.9 m line mark.

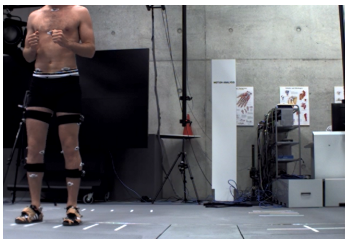

(j) Ending position on 1.9 m line mark.

Figure 4.5: Example of LSJ task with left foot contact on the force platform.

Participants were asked to perform the test wearing adidas München (n=8; Fig. 4.6a) or adidas Samba (n=17; Fig. 4.6b) shoes, in order to have similar traction on the concrete laboratory floor, where the tests were carried out.

(a) adidas München.

(b) adidas Samba.

Figure 4.6: Shoes used during the test.

4.3.4 Data processing

4.3.4.1 Conversion of the inertial measurement units' raw accelerations into the global system

Each IMU outputs the raw accelerometer, magnetometer and gyroscope data measured along its axes. All data were processed using Matlab R2019a (Mathworks, Natick, MA, USA). A Kalman filter system object, *ahrsfilter*, available in the software, was used to fuse each sensor's raw data in order to refer the device orientation to a North-East-Down (NED) coordinate system (Fig. 4.7). A sensor fusion approach to calculate the sensors' orientations into the global system was chosen over gyroscope integration because of its higher performance during movements involving impacts, and the use of an extended Kalman filter for its benefits over other fusion techniques, such as a complementary filter approach, as was reported in section 2.4. This orientation was defined for each sensor by a rotation matrix (${}^{NED}R_{IMU}$) having in each column the coordinates of each sensor's local orientation axis with respect to the global reference system:

$$ {}^{NED}R_{IMU} = \begin{bmatrix} \cos\theta_{x_{NED}x_{IMU}} & \cos\theta_{x_{NED}y_{IMU}} & \cos\theta_{x_{NED}z_{IMU}} \\ \cos\theta_{y_{NED}x_{IMU}} & \cos\theta_{y_{NED}y_{IMU}} & \cos\theta_{y_{NED}z_{IMU}} \\ \cos\theta_{z_{NED}x_{IMU}} & \cos\theta_{z_{NED}y_{IMU}} & \cos\theta_{z_{NED}z_{IMU}} \end{bmatrix} \tag{4.1} $$

The raw accelerations measured by each IMU (a_{IMU}) were converted into the IMU global NED coordinate system by the following:

$$ \overrightarrow{a_{NED}} = {}^{NED}R_{IMU}\ \overrightarrow{a_{IMU}} \tag{4.2} $$

Once defined in the NED system, the accelerations (a_{NED}) were converted into the laboratory global system (a_{Lab}), in order to be aligned with the force platform measurements, by the following:

$$ \overrightarrow{a_{Lab}} = {}^{Lab}R_{NED}\ \overrightarrow{a_{NED}} \tag{4.3} $$

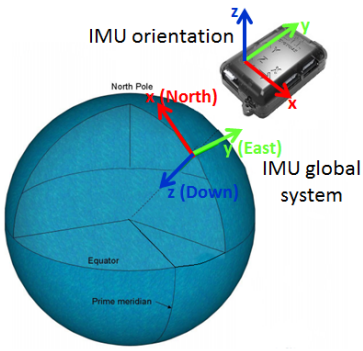

Figure 4.7: IMU local and global coordinate systems.

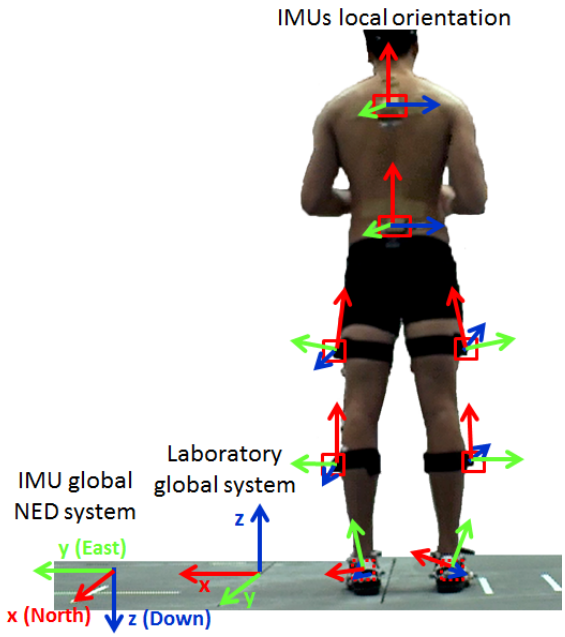

Figure 4.8: IMUs' local coordinate systems, IMU global NED system and laboratory global system.

${}^{Lab}R_{NED}$ is the rotation matrix describing the orientation of the NED system compared to the laboratory global coordinates, which was calculated as:

$$
\begin{aligned}
{}^{Lab}R_{NED} &= R_z\left(\frac{\pi}{2}\right) R_y(0)\, R_x(\pi) = \\
&= \begin{bmatrix} \cos\left(\frac{\pi}{2}\right) & -\sin\left(\frac{\pi}{2}\right) & 0 \\ \sin\left(\frac{\pi}{2}\right) & \cos\left(\frac{\pi}{2}\right) & 0 \\ 0 & 0 & 1 \end{bmatrix} \begin{bmatrix} \cos 0 & 0 & \sin 0 \\ 0 & 1 & 0 \\ -\sin 0 & 0 & \cos 0 \end{bmatrix} \begin{bmatrix} 1 & 0 & 0 \\ 0 & \cos\pi & -\sin\pi \\ 0 & \sin\pi & \cos\pi \end{bmatrix}
\end{aligned} \tag{4.4}
$$

where $\frac{\pi}{2}$ and π were defined by analysing the north and z axes orientation.

Equations 4.1 to 4.4 were used to calculate the orientation of the raw accelerations into the laboratory system for the static and movement trials, in order to subtract the static values from the dynamic ones. The data given as input for the static trial were the mean values calculated over the static recording.

4.3.4.2 Filtering

Due to the consistency of the movement, a single trial was analysed in order to select the appropriate filter cut-off frequency. The power spectral density (PSD) of each IMU global acceleration (frequency resolution: 0.14 Hz) was calculated. The visual inspection of the PSD (Fig. 4.9) revealed different oscillatory responses between segments due to location and attachment method, suggesting that each sensor and axis required the selection of an individual filter cut-off frequency, which, however, could not be selected from the PSD.

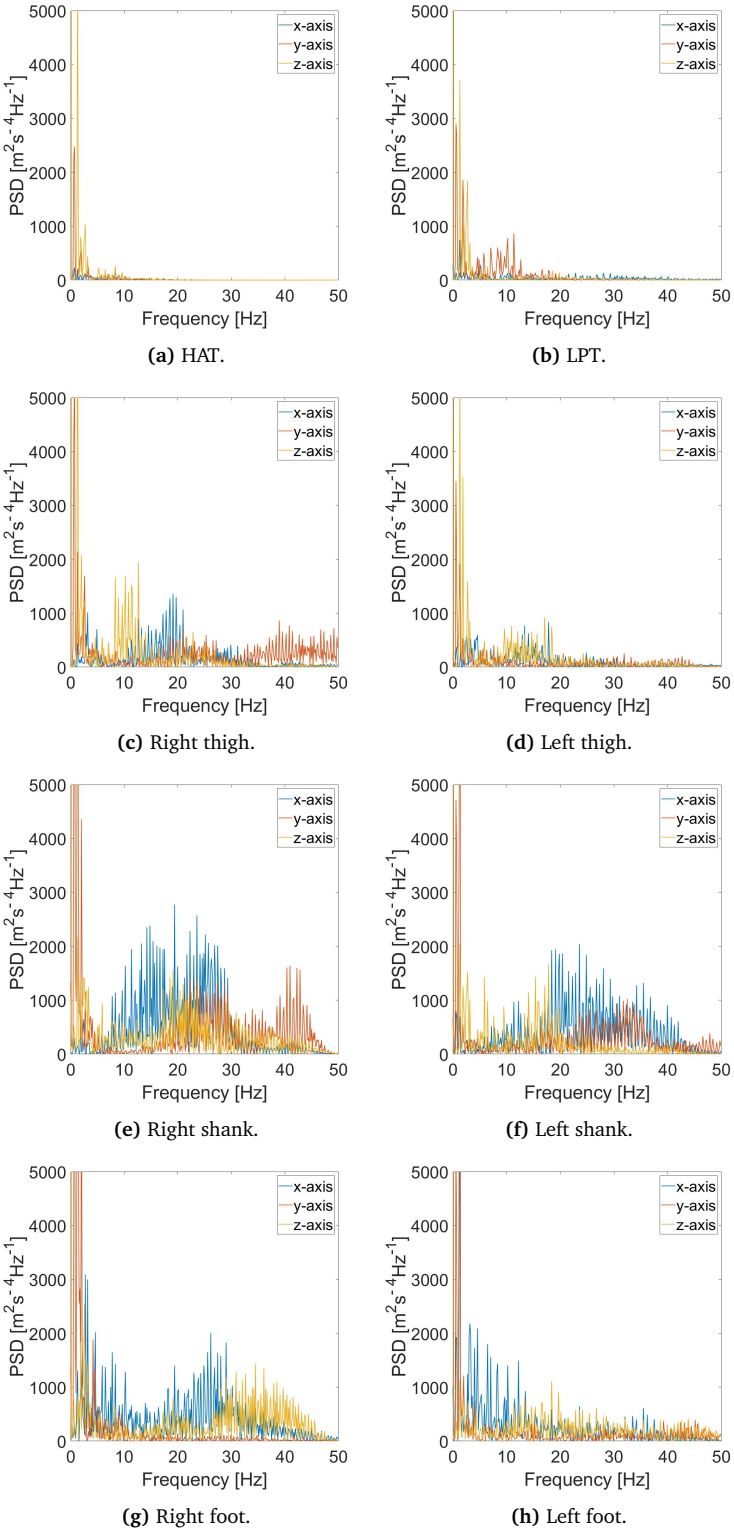

(a) HAT. **(b)** LPT.

(c) Right thigh. **(d)** Left thigh.

(e) Right shank. **(f)** Left shank.

(g) Right foot. **(h)** Left foot.

Figure 4.9: Example of PSD calculated for each IMU global acceleration during one trial (sample frequency of 100 Hz). X, y and z refer to the laboratory global system axes of figure 4.8.

From the markers' locations, the CoM trajectory of each segment was calculated and its acceleration was obtained by double differentiation. The accelerations were filtered using a second order forward-backward low-pass Butterworth filter with cut-off

frequency of 30 Hz, selected from the analysis of the PSD (frequency resolution: 0.14 Hz; Fig. 4.10), calculated for each segment CoM.

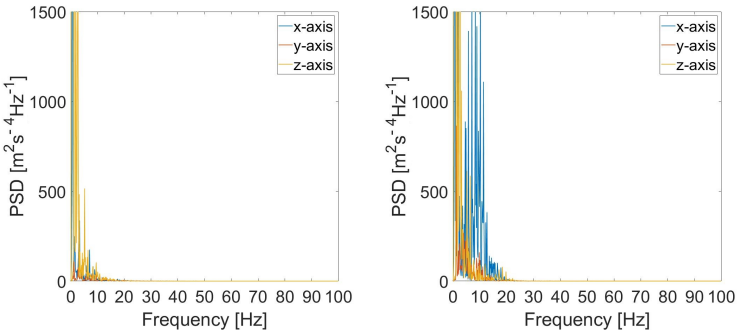

(a) HAT.

(b) LPT.

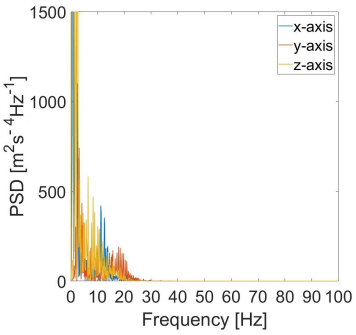

(c) Right thigh.

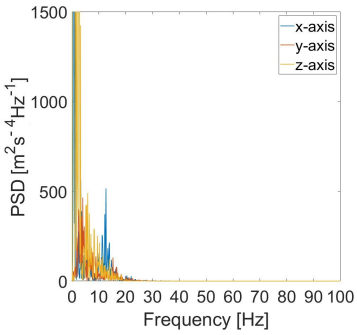

(d) Left thigh.

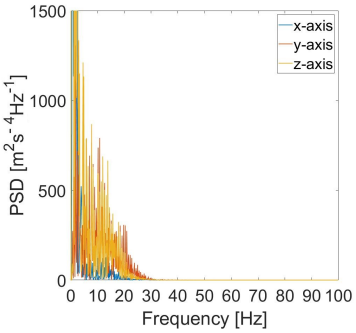

(e) Right shank.

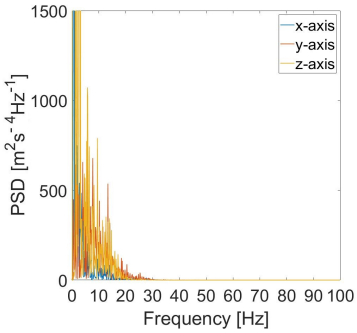

(f) Left shank.

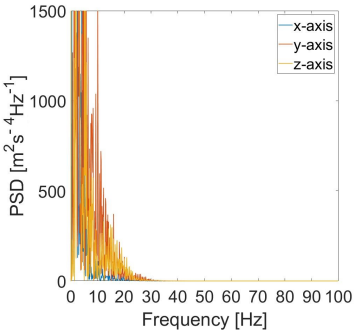

(g) Right foot.

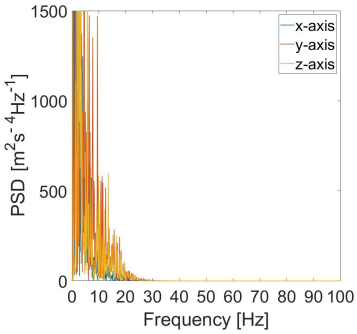

(h) Left foot.

Figure 4.10: Example of PSD calculated for each segment CoM acceleration during one trial. The CoM acceleration was obtained from the markers' trajectories data (sample frequency of 200 Hz).

The same filter was applied to the IMUs' global accelerations and five cut-off frequencies (10, 20, 30, 40 and 50 Hz) were used for each sensor location and along each axis. These were compared with the correspondent filtered CoM accelerations obtained from the markers' trajectories, in order to identify the cut-off frequency that leads to the best visual match. The details of the selected cut-off frequencies are reported in table 4.1 and an example of best visual match is shown in figure 4.11.

Table 4.1: Cut-off frequencies related to each sensor and axis, where x, y and z are the medio-lateral, antero-posterior and vertical axis of the laboratory global system (Fig. 4.8), respectively.

Sensor	Cut-off frequency [Hz]		
location	x	y	z
T4	30	30	30
midPSIS	20	20	30
Thighs	30	30	40
Shanks	20	30	30
Feet	50	50	50

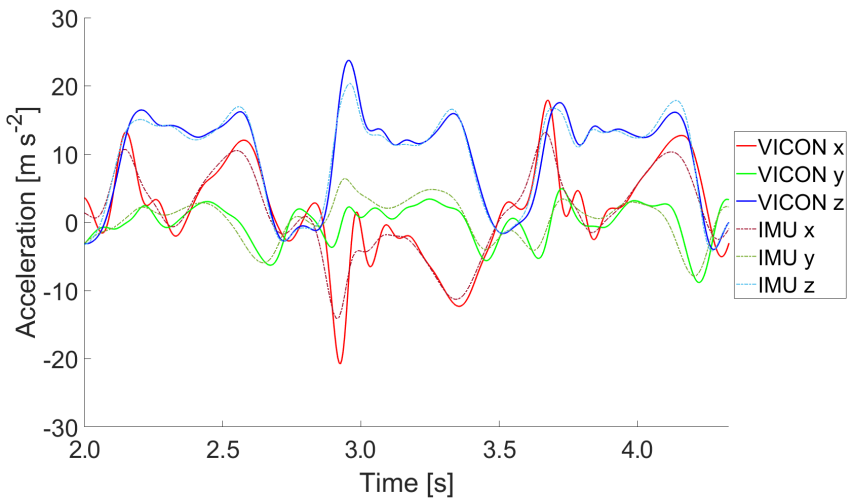

Figure 4.11: Example of the comparison between global acceleration calculated from the markers' trajectories (solid line) and from the IMU (dash-dotted line) for the midPSIS location after filtering with the individually selected cut-off frequencies for each axis, where x, y and z are represented in red, green and blue and correspond to the medio-lateral, antero-posterior and vertical axis of the laboratory global system (Fig. 4.8), respectively.

The IMU global accelerations were synchronised with the motion capture and force platform's recordings by matching the highest peak of the foot vertical acceleration during the first stance phase on the force platform for each trial (Fig. 4.12). This value corresponds to the first peak of the foot acceleration with 25 m s^{-2} minimum value, which was identified through the *findpeaks* Matlab function.

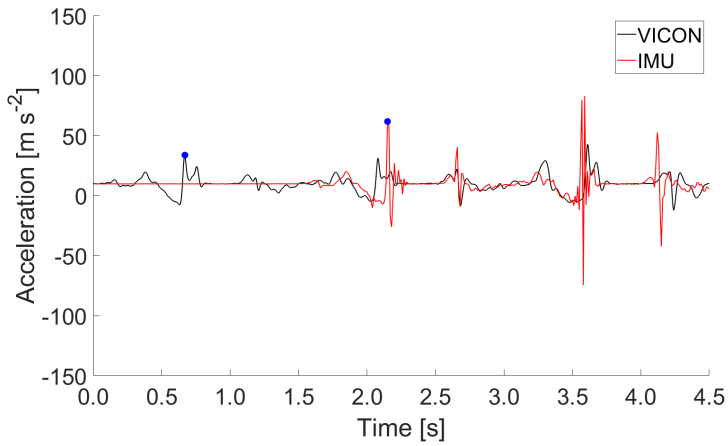

(a) Peak identification before synchronisation.

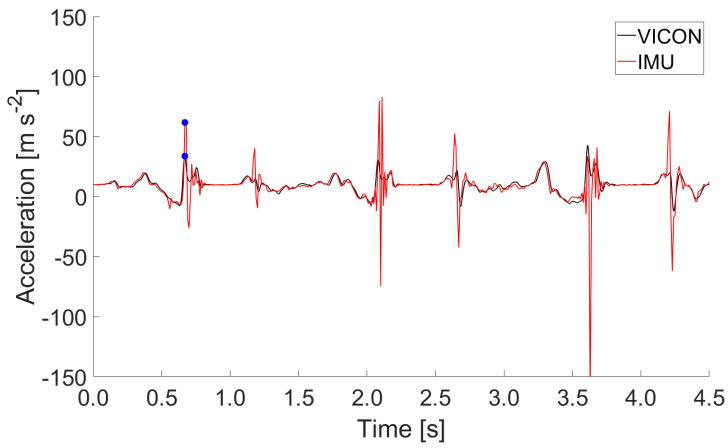

(b) Peak matching after synchronisation.

Figure 4.12: Foot vertical global acceleration calculated from the markers' trajectories (black line) and from the IMU (red line) before and after synchronisation, achieved by identifying the first peak over 25 m s^{-2} of each signal (blue markers).

4.3.4.3 Ground reaction force estimation

GRF components were estimated using Newton's second Law of Motion:

$$\overrightarrow{GRF} = \sum_{i=1}^{8} m_i \left(\overrightarrow{a_i} - \overrightarrow{g}\right)$$
$$\begin{bmatrix} F_{M-L} \\ F_{A-P} \\ F_V \end{bmatrix} = \sum_{i=1}^{8} m_i \left(\begin{bmatrix} a_x \\ a_y \\ a_z \end{bmatrix}_i - \begin{bmatrix} 0 \\ 0 \\ 9.81 \end{bmatrix} \right) \tag{4.5}$$

where $F_{M\text{-}L}$, $F_{A\text{-}P}$ and F_V are the medio-lateral, antero-posterior and vertical GRF component, respectively; a_i is the filtered IMU acceleration in the global system of the i-th sensor, g is the acceleration of gravity and m_i is the mass of each one of the eight segments considered, highlighted in figure 4.13.

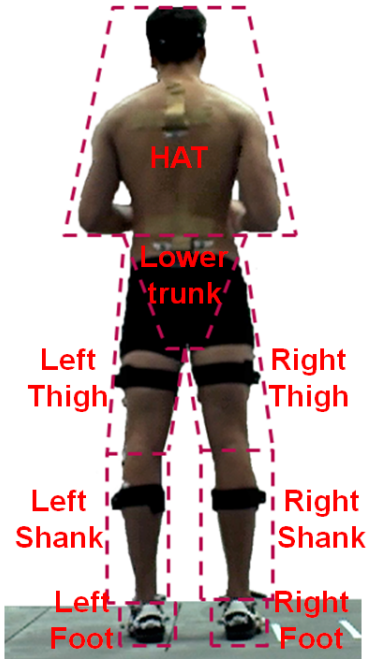

Figure 4.13: Body segments.

The mass of each segment was calculated using Zatsiorky-Seluyanov's inertia parameters [125], chosen since they were determined from 100 male Caucasian active subjects with mean age of 24 years, similar to the participant sample of this study. Zatsiorky-Seluyanov's segment masses are reported in table 4.2, with the addition of the HAT segment, defined for this study as the sum of head and neck, arms, hands, upper and middle trunk, and which mass was calculated as:

$$m_{HAT} = m_{head} + m_{uppertrunk} + m_{middletrunk} + 2\left(m_{upperarm} + m_{forearm} + m_{hand}\right) \quad (4.6)$$

Table 4.2: Body segments with their mass percentages [125].

Segment	Mass [% BW]
Head and neck	6.94
Upper trunk	15.96
Middle trunk	16.33
Upper arm	2.71
Forearm	1.62
Hand	0.61
HAT	49.11
Lower trunk	11.17
Thigh	14.16
Shank	4.33
Foot	1.37

4.3.5 Statistical analysis

The LSJ movement presents high horizontal accelerations, and being performed in the frontal plane, exhibits high accelerations in the medio-lateral direction, but negligible values along the antero-posterior axis. Therefore, only the GRFs in the medio-lateral and vertical directions were considered.

The mean value of measured and estimated GRFs in the medio-lateral and vertical directions were calculated over each one of the four stance phases recorded during the movement analysed, and compared using RMSE, normalised RMSE (nRMSE), normalised with respect to the mean measured GRF for each stance phase, and relative error (RelErr). nRMSE and RelErr are calculated through the following equations for each stance phase, and applied to the vertical and medio-lateral force components separately:

$$nRMSE = \frac{RMSE}{\frac{\sum_1^N F_{FP}}{N}} \cdot 100 \tag{4.7}$$

$$RelErr = \left| \frac{F_{IMU} - F_{FP}}{F_{FP}} \right| \cdot 100 \tag{4.8}$$

where F_{FP} and F_{IMU} are the step-averaged measured and estimated GRFs, and N is the total number of trials analysed for the specific stance phase. The RelErr was rated as very low ($< 5\%$), low ($5-10\%$), moderate ($10-15\%$), high ($15-20\%$) and very high ($> 20\%$), according to Verheul et al. [111], who based these values on meaningful performance or injury related differences in GRF.

4.4 Results

Table 4.3 shows RMSE, nRMSE and RelErr. The RMSE ranges between 43.4 and 76.2 N and between 55.9 and 65.7 N for the vertical and medio-lateral GRF, respectively, which correspond to nRMSE ranges of 4.4 and 7.5% and 10.6 and 12.8%.

Table 4.3: RMSE, nRMSE and RelErr for estimated vertical (F_V) and medio-lateral ($F_{M\text{-}L}$) GRF components for each stance phase.

	F_V			F_{M-L}			n
Stance phase	RMSE [N]	nRMSE [%]	RelErr [%]	RMSE [N]	nRMSE [%]	RelErr [%]	
1st (Fig. 4.5b)	43.4	4.4	3.2 ± 2.8	55.9	12.0	10.8±5.4	120
2nd (Fig. 4.5d)	52.2	5.2	3.8 ± 3.2	65.7	12.8	10.7±6.5	150
3rd (Fig. 4.5f)	76.2	7.5	5.4 ± 4.6	65.2	12.1	9.8±6.3	149
4th (Fig. 4.5h)	71.6	7.1	5.5 ± 4.3	57.3	10.6	8.3±5.6	150

A good and bad example, based on the RMSE, of the comparison of the vertical and

medio-lateral GRFs measured by the force platform and estimated by the IMUs are shown in figures 4.14 and 4.15, respectively.

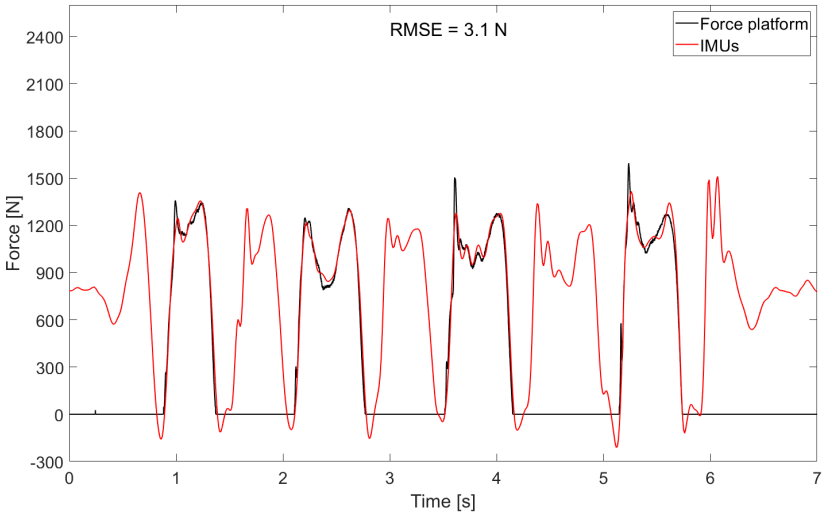

(a) Vertical components of GRF - good result.

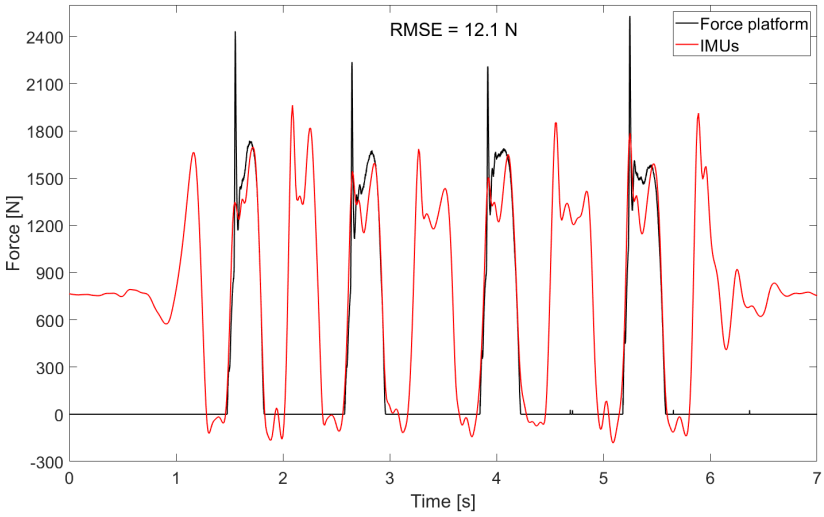

(b) Vertical components of GRF - bad result.

Figure 4.14: Good and bad examples of vertical GRF measured by the force platform (black) and estimated (red) through the IMUs.

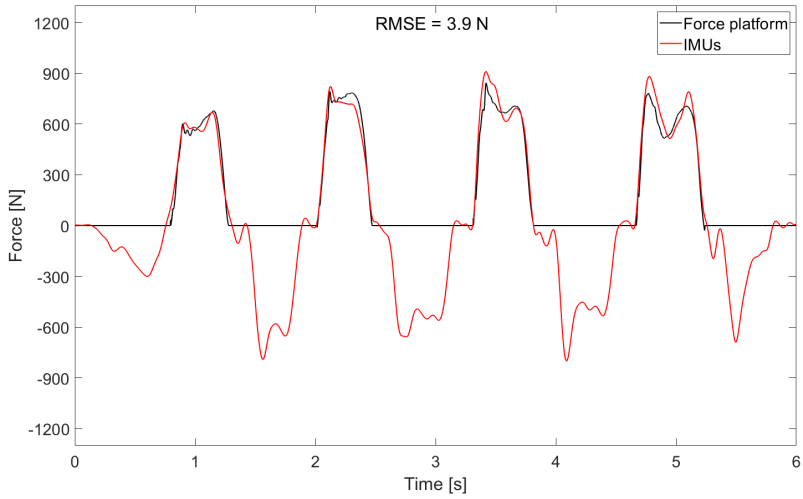

(a) Medio-lateral component of GRF - good result.

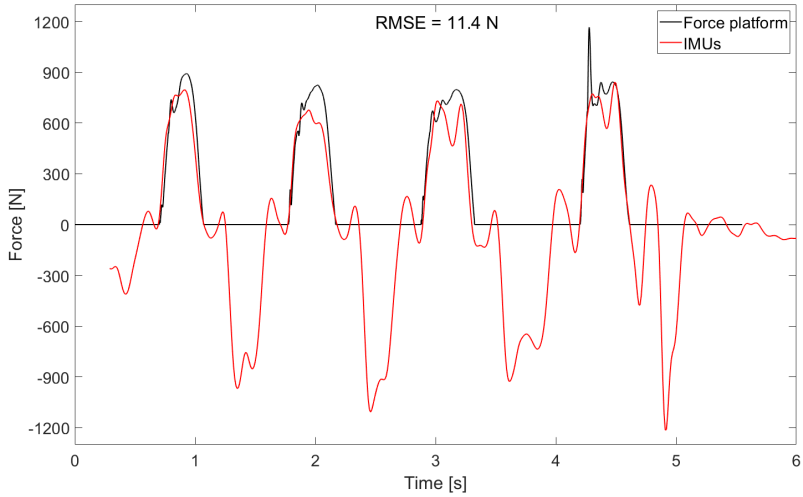

(b) Medio-lateral component of GRF - bad result.

Figure 4.15: Good and bad examples of medio-lateral GRF measured by the force platform (black) and estimated (red) through the IMUs.

The magnetometers' readings were analysed in order to identify if interferences were present in the laboratory environment. Figure 4.16 reports the absolute value of the magnetic field calculated for each sensor during a single trial with left foot contacts on the force platform, and compared with the Earth's magnetic field of the testing location, equal to 48.8 µT [126]. A constant value close to the Earth's magnetic field for the duration of the trial would be expected if no interference was present. However, as can be seen from the figure, the sensors placed on the lower limbs present oscillations in the magnetometers' readings, therefore, the sensors closer to the ground were affected by ferromagnetic materials, such as the force platform. It could be seen also that the IMUs affixed on the right lower limb present more oscillations compared to the left ones; these oscillations correspond with the stance phases over the force platform with the left foot and to the swing phase of the right lower limb over it.

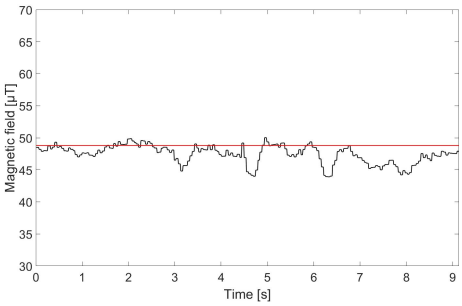

(a) HAT.

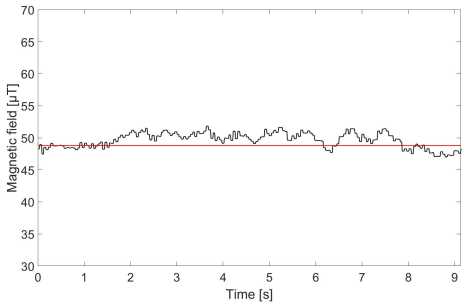

(b) LPT.

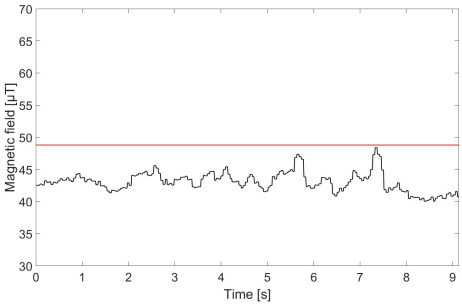

(c) Right thigh.

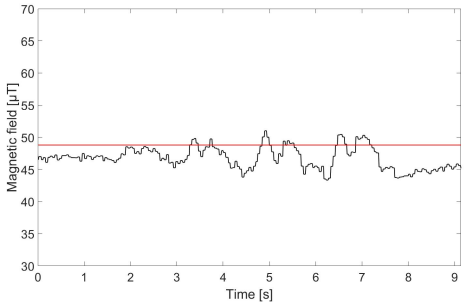

(d) Left thigh.

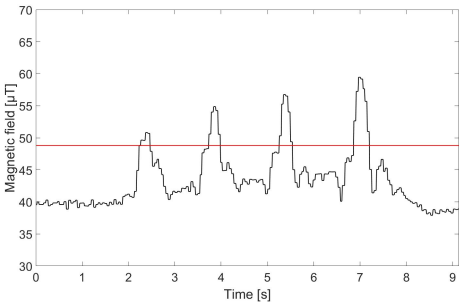

(e) Right shank.

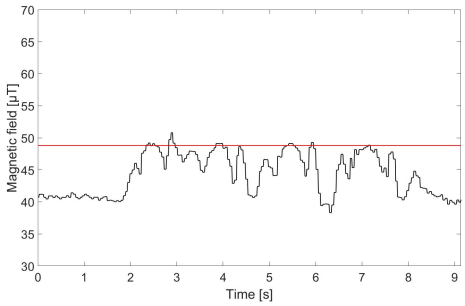

(f) Left shank.

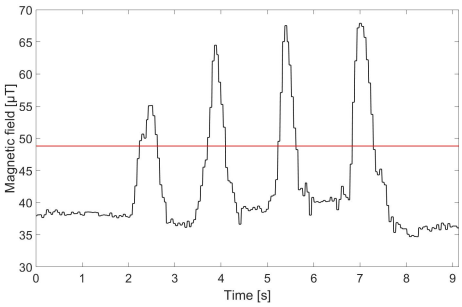

(g) Right foot.

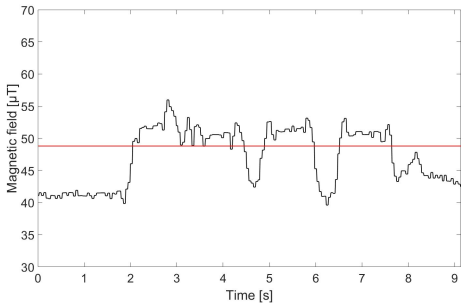

(h) Left foot.

Figure 4.16: Magnetic field measured by each sensor (black line) compared to the Earth's magnetic field equal to 48.8µT (red line).

To evaluate the effect of the magnetometers' readings on the GRF estimation, the force components were estimated from the accelerations derived from the markers' trajectories using equation 4.5, and compared with the IMU results and the force platform's measurement. This comparison is shown in figure 4.17 and highlights how an incorrect magnetometer reading affects the shear force estimation, when the sensors' orientations in the global system are calculated through a NED system.

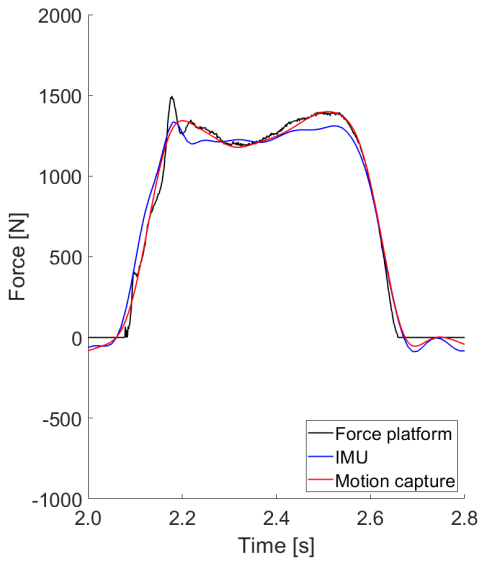

(a) Vertical force.

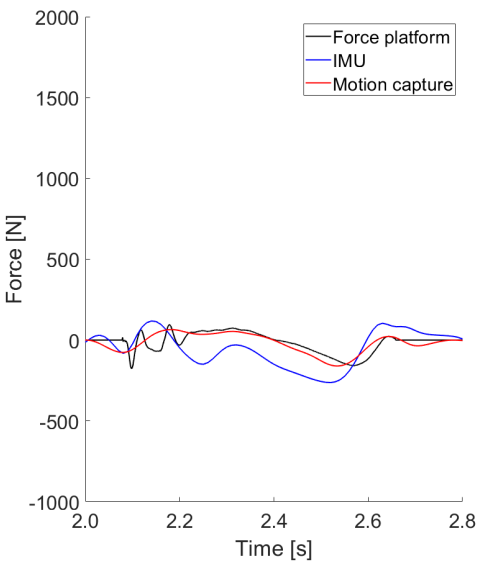

(b) Antero-posterior force.

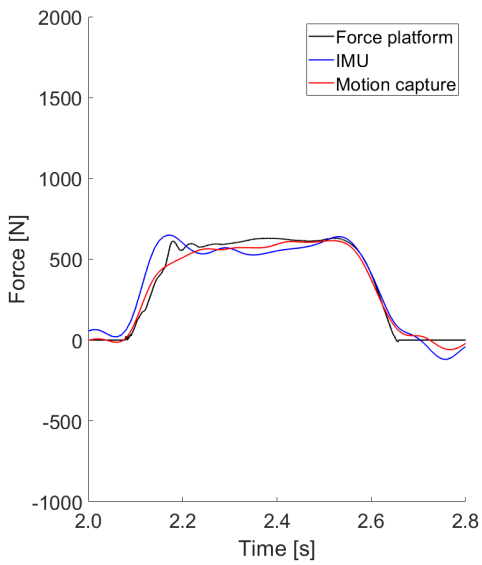

(c) Medio-lateral force.

Figure 4.17: Effect of the magnetometer interference on the GRF estimation. The second stance phase of a trial is reported as example.

The raw accelerations recorded by the IMUs were analysed in comparison to the acceleration derived from the markers' trajectories. The values of one trial are reported in figure 4.18 to show that the sensors affixed to shanks and feet segments reach the ±16 g sensor range (Fig. 4.18a), whereas, the accelerations of the same segments derived from the markers' trajectories do not exceed ±10 g (Fig. 4.18b).

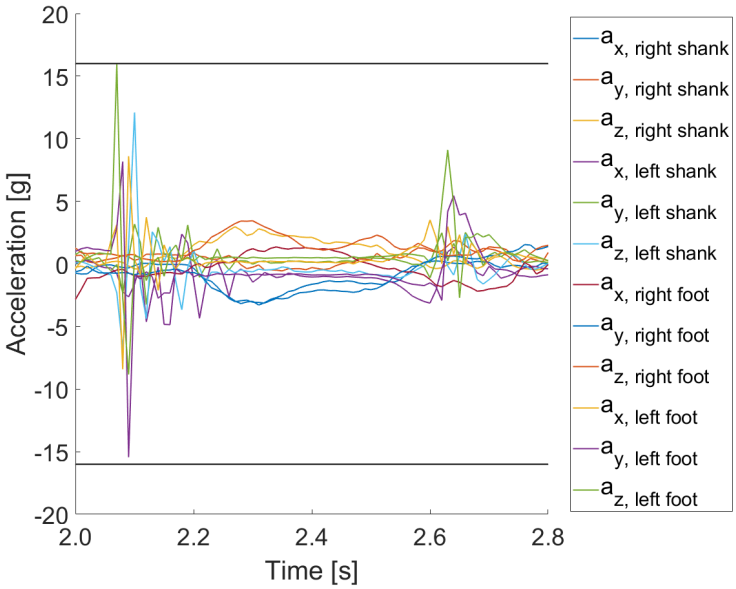

(a) IMUs' raw accelerations.

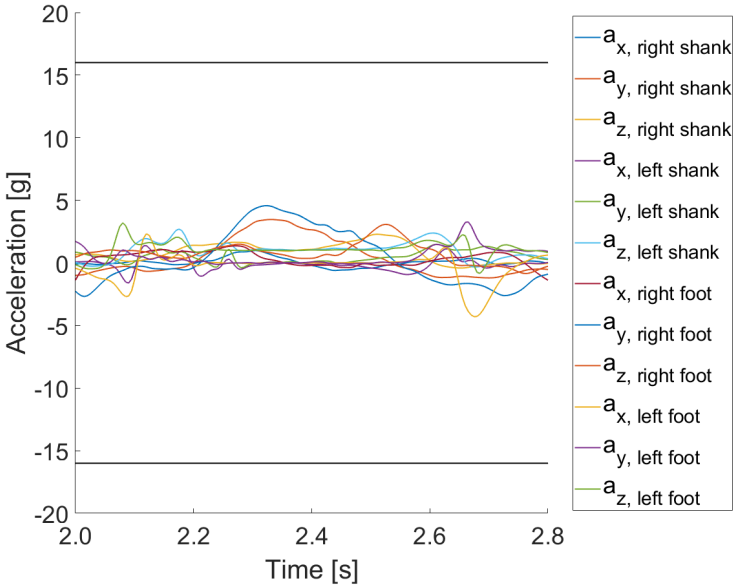

(b) Markers' accelerations.

Figure 4.18: Shanks and feet accelerations recorded by IMUs and derived from the markers' trajectories. The second stance phase of a trial is reported as example.

4.5 Discussion

The purpose of this chapter was to identify a method able to estimate GRFs from IMUs with good accuracy, especially in the horizontal direction, which is considered a critical factor related to performance during football-specific movements (Sec. 2.3.2.4). The graphical comparison (Fig. 4.14 and 4.15) of the instantaneous values of measured and estimated forces, shows that the IMUs are able to detect the stance phases with good alignment both in the vertical and medio-lateral directions. Whereas, the errors reported in table 4.3 highlight that the vertical force was estimated with higher accuracy than the medio-lateral component. The ability of IMUs to estimate the vertical force is related to the distance jumped during the exercise, with the error increasing from the first to third stance phase. Whereas this relationship is not present in the medio-lateral direction. According to the error rating used by Verheul et al. [111], the vertical GRF was estimated with low and very low errors during each stance phase, whereas the medio-lateral component was estimated with low to moderate errors with the highest errors during the first and second stance phases.

Previous research [107, 108] estimated GRFs from IMU during sprint and cutting manoeuvres, however the results could be compared to the present work, since they all involve movements with high impacts and accelerations in the horizontal direction. The instantaneous forces showed a good improvement compared to the GRF time history reported by Gurchiek et al. [108] in figure 2.16. The comparison between step-averaged measured and estimated forces with the previous studies (Table 4.4), revealed a similar estimation error for the vertical GRF, with RMSE between 43.4 and 76.2 N in this study comparable with the values of 54.2 N and 77.1 N obtained by Gurchiek et al. [108] for sprint and change of direction, respectively, and mean RelErr between 3.2 and 5.5% for this study better than the 7.3% found in sprinting by Setuain et al. [107]. Whereas, RMSE ranging between 55.9 and 65.7 N and

Table 4.4: RMSE and RelErr comparison between this study and previous research for estimated vertical (F_V) and medio-lateral ($F_{M\text{-}L}$) GRF components.

Study	Movement	F_V		F_{M-L}	
		RMSE [N]	RelErr [%]	RMSE [N]	RelErr [%]
This study	LSJ 1st stance (Fig. 4.5b)	43.4	3.2±2.8	55.9	10.8±5.4
	LSJ 2nd stance (Fig. 4.5d)	52.2	3.8±3.2	65.7	10.7±6.5
	LSJ 3rd stance (Fig. 4.5f)	76.2	5.4±4.6	65.2	9.8±6.3
	LSJ 4th stance (Fig. 4.5h)	71.6	5.5±4.3	57.3	8.3±5.6
Setuain et al. [107]	Sprint		7.3±8.0		45.3±55.0
Gurchiek et al. [108]	Sprint acceleration	77.1		66.3	
	Change of direction	54.2		163.5	

mean RelErr between 8.3 and 10.8% represent a good improvement in the estimation of medio-lateral force compared to the values of 66.3 N, 163.5 N and 45.3% calculated for RMSE during sprint and change of direction [108] and mean RelErr during sprint [107], respectively. Gurchiek et al. [108] reported much larger errors in the estimation of the instantaneous force compared to the step-averaged values, in particular in the horizontal direction, whereas the same could not be said in the present study with the instantaneous estimated forces presenting a visually good match with the measured values, especially along the vertical direction (Fig. 4.14 and 4.15).

Previous studies [107, 108] predicted GRFs during sprint and cutting manoeuvres using Newtonian mechanics from the data of a single IMU sensor applied on the sacral region, where the whole-body's CoM is considered to be located; however, the high errors obtained in the estimation of shear forces, highlighted the need for an improvement. The authors suggested that these high errors could be related to the use of a single sensor and its position, since the subject's CoM could move from the sacral region, due to the large asymmetries and variations in body configuration throughout the movement analysed. A study from Verheul et al. [111] confirmed that the use of a single point is not able to accurately represent the whole-body biomechanical loads during dynamic tasks. The authors estimated the resultant GRF from kinematics, comparing all combinations of segments from a minimum of one to the maximum of fifteen, suggesting that a minimum of two and three segments was required for low and moderate speed running, respectively, eight segments for cutting manoeuvres and eleven for accelerations in order to achieve moderate or lower errors; whereas high or very high errors were found for the highest intensity tasks, such as deceleration and high speed running, regardless of the number of segment considered. Moreover, the authors found that the trunk is the main contributor and must be included in all the segment combinations. For this reason, in the present study the use of a multiple-sensor approach representing a Lower Limb Trunk (LLT) model representation was analysed. The choice of using eight sensors was limited by the availability, however the participants were asked to keep their arms flexed and close to the torso during the movement, thus the upper body can be considered as a single segment. The trunk was divided into two links (HAT, comprising upper and middle part of the trunk, and lower trunk) based on the segments considered by Verheul et al. [111] (trunk and pelvis) and on the study from Kodama and Watanabe [95], where, during sit to stand and squat motion, GRFs were estimated with better accuracy when the trunk was divided into two or three links compared to a configuration that considered the trunk as a single segment, no matter if the two links were split as upper-middle and lower trunk or upper and middle-lower trunk (Sec. 2.4.1.1).

Some limitations were identified in this study. In section 2.4.1.1, a limitation found

in some studies was reported as the accelerometer range, which was not able to capture the peak acceleration at very high impact loadings [101]. Therefore, the raw accelerometers' recordings were analysed. Figure 4.18 shows that the accelerations of shanks and feet segments exceed the ±16 g accelerometer range when measured with the IMUs, whereas the same accelerations are lower than ±10 g when derived from the markers' trajectories. This suggests that the high accelerations recorded by the IMUs are a consequence of the attachment methods and the sensor's accelerometer range is large enough to analyse this football-related movement. Different oscillatory responses were observed between sensors, due to different locations and attachment methods, therefore cut-off frequencies individually selected for each segment were used. However, different oscillatory responses were present also between participants, which affect the estimation of GRFs (Fig. 4.19) and suggests that different cut-off frequencies should not be considered only in relation to each sensor but also individually selected for each participant.

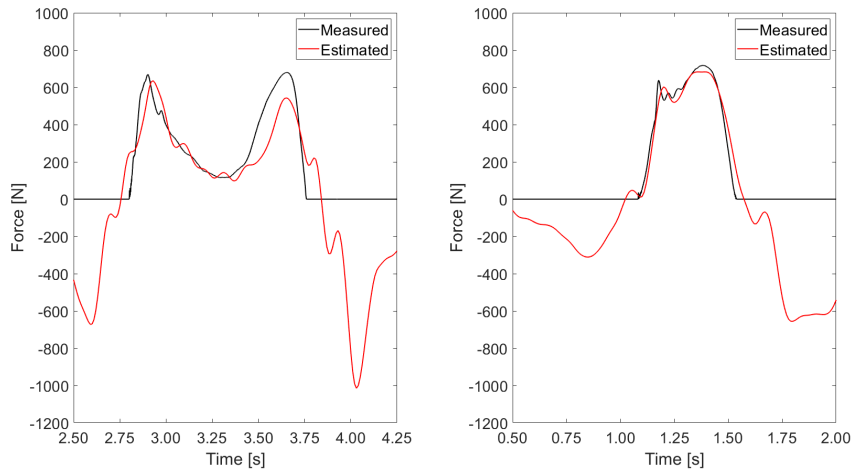

(a) High oscillations.

(b) Low oscillations.

Figure 4.19: Example of different oscillatory responses on the medio-lateral GRF estimation.

The consideration of different body segments implies that the acceleration measured by each sensor corresponds to that of the segment CoM and, furthermore, the segment mass should be individualised; however, not all the sensors were placed in correspondence of the segment CoM and the inertia parameters considered are based on average values found in the literature, even if from a sample similar to the current study. Finally, this analysis revealed the presence of magnetic interferences in the laboratory environment, which affects the sensors' orientations and, consequently, the final results in the medio-lateral direction (Fig. 4.17). If the method will be used in the field, magnetic interferences should not be present and no corrections in the sensors' orientations are required, whereas if the method is used in presence of ferro-magnetic materials, the sensors' orientations can be estimated from markers' trajectories using an optoelectronic motion capture system.

4.6 Conclusion

In this chapter a method to estimate 3D GRFs using eight IMU sensors was presented. The technique was validated during a LSJ movement, with very low to low relative errors in the estimation of the vertical GRF and low to moderate errors for the medio-lateral force component. These results were similar to those of previous studies when estimating the force in the vertical direction, whereas a good improvement along the medio-lateral axis was achieved by using a multiple-sensor approach compared to a single sensor one. The movement analysed is relevant to football because of the high medio-lateral accelerations recorded, however, some improvements are necessary to use the method in-field for football-specific movements and overcome the limitations previously outlined. For this reason, a further validation study will be presented in the next chapter.

Chapter 5

Use of inertial measurement units to estimate ground reaction forces during football-specific movements

5.1 Introduction

In the previous chapter (Ch. 4), a method based on a multiple-sensor Newtonian mechanics approach to estimate 3D GRFs was presented. The low to moderate errors, obtained in the medio-lateral force prediction during the LSJ movement analysed, showed a good improvement compared to previous research, therefore, an IMU-based method represents a good candidate to evaluate shoe-surface interaction in the field and its consequences on athletic performance.

The LSJ movement analysed in the previous chapter presents high medio-lateral accelerations, however, it is a football-relevant but not specific task [124], therefore, the applicability of the method to football-specific manoeuvres, replicating a real game environment, needs to be investigated. As reported in section 2.1, football movements are characterised by high acceleration starts, quick sprints and rapid changes in direction [3]. The majority of the change of direction tasks during a match play are between 0° and 90°, with numbers six times higher than manoeuvres between 90° and 180° [23] (Sec. 2.1); and faster performances are associated with the application of greater braking force on the steps prior to turning [82, 84, 85] (Sec. 2.3.2.4). Therefore, it is important to evaluate acceleration steps, changes of direction, in particular between 0° and 90°, and deceleration steps in the forward direction prior them, to validate a GRF estimation method for in-field football-specific movements.

Limitations, identified in the previous chapter (Ch. 4), needs to be addressed, such as the presence of different oscillatory responses due to sensors' attachment methods

and locations, sensor placement not corresponding with the segment's CoM and the presence of magnetic interferences in the laboratory environment.

In this chapter, a new study, carried out to improve the method previously described to estimate GRFs, will be presented and validated during football-specific movements.

5.2 Aim and objectives

The aim of this chapter is to improve the method previously developed to estimate 3D GRFs using multiple IMUs.

To achieve this, the following objectives have been identified:

1. develop an improved method to estimate 3D GRFs from IMUs;
2. validate the proposed method for football-specific movements against force platform's measurements.

5.3 Methods

5.3.1 Participants

After ethical approval from Sheffield Hallam University Research Ethical Committee, three male participants (age: 21.7±1.9 years; mass: 75.2±3.8 kg; stature: 1.77±0.03 m) volunteered to take part in the study. Participants were healthy and physically active.

A higher number of participants were initially recruited, however, COVID-19 affected the data collection. The data available comprise a total of 208 valid foot contacts on the force platforms, representing five different movements (acceleration, deceleration, 45° cut, 90° cut and 180° turn) with measured impact peak forces ranging between 6.99 and 57.69 N kg^{-1} in the vertical direction and between 0.91 and 24.91 N kg^{-1} in the horizontal direction. These provide a wide range of forces regardless the small number of participants.

5.3.2 Experimental set-up

A 24-camera optoelectronic motion capture system (Qualisys Oqus 7+, Qualisys AB, Gothenburg, Sweden; motion capture volume: 22 x 12 x 2 m) and four 60 x 90 cm force platforms (Optima-BMS, AMTI, Watertown, MA, USA), both sampling at 200 Hz were used. The same sensors described in section 4.3.2 were utilised.

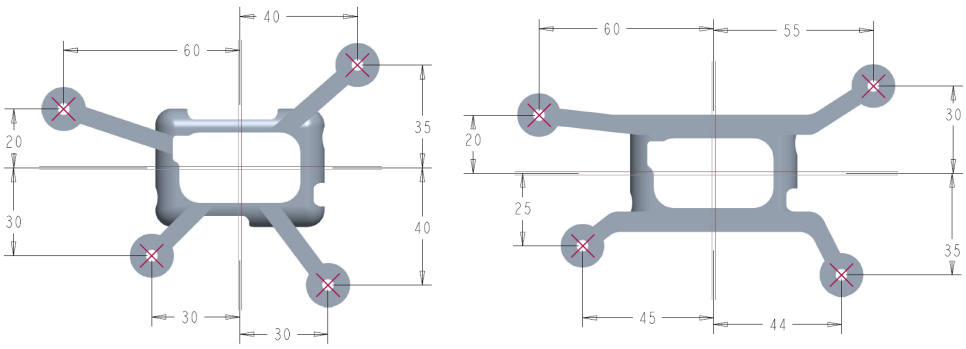

(a) Foot sensor mount design.

(b) HAT, LPT, thigh and shank sensor mount design.

Figure 5.1: Sensor mount technical drawings with measurements in mm.

The IMU attachment method used in this study follows the assessment presented in appendix B. This IMU placement method addresses one of the limitations highlighted in the previous chapter (Ch. 4), by reducing the undesired noises due to the oscillations of the sensors compared to the body segment, and to tissue artefacts. The orientation of each sensor was obtained from the location of four retro-reflective markers (diameter of 12.5 mm) applied on a light weight rigid frame, specifically designed to house them and be mounted on each IMU sensor. The mass of each sensor mount with markers is 8.98 ± 0.15 g. Two different sensor mount designs were designed. One for the sensors placed on the feet (Fig. 5.1a) to avoid any limitation to the ankle range of motion; and the second for all the other sensors (Fig. 5.1b) to allow and facilitate the placement of the elastic auto-adhesive bandage, which, as explained in appendix B, was used to improve the attachment method technique by reducing the presence of undesired noises. The sensor mounts present a reinforcement on the bottom part of each rod to minimise any vibrations during the high intensity movements analysed that involve an impact. They were 3D printed and attached on top of each sensor through double sided tape. The use of the sensor mounts overcome the effect of magnetic interferences present in the laboratory environment in the determination of the IMUs' headings, which was identified as another limitation in the previous chapter (Ch. 4).

The analysis of whole body kinetics through the use of body segments implies that the acceleration measured by each sensor corresponds to that of the respective segment CoM; however, in the previous chapter (Ch. 4), it was highlighted that not all the sensors were placed in correspondence with the segment CoM. For this reason, each segment CoM was determined before attaching the sensors. These values were derived from the inertia parameters defined by Zatsiorsky-Seluyanov [125], reported in table 5.1, where the CoM is referred as the distance from the proximal endpoint expressed as percentage of the total segment length. The anatomical landmarks, representing the proximal and distal endpoints, are reported in figure 5.2.

Table 5.1: Body segment inertia parameters, defined by Zatsiorsky-Seluyanov [125].

Segment	Proximal endpoint	Distal endpoint	Mass [% BW]	Length [%]	CoM [%]
Head and neck	VERT	C7	6.94	13.95	50.02
Upper arm	ACR	EJC	2.71	19.06	59.40
Forearm	EJC	WJC	1.62	15.45	45.74
Hand	WJC	MET3	0.61	4.95	79.00
Upper Part Trunk (UPT)	SUPR	XYPH	15.96	9.80	29.99
Middle Part Trunk (MPT)	XYPH	OMPH	16.33	12.38	45.02
Lower Part Trunk (LPT)	OMPH	MIDH	11.17	8.37	61.15
Thigh	ASIS	TIB	14.16	24.25	45.49
Shank	TIB	SPHY	4.33	24.93	40.47
Foot	HEEL	TTIP	1.37	14.82	44.15

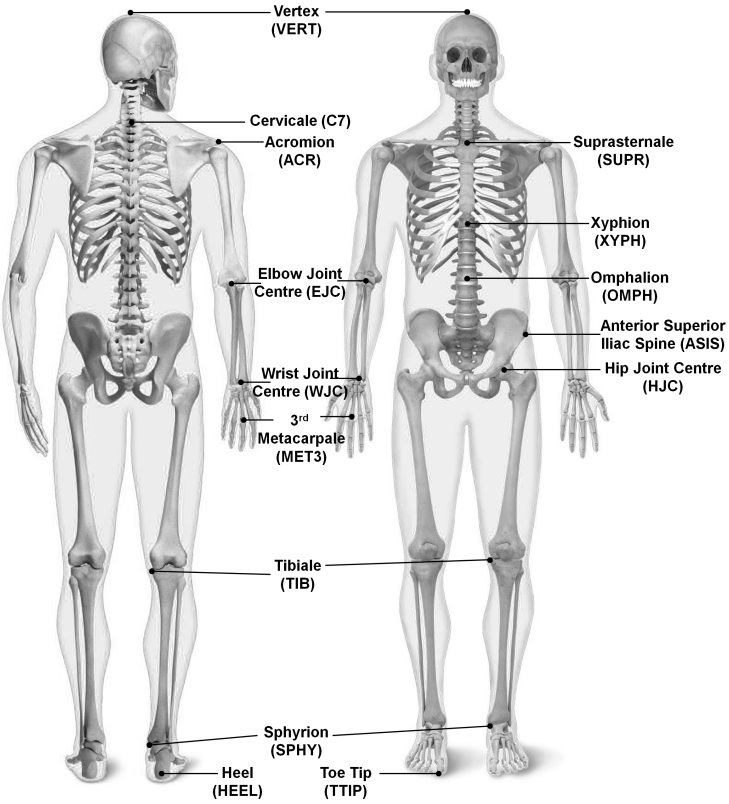

Figure 5.2: Back and front view of the body landmarks.

The details of each segment attachment method and location, as well as each segment mass, are reported in the following pages, with $d(a-b)$ defined as the distance between points a and b. Each body segment mass was defined as a percentage of the total body mass; however, additional masses were applied to each segment, such as IMU, sensor mount, auto-adhesive bandage, velcro, heart rate monitor, thermoplastic and shoes. Thus, a comparison, between adding these additional masses individually to the specific segments or considering them as part of each segment mass percentage of the total body mass, was performed. No differences were found, due to the negligible amount of mass of these elements compared to those of the body segments,

(a) Front view. **(b)** Back view.

Figure 5.3: Sensors' attachment locations.

thus, the latter option was chosen. The mass values used are derived from Zatsiorky-Seluyanov's inertia parameters [125] (Table 5.1).

5.3.2.1 Foot segment

Segment mass: 1.37% BW
Sensor attachment location: on the shoe, over the laces.
Sensor attachment method: the sensor was fixed, through adhesive velcro, to a 40 x 70 mm thermoplastic plate (Fig. 5.4a), which was attached to the subject's shoe through double sided tape, and secured with medical tape (Fig. 5.4b).

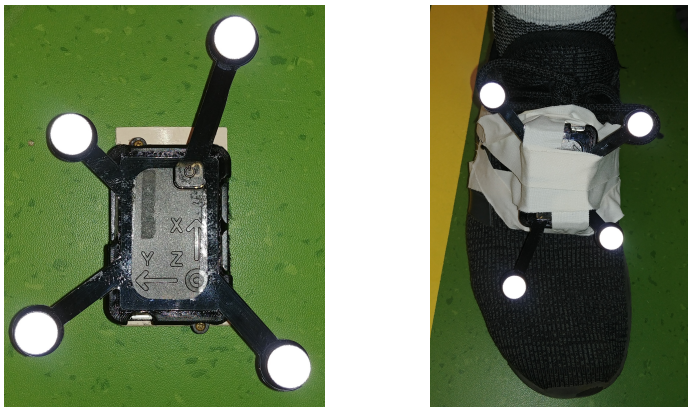

(a) Sensor and sensor mount with markers over the 40 x 70 mm thermoplastic plate. **(b)** Sensor attachment.

Figure 5.4: Foot sensor attachment method.

5.3.2.2 Shank segment

Segment mass: 4.33% BW
Sensor attachment location: over the tibia bone at 0.4047 *d(TIB – SPHY)* from TIB.
Sensor attachment method: the sensor was attached to the skin through adhesive velcro and further secured with tape and a 75 mm wide elastic auto-adhesive bandage wrap around the subject's shank (Fig. 5.5b).

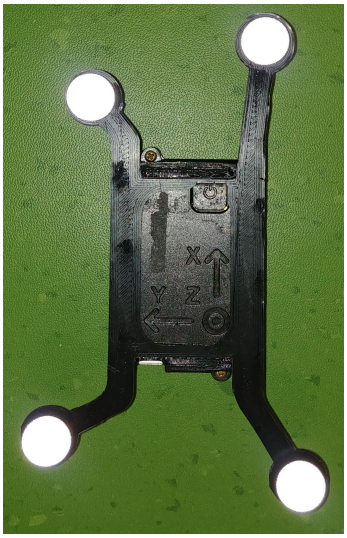

(a) Sensor and sensor mount with markers.

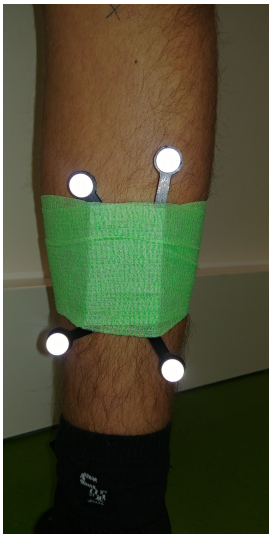

(b) Sensor attachment.

Figure 5.5: Shank sensor attachment method.

5.3.2.3 Thigh segment

Segment mass: 14.16% BW
Sensor attachment location: on the lateral aspect of the thigh, over the fascia lata, at 0.4549 *d(ASIS – TIB)* from ASIS.
Sensor attachment method: the sensor was fixed, through adhesive velcro, to a 50 x 100 mm thermoplastic plate (Fig. 5.6a), which was attached to the subject's skin through double sided tape, and secured with medical tape and a 75 mm wide elastic auto-adhesive bandage wrap around the subject's thigh (Fig. 5.6b).

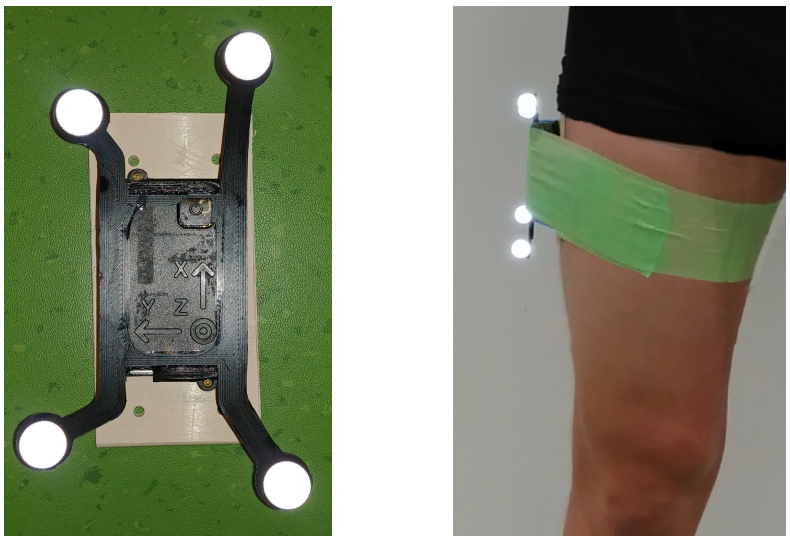

(a) Sensor and sensor mount with markers over the 50 x 100 mm thermoplastic plate.

(b) Sensor attachment.

Figure 5.6: Thigh sensor attachment method.

5.3.2.4 LPT segment

Segment mass: 11.17% BW
Sensor attachment location: midPSIS.
Sensor attachment method: the sensor was attached to the skin, through the use of adhesive velcro and secured with tape and a 75 mm wide elastic auto-adhesive bandage wrap around the subject's waist (Fig. 5.7).

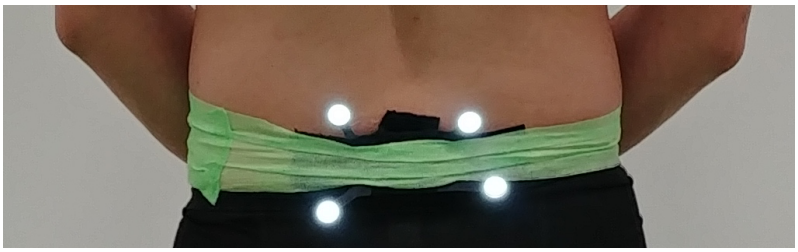

Figure 5.7: LPT sensor attachment method.

5.3.2.5 HAT segment

Segment mass: 49.11% BW (eq. 4.6)
Sensor attachment location: over the sternum at 6.33% H_{tot} from SUPR (eq. 5.4).

The CoM of a combination of segments is calculated through the following formulas:

$$CoM_x = \frac{\sum_i m_i x_i}{\sum_i m_i} \tag{5.1}$$

$$CoM_y = \frac{\sum_i m_i y_i}{\sum_i m_i} \tag{5.2}$$

$$CoM_z = \frac{\sum_i m_i z_i}{\sum_i m_i} \tag{5.3}$$

Since the HAT segment CoM is calculated to attach the sensor, and the body presents bilateral symmetry, only the CoM value on the vertical axis (y-axis in figure 5.8) needed to be calculated. The SUPR was used as proximal endpoint, and the upper arm was considered as kept along the trunk with the elbow flexed at 90° (Fig. 5.8), angle chosen as a mean representative value during running.

$$\begin{aligned} CoM_{HAT} =& \frac{\sum_1^9 m_i d(SUPR - CoM_i)}{\sum_1^9 m_i} \\ & -m_{head}[d(SUPR-C7)+(1-CoM_{head})L_{head}] \\ & +m_{UPT}CoM_{UPT}L_{UPT} \\ & +m_{MPT}[d(SUPR-XYPH)+CoM_{MPT}L_{MPT}] \\ & +2m_{upperarm}CoM_{upperarm}L_{upperarm} \\ & +2m_{forearm}[d(SUPR-EJC)+CoM_{forearm}L_{forearm}] \\ & +2m_{hand}[d(SUPR-WJC)+CoM_{hand}L_{hand}] \\ =& \frac{}{m_{head}+m_{UPT}+m_{MPT}+2(m_{upperarm}+m_{forearm}+m_{hand})} \\ =& 6.33H_{tot} \end{aligned} \tag{5.4}$$

where H_{tot} is the subject stature and

$$d(SUPR-C7) = 4.1\%H_{tot} \tag{5.5}$$

$$d(SUPR-XYPH) = L_{uppertrunk} \tag{5.6}$$

$$d(SUPR-EJC) = d(ACR-EJC) = L_{upperarm} \tag{5.7}$$

$$d(SUPR-WJC) = d(ACR-EJC) + d(EJC-WJC) = L_{upperarm} + L_{forearm} \tag{5.8}$$

The ACR was considered at the same height on the longitudinal axis compared to the SUPR, since mean anthropometric values [127] showed a difference of 2 mm when

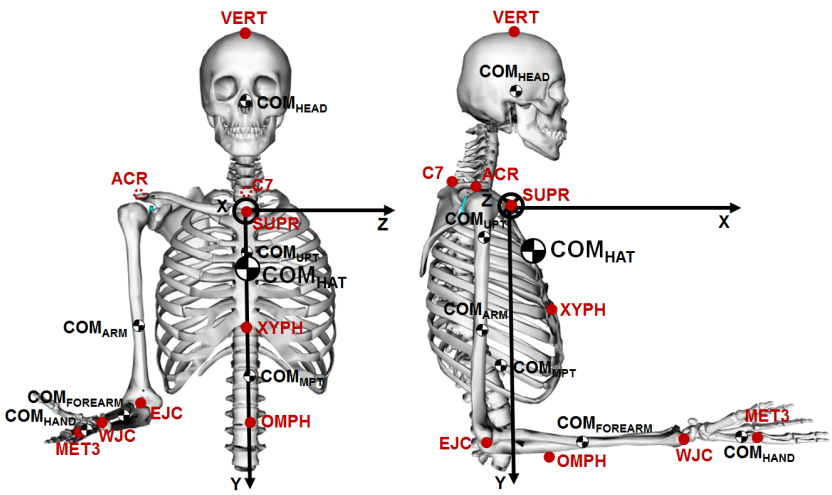

Figure 5.8: HAT CoM and endpoints.

measuring SUPR and ACR vertical height on male subjects sitting, which can be considered negligible.

Sensor attachment method: the sensor was attached with adhesive velcro to a heart rate monitor band, used to keep the sensor in place, and further secured with a 75 mm wide elastic auto-adhesive bandage wrap around the subject's torso (Fig. 5.9).

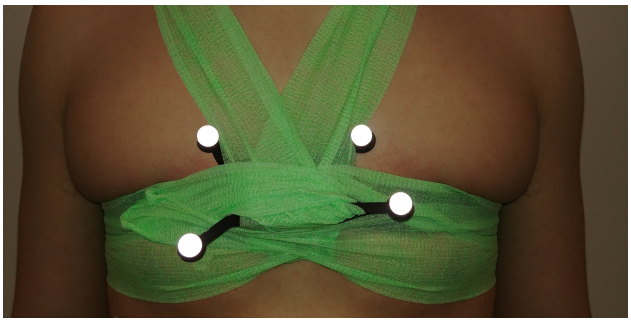

Figure 5.9: HAT sensor attachment method.

5.3.3 Protocol

Before the test, participants completed a self-directed warm-up routine, involving jogging, skip, side-stepping, sprint and stretching; extra time was given to familiarise with the tasks.

The participant's body weight was measured while standing on the force platform in a static position for three seconds. Participants were asked to start each trial from a T-pose, to be kept for three seconds, and to complete three trials of the following movements:

- 5 m straight acceleration, starting close to the force platforms in order to perform the first step on top of them (Fig. 5.10a);
- 45° change of direction using the right leg to push off during the side cut, preceded by a 7.5 m straight acceleration and followed by 3 m sprint (Fig. 5.10b);
- 45° change of direction using the left leg to push off during the side cut, preceded by a 7.5 m straight acceleration and followed by 3 m sprint (Fig. 5.10c);
- 90° change of direction using the right leg to push off during the side cut, preceded by a 7.5 m straight acceleration and followed by 3 m sprint (Fig. 5.10e);
- 90° change of direction using the left leg to push off during the side cut, preceded by a 7.5 m straight acceleration and followed by 3 m sprint (Fig. 5.10a);
- 180° change of direction using the dominant leg to push off during the turn, preceded and followed by 7.5 m straight acceleration (Fig. 5.10f).

In order to ensure the correct change of direction angle, poles were used to limit the movement.

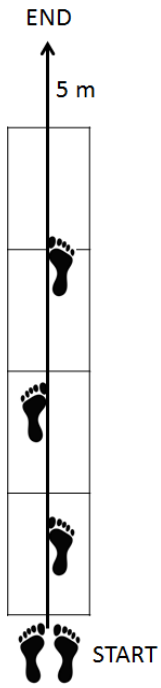

(a) 5 m sprinting acceleration.

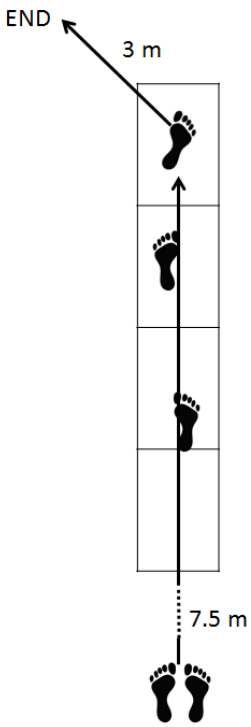

(b) 45° change of direction using the right leg to push off during the side cut.

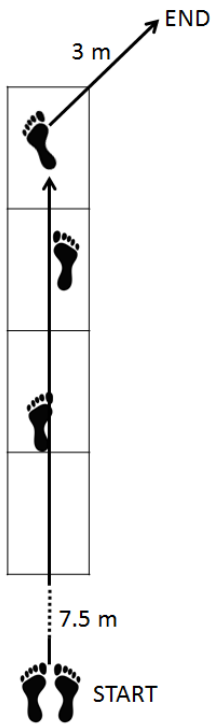

(c) 45° change of direction using the left leg to push off during the side cut.

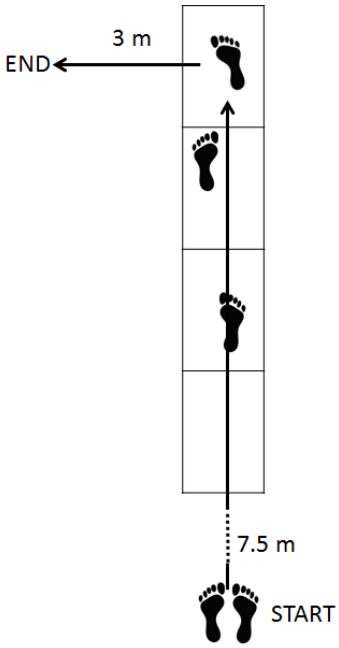

(d) 90° change of direction using the right leg to push off during the side cut.

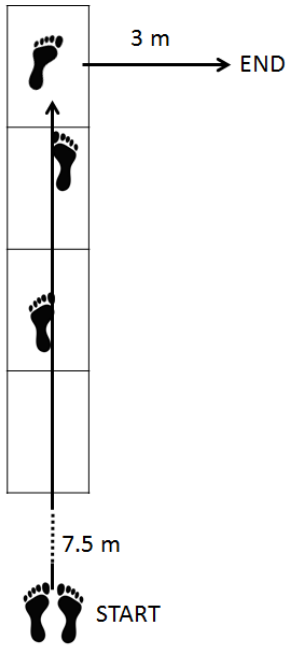

(e) 90° change of direction using the left leg to push off during the side cut.

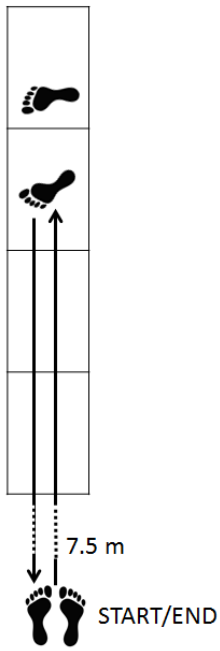

(f) 180° change of direction using the right leg to push off during the turn.

Figure 5.10: Movements performed.

5.3.4 Data processing

5.3.4.1 Conversion of the inertial measurement units' raw accelerations into the global system

IMU local axes' orientations were affected by the magnetic interference present in the laboratory environment. For this reason, the orientation of each sensor's local coordinate system was determined from the coordinates of the four markers applied on each sensor through the 3D printed sensor mount. Before achieving this, the IMUs' recordings needed to be synchronised with the motion capture data.

The IMUs' raw accelerations were transformed into the laboratory global coordinate system using equations 4.1 to 4.3, where ${}^{Lab}R_{NED}$ is the rotation matrix describing the orientation of the IMU NED system compared to the motion capture coordinate system and was calculated as:

$$ {}^{Lab}R_{NED} = R_z\left(\frac{3}{4}\pi\right) R_y(0)\, R_x(\pi) \tag{5.9} $$

with $\frac{3}{4}\pi$ and π determined by measuring the orientation of the magnetic north with respect to the laboratory.

A single point for each cluster of markers was calculated for each time instant as:

$$ T(t) = \frac{1}{4}\sum_{i=1}^{4} c_i(t) \tag{5.10} $$

where $c_i(t)$ represents the 3D coordinates of the marker i belonging to the cluster at time t. The acceleration of point T ($a_T(t)$) in the motion capture coordinate system was determined by double differentiation.

The IMUs' global accelerations were synchronised with the motion capture and force platform data by matching the highest peak of the vertical acceleration recorded on the foot, with which the first step of acceleration is performed, with the correspondent a_T value. This point corresponds to the first peak of the foot acceleration with 25 m s^{-2} minimum height, which was identified through the *findpeaks* Matlab function.

Each cluster coordinate system was determined for each time sample from the marker coordinates. An example of the coordinate system calculation is reported in figure 5.11, which orientation can be determined through the following equations:

$$ \overrightarrow{k} = \frac{c_1 - c_3}{\|c_1 - c_3\|} \tag{5.11} $$

$$ \overrightarrow{j} = \frac{\overrightarrow{k} \times (c_2 - c_4)}{\|\overrightarrow{k} \times (c_2 - c_4)\|} \tag{5.12} $$

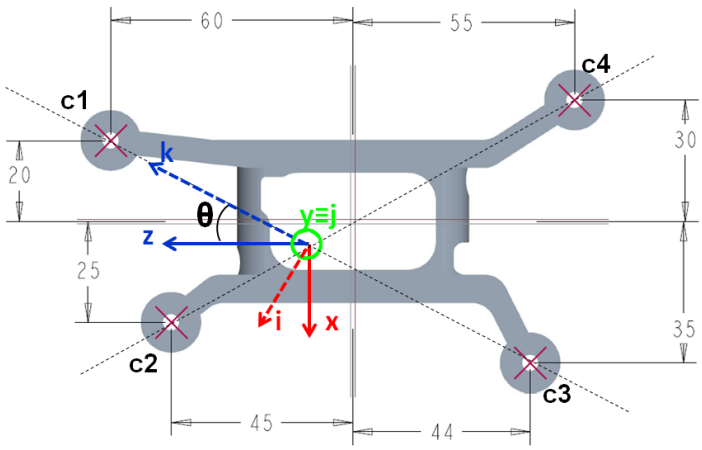

Figure 5.11: Example of coordinate system calculated with the non optimal estimator (dashed lines) and sensor local coordinate system (continuous lines).

$$\vec{i} = \vec{j} \times \vec{k} \tag{5.13}$$

$$^{MoCap}R_{cluster} = \left[\vec{i} \quad \vec{j} \quad \vec{k}\right] \tag{5.14}$$

The cluster coordinate system was rotated about the y-axis at an angle θ, determined from the details of the sensor mount technical design (Fig. 5.11), in order to obtain the real sensor axis orientation with respect to the motion capture coordinate system (Fig. 5.12), and overcome the effect of the magnetic interference:

$$^{MoCap}R_{IMU} = R_y(\theta)^{MoCap}R_{cluster} \tag{5.15}$$

The raw accelerations measured by each IMU (a_{IMU}) were converted into the motion capture coordinate system through the following formula:

$$\overrightarrow{^{MoCap}a_{IMU}} = ^{MoCap}R_{IMU}\,\overrightarrow{a_{IMU}} \tag{5.16}$$

Once defined in the motion capture coordinate system, the accelerations $\left(^{MoCap}a_{IMU}\right)$ were converted into the global coordinate system, defined in accordance with the movements analysed. X was defined as the forward axis, pointing in the direction of travel towards the change of direction, z the vertical axis pointing upwards and y the medio-lateral axis directed from right to left (Fig. 5.12).

The accelerations in the global coordinate system (a_{Gl}) were determined as follows:

$$\overrightarrow{a_{Gl}} = ^{Gl}R_{MoCap}\,\overrightarrow{^{MoCap}a_{IMU}} \tag{5.17}$$

where the global coordinate system is rotated 180° about the z-axis compared to the motion capture one. Finally, also the force platforms' recordings were transformed into the global coordinate system to allow the result comparison.

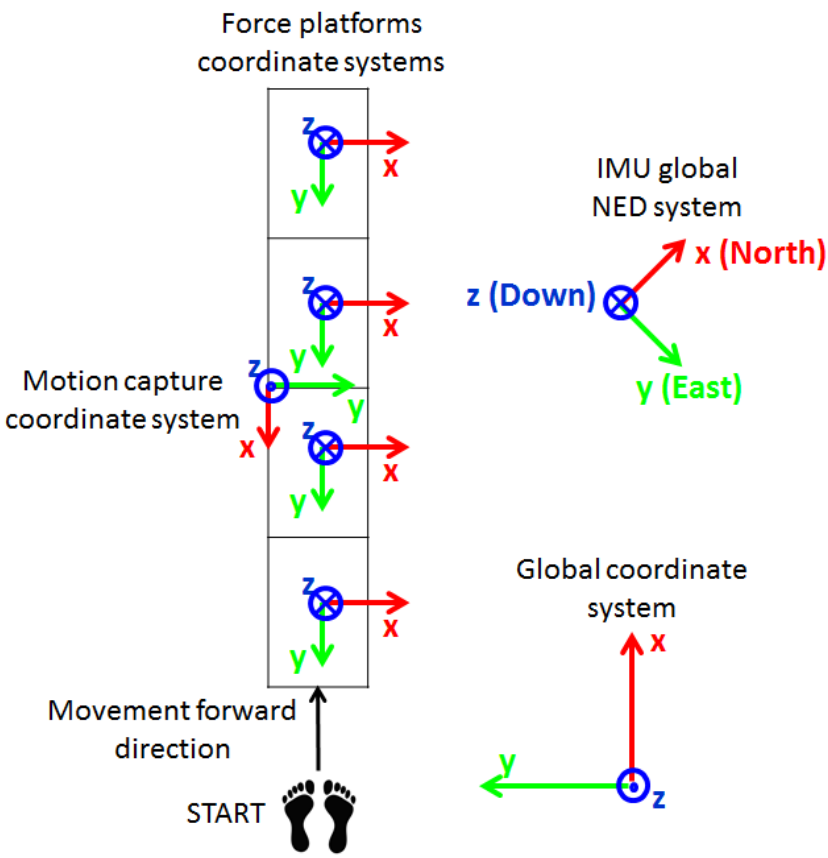

Figure 5.12: Coordinate systems of IMUs, motion capture and force platforms with respect to the final global coordinate system, defined in accordance with the movements analysed.

In order to evaluate the effect of the magnetic interference on the sensor heading determination and the benefit in the use of the sensor mount, the 3D GRFs were estimated from the unfiltered accelerations of each segment, calculated in the global coordinate system through three different methods. These accelerations were substituted into equation 4.5 to use the method described in the previous chapter (Ch. 4). The first method considers the magnetometers' recordings, by using equations 4.1 to 4.3 (IMU in figure 5.13), the second method uses the IMU accelerations and the sensor mounts' orientations (eq. 5.14 to 5.17; IMU+Qualisys in figure 5.13), and the third method considers the acceleration of the centre of each cluster ($a_T(t)$; Qualisys in figure 5.13). The third method was expected to match the results obtained through the second method, but with twice the temporal resolution, since IMU and motion capture sample frequencies were 100 and 200 Hz, respectively. A comparison of the results obtained for each method for a 90° change of direction performed with the right leg is reported in figure 5.13. As it can be seen, the magnetic interference present in the laboratory affects the estimation of the forces along the horizontal axes; whereas the calculation of the IMU accelerations into the global system through the use of the clusters' orientations helps to address this limitation.

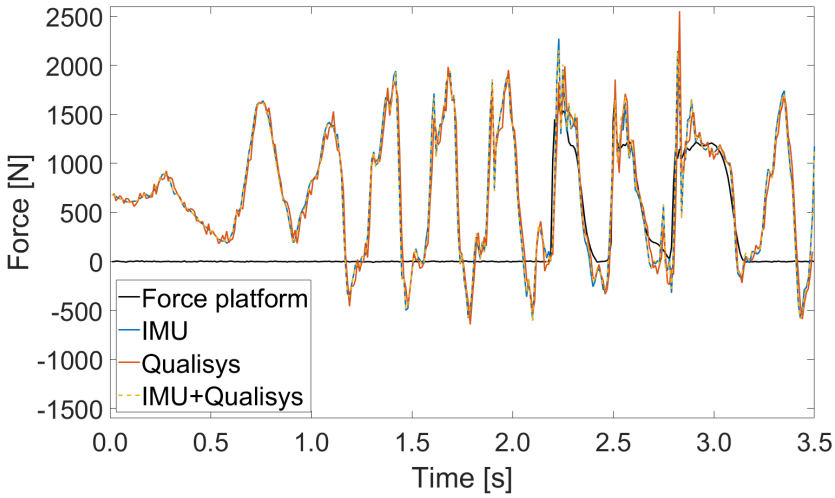

(a) Vertical force.

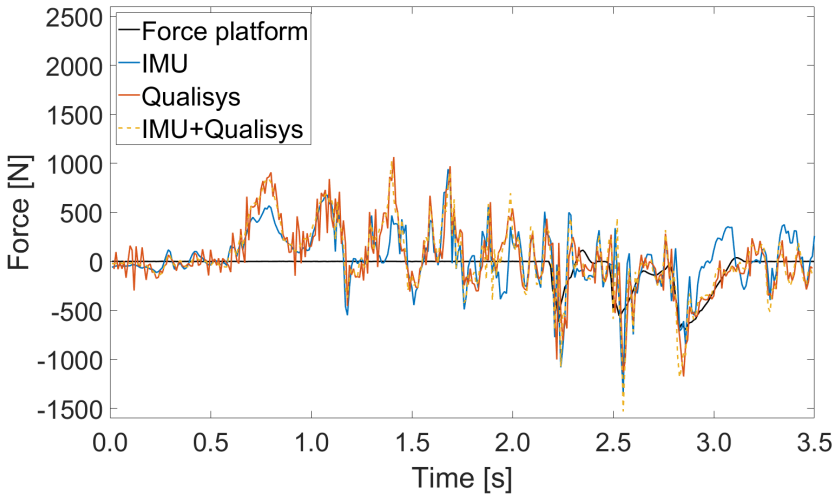

(b) Antero-posterior force.

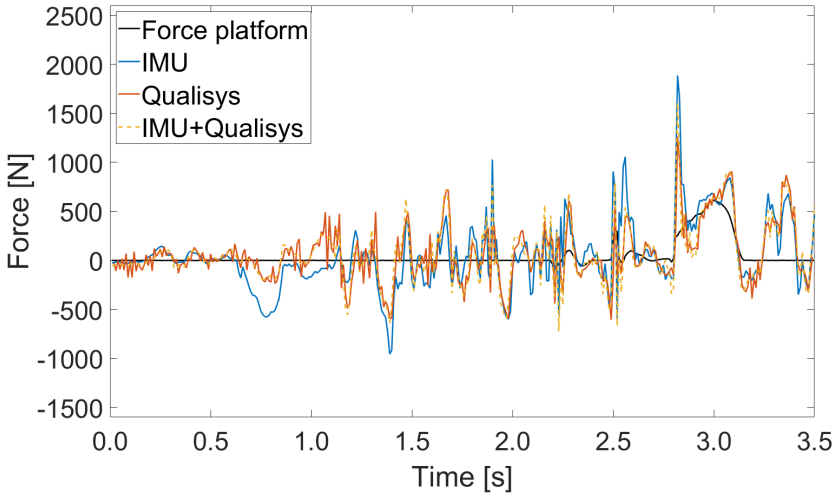

(c) Medio-lateral force.

Figure 5.13: Example of magnetic interference effect during a 90° change of direction trial.

5.3.4.2 Ground reaction force estimation

The GRF estimation, through the method described in the previous chapter (Ch. 4) using Newtonian mechanics, lead to a series of limitations when applied to the football-specific movements considered in this study. In particular, the use of the filters chosen previously resulted in the loss of deceleration steps and of important information during the beginning of the stance phase; but when lower cut-off frequencies or no filtering were considered, undesired noise was present, and forces during the flight phases were estimated. Therefore, the identification of a different technique to predict the GRFs was necessary.

The analysis over the time of the GRFs, measured with the force platforms, and the accelerations in the global system of individual segments revealed a correspondence between specific segments' acceleration peaks and GRF impact peaks, which differ between movements and axes. Therefore, an approach similar to the one described by Clark et al. [112, 113] was used. The details of the method used by Clark et al. [112, 113] are reported in section 2.4.1.5. To summarise, the authors developed a two-mass model by overlapping two individual force-time waveforms, which describe the collision of the lower limb with the running surface and the motion of the remainder of the body mass throughout the stance phase. The authors found that these two mechanical phenomena acting in parallel are sufficient to predict the vertical GRF during steady-speed level running, where no net vertical displacement of the CoM over each step and constant speed were assumed.

The high-intensity movements considered in this study present mechanical differences within each task, since the body's CoM does not move at constant speed and with constant vertical height, and has different positions respect to the CoP when the athletes accelerate, decelerate or prepare and perform changes of direction of different angles. For these reasons, it was not assumed that the estimation of the GRFs can be limited to a model based on only two segments, and a more complex approach than the evaluation of the remainder of the body mass contribution should be considered.

Each task was divided into sub-tasks (Table 5.2) and each one was individually analysed along the three axes. All the trials recorded for each participant were considered in the definition and validation of the method, due to the small sample size.

First of all, when analysing each individual step, the stance phase events needed to be identified. For the force platform measurement, each touch-down and take-off event was selected from the vertical force component using a 20 N threshold. The stance phase events for the IMUs could be identified from the synchronisation with the force platform, however, this approach can not be used in the field, thus a relationship between the stance phase events and IMUs' accelerations was investigated.

Table 5.2: Sub-tasks considered for each task.

Straight acceleration	Cutting movement	Turning movement
First step of acceleration	Deceleration	Deceleration
Acceleration steps after first	Step prior change of direction	Step before turning
	Change of direction step	Turning step
		Step after turning
		Acceleration steps after turning

It was concluded that the touch-down can be determined from the minimum value of the shank or foot vertical global acceleration found before the highest peak preceding a period of relatively constant acceleration, at the end of which the peak found in the antero-posterior foot raw acceleration could be associated with the take-off event (Fig. 5.14).

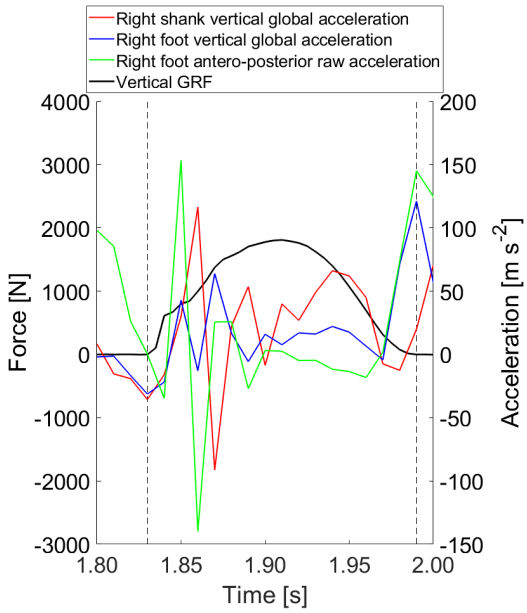

Figure 5.14: Example of stance phase identification.

The process to identify the method to estimate the GRFs was the same for each sub-task and axis, thus the general approach is described in the following paragraphs, in parallel to an example. The sub-task reported as example is the second step of acceleration and the GRF estimation along the antero-posterior axis was considered (Fig. 5.15a). The steps of the process are reported in figure 5.15.

The accelerations measured by each IMU were plotted against the GRF measured with the force platform, in order to identify the segment or combination of segments responsible for the impact peaks recorded at the beginning of the stance phase. Once the specific segment or segments were identified, the percentage of mass involved was investigated. Differently from Clark et al. [112,113], the mass percentages considered were not arbitrary values but consisted in the mass percentage of the selected segment

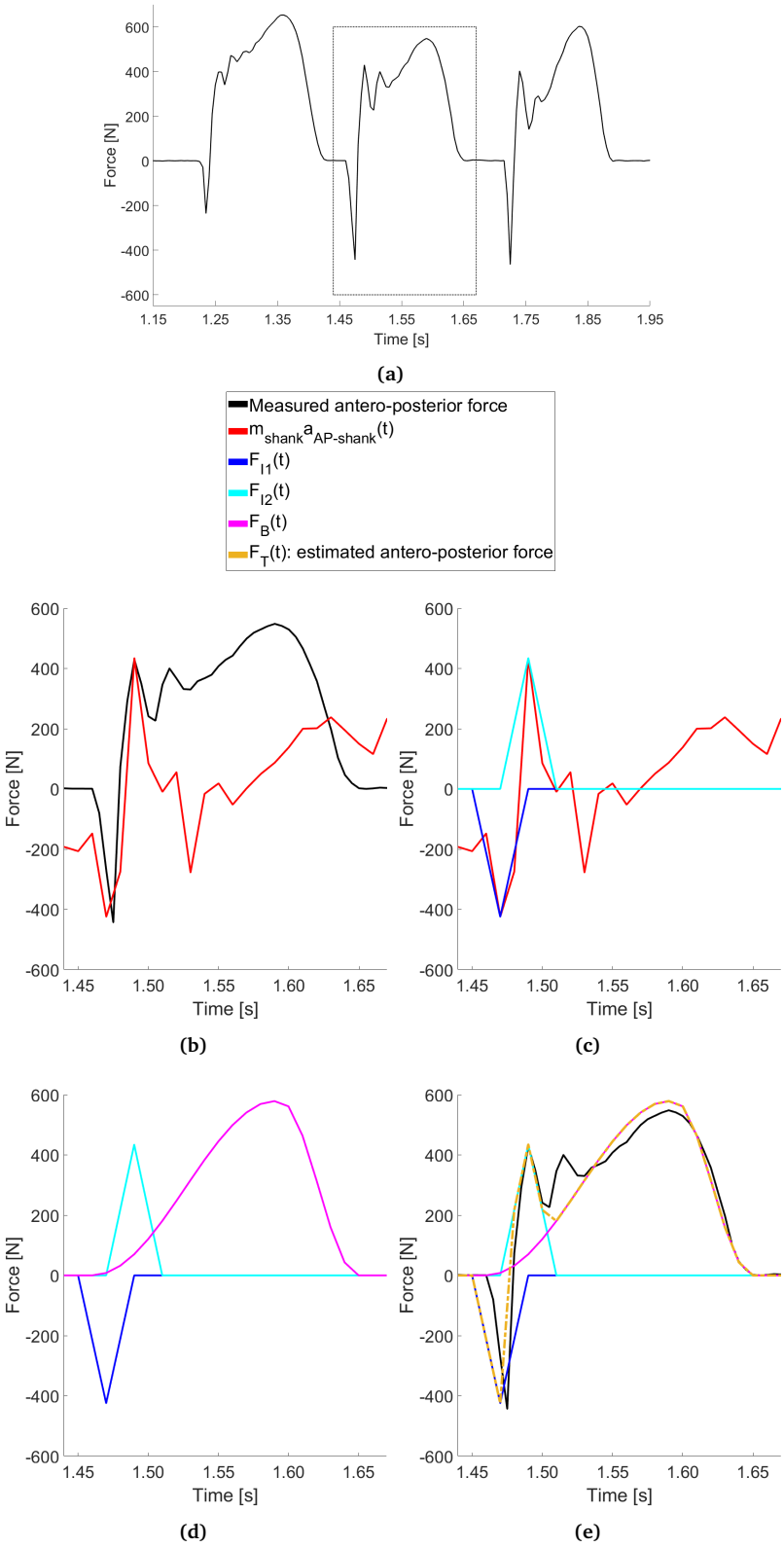

Figure 5.15: Example of the steps of the GRF estimation process.

or the sum of this specific segment mass with the distal and proximal ones, where all values were derived from Zatsiorsky-Seluyanov's inertia parameters (Table 5.1). This approach was followed since it was assumed that a mechanical explanation could al-

ways be possible by investigating the position of the CoM compared to the CoP. In the example (Fig. 5.15b), the measured GRF presents a negative and a positive impact peak during the beginning of the stance phase, with the same peak locations identified in the shank acceleration curve profile; in order to obtain the best magnitude fit, different mass percentages were analysed: shank mass (4.33% BW), sum of shank and foot mass (5.70% BW) and lower limb mass (19.86% BW); data from table 5.1. The best fit was found by considering the shank segment mass percentage.

The forces associated with the negative and positive impact peaks, F_{I1} and F_{I2} respectively (Fig. 5.15c), were calculated using equation 2.1:

$$F_{I1}(t) = \frac{m_{shank} a_{shank}(B_{I1})}{2}\left[1+\cos\left(\frac{t-B_{I1}}{0.02}\pi\right)\right] \text{ for } B_{I1}-0.02 \leq t \leq B_{I1}+0.02 \tag{5.18}$$

$$F_{I2}(t) = \frac{m_{shank} a_{shank}(B_{I2})}{2}\left[1+\cos\left(\frac{t-B_{I2}}{0.02}\pi\right)\right] \text{ for } B_{I2}-0.02 \leq t \leq B_{I2}+0.02 \tag{5.19}$$

where B_{I1} and B_{I2} are the first and second peak centre locations, respectively. A constant value of 0.02 s was chosen as the half-width time interval (variable C in equation 2.1), because the impulse profile can be considered symmetric, and this value represents a good match for the impact peak durations. This number was representative for the impact peak half-width time interval for most of the sub-tasks and directions, however this could be limited by the low sample frequency of the IMUs' recordings.

To determine the remainder part of the force curve profile, the use of the total GRI was compared with the CoM acceleration, considered as the LPT segment acceleration, and the sum of multiple segments accelerations. The best fit in the force amplitude determination was found by considering the acceleration of each one of the segments not contributing during the impact. In the example, the force curve $F_B(t)$ (Fig. 5.15d) was calculated, using equation 2.2, as:

$$F_B(t) = \begin{cases} \overline{\sum_{i=1}^{7} m_i a_i(t)}\left[1+\cos\left(\frac{t-(t_0+0.7t_C)}{0.7t_C}\pi\right)\right] & \text{for } t_0 \leq t \leq t_0+0.7t_C \\ \overline{\sum_{i=1}^{7} m_i a_i(t)}\left[1+\cos\left(\frac{t-(t_0+0.7t_C)}{0.3t_C}\pi\right)\right] & \text{for } t_0+0.7t_C < t \leq t_f \end{cases} \tag{5.20}$$

where t_0 is the initial contact time, t_f the final contact time, t_C the contact time, m_i and a_i the mass and acceleration of the i-th segment, where the only segment excluded in the calculation of this example was the shank of the stance leg, considered in F_{I1} and F_{I2}. In this example, the peak centre location was identified as the 70% of the stance phase, which corresponds to an arbitrary value determined from the observation of the measured GRF, where a constant location was identified. For the majority of the other sub-tasks and axes, the peak centre location corresponds to the acceleration peak of a specific segment, which is part of the remainder of the body mass contribution.

Finally, the total force $F_T(t)$ was calculated through the combination of the previous forces (Fig. 5.15e) as:

$$F_T(t) = \begin{cases} F_{I1}(t) & \text{for } t_0 \leq t \leq B_{I1} \\ F_{I2}(t) & \text{for } B_{I1} < t \leq B_{I2} \\ max(F_{I2}, F_B) & \text{for } B_{I2} < t \leq t_f \end{cases} \tag{5.21}$$

5.3.5 Statistical analysis

Due to the small amount of participants, all trials were considered in the calculation of the errors, which were evaluated for each sub-task separately. Measured and estimated GRFs were normalised to each participant's body mass and the resultant GRF was calculated from the three individual force components, in order to evaluate the method and compare it with previous research. The accuracy of the proposed method to estimate the GRFs was assessed using functional limits of agreement (FLoA) [128], and absolute and relative curve RMSE. Moreover, the following GRF loading characteristics were calculated: impulse, impact peak, loading rate, and active peak. The errors in the estimation of these characteristics were defined as the percentage difference between the measured and estimated data. Curve RMSE was rated as very low (< 1 N kg^{-1}), low ($1-2$ N kg^{-1}), moderate ($2-3$ N kg^{-1}), high ($3-4$ N kg^{-1}) or very high (> 4 N kg^{-1}), and estimated GRF loading characteristics errors were rated as very low ($< 5\%$), low ($5-10\%$), moderate ($10-15\%$), high ($15-20\%$) or very high ($> 20\%$), according to Verheul et al. [111]. The accuracy in the selection of the stance phase events was evaluated by comparing the contact times through the RMSEs.

Spearman's rank correlation coefficients were calculated for the GRF loading characteristics and the contact times, in order to evaluate the ability of the method to correctly rank these variables. High correlations (> 0.70) will provide the possibility to use these variables to rank shoe-surface interactions and identify the conditions that allow players to utilise the highest amount of traction and to achieve better performances.

All data were processed using Matlab R2019a (Mathworks, Natick, MA, USA).

5.4 Results

The best and representative results for each sub-task were identified from the absolute RMSE as the steps with the lowest value and the error closer to the mean, respectively. These are reported in figures 5.16 and 5.17.

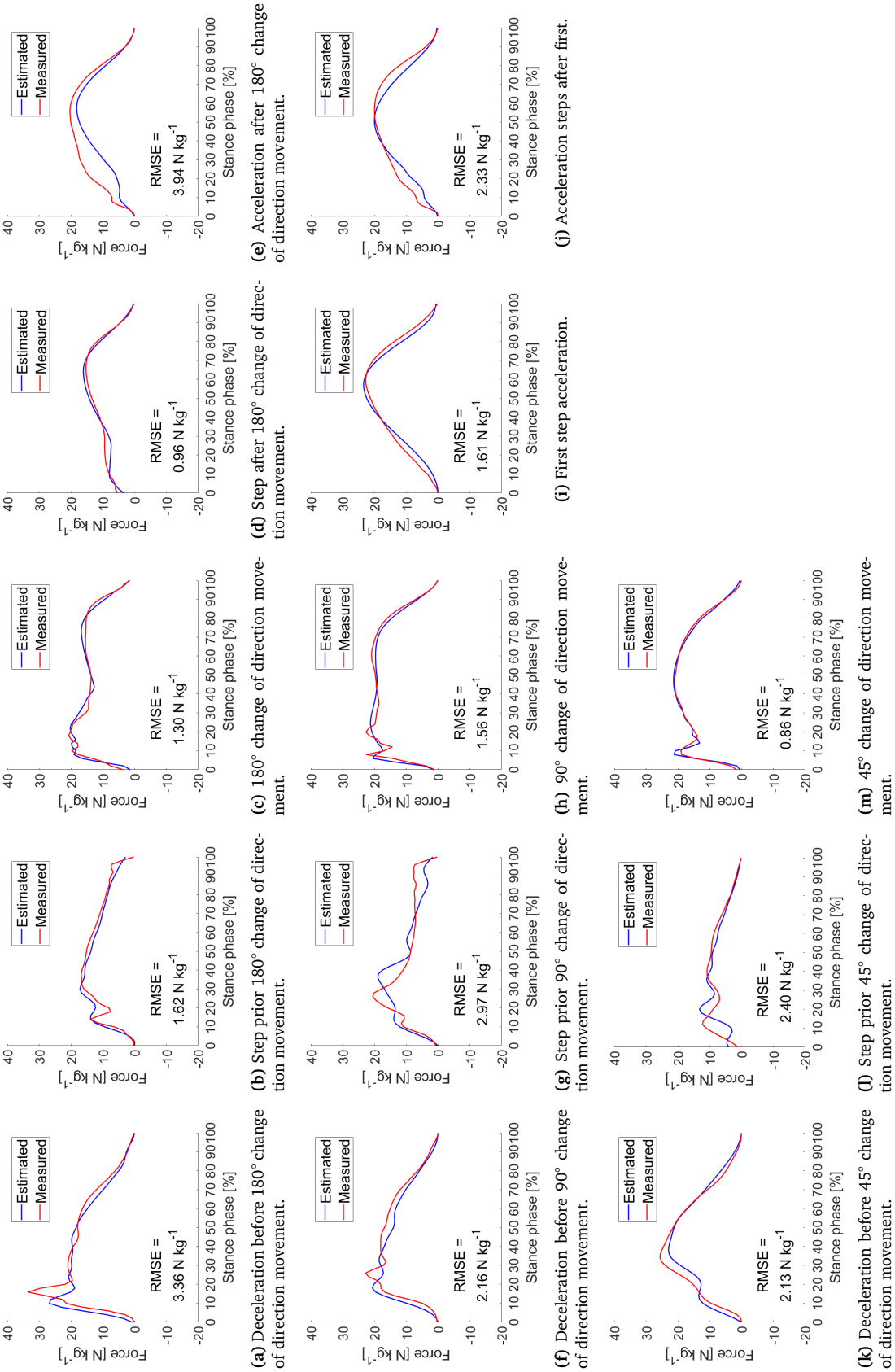

(a) Deceleration before 180° change of direction movement.

(b) Step prior 180° change of direction movement.

(c) 180° change of direction movement.

(d) Step after 180° change of direction movement.

(e) Acceleration after 180° change of direction movement.

(f) Deceleration before 90° change of direction movement.

(g) Step prior 90° change of direction movement.

(h) 90° change of direction movement.

(i) First step acceleration.

(j) Acceleration steps after first.

(k) Deceleration before 45° change of direction movement.

(l) Step prior 45° change of direction movement.

(m) 45° change of direction movement.

Figure 5.16: Best measured (red line) and estimated (blue line) GRF curve profiles for each movement analysed.

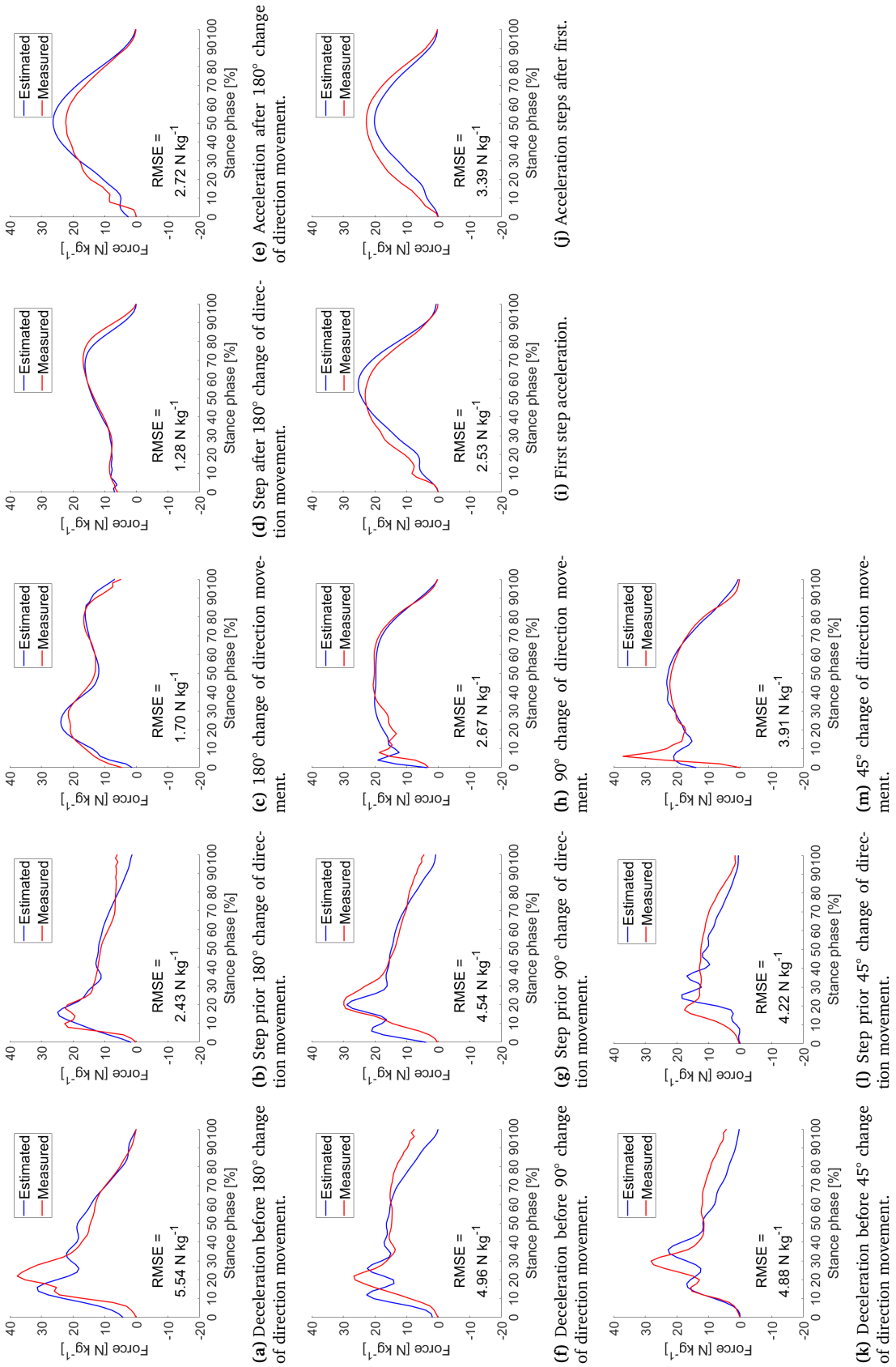

(a) Deceleration before 180° change of direction movement.
(b) Step prior 180° change of direction movement.
(c) 180° change of direction movement.
(d) Step after 180° change of direction movement.
(e) Acceleration after 180° change of direction movement.
(f) Deceleration before 90° change of direction movement.
(g) Step prior 90° change of direction movement.
(h) 90° change of direction movement.
(i) First step acceleration.
(j) Acceleration steps after first.
(k) Deceleration before 45° change of direction movement.
(l) Step prior 45° change of direction movement.
(m) 45° change of direction movement.

Figure 5.17: Representative measured (red line) and estimated (blue line) GRF curve profiles for each movement analysed.

To aid interpretation of the RMSE, its distribution for each movement is reported for the resultant force in figure 5.18.

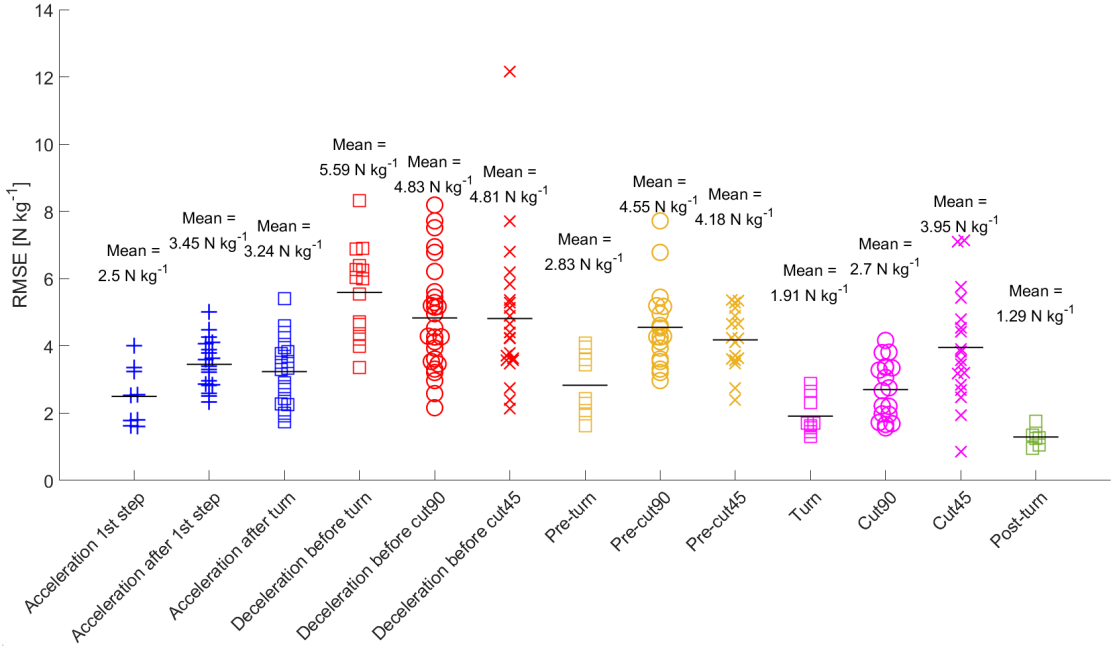

Figure 5.18: Resultant GRF curve RMSE distribution for each sub-task (Table 5.2).

The FLoA were calculated for each sub-task of the five movements performed, and for each one of them the measured and estimated resultant GRF comparison is reported in figures 5.19 to 5.21. The best accuracy in the force curve profile was achieved during the mid-stance for each sub-task, and the worst in the first 30% of the stance phase when impact peaks are present. A comparison between the sub-tasks shows that the errors increase with the movement intensity, with the deceleration steps presenting the worst results and larger limits of agreement both in the mid-stance and in the impact peak force estimation, and the changes of direction steps having the best results in the overall force curve profile.

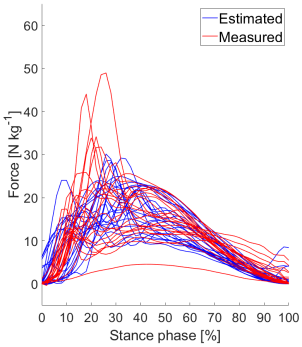

(a) Deceleration before 45° change of direction movement curve profile.

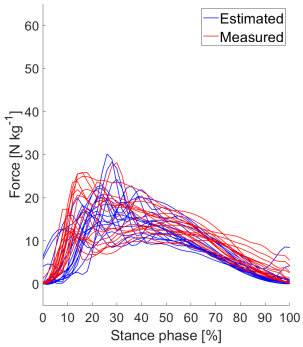

(b) Step prior 45° change of direction movement curve profile.

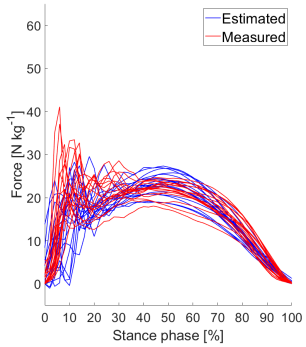

(c) 45° change of direction movement curve profile.

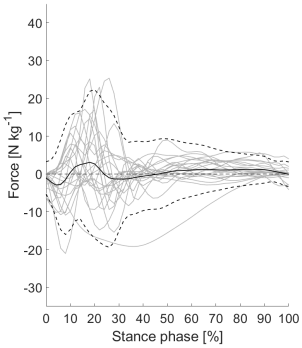

(d) Deceleration before 45° change of direction movement FLoA.

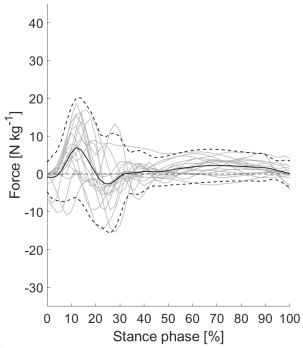

(e) Step prior 45° change of direction movement FLoA.

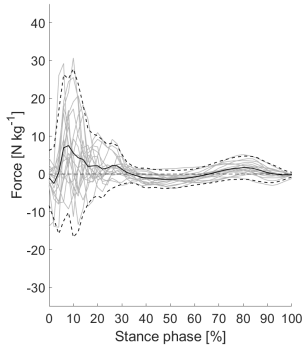

(f) 45° change of direction movement FLoA.

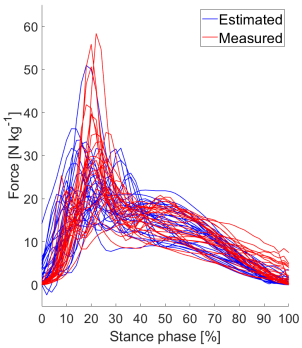

(g) Deceleration before 90° change of direction movement curve profile.

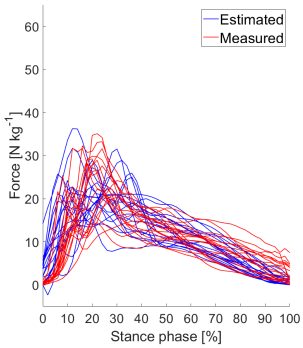

(h) Step prior 90° change of direction movement curve profile.

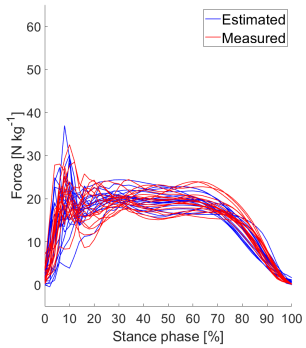

(i) 90° change of direction movement curve profile.

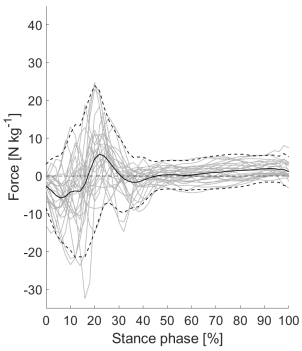

(j) Deceleration before 90° change of direction movement FLoA.

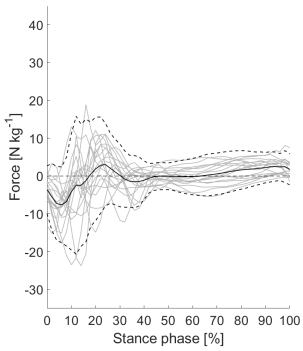

(k) Step prior 90° change of direction movement FLoA.

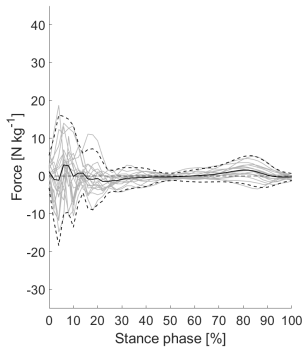

(l) 90° change of direction movement FLoA.

Figure 5.19: Resultant GRF curve profile and FLoA for 45° and 90° change of direction tasks.

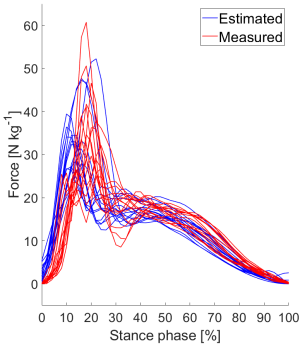

(a) Deceleration before 180° change of direction movement curve profile.

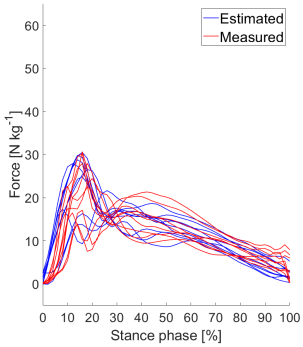

(b) Step prior 180° change of direction movement curve profile.

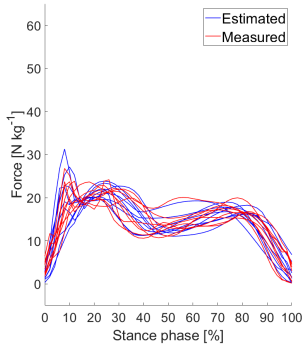

(c) 180° change of direction movement curve profile.

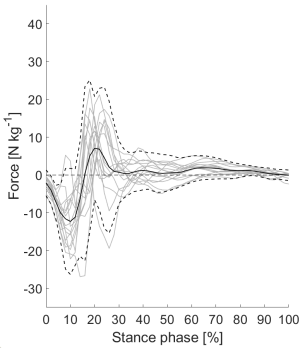

(d) Deceleration before 180° change of direction movement FLoA.

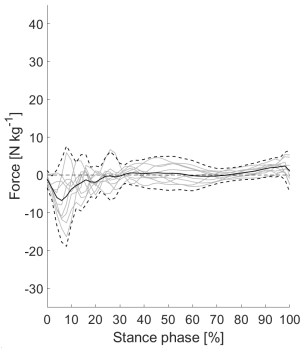

(e) Step prior 180° change of direction movement FLoA.

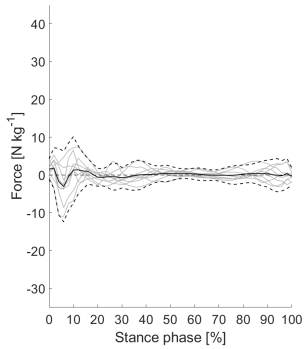

(f) 180° change of direction movement FLoA.

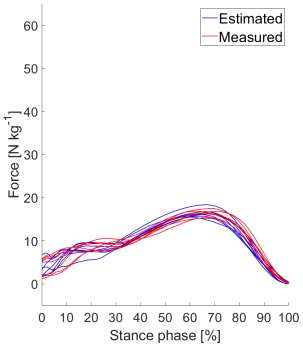

(g) Step after 180° change of direction movement curve profile.

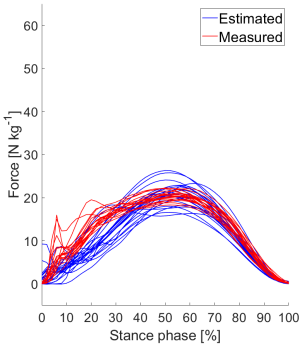

(h) Acceleration after 180° change of direction movement curve profile.

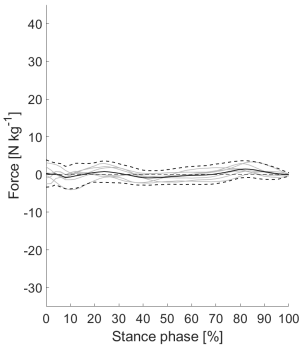

(i) Step after 180° change of direction movement FLoA.

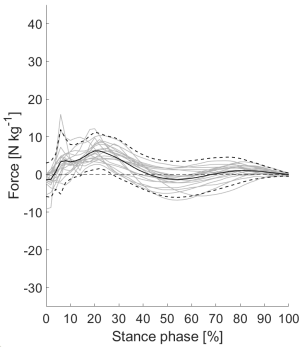

(j) Acceleration after 180° change of direction movement FLoA.

Figure 5.20: Resultant GRF curve profile and FLoA for 180° change of direction task.

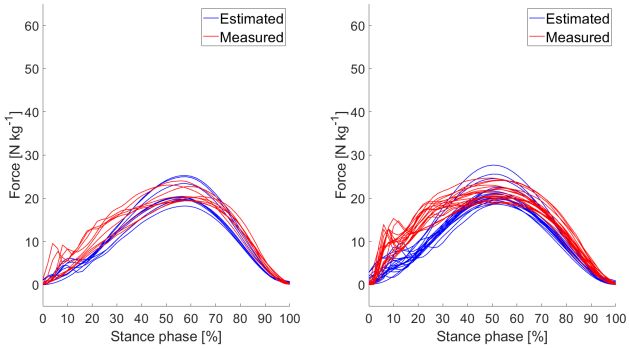

(a) First step of acceleration curve profiles.

(b) Acceleration steps after first curve profiles.

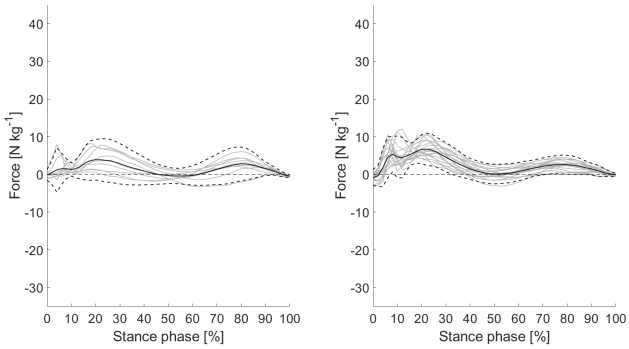

(c) First step of acceleration FLoA.

(d) Acceleration steps after first FLoA.

Figure 5.21: Resultant GRF curve profile and FLoA for the acceleration steps.

In tables 5.3 to 5.7 are reported the curve absolute and relative RMSE, and the GRF loading characteristics errors obtained for each sub-task in the estimation of resultant, horizontal, vertical, antero-posterior and medio-lateral force, respectively. As it can be seen from table 5.3, the resultant GRF errors are related to the intensity of the task, with lower RMSE obtained for the slowest movement analysed, or rather, turn (1.91 ± 0.6 N kg^{-1}) and post-turn (1.29 ± 0.3 N kg^{-1}) steps, and higher errors for the deceleration steps ($4.81 - 5.59$ N kg^{-1}), which represent the sub-task of higher intensity and with larger impacts. This trend is confirmed also for the same type of movement, in particular the errors for the change of direction manoeuvres equal to 1.91, 2.70 and 3.95 N kg^{-1} for 180°, 90° and 45°, respectively, since cutting manoeuvres of smaller angles are performed at higher intensity; and in the deceleration, with errors of 4.81, 4.83 and 5.59 N kg^{-1} for 45°, 90° and 180° changes of direction angle, where an increase in the cutting angle needs to be performed at a lower speed, thus higher decelerations are required. Moderate to low errors were obtained for the impulse errors ($2.4 - 13.7$%), with the exception of the acceleration steps after the first one (18.4%) and the deceleration before the 45° change of direction (18.5%); and for the active peak force error ($3.6 - 11.6$%), with the exception of the deceleration before the 45° cut manoeuvre (15.6%) and the step prior the 90° cut (17.7%). The

impact peak force was predicted with low to moderate errors for the turn movement and the steps before it, including the deceleration (5.1 − 13.4%), whereas the impact peak force for all the other sub-tasks and all the loading rates were estimated with high or very high errors (15.5 − 60.3% and 22.7 − 86.1%, respectively).

The vertical force (Table 5.5) was predicted with the same trend highlighted for the resultant force curve RMSE, with turn and post-turn stance phases reporting the lowest errors (1.78 ± 0.6 N kg^{-1} and 1.58 ± 0.7 N kg^{-1}, respectively); deceleration steps with the highest errors, which increase with the change of direction angle (4.37, 4.39 and 5.41 N kg^{-1} for 45°, 90° and 180°, respectively); and errors increasing from 1.78, 2.52 to 4.12 N kg^{-1} for the 180°, 90° and 45° change of direction tasks. Moderate to low errors were obtained for the active peak force errors (3.7 − 14.9%), with the exception of the deceleration before the 45° cut manoeuvre (17.6%). Impulses were estimated with low to very low errors for the changes of direction and the steps before and after the turn (2.4 − 8.7%); moderate errors for the first step of acceleration, deceleration before 90° and 180° changes of direction, and the step prior the 90° cutting manoeuvre (11.0 − 14.2%); and high to very high errors for the acceleration steps after the first one and after the turn, and all the steps analysed before the 45° cut (15.6 − 21.5%). Similarly to the resultant force, the vertical GRF impact peaks and loading rates were predicted with high to very high errors, with the exception of the impact peaks estimated in the steps before the turn stance phases.

The horizontal force (Table 5.4) curve RMSE presents the same trend as the other forces considered for the changes of direction, with the error increasing from 1.68 to 1.86 and 2.33 N kg^{-1} for the change of direction angle increasing from 45° to 90° and 180°, respectively; whereas the same trend was not found for the deceleration steps. Active peak force and impulse errors were estimated with lower accuracy compared to the vertical force. With the former estimated with low to moderate errors (9.2 − 11.9%) for the acceleration, excluding the first step, the stance phases prior and post turn, and all the changes of direction. The latter reporting very low to moderate errors (4.6 − 14.3%) for the second and third step of acceleration, acceleration after turn, deceleration before 90° change of direction manoeuvre, and all the changes of direction and the steps prior them.

Table 5.3: RMSE, impulse, impact peak, loading rate and active peak errors of the resultant GRF estimated for each sub-task. Values are mean ± standard deviations and either absolute and relative errors compared to the resultant GRF component measured with the force platforms. Very low, low, moderate, high and very high errors are highlighted with dark green, light green, yellow, light red and dark red colours, respectively.

	RMSE		Impulse error		Impact peak error		Loading rate error		Active peak error	
	[N kg^{-1}]	[%]	[N s kg^{-1}]	[%]	[N kg^{-1}]	[%]	[N kg^{-1} s^{-1}]	[%]	[N kg^{-1}]	[%]
Acceleration - first step	2.50±0.9	20.1±6.7	0.34±0.2	13.7±7.7	2.37±2.3	39.4±28.8	335.4±402.8	69.7±51.4	−0.26±1.0	3.6±2.7
Acceleration - second and third step	3.45±0.7	25.5±5.4	0.41±0.1	18.4±4.1	5.99±1.4	60.3±17.9	621.0±338.5	86.1±44.6	0.16±1.3	4.5±3.7
Acceleration after turn	2.92±0.9	23.0±7.2	0.29±0.2	12.3±7.2	3.52±5.0	42.9±37.7	43.5±722.4	63.3±45.4	−0.69±1.7	6.6±6.8
Deceleration before turn	5.59±1.4	43.3±11.7	0.15±0.2	11.3±6.3	1.94±5.8	13.4±10.4	−471.8±417.3	37.6±22.0	1.61±1.9	10.0±9.4
Deceleration before cut 90°	4.83±1.6	41.0±12.3	0.14±0.2	11.1±6.6	3.70±8.3	24.8±15.4	−140.7±414.6	34.7±22.2	−0.40±2.4	11.6±6.4
Deceleration before cut 45°	4.81±2.1	62.0±96.0	0.10±0.3	18.5±28.0	1.63±6.6	28.0±30.8	71.1±302.6	34.3±16.9	−1.20±4.8	15.6±28.5
Post-turn	1.29±0.3	13.0±2.8	0.05±0.2	5.1±3.6					0.65±0.9	9.1±6.8
Pre-turn	2.83±0.9	24.9±8.5	−0.08±0.2	6.4±3.7	−0.47±1.5	5.1±3.4	−106.1±275.3	22.7±15.1	0.19±1.8	9.5±5.9
Pre-cut 90°	4.55±1.2	41.6±11.3	0.10±0.3	10.0±7.4	1.31±6.1	23.9±13.7	−277.4±381.7	38.0±24.1	−0.57±4.4	17.7±8.3
Pre-cut 45°	4.18±0.9	41.8±8.9	0.22±0.2	13.7±5.5	−0.40±3.5	15.5±10.2	180.2±264.2	42.4±20.0	0.70±2.2	8.2±9.4
Turn	1.91±0.6	13.0±4.1	0.00±0.3	2.4±2.0	−0.54±4.2	12.4±9.2	−92.6±97.6	24.5±6.2	0.17±1.3	4.4±3.3
Cut 90 °	2.70±0.9	17.5±5.5	0.13±0.2	3.1±3.3	−1.45±4.9	16.2±12.7	−251.9±346.9	35.1±23.6	0.15±1.3	4.0±4.8
Cut 45°	3.95±1.7	24.3±9.5	0.20±0.2	6.0±3.9	5.07±6.2	21.8±18.8	296.6±530.8	46.4±26.3	−0.83±1.2	4.6±3.5

Table 5.4: RMSE, impulse, impact peak, loading rate and active peak errors of the horizontal GRF component estimated for each sub-task. Values are mean ± standard deviations and either absolute and relative errors compared to the horizontal GRF component measured with the force platforms. Very low, low, moderate, high and very high errors are highlighted with dark green, light green, yellow, light red and dark red colours, respectively.

	RMSE		Impulse error		Impact peak error		Loading rate error		Active peak error	
	[N kg^{-1}]	[%]	[N s kg^{-1}]	[%]	[N kg^{-1}]	[%]	[N kg^{-1} s^{-1}]	[%]	[N kg^{-1}]	[%]
Acceleration - first step	1.39±0.5	28.4±7.1	0.18±0.1	18.6±11.1	−1.1±1.4	36.5±30.0	−9.9±207.4	74.4±36.4	1.21±0.7	15.3±9.1
Acceleration - second and third step	1.24±0.4	28.4±6.6	0.05±0.1	10.4±9.2	−0.1±2.0	40.9±28.2	27.3±260.1	57.0±35.6	0.51±0.9	11.5±8.6
Acceleration after turn	1.45±0.7	30.9±13.5	0.03±0.1	8.6±8.6	0.0±2.4	26.8±31.9	−137.7±443.7	59.9±41.0	−0.34±1.2	11.9±8.9
Deceleration before turn	2.77±0.9	55.9±17.5	0.16±0.1	21.6±15.6	6.7±4.3	50.7±31.3	58.7±194.7	35.0±21.7	1.86±1.7	20.1±17.4
Deceleration before cut 90°	3.22±1.1	56.0±19.3	−0.01±0.2	13.4±9.7	0.2±4.8	32.7±13.3	−100.2±235.0	38.4±27.2	0.00±2.2	18.3±11.7
Deceleration before cut 45°	2.77±1.0	98.7±136.9	0.02±0.2	23.7±29.0	0.0±4.8	37.7±35.7	−100.3±336.1	43.9±41.2	−0.45±2.1	26.5±24.6
Post-turn	1.26±0.8	25.8±14.1	−0.20±0.2	13.0±12.1					0.36±0.6	12.9±7.3
Pre-turn	2.26±1.0	34.5±17.2	−0.04±0.2	9.2±5.4	−1.9±2.3	14.4±10.5	−163.0±240.8	34.3±29.4	0.13±1.5	9.2±10.7
Pre-cut 90°	3.55±1.2	61.8±22.2	−0.02±0.2	12.8±11.0	−0.6±4.4	29.9±13.3	−185.4±244.8	44.1±27.3	0.67±3.1	31.2±9.6
Pre-cut 45°	2.26±0.6	63.2±16.3	0.03±0.1	14.3±11.7	−1.0±2.8	29.1±14.0	−22.3±292.2	36.9±30.8	−0.29±1.6	19.4±13.0
Turn	1.68±0.3	18.6±2.9	0.17±0.2	4.6±3.4	−0.0±1.7	8.6±6.9	6.5±45.1	13.8±8.7	0.79±1.5	9.8±8.5
Cut 90 °	1.86±0.6	21.7±6.7	0.16±0.2	6.9±5.6	0.8±3.0	16.8±18.4	37.0±136.3	27.6±21.7	−0.11±1.9	10.4±10.3
Cut 45°	2.33±0.6	30.2±6.6	0.16±0.2	10.7±6.8	−0.2±4.2	24.7±15.3	−56.3±353.0	37.3±24.7	0.18±1.2	9.8±7.3

Table 5.5: RMSE, impulse, impact peak, loading rate and active peak errors of the vertical GRF component estimated for each sub-task. Values are mean ± standard deviations and either absolute and relative errors compared to the vertical GRF component measured with the force platforms. Very low, low, moderate, high and very high errors are highlighted with dark green, light green, yellow, light red and dark red colours, respectively.

	RMSE		Impulse error		Impact peak error		Loading rate error		Active peak error	
	[N kg^{-1}]	[%]	[N s kg^{-1}]	[%]	[N kg^{-1}]	[%]	[N kg^{-1} s^{-1}]	[%]	[N kg^{-1}]	[%]
Acceleration - first step	2.46±0.8	21.6±7.0	0.32±0.2	14.2±8.1					−0.70±1.0	4.6±3.0
Acceleration - second and third step	3.61±0.8	28.5±6.4	0.44±0.1	21.4±5.2	6.0±0.4	75.6±10.3	565.8±159.0	105.4±11.0	0.21±1.4	5.1±3.9
Acceleration after turn	2.93±0.8	25.2±7.1	0.32±0.2	15.6±8.5	1.3±4.8	32.6±38.2	261.5±446.8	74.0±31.4	−0.59±1.7	7.1±6.4
Deceleration before turn	5.41±1.4	46.4±14.4	0.10±0.2	11.0±6.6	−0.3±5.5	12.6±10.4	−559.8±413.6	42.6±27.1	1.36±1.2	8.5±7.2
Deceleration before cut 90°	4.39±1.6	43.3±13.0	0.20±0.2	14.0±9.5	2.6±7.3	23.8±17.6	−126.7±355.6	29.8±21.6	−0.33±2.3	11.9±7.5
Deceleration before cut 45°	4.37±2.0	61.5±95.5	0.13±0.3	21.5±28.0	1.0±7.3	36.7±24.1	87.8±325.7	37.5±16.6	−0.48±4.8	17.6±28.1
Post-turn	1.58±0.7	18.1±8.1	0.23±0.2	8.7±5.9					0.45±0.9	6.1±9.6
Pre-turn	2.29±0.7	24.6±7.4	−0.05±0.1	6.9±4.6	−0.1±1.6	5.8±6.2	−45.1±273.4	17.8±19.6	−0.10±1.5	9.3±8.1
Pre-cut 90°	3.92±1.0	42.8±11.5	0.18±0.2	12.6±10.6	0.4±6.1	25.0±17.6	−131.9±207.4	27.3±17.1	−0.09±3.3	14.9±9.4
Pre-cut 45°	3.91±1.0	42.4±10.9	0.25±0.2	17.3±8.1	−0.4±4.5	27.5±12.9	181.4±208.8	45.4±24.9	0.81±2.4	11.5±9.1
Turn	1.78±0.6	15.2±5.4	−0.08±0.3	2.4±3.1	−1.9±5.0	16.6±15.3	−97.7±77.1	21.8±15.5	−0.89±1.0	7.0±2.6
Cut 90 °	2.52±0.8	19.7±6.0	0.09±0.2	3.1±2.9	−1.2±5.8	23.3±17.1	−209.1±408.4	43.7±23.0	0.27±0.8	3.7±2.4
Cut 45°	4.12±1.7	29.1±11.5	0.19±0.2	7.6±5.1	5.3±6.4	28.4±19.7	349.6±547.9	48.9±31.4	−1.23±1.0	6.3±3.9

Table 5.6: RMSE and impulse errors of the antero-posterior GRF component estimated for each sub-task. Values are mean ± standard deviations and either absolute and relative errors compared to the antero-posterior GRF component measured with the force platforms. Very low, low, moderate, high and very high errors are highlighted with dark green, light green, yellow, light red and dark red colours, respectively.

	RMSE		Impulse error	
	[N kg^{-1}]	[%]	[N s kg^{-1}]	[%]
Acceleration - first step	1.49±0.6	32.2±11.0	0.23±0.1	27.4±12.3
Acceleration - second and third step	1.47±0.5	38.7±11.9	0.09±0.1	17.1±10.7
Acceleration after turn	1.71±0.8	−40.2±17.4	−0.09±0.1	13.5±10.4
Deceleration before turn	2.77±0.9	−58.8±18.6	−0.18±0.1	25.0±17.3
Deceleration before cut 90°	3.03±1.1	−56.3±20.0	−0.04±0.2	15.0±10.5
Deceleration before cut 45°	2.63±1.0	−41.3±222.2	−0.05±0.2	36.6±57.1
Post-turn	1.29±0.7	−27.1±113.5	0.21±0.2	14.0±11.5
Pre-turn	2.16±1.0	−34.0±17.8	0.01±0.1	9.5±4.7
Pre-cut 90°	3.30±1.2	−61.0±24.7	−0.05±0.2	14.2±11.8
Pre-cut 45°	2.03±0.7	−74.4±25.9	−0.03±0.1	19.3±14.6
Turn	1.70±0.3	−19.0±2.8	−0.16±0.2	4.4±3.2
Cut 90 °	1.59±0.5	−28.5±8.8	−0.07±0.2	7.4±4.8
Cut 45°	1.99±0.5	−102.3±46.1	0.10±0.2	33.0±34.8

Table 5.7: RMSE and impulse errors of the medio-lateral GRF component estimated for each sub-task. Values are mean ± standard deviations and either absolute and relative errors compared to the medio-lateral GRF component measured with the force platforms. Very low, low, moderate, high and very high errors are highlighted with dark green, light green, yellow, light red and dark red colours, respectively.

	RMSE		Impulse error	
	[N kg^{-1}]	[%]	[N s kg^{-1}]	[%]
Acceleration - first step	0.69±0.3	−30.7±471.2	0.07±0.1	113.5±55.6
Acceleration - second and third step	0.86±0.4	114.0±45.2	0.08±0.1	71.1±39.0
Acceleration after turn	1.12±0.5	−381.8±1376.8	0.00±0.1	92.6±118.0
Deceleration before turn	1.19±0.6	138.7±210.4	0.05±0.1	106.0±897.5
Deceleration before cut 90°	2.09±0.8	152.0±102.7	−0.14±0.1	44.6±33.9
Deceleration before cut 45°	1.61±0.7	280.7±870.0	0.00±0.1	31.2±40.3
Post-turn	0.65±0.4	116.9±303.9	−0.02±0.2	138.7±369.9
Pre-turn	1.56±0.3	471.7±923.9	−0.03±0.1	139.4±747.4
Pre-cut 90°	2.34±0.8	183.5±111.4	−0.19±0.1	53.7±34.9
Pre-cut 45°	1.56±0.6	99.8±49.3	0.02±0.1	21.2±24.0
Turn	0.91±0.2	−717.8±784.1	−0.08±0.1	207.0±241.4
Cut 90 °	1.74±0.5	30.6±7.7	0.18±0.2	11.9±8.0
Cut 45°	2.32±0.6	35.7±8.1	0.30±0.2	22.3±15.0

In the following tables (Tables 5.8 and 5.9), the Spearman's rank correlation coefficient calculated for each GRF loading characteristic considered is reported for all the sub-tasks. The impulse calculated during the change of direction stance phases is ranked with high or very high correlation (> 0.70) in both the vertical and horizontal directions, regardless the angle; whereas only the vertical impulse can be ranked with high precision for the acceleration steps. The active peak force in the vertical direction was ranked with high to very high correlation for all the sub-tasks, with the exception of the acceleration after the turning manoeuvre and the deceleration before

the 45° change of direction; whereas the active peak force in the horizontal direction was ranked with high to very high agreement for the first step of acceleration, the step after the turn and the 45° change of direction task. The contact time was estimated with a RMSE of 14 ms and a very high agreement of 0.97 was obtained for the Spearman's rank correlation coefficient.

Table 5.8: Spearman's rank correlation coefficient for impulse and active peak force. High and very high correlation are highlighted with darker green.

	Impulse					Active peak		
	AP	ML	V	H	R	V	H	R
Acceleration - first step	0.28	0.33	0.82	0.32	0.78	0.92	0.73	0.85
Acceleration - second and third step	0.59	0.32	0.88	0.54	0.87	0.80	0.55	0.82
Acceleration after turn	0.67	0.41	0.52	0.64	0.56	0.44	0.60	0.31
Deceleration before turn	0.45	0.82	0.59	0.54	0.61	0.85	0.56	0.42
Deceleration before cut 90°	0.81	0.43	0.88	0.81	0.86	0.81	0.61	0.76
Deceleration before cut 45°	0.48	0.49	0.66	0.49	0.69	0.63	0.56	0.70
Post-turn	0.79	0.57	0.29	0.79	0.46	0.80	0.80	0.60
Pre-turn	0.92	0.20	0.82	0.92	0.87	0.76	0.62	0.74
Pre-cut 90°	0.75	0.52	0.92	0.80	0.91	0.81	0.54	0.93
Pre-cut 45°	0.46	0.71	0.85	0.63	0.88	0.88	0.69	0.94
Turn	0.75	0.62	0.97	0.73	0.97	0.74	0.57	0.60
Cut 90 °	0.94	0.63	0.97	0.90	0.96	0.85	0.47	0.77
Cut 45°	0.50	0.78	0.77	0.81	0.89	0.90	0.84	0.92

Table 5.9: Spearman's rank correlation coefficient for impact peak force and loading rate. High and very high correlation are highlighted with darker green.

	Impact peak			Loading rate		
	V	H	R	V	H	R
Acceleration - first step	0.00	0.61	0.50	0.00	0.32	−0.50
Acceleration - second and third step	0.80	0.71	−0.40	1.00	0.45	−0.60
Acceleration after turn	0.50	0.36	0.60	−1.00	0.48	−0.40
Deceleration before turn	0.66	−0.06	0.75	0.23	0.32	0.39
Deceleration before cut 90°	0.72	0.44	0.74	0.69	0.44	0.49
Deceleration before cut 45°	0.68	−0.02	0.69	0.59	0.56	0.71
Post-turn						
Pre-turn	0.98	0.68	0.92	0.40	−0.07	0.30
Pre-cut 90°	0.51	0.44	0.66	0.60	0.34	0.31
Pre-cut 45°	0.82	−0.01	0.79	0.34	0.65	0.21
Turn	0.40	0.54	0.60	0.00	0.94	0.60
Cut 90 °	0.23	0.49	0.34	0.55	0.73	0.52
Cut 45°	0.11	0.27	0.19	0.11	0.64	0.28

Figure 5.22 shows the comparison between the raw accelerations recorded by the IMUs placed on the foot and shank segments (Fig. 5.22b) and the unfiltered accelerations calculated from the centre of the cluster (a_T) applied to the same sensors (Fig. 5.22a), during a 180° change of direction movement trial; where the centre of the cluster was determined from the markers' trajectories captured with the optical motion capture system. It is evident that the accelerations at the time the lower limb

impacts the ground exceed the ±16g limit, of a quantity up to four times this limit during the decelerations steps.

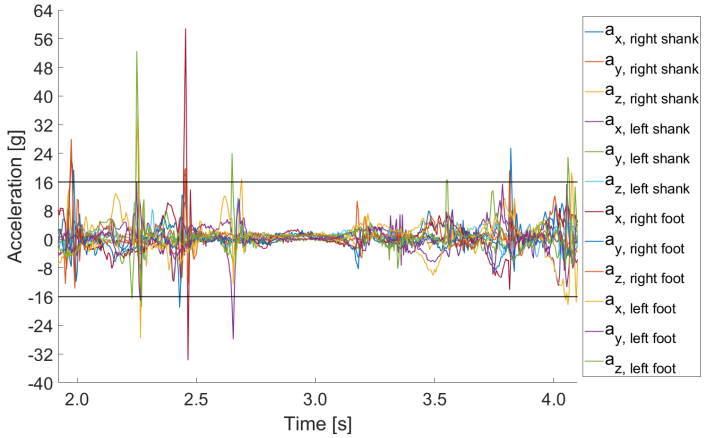

(a) Markers' accelerations.

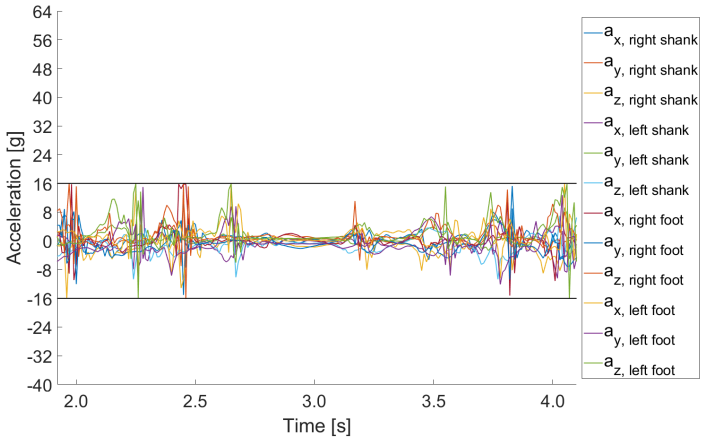

(b) IMUs' accelerations.

Figure 5.22: Accelerometer range limit, comparison between markers and IMUs' accelerations.

Another limitation is reported in figure 5.23, where two consecutive steps, recorded during a 180° change of direction movement trial, show that the impact peak force is affected not only by the accelerometer range limit, but from the 100 Hz sample frequency as well. This is highlighted by the comparison between the measured shank accelerations, with the left leg peak acceleration (red line) appearing as cut.

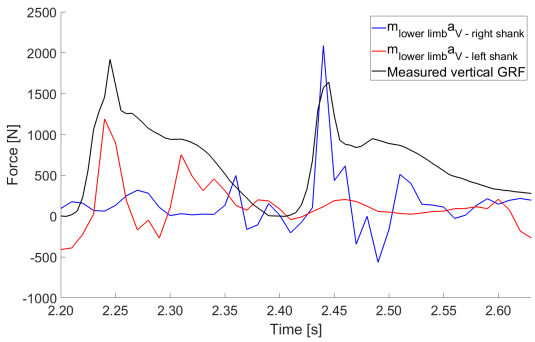

Figure 5.23: Example of the IMU sample frequency limitation.

In order to further examine the extent of these limitations, the method just described to estimate the 3D GRFs from the IMUs was applied to the unfiltered accelerations derived from the location of the centre of the clusters (a_T) for a sprint trial. The results are reported in figure 5.24.

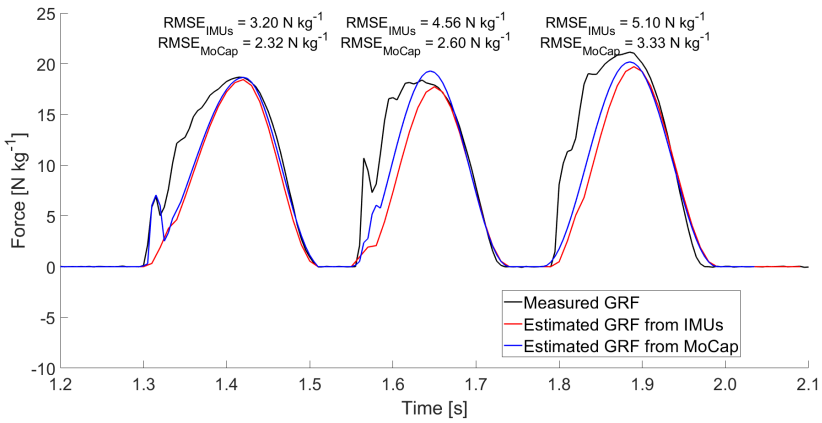

(a) Vertical GRF component.

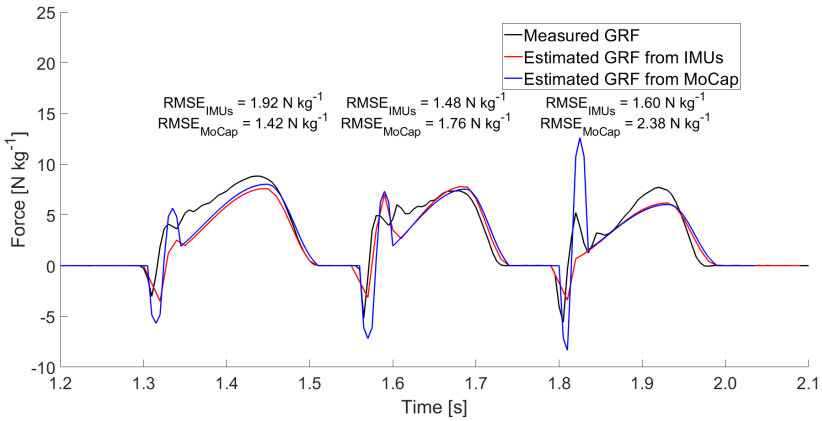

(b) Antero-posterior GRF component.

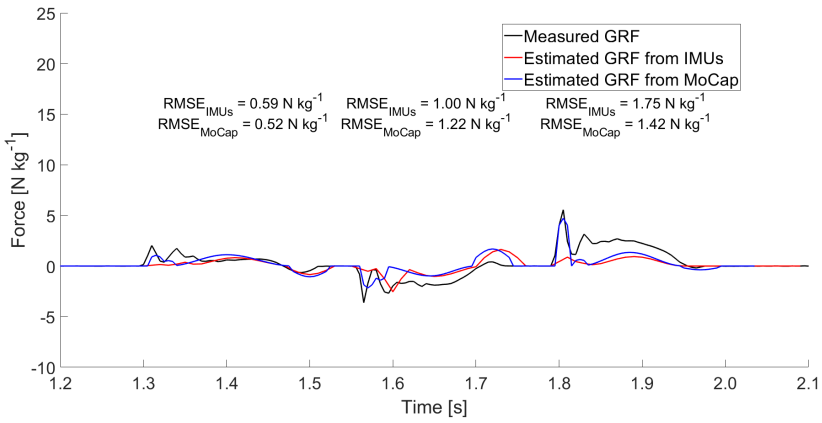

(c) Medio-lateral GRF component.

Figure 5.24: Comparison of 3D GRFs measured from the force platform (black line) and estimated from inertial (red line) and optical (blue line) motion captures, sampling respectively at 100 and 200 Hz.

5.5 Discussion

This study aimed to improve the 3D GRF estimation method compared to what was previously presented and to assess its validity during a range of high intensity football-specific tasks. Eight IMUs were attached on the body segments listed in sections 5.3.2.1 to 5.3.2.5 creating a LLT model. Each body segment is composed of a rigid and a non-rigid part, the former is represented by bones and the latter by muscles and other soft tissues, which are not rigidly attached to the skeletal part but they are linked to it through elastic and viscous connections, and act as a wobbling mass (term introduced by Gruber et al. [129]). This wobbling mass represents more than 80% of the total mass of the segment, and it can move and rotate relative to the bone becoming the source of skin-motion artefacts [130], which effect is highly variable between subjects due to factors such as differences in the amount and properties of the soft tissue covering the bones [131, 132]. During impacts, as those produced when athletes sprint, decelerate or change direction, the wobbling mass moves with respect to the underlying bone, producing vibrations and decelerating slower than the bone. This produces big differences during the impact phase, when the wobbling mass moves downwards practically unrestrained, and becomes negligible after the impact, in the active phase, when the movement is muscularly decelerated and considerably smaller accelerations occur [129, 130, 133]. The measurements of skin-mounted sensors are affected by wobbling masses, which cause a signal distortion. Several studies [131, 134, 135] compared the output of accelerometers mounted on the skin or directly to the bone and found that the mass of skin-mounted accelerometers must be as low as possible in order to obtain accurate measurements. When extra mass is added to the structure, the accelerometer and its supporting apparatus effectively become part of the vibrating system and are themselves the source of the high-frequency component. Forner-Cordero et al. [132] compared different sensor attachments characterised by different levels of tightness and mass of the bandage. The authors calculated the natural frequency of the attachment from the accelerometer signal during a heel drop from tiptoes movement to determine which attachment was the most appropriate for their biomechanical measurements. The natural frequency is determined by two factors, the amount of mass and the stiffness of the system and when the natural frequency is very close to or below the frequencies of interest, a measurement distortion will occur [131]. The authors concluded that the sensor has to be firmly attached to the skin with a preload compressing the soft tissue and increasing the stiffness of the sensor attachment. Moreover, they found that the mass of the elastic bandage did not affect the measurements significantly, therefore, the added mass becomes source of vibration only when the preload significantly exceeds the value required to overcome skin damping.

In this study, improvements were made in order to address the limitations outlined in the previous chapter (Ch. 4). Sensor mount frames were used to estimate the orientation of each sensor, addressing the magnetic interference problem, which will not be necessary for the use in the field, since magnetic interferences should not be present and, therefore, the sensors' heading measurements should be reliable. The sensors were placed in correspondence of each segment CoM, as required by a multi-segment acceleration approach; and the attachment method was improved specifically for each location in order to reduce the amount of oscillations and their variability between individuals and segments. The mass added to each segment represents an increase of 2% or lower of the total segment mass, with the exception of the feet where the added mass still represents a low addition compared to the shoe mass, therefore, it can be assumed that the benefit of the firm attachment method used compensate the increased vibrations due to the additional mass. However, future work should consider the use of lighter and smaller sensors. Moreover, the different attachment methods were compared in appendix B by observing the differences in PSD at the higher frequency components, future work should quantify the natural frequency of the attachment from the accelerometer signal during a simple movement involving impacts, such as a heel drop from tiptoes as proposed by Forner-Cordero et al. [132], before the biomechanical measurements of interest to provide an objective guide to determine if the skin-mounted sensors are attached properly.

Despite the improvements made to address the limitations outlined in the previous chapter (Ch. 4), the application of the same method to estimate 3D GRF during football-specific movements presented new challenges. As expected, the reduced presence of noise in the measurements due to the improved sensor attachment technique, led to the unsuitability of the cut-off frequencies previously selected, with the loss of some steps and of important information during the beginning of the stance phase. In addition, the use of Newton's Second Law of Motion assumes the body segments as rigid with fixed inertial parameters, instead the human body consists mainly of deformable soft tissue, that during impacts moves in a wave-like manner leading to segment shape and inertial parameter changes, therefore, assuming human limbs behaving as rigid bodies ignores a real set of forces occurring within the human body and potential mechanisms of passive force transfer and energy dissipation [133]. Therefore, the identification of a different technique to estimate the GRFs for these high-intensity movements was necessary.

Clark et al. [112, 113] found that two mechanical phenomena, the collision of the lower limb with the surface and the motion of the remainder of the body mass throughout the stance phase, are sufficient to estimate the vertical GRF component during steady-speed level running. The same approach was extended to all force compo-

nents and was found to be appropriate. However, when analysing the GRFs in the three dimensions of space and for football-specific movements, the collision of the lower limb with the surface could not be reduced to the deceleration recorded on a single body landmark, as done by Clark et al. [112, 113], but requires the examination of the contribution of each one of the three segments forming the lower limb, relative to the specific movement analysed.

This study disagrees with Clark's conclusion that the effective mass may be mechanically incorrect and unnecessary for accurate modelling. Different mass percentages, resulting from the combination of the lower limb segment masses, were analysed and it was concluded that the use of arbitrary values can be avoided. In the example presented in section 5.3.4.2, shank mass (4.33% BW), sum of shank and foot mass (5.70% BW) and lower limb mass (19.86% BW) were compared and a good fit was found by considering the shank segment mass percentage, rather than using an arbitrary value of 8.00% BW as done by Clark et al. [112, 113]. In general, higher mass percentages need to be considered during the impact phase when the movement is performed at a higher intensity, such as during deceleration steps. Moreover, when more than one impact peak is present, the mass percentage increases for the second peak compared to the first one, which is associated with a more vertical alignment of the body's CoM on the CoP.

Three studies [107–109] were found in the literature that used IMU to estimate step-averaged and instantaneous 3D GRFs during football-specific movements. Of these, two studies reported the step-averaged errors both in the vertical and horizontal direction and were considered for comparison with the errors obtained in the work reported in the previous chapter (Ch. 4) and this study (Table 5.10). Both Setuain et al. [107] and Gurchiek et al. [108] applied Newton's second Law of Motion to the acceleration of a single sensor attached on the subjects' upper or lower back, and the results highlight the need of an improvement in the estimation of shear forces. As it can be seen

Table 5.10: RMSE and RelErr comparison between this study and previous research for estimated vertical (F_V) and horizontal (F_H) GRF components.

Study	Movement	F_V		F_H	
		RMSE [N]	RelErr [%]	RMSE [N]	RelErr [%]
This study	Sprint acceleration	173.3	30.2±51.2	46.8 (AP: 55.3, ML: 36.1)	16.8±21.6
	Change of direction	71.2	10.9±40.1	61.6 (AP: 54.1, ML: 77.6)	7.8±6.3
Ch. 4 study	LSJ 1st stance (Fig. 4.5b)	43.4	3.2±2.8	55.9	10.8±5.4
	LSJ 2nd stance (Fig. 4.5d)	52.2	3.8±3.2	65.7	10.7±6.5
	LSJ 3rd stance (Fig. 4.5f)	76.2	5.4±4.6	65.2	9.8±6.3
	LSJ 4th stance (Fig. 4.5h)	71.6	5.5±4.3	57.3	8.3±5.6
Setuain et al. [107]	Sprint		7.3±8.0		45.3±55.0
Gurchiek et al. [108]	Sprint acceleration	77.1		AP: 37.7, ML: 66.3	
	Change of direction	54.2		AP: 97.5, ML: 163.7	

from table 5.10, the results obtained with the methods presented in this and the previous chapter provide lower errors in the horizontal direction, whereas, in the vertical direction similar errors were obtained when comparing previous work with the data from chapter 4, but worse results for this study. In addition to the step-averaged errors, Gurchiek et al. [108] compared also the instantaneous force (Fig. 2.16), which showed larger errors in comparison to the vertical and horizontal step-averaged forces both for the sprint and change of direction tasks. This suggests that the use of the step-averaged force to compare the results may be a limit and it is not representative of the accuracy in the prediction of GRF loading characteristics, which are the parameters of interest to understand the mechanisms of shoe-surface interaction, and the consequences for athletic performance and injury risk. The instantaneous forces estimated both during the LSJ with the method presented in the previous chapter (Fig. 4.14 and 4.15) and during football-specific tasks with the method reported in this study (Fig. 5.19 to 5.21) show a better fit with the forces measured by the force platforms compared to the studies reported in the literature. Therefore, the method presented in this chapter to estimate GRFs represents an improved method to estimate the forces in both the vertical and horizontal direction compared to previous research.

Some of the results obtained in this study can be directly compared to those of Verheul et al. [111]. The authors estimated the resultant GRF for dynamic and high intensity movements applying Newton's second Law of Motion to the body segment accelerations derived from the markers' trajectories recorded with an optoelectronic motion capture system. In table 5.11, the force curve profile, impulse and impact peak force errors are reported for second or third step of acceleration, deceleration to complete stop and 90° change of direction; movements that can be compared to three of the sub-tasks considered in this study. A deceleration to complete stop was not recorded in the current study, and the deceleration before the turning manoeuvre was considered for comparison, since it requires to stop the body before accelerating in the opposite direction. However, differences could be present; such as a rotation of the body before turning in order to be aligned into the new intended direction, which

Table 5.11: Comparison between the results obtained in this study with those of Verheul et al. [111] for GRF curve profile, impulse and impact peak force errors in the resultant direction for acceleration, deceleration and change of direction tasks.

	RMSE [N kg^{-1}]		Impulse error [%]		Impact peak error [%]	
	Verheul et al. [111]	This study	Verheul et al. [111]	This study	Verheul et al. [111]	This study
Acceleration	2.82±0.7	3.45±0.7	9.1±4	18.4±4	28.5±33	60.3±18
Deceleration	5.77±1.8	5.59±1.4	11.1±6	11.3±6	15.0±9	13.4±10
Change of direction	2.67±0.7	2.70±0.9	3.8±2	3.1±3	9.8±8	16.2±13

could result in a different distribution of the forces especially in the horizontal direction. Instantaneous forces and impulses for deceleration and change of direction tasks were estimated with similar accuracy in this study compared to the values obtained by Verheul et al. [111]. Impact peak was estimated with better and worse accuracy for deceleration and change of direction tasks respectively. Higher errors were obtained in this study for the acceleration task. The loading rate errors are not reported, since very high errors were found for both studies.

Different accuracies were achieved in the estimation of the GRF curve profiles and loading characteristics in this study (Fig. 5.19 to 5.21; Tables 5.3 to 5.5). Overall, between all tasks analysed, lower errors were found in the mid-stance phase, around the active peak event, and considerably higher errors were obtained for the impact peaks, in the first 30% of stance phase. The comparison between tasks, showed that the accuracy in the force curve profile estimation is related to movement intensity, with the most intensive movement, the decelerations steps, presenting higher RMSE and larger limits of agreement regardless of the percentage of the stance phase analysed. The same relationship was found for the force curve RMSE, with the error increasing with the change of direction angle increasing or decreasing for deceleration or cutting stance phases, respectively; since changing direction of a bigger angle is performed at lower speed, thus requires higher decelerations and impacts to slow down the body's CoM. Moderate to low errors were obtained, both in the vertical and horizontal direction, in the estimation of the active peak force for all the changes of direction, the acceleration, excluding the first step, and the steps prior and post the turning movement; and in the impulse estimation for all the changes of direction, all the steps preceding the 90° cut and those directly preceding and following the turn (Tables 5.4 to 5.5). Impact peak force and loading rate were predicted with high errors (Tables 5.4 to 5.5) because of the two main limitations found in this study, the accelerometer range and the sample frequency limited to ±16 g and 100 Hz, respectively.

The low sample frequency of the IMU recordings and the IMU's accelerometer range limit of ±16 g (Fig. 5.22 and 5.23) are thought to affect the definition of the impact peak force amplitude and time interval, with the former that should be equal to double the average force over the time interval because of the simple properties of the risen cosine bell function [113], and the latter corresponding to an arbitrary value constant between sub-tasks. The impact peak force occurs after 0.02 to 0.04 s [136, 137], therefore, only 2 to 4 samples are available when trying to describe it with a sample frequency of 100 Hz. Moreover, figure 5.22 highlights that impact peak accelerations can be 3 to 4 times higher compared to the measurement range limit of the sensors used in this study. Due to these limitations, as shown in figure 5.23, the timing and magnitude of segmental accelerations result distorted and attenuated,

with consequent loss of information when attempting to estimate the impact peak force. The method described in this chapter was used to estimate the 3D GRFs from the accelerations derived from the location of the centre of the clusters (a_T) for a sprint trial to further analyse the effect of the sensors' limitations on the impact peak force prediction. The accelerations derived from the motion capture recordings do not have a limited range and are recorded at double the sample frequency of that used for the IMUs, however they are likely to be susceptible to noise due to double differentiation. The results are shown in figure 5.24 and highlight the differences in the estimation of the impact peak force. It is important to report that the method was developed using the IMU recordings, thus different mass percentages could be necessary to obtain a better fit, and the width of the impact time interval could be defined from the acceleration data, rather than using an arbitrary value. This suggests that the use of sensors with a minimum of 500 Hz and minimum measurement range of ±60 g would give the possibility of describing the impact peak force with 10 to 20 samples, which might allow the improvement of the impact peak force estimation.

Verheul et al. [111] analysed the minimum number of segments required to estimate the GRFs with moderate or lower errors, concluding that a minimum of eight segments was required for cutting movements and eleven for accelerations, whereas for the highest intensity tasks, such as decelerations, high or very high errors were found regardless of the number of segments used. These findings were confirmed by this study, where moderate or lower errors were found in the estimation of force curve profiles and impulses for all the cutting manoeuvre tasks by using eight segments (Table 5.3). However, Verheul et al. [111] reported only the errors obtained with a fifteen segment model, which are comparable with those obtained in this study; therefore, it represents an improved method to estimate the GRFs during a 90° cutting task. The higher errors obtained for the acceleration steps in this study could be related to the number of body segments considered; thus, the application of this GRF estimation technique to an eleven body segment model should be investigated for this specific task. Finally, the high or very high errors (RMSE > 3 N kg^{-1}) obtained in this study for the deceleration steps (Table 5.3) could suggest, as stated by Verheul et al. [111], that very high intensity movements could not be accurately represented by a multi-segment body approach. However, the force curve profile of this movement is largely influenced by the impact peak; thus, different results and conclusions could be drawn if the method was not limited by the accelerometer range. These results show that the technique presented in this chapter has a good potential to estimate 3D GRFs during high intensity movements and should be explored further with improved IMUs.

In section 2.3.2.4, it was reported that a faster change of direction time performance is associated with the ability to decelerate predominantly on the penultimate step before

turning, since the application of a higher braking force, allows the body to be rotated and aligned into the new intended direction more effectively [82, 84, 85]. Therefore, the possibility given by an IMU in-field based method to estimate the GRFs and contact times for subsequent steps in a large testing area represents a great benefit for performance evaluation. Faster performances are also related to significantly shorter ground contact times, greater horizontal peak forces, lower vertical impact forces and greater medial distances of the CoM from the CoP [82, 83]. The method presented in this chapter predicts impact peak forces with high to very high relative errors, ranging between 15.5 and 60.3% in the resultant direction, but showing the possibility to be improved with better IMUs. Whereas, the method allows prediction of the contact time for a variety of high-intensity movements with RMSE of 14 ms, giving the possibility to directly evaluate performance in field-based research. In addition to the contact time prediction, the method showed its reliability also in the estimation of the active peak force. A study from Morio et al. [89] (Sec. 2.3.3) found a significant correlation for both static and dynamic friction with traction perception during a forward cutting manoeuvre performed over a force platform with different shoe and surface conditions. For this reason, the active peak force represents another valuable measurement for in-field testing, giving the possibility to compare utilised traction with traction perception. From table 5.8, it can be concluded that a reliable ranking of shoe-surface conditions is possible for the changes of direction, regardless the angle of the manoeuvre, through the calculation of the impulse, and for the first step of acceleration through the estimation of the active peak force. These GRF loading characteristics were estimated with relative errors ranging between 2.4 and 7.6% and between 4.6 and 15.3% in the vertical and horizontal directions, respectively. Therefore, this method provides the possibility to compare and rank different shoe-surface conditions in the field in both the vertical and horizontal direction, representing an improvement compared to previous research [107, 108].

As already reported, this study highlights two main limitations, regarding sample frequency and accelerometer range. As shown in figure 5.24, these affect the results, especially for the instantaneous GRF, the impact peak force and the loading rate errors. Another limitation is the small number of participants taken part to this study, which could have led to subject-specific definitions not valid for a wider population sample. Thus, future work should develop the method using new generation IMUs, able to record accelerations with a minimum range of ±60 g and a minimum sample frequency of 500 Hz to improve the estimation of GRFs during the first 30% of the stance phase, and validate it with a bigger sample size to avoid any subject-specific definition and check the reliability on a higher number of movement techniques.

5.6 Conclusion

A new method for the estimation of 3D GRFs was presented in this chapter. Instantaneous force components and GRF loading characteristics were predicted during high-intensity football-specific movements, through the use of eight IMUs and the consideration of two mechanical phenomena: the collision of the lower limb with the surface and the motion of the remainder of the body mass throughout the stance phase.

Different levels of accuracy were obtained between tasks, with the errors increasing with the movement intensity. However, the results show the validity of the method in the estimation of the GRFs during change of direction stance phases, of the active peak force for the majority of the movement considered and of the contact time. Therefore, this method represents an improvement compared to the current state of the art and can be used in the field to evaluate shoe-surface interaction and its relationship with performance and traction perception during football-specific movements.

In the next chapter, the method will be applied in the field to compare four different football shoe-surface conditions during an agility course.

Chapter 6

Effect of football hybrid turf surfaces on players' performance and traction perception

6.1 Introduction

In chapter 1, it was highlighted how in recent years, football playing surfaces and footwear design significantly evolved in order to assist the player in enhancing performance and to reduce injury risk. The research focused on the improvement of playing surfaces result in the development of hybrid turf surfaces, which combine the feel, look and comfort of natural grass with the resilience and resistance to tearing, divots and adverse climatic conditions of artificial turf [12]. Nowadays, these surfaces are installed all over the world and became the dominant surface for the major professional leagues, especially in the UEFA regions. However, whilst natural grass and artificial turf surfaces have been widely analysed [27, 49, 50, 62, 66, 70–72], information regarding hybrid turf surfaces' mechanical properties, interaction with shoes and effect on player movement are still lacking.

In chapter 3, it was possible to identify the mechanical property ranges of hybrid turfs used in match play and compare them with those of natural grass surfaces. In this chapter, the method previously described (Ch. 5) will be used to estimate 3D GRFs through eight IMUs, while participants complete an agility course on two hybrid turf surfaces of different construction, wearing in turn two pairs of shoes characterised by different studs' shape and outsole rigidity. This will allow the evaluation of shoe-surface interaction and its effect on players' performance and traction perception, where player's perception of changes in shoe-surface interaction will be assessed through a questionnaire.

The data collection presented in this chapter was carried out before the study reported previously (Ch. 5).

6.2 Aim and objectives

The aim of this chapter is to evaluate the effect of two football hybrid turf surfaces and two shoes on players' performance and traction perception.

To achieve this, the following objectives have been identified:

1. develop an agility course to represent high-intensity football-specific movements;
2. characterise the mechanical properties of the football hybrid turfs;
3. evaluate performance based on GRFs and time to complete the course;
4. evaluate players' perception;
5. identify any relationship between football shoe-surface interaction, performance time, traction perception and mechanical characteristics of the surfaces.

6.3 Methods

6.3.1 Participants

After the study was approved by Sheffield Hallam University Research Ethics Committee, twenty male participants (age: 23.1 ± 3.7 years; mass: 77.5 ± 7.9 kg; stature: 1.81 ± 0.04 m), wearing shoes UK size 8.5 to 10.5, free from injuries and with different levels of football experience, volunteered to take part in the study. Participants were classified regarding their football level into competitive (n = 9), recreational (n = 10) and not competing in official leagues (n = 1) players.

6.3.2 Experimental set-up

6.3.2.1 Environment

The tests were completed over 24 days with mean temperature of 19.1 ± 5.2°C and relative humidity of 55.8 ± 9.5%. One test was performed under rainy conditions.

6.3.2.2 Surfaces

The tests were carried out on two different hybrid turf surfaces: a reinforced root-zone (Fibrelastic, Mansfield Sand, Sutton-in-Ashfield, UK) and a stitched-based system (SISgrass, SIS Pitches, Maryport, UK), which are located at adidas headquarters in Herzogenaurach, Germany. At time of testing the surfaces were less than six months

(a) SISgrass.

(b) Fibrelastic.

Figure 6.1: Hybrid turf surfaces with the artificial component highlighted.

old, where lifespan of more than 15 years is expected, subject to hours of play and maintenance.

6.3.2.3 Shoes

Participants were asked to wear in turn two different pairs of shoes, adidas Nemeziz 19.1 and Predator 19.1, three different sizes were available (8.5, 9.5 and 10.5 UK).

(a) adidas Nemeziz, side view.

(b) adidas Predator, side view.

(c) adidas Nemeziz outsole.

(d) adidas Predator outsole.

(e) adidas Nemeziz forefoot studs.

(f) adidas Predator forefoot studs.

Figure 6.2: adidas shoes used during the test.

Both shoes were firm grass designs with 12 moulded plastic studs with the same distribution and length; the shoes differ for studs' geometry, outsole construction and ankle support. adidas Nemeziz 19.1 has cylindrical studs, flexible outsole and low ankle profile cut. adidas Predator 19.1 has prismatic studs, a more rigid outsole and heel structure compared to the Nemeziz, and a sock-like fit. The shoe mass is 220 g and 230 g for Nemeziz and Predator, respectively.

6.3.2.4 Devices

Mechanical tests were carried out with an AA and a rotational traction test device. The moisture content was measured through a HH2 Moisture Meter (Delta-T Devices, Cambridge, UK). The devices were described in section 3.1.1.1, 3.1.1.3 and 3.1.1.4, respectively.

The IMU sensors, described in section 4.3.2, were used to estimate the 3D GRFs and contact times. The sensors' locations and attachment methods (Fig. 6.3) are as described in the previous chapter (Sec. 5.3.2).

(a) Front view. **(b)** Back view.

Figure 6.3: Sensors' location and attachment methods.

A GoPro Hero 7 silver (GoPro, San Mateo, CA, USA) camera was used to record at 60 Hz the participants performing the course, and timing gates (Smartspeed Pro, Fusion sport, Boulder, CO, USA) were used to record the performance time needed to complete the course.

6.3.2.5 Agility course

The knowledge of football movements is crucial in the design of an agility course, which should be suitable to evaluate shoe-surface interaction and be representative of the actions recorded during match-play. In the literature review (Sec. 2.1), it was reported that high and very high intensity movements are the most crucial moments of the game, since they contribute directly to win the ball possession, score a goal or prevent one. These high intensity actions have a mean duration of 13.1 ± 3.2 s [23] and involve acceleration, maximal speed and agility [24]. Agility is the ability to change direction, start and stop quickly [24], usually occurring as reaction to a sudden external stimulus, such as avoiding another player or following the bounce of the ball [86]. Many changes of direction are observed during match play, with a mean of approximately 600 turns between 0° and 90°, 100 between 90° and 180°, and 10 for greater angles [23]. Therefore, the agility course was designed in order to involve accelerations, decelerations, anticipated and unpredicted changes of direction; have a balanced design between left and right cutting manoeuvres, in order to perform them evenly with right and left leg and at similar speed; fit inside the 15 x 15 m space available for each surface; and be completed within the mean time recorded for high intensity actions during match play.

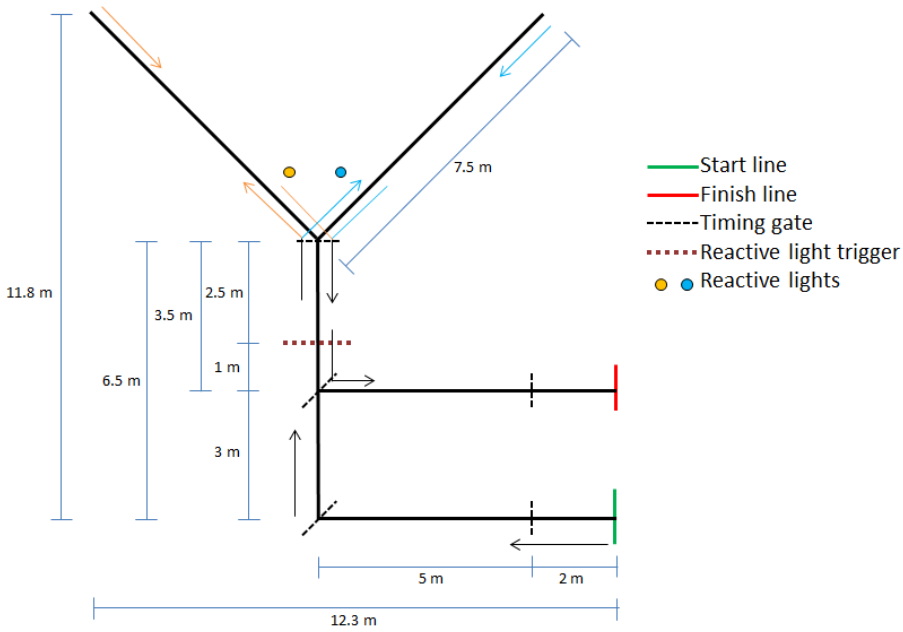

Figure 6.4: Agility course schematic representation.

Figures 6.4 and 6.5 show the agility course final design and its configuration on the testing site. The total course distance is 39 m and comprises a 7 m straight acceleration; a 180° change of direction performed using the dominant leg to push off during the turn; two 90° changes of direction, one turning to the left and one to the right, in order to be performed using the right or left leg to push off during the side cut, respectively; and two 45° changes of directions, one to the left and one to the right. All movements were constrained using obstacles in order to get changes of direction as close as possible to the desired angles; a reactive light was used to recreate the external stimulus to command an unpredicted change of direction movement. The light was actioned by a trigger placed 2.5 m before the change of direction.

(a) View 1.

(b) View 2.

(c) View 3.

Figure 6.5: Different views of the agility course set-up. The course schematic representation is added to the photos to highlight the set-up.

One to three participants were analysed on each day with the course kept in the same location. Between days, the course was slightly moved inside the available space, in order for the movements to not be affected by surface wear or compaction.

6.3.3 Protocol

6.3.3.1 Surface mechanical tests

The AA device was used to assess the shock absorption and vertical deformation of the two hybrid turf surfaces on which the biomechanical tests were carried out. The testing protocol is described in section 3.1.1.1, with the difference that the three drops were performed at two different locations, rather than nineteen for each surface, due to the smaller area of the pitches. The surfaces were tested a total of three times for shock absorption and twice for vertical deformation, on different days, but at the same locations. The rotational traction test was carried out once at three different locations for each surface, following the protocol described in section 3.1.1.3. After each participant, the moisture content of each surface was measured twice at four locations, kept constant over the measurements.

(a) AA Berlin. **(b)** AA Stuttgart.

Figure 6.6: AA set-up for shock absorption and vertical deformation measurements.

6.3.3.2 Biomechanical tests

Before the tests, participants completed a warm-up routine involving low intensity running, side stepping, high knees, butt kicks and sprints. Additional time was given for self-directed stretching. Upon conclusion of the warm-up, participants were allowed as many warm-up repetitions of the course as necessary. Each participant performed

three trials of the agility course for each shoe-surface condition. The first condition was chosen by alternating the starting surface between participants, who were left free to choose the first pair of shoes to wear. This was followed by three trials with the second pair of shoes on the same surface, before moving to the next field with the same shoes, and finally change to the first pair of shoes on the second surface. This structured order was selected to move trigger, lights, electrical cables, camera and timing gates a single time and avoid the participants to cool-down. Before each condition, participants were given time to become familiar with the changes. Participants were asked to start each trial from a T-pose to be kept for three seconds. This was necessary in order to record a static trial before the movement and to correctly estimate the sensor axes.

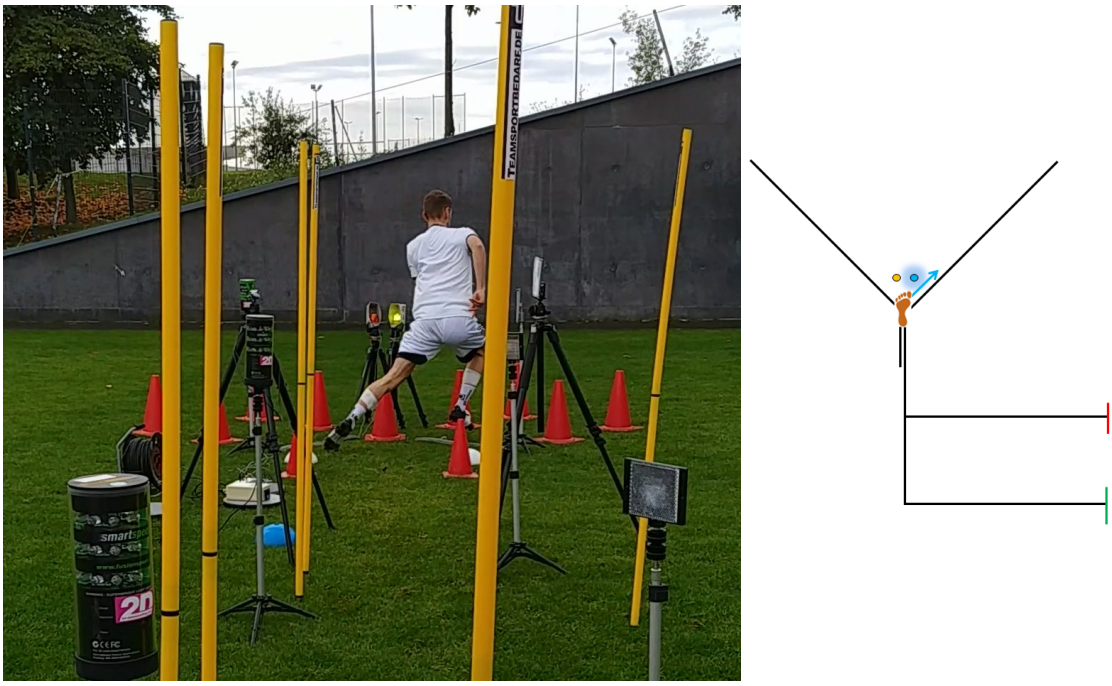

(a) Unpredicted 45° change of direction task.

(b) 90° change of direction task.

Figure 6.7: Photos of two change of direction tasks. The specific step shown in each photo is highlighted in orange in the course schematic on the right of each photo. On the top picture, the light is indicating the direction of the cutting task.

The direction of the unpredicted change of direction was communicated through a system comprising two reactive lights. A single light, defined by a manual pre-selection, switches on when the participant activates the trigger. A Matlab code was written in order to randomise the direction of the unpredicted 45° cutting task, with the constraint that, if for a shoe-surface condition all the three trials were performed pushing off with the same leg, at least one trial of each other condition had to be performed in the same direction.

A minimum of three minutes was given to rest between trials performed with the same shoe-surface combination, and a minimum of six minutes between conditions. The rest time was related to the amount of time required to complete each questionnaire section, change shoes and to become familiar with the new interaction.

6.3.3.3 Subjective-sensory data tests

A visual analogue scale (VAS) questionnaire was developed for this study and used to assess perception. Participants answered by drawing a vertical line on a 10 cm long horizontal line, where the left and right extremities represent a score equal to zero or ten, and were indicated in the questionnaire as "too low/very poor/very slow" and "too high/very good/very fast", respectively, depending on the question. The middle of the line was marked and represented neutrality.

The questionnaire consists of five sections. The first included general information regarding playing style and traction preferences; the others asked to assess surface properties, fatigue, traction and time perception for each shoe-surface combination, through the following questions:

1. How do you rate the pitch hardness?
2. How do you rate the pitch shock absorption?
3. How do you rate the fatigue effect on your muscles and tendons?
4. How do you rate the overall control of your foot with this shoe on this pitch?
5. How do you rate the traction offered by this shoe on this pitch during straight acceleration?
6. How do you rate the traction offered by this shoe on this pitch during cutting movements?
7. How do you rate the traction offered by this shoe on this pitch during turning movements?
8. How do you rate the overall traction performance?
9. How do you rate your perceived running time?

Each shoe-surface interaction section of the questionnaire was filled after completing the three trials of the course with that specific shoe-surface condition. Participants

were asked to focus on traction perception while completing the agility course and were made aware of the specific questions before the test.

6.3.4 Data processing

6.3.4.1 Surface mechanical tests

The AA measures the shock absorption and vertical deformation values after each impact from formulas 3.1 and 3.2, respectively (Sec. 3.1.1.1), and calculates the mean value of the second and third impacts for each location. As previously said, three tests on two different locations were carried out with the AA Berlin and two tests on two locations with the AA Stuttgart; the mean between tests and locations was calculated for each variable.

In chapter 3, the mechanical property ranges of the three different hybrid turf construction systems were reported. The data from shock absorption and vertical deformation did not include whether the measurements were performed with an AA or an AAA device; however, as reported in section 3.5, the comparison of the number of surfaces tested for energy restitution with those on which shock absorption and vertical deformation were measured, suggested that the latter device was used. Colino et al. [138] stated that the two devices could be used interchangeably, with almost perfect reliability, by minimising the slight deviations between the two devices using the following equations:

$$SA_{AAA} = \frac{SA_{AA} - 10.117}{0.852} \tag{6.1}$$

$$VD_{AAA} = \frac{VD_{AA} + 0.583}{0.925} \tag{6.2}$$

Therefore, in order to identify where the hybrid turf surfaces, on which the data collection was carried out, sit compared to those included in the Labosport ScorePlay™ database, these equations were applied to the mean values calculated from the tests. The mean value of rotational traction measured on the three locations was calculated, as well as of the moisture content measured on the different locations between the tests.

6.3.4.2 Biomechanical tests

Of the twenty participants taking part in this study, one was excluded from the analysis of performance time (Pa06) and two (Pa03 and Pa10) from that of the estimation of GRFs, because of missing data.

For each participant, one trial for each shoe-surface combination was selected for

analysis. These trials were chosen from those where the participant performed the unpredicted change of direction pushing off with the same leg. For each participant, some aspects were kept into consideration in the selection: 45° change of direction performed as a side cut, not a cross cut; 180° turning manoeuvre and first step of acceleration at the start of the course performed with the same leg between all the conditions; no subsequent steps performed with the same leg; and no loss of data during the whole course. If multiple trials met these conditions, the fastest one was chosen.

Since the data collection was carried out in the field, the magnetometers' recordings were not affected by interferences, thus, the raw accelerations measured by each IMU were converted into the IMU global NED coordinate system as explained in section 4.3.4.1, using equation 4.2.

The stance phase events were manually selected, by using the shank and foot vertical global accelerations for the touch-down and the foot antero-posterior raw accelerations for the take-off event, as described in the previous chapter (Sec. 5.3.4.2). Once the stance phase events were selected, the video recordings were used to count the total number of steps needed to perform the course and identify the steps corresponding to the changes of direction. The take-off events of each change of direction were used to divide the recording into five sections, in order to convert the accelerations, defined in the NED system, into a global coordinate system specific for each movement analysed inside the agility course. As in the previous chapter (Ch. 5), each system was defined in order for the x-axis to point in the direction of travel towards the change of direction, the z-axis to point upwards, and the y-axis representing the medio-lateral axis, directed from right to left (Fig. 6.8).

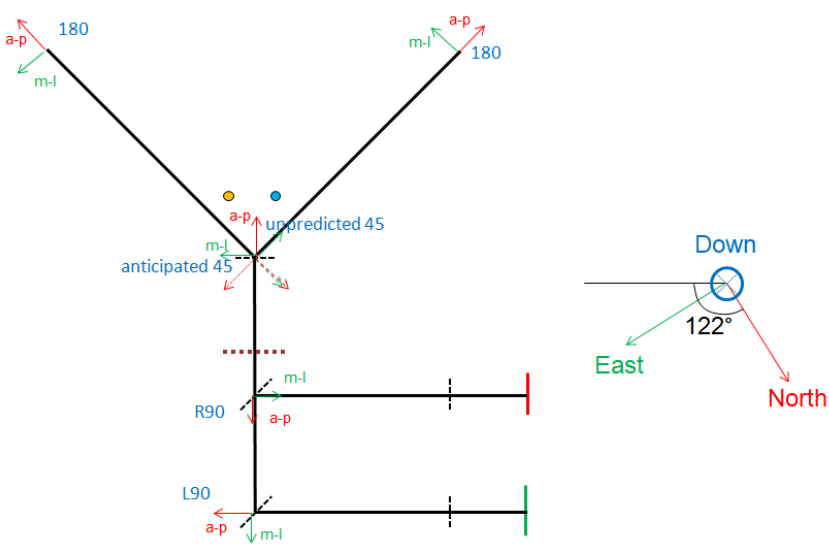

Figure 6.8: Reference systems in the agility course.

The 3D GRFs were estimated from the eight IMUs using the method described in the previous chapter (Sec. 5.3.4.2). Figure 6.9 shows an example of the steps necessary to complete the agility course, and highlights through black feet that participants required a number of steps for which a validation had not been performed. The coloured feet represent the steps for which the GRFs were estimated, with the different colours indicating the various tasks. A maximum of three steps were validated before each change of direction, divided into deceleration and step prior to the change of direction sub-tasks; whereas the acceleration steps directly following the changes of direction could be estimated only for the 180° turn (Table 5.2).

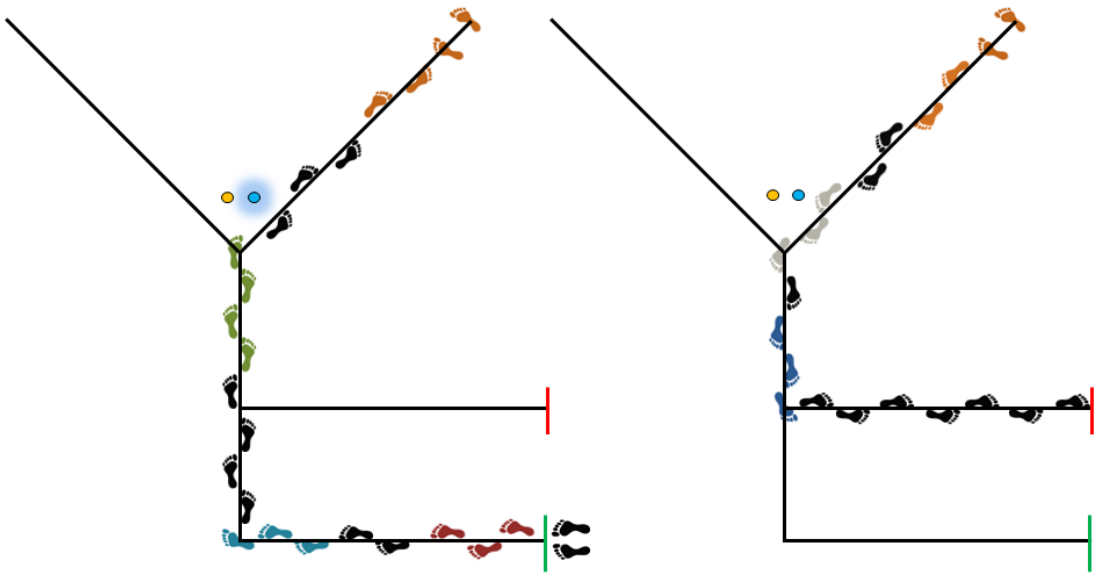

Figure 6.9: Course schematic with the steps necessary to complete the course. The coloured feet represent the stance phases analysed, whereas the black feet indicate those for which a validation had not been performed. Each colour represents a different task, specifically red, light blue, green, orange, grey and blue correspond respectively to straight acceleration, 90° cut performed pushing off with the left leg, unpredicted 45° cut (in the picture it is performed pushing off with the left leg following the switch on of the light on the right) 180° turn (in the picture it is performed with the right leg), anticipated 45° cut (in the picture it is performed pushing off with the right leg), and 90° cut performed pushing off with the right leg.

An example of the estimated 3D GRFs during the agility course for one participant and the four shoe-surface conditions is reported in figure 6.10, the coloured squared refers to the feet colours of figure 6.9.

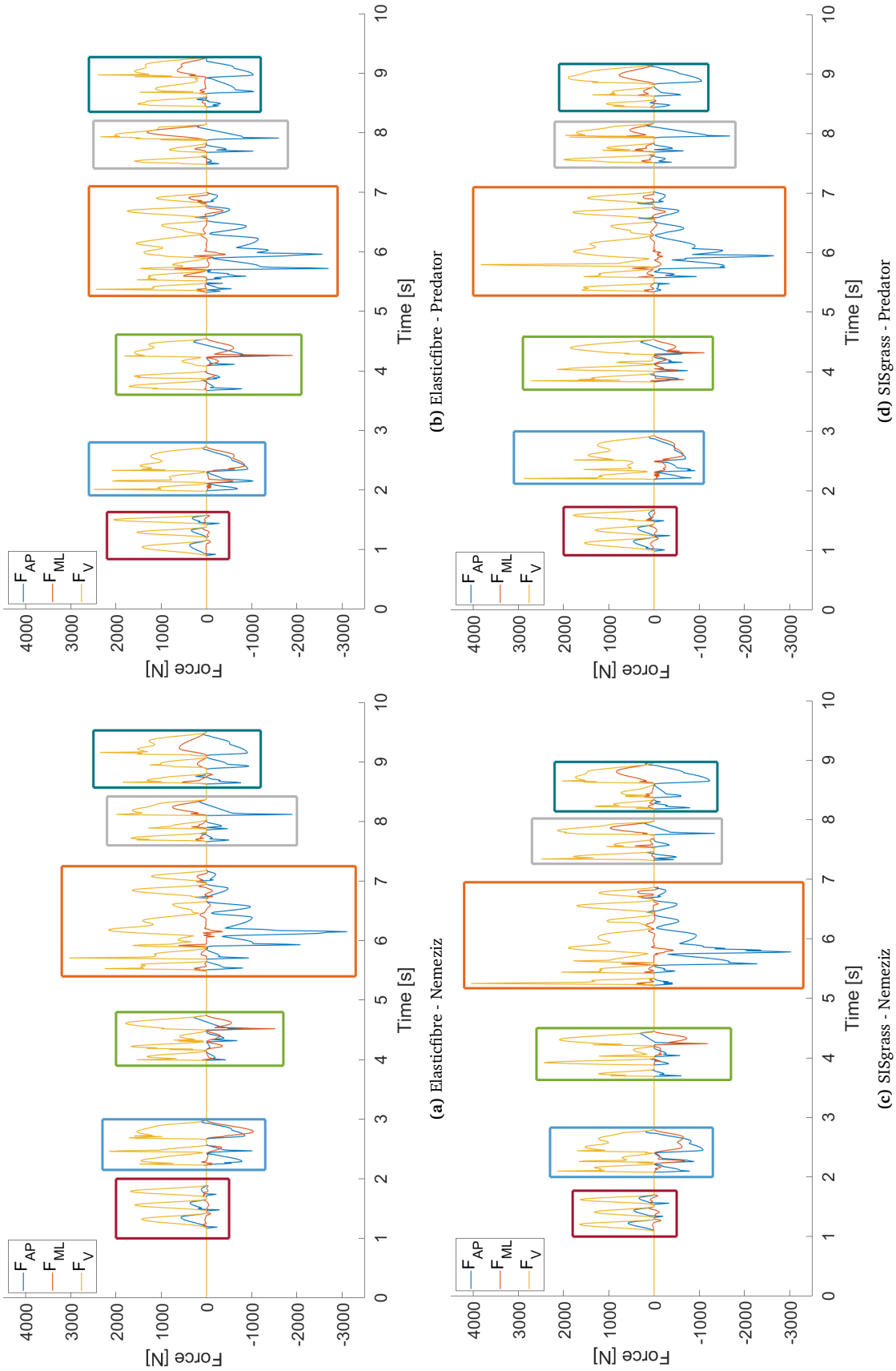

Figure 6.10: GRFs estimated for one participant for each condition. The squared colours refers to the tasks highlighted with the feet of the same colour of figure 6.9.

6.3.5 Statistical analysis

6.3.5.1 Surface mechanical tests

In chapter 3, the mechanical properties' ranges of hybrid turf surfaces tested by Labosport, as part as their ScorePlay™ dataset, were graphically reported as beeswarm plots to represent their distribution and display individual measurements without overlapping (Fig. 3.10 and 3.9). In order to compare the surfaces, on which this study was carried out, with elite level playing surfaces, the mean values, calculated for each mechanical property tested on the surfaces, is reported inside the plots.

6.3.5.2 Biomechanical tests

The repeatability of the manual selection of the stance phase events was assessed using a two-way fixed intra-class correlation coefficient ICC(3,1) test. A single trial was considered and the events were selected five times at intervals of 1.5 hours by the same researcher.

For each participant and shoe-surface condition, the best performance time was selected between the trials with the unpredicted change of direction performed pushing off with the same leg. Active peak force and impulse were calculated for each step analysed from the vertical and horizontal GRF components. The contact time of each stance phase was calculated for comparison as well.

The individual steps analysed were grouped into acceleration, deceleration and change of direction tasks (Fig. 6.11); for each grouped movement the mean value of the GRF loading characteristics (i.e. impulse and active peak force) and the contact time were calculated to compare each shoe-surface condition within and between participants. Two-way analysis of variance (ANOVA) tests were used to identify significant differences between surface conditions (Fibrelastic vs SISgrass) and shoe conditions (Nemeziz vs Predator) within and between participants for performance time, active peak force and impulse along the vertical and horizontal directions, and contact time during acceleration, deceleration and change of direction tasks. Alpha was set to 0.05 for all tests. For each ANOVA test, Cohen's effect size (d) was calculated by dividing the mean difference between the two groups by the pooled standard deviation. According to Cohen [139], values of 0.20, 0.50 and 0.80 correspond to small, medium and large effect sizes, respectively.

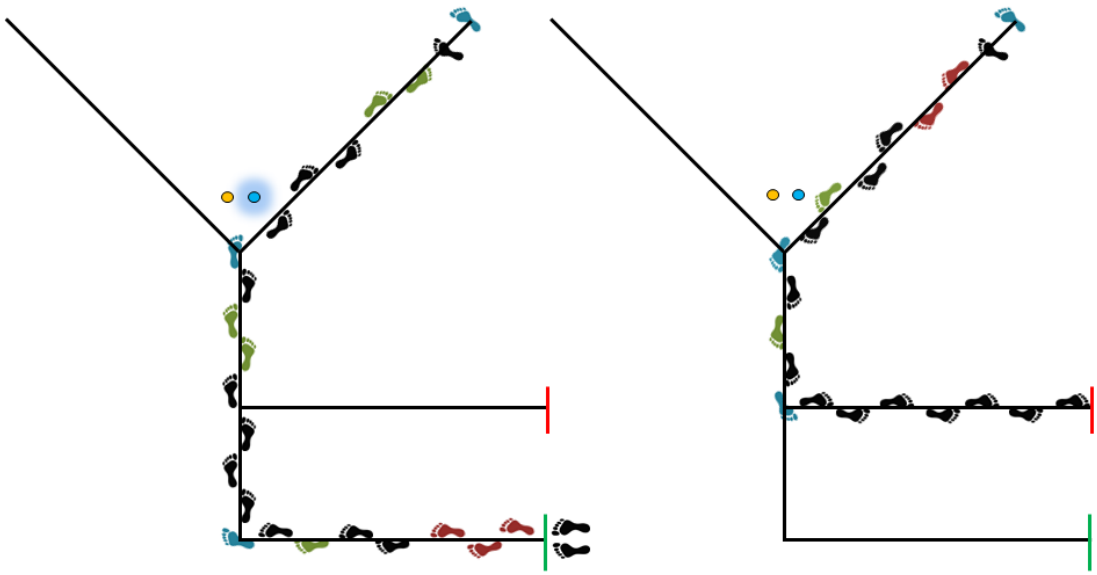

Figure 6.11: Course schematic with the steps necessary to complete the course. The coloured feet represent the stance phases corresponding to each group of movements: red for acceleration steps, green for deceleration steps, and blue for change of direction steps.

6.3.5.3 Subjective-sensory data tests

For each one of the questions reported in section 6.3.3.3, the presence of between participants significant differences between surface or shoe conditions were investigated through a two-way ANOVA test and Cohen's *d* effect size. Alpha was set to 0.05.

One participant (Pa20) was excluded from the analysis, since the 10 cm VAS was interpreted as a three point scale.

6.3.5.4 Relationship between biomechanical and subjective-sensory data

Spearman's rank correlation coefficient was used to assess the relationship between GRF loading characteristics and traction perception, and between the performance time with the time perception and the overall traction perception. The former correlation considers the first step of acceleration and the individual changes of direction (Fig. 6.12), steps for which the IMU method was demonstrated able to rank the data with strong correlation (Ch. 5), and the traction perceived during the related movement, or rather during acceleration, cutting and turning tasks. The correlation is rated as positive or negative, depending on the sign, and ranked as negligible ($0-0.30$), low ($0.30-0.50$), moderate ($0.50-0.70$), high ($0.70-0.90$) or very high ($0.90-1.00$) [140].

All data were processed using Matlab R2019a (Mathworks, Natick, MA, USA).

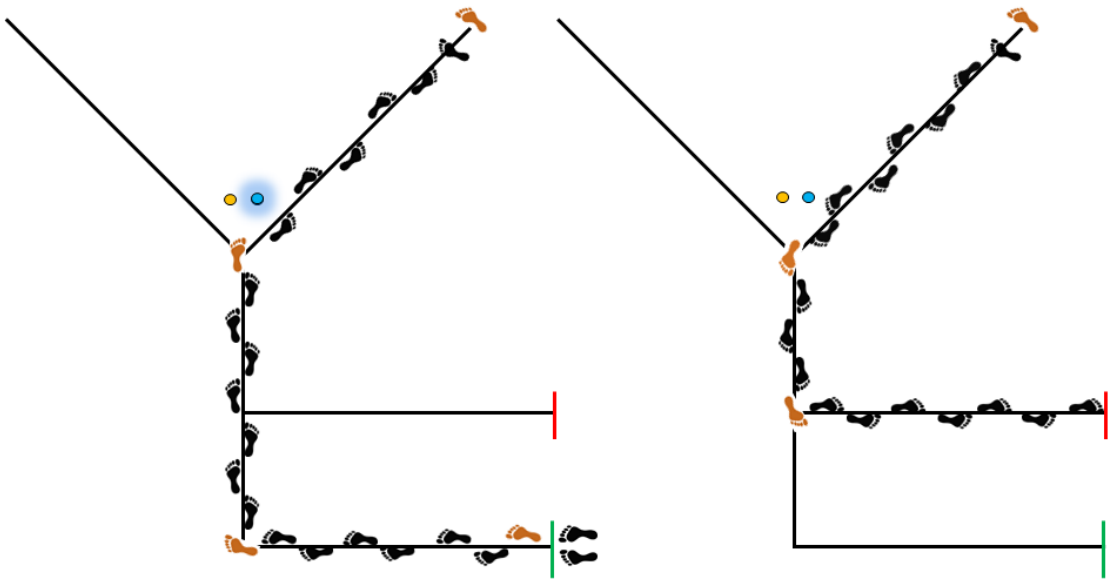

Figure 6.12: Course schematic with the first step of acceleration and the individual changes of direction highlighted.

6.4 Results

6.4.1 Surface mechanical tests

In table 6.1, the mean values calculated for each mechanical property tested are reported for both surfaces. The mean was examined for consistency with the Labosport ScorePlay™ dataset analysis (Ch. 3), where a single value for each sport surface tested was reported. These mean values are also displayed in figure 6.13 as green asterisks inside the beeswarm plots representing the ranges and distribution of each mechanical property tested by Labosport.

Table 6.1: Mean value calculated for each mechanical property for each surface.

	Fibrelastic	SISgrass
Shock absorption	37.0 %	41.7 %
Vertical deformation	3.7 mm	3.3 mm
Rotational traction	48.0 Nm	57.3 Nm
Moisture content	20.0 %	20.0 %

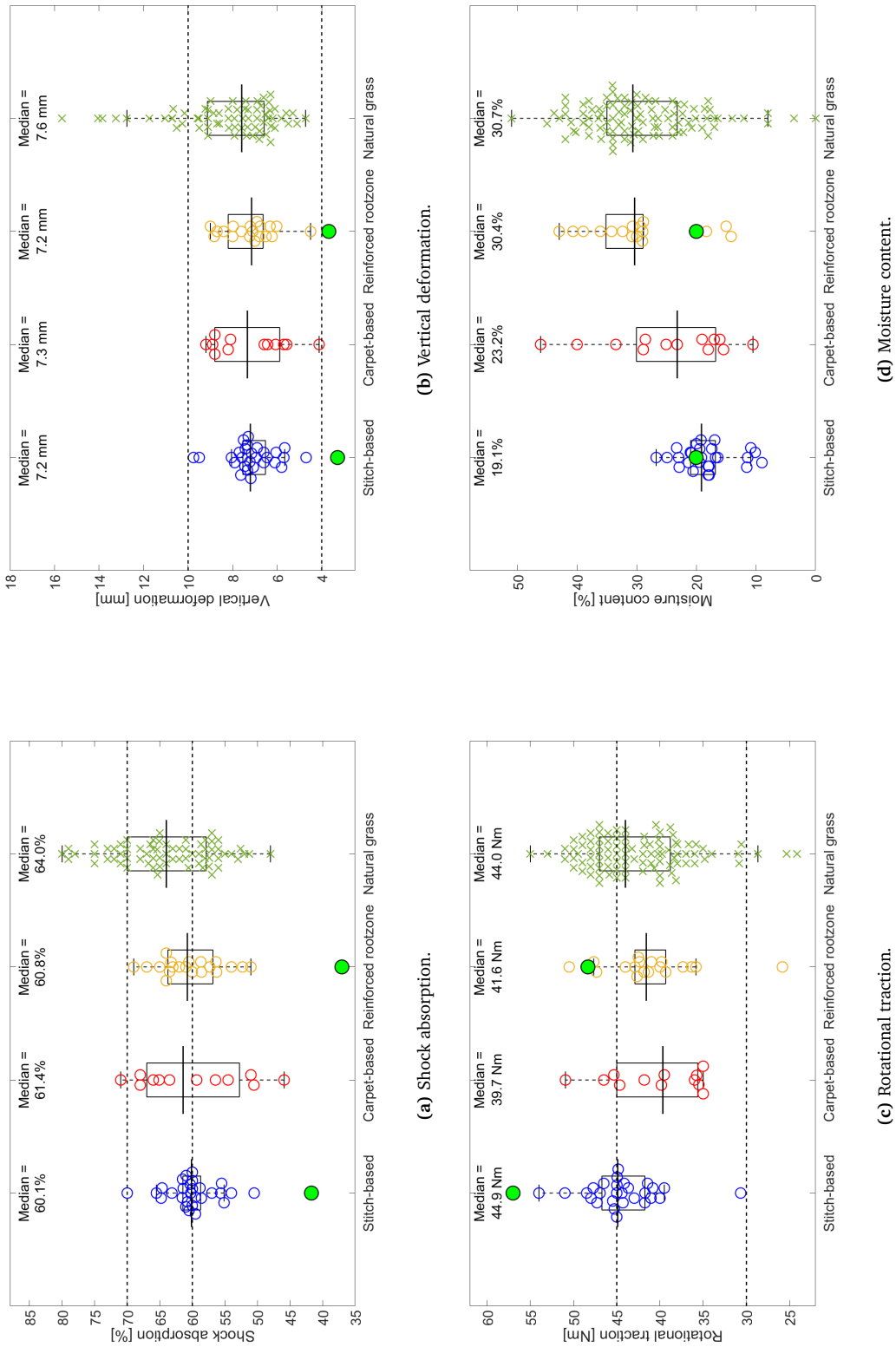

Figure 6.13: Comparison of shock absorption, vertical deformation, rotational traction and moisture content between stitched-based, carpet-based, reinforced rootzone hybrid turf systems and natural grass surfaces used in match play (data from Labosport ScorePlay^{TM} dataset) and the surface tested in the current work, which results are indicated with a green asterisk.

6.4.2 Biomechanical tests

An ICC(3,1) = 1 was found for the manual selection of the stance phase events repeatability. In addition, the standard deviation for each event was calculated and ranged between 0 and 18 ms, with a mean value of 1.8 ms, were obtained, where 10 ms is the time difference between samples; confirming the high accuracy in the stance phase events manual selection.

6.4.2.1 Performance time

In table 6.2, the mean performance times between participants for each condition are reported, as well as the two-way ANOVA test results. No significant differences were found between surface or shoe conditions.

Table 6.2: Performance time reported as mean ± standard deviations for each shoe-surface condition and two-way ANOVA test p-value results with Cohen's d effect sizes (n=76).

	Fibrelastic Nemeziz	Fibrelastic Predator	SISgrass Nemeziz	SISgrass Predator	Surfaces p	Surfaces d	Surfaces F	Shoes p	Shoes d	Shoes F
Performance time	8.87 ± 0.38 s	8.94 ± 0.45 s	8.96 ± 0.52 s	8.99 ± 0.41 s	0.517	0.151	0.420	0.590	0.125	0.290

The best performance times for each participant and shoe-surface combination are reported in table 6.3, together with the results of the two-way ANOVA test. Statistical significant differences were identified between surfaces for participant Pa03 ($p = 0.035$, $d = 7.569$, $F = 324.974$) and for both shoe ($p = 0.032$, $d = 1.335$, $F = 383.041$) and surface ($p = 0.031$, $d = 1.495$, $F = 429.082$) conditions for participant Pa05.

Table 6.3: Best performance times for each participant and shoe-surface combination; and two-way ANOVA test p-values and Cohen's d effect sizes (n=4).

	Fibrelastic Nemeziz [s]	Fibrelastic Predator [s]	SISgrass Nemeziz [s]	SISgrass Predator [s]	Surfaces p	Surfaces d	Surfaces F	Shoes p	Shoes d	Shoes F
Pa01	9.126	9.146	8.581	8.928	0.258	2.195	5.444	0.463	0.625	1.260
Pa02	9.055	9.053	8.774	8.948	0.272	2.218	4.810	0.507	0.573	0.955
Pa03	8.626	8.585	8.978	8.900	0.035	7.569	324.974	0.192	0.252	10.344
Pa04	8.293	8.192	8.077	8.369	0.937	0.126	0.010	0.712	0.684	0.236
Pa05	9.241	9.371	9.089	9.233	0.031	1.495	429.082	0.032	1.335	383.041
Pa07	8.826	9.433	9.243	9.192	0.834	0.289	0.072	0.553	1.154	0.714
Pa08	8.715	8.668	8.878	9.156	0.295	2.309	4.012	0.607	0.449	0.505
Pa09	9.065	9.033	9.199	9.499	0.322	1.989	3.266	0.568	0.553	0.652
Pa10	9.671	9.847	9.499	9.799	0.327	0.633	3.148	0.162	2.666	14.736
Pa11	9.003	8.915	9.382	9.133	0.168	2.261	13.750	0.284	0.771	4.381
Pa12	9.000	9.435	10.521	9.569	0.444	1.581	1.424	0.773	0.339	0.139
Pa13	8.464	8.661	8.905	8.683	0.468	1.560	1.221	0.962	0.057	0.004
Pa14	9.241	9.298	8.911	9.365	0.628	0.575	0.439	0.420	1.518	1.657
Pa15	8.768	8.781	8.703	8.500	0.355	1.701	2.566	0.541	0.659	0.774
Pa16	9.020	8.988	8.719	8.746	0.069	12.969	84.702	0.946	0.013	0.007
Pa17	9.118	9.394	9.118	9.166	0.500	0.814	1.000	0.390	1.421	2.019
Pa18	7.983	8.115	8.280	8.356	0.066	3.532	92.297	0.167	0.544	13.796
Pa19	8.405	8.283	8.270	8.288	0.524	1.054	0.862	0.593	0.770	0.552
Pa20	8.901	8.749	9.040	9.068	0.238	2.963	6.474	0.616	0.356	0.475

6.4.2.2 Ground reaction force loading characteristics and contact time during the acceleration task

For each participant, the GRF loading characteristics and the contact time were calculated for each individual step, assigned to the acceleration task (red feet in Fig. 6.11). GRF loading characteristics and contact time mean values and differences between participants are reported in tables 6.4 and 6.5, respectively. Statistical significant differences were found between shoes in the horizontal active peak force ($p < 0.001$, $d = 0.997$, $F = 69.225$), vertical ($p < 0.001$, $d = 0.459$, $F = 16.176$) and horizontal impulse ($p < 0.001$, $d = 0.831$, $F = 50.353$) and contact time ($p < 0.001$, $d = 0.493$, $F = 18.232$); and between surfaces for the vertical impulse ($p < 0.001$, $d = 0.517$, $F = 20.183$) and contact time ($p = 0.005$, $d = 0.318$, $F = 7.844$).

Table 6.4: Between participants active peak force, impulse, and contact time mean ± standard deviation for each shoe-surface condition and variable for the acceleration task.

	Fibrelastic Nemeziz	Fibrelastic Predator	SISgrass Nemeziz	SISgrass Predator
Vertical active peak [N kg^{-1}]	20.02±2.32	20.08±2.45	19.58±2.82	20.08±3.02
Horizontal active peak [N kg^{-1}]	5.78±1.88	5.82±2.02	6.14±2.39	5.68±2.48
Vertical impulse [N s kg^{-1}]	2.14±0.23	2.19±0.37	2.12±0.35	2.17±0.32
Horizontal impulse [N s kg^{-1}]	0.68±0.20	0.70±0.24	0.73±0.28	0.66±0.25
Contact time [s]	0.21±0.03	0.22±0.03	0.22±0.03	0.22±0.03

Table 6.5: Between participants active peak force, impulse, and contact time two-way ANOVA test results for the acceleration task.

	Surfaces			Shoes			n
	p	d	F	p	d	F	
Vertical active peak	0.070	0.213	3.304	0.497	0.077	0.463	286
Horizontal active peak	0.559	0.059	0.343	< 0.001	0.997	69.225	279
Vertical impulse	< 0.001	0.517	20.183	< 0.001	0.459	16.176	288
Horizontal impulse	0.431	0.085	0.623	< 0.001	0.831	50.353	288
Contact time	0.005	0.318	7.844	< 0.001	0.493	18.232	288

In tables 6.6 to 6.10, mean ± standard deviation and within participant results for the two-way ANOVA test are reported for vertical and horizontal active peak force, vertical and horizontal impulse and contact time, respectively. Differences were found especially between shoe conditions for the horizontal active peak force (78% of participants), vertical (50% of participants) and horizontal (56% of participants) impulses.

Table 6.6: Within participant mean ± standard deviation for each shoe-surface condition vertical active peak force from the acceleration task, and two-way ANOVA test results.

	Fibrelastic Nemeziz [N kg^{-1}]	Fibrelastic Predator [N kg^{-1}]	SISgrass Nemeziz [N kg^{-1}]	SISgrass Predator [N kg^{-1}]	Surface			Shoe			
					p	d	F	p	d	F	n
Pa01	17.99±2.0	17.82±2.8	18.04±2.5	18.70±2.2	0.795	0.077	0.070	0.001	1.728	18.924	16
Pa02	19.54±2.1	20.94±1.9	18.50±0.7	20.45±1.3	0.647	0.242	0.220	0.390	0.471	0.797	16
Pa04	20.29±0.9	20.03±2.5	20.99±1.5	17.82±0.5	0.980	0.013	< 0.001	0.510	0.366	0.462	16
Pa05	19.21±1.6	17.95±1.1	17.85±1.0	18.27±0.5	0.035	1.225	5.928	0.180	0.568	2.075	16
Pa06	20.46±1.5	10.06±3.3	18.65±1.7	20.99±2.3	0.126	0.550	2.701	0.001	1.965	17.820	16
Pa07	19.63±1.3	20.49±1.0	18.90±0.8	18.72±1.7	0.294	0.541	1.203	0.147	0.799	2.410	16
Pa08	19.11±1.8	20.36±2.5	19.62±1.5	20.90±2.0	0.027	1.107	6.342	0.536	0.243	0.407	16
Pa09	20.79±2.3	20.08±3.1	19.35±2.8	25.08±2.7	0.300	0.557	1.173	0.301	0.555	1.167	16
Pa11	19.77±1.4	20.55±0.7	18.44±0.7	22.18±3.4	0.638	0.259	0.232	0.925	0.051	0.009	16
Pa12	21.70±2.3	21.69±2.9	20.07±2.1	22.27±3.0	0.001	1.402	20.361	0.001	1.250	17.483	16
Pa13	19.83±1.6	20.55±0.9	21.31±4.3	20.51±0.5	0.578	0.298	0.328	0.396	0.467	0.776	16
Pa14	18.91±2.8	17.95±2.4	20.13±7.2	18.78±2.7	0.919	0.031	0.011	0.001	1.646	17.640	16
Pa15	18.45±1.0	18.22±0.7	19.85±2.1	18.67±3.5	0.664	0.179	0.199	0.064	0.908	4.172	16
Pa16	19.01±0.8	20.10±1.1	18.37±2.3	17.57±2.6	0.456	0.401	0.595	0.354	0.508	0.929	16
Pa17	20.90±2.2	20.46±1.5	20.31±2.1	20.07±2.2	< 0.001	2.136	43.990	0.932	0.019	0.008	16
Pa18	18.39±1.5	19.98±2.4	19.80±1.7	17.33±1.1	0.066	1.070	4.106	0.492	0.330	0.504	16
Pa19	24.62±1.3	22.84±0.9	21.51±0.6	22.87±2.1	0.602	0.269	0.287	0.549	0.310	0.381	16
Pa20	21.71±1.2	21.33±1.6	20.71±2.1	19.29±0.8	0.506	0.358	0.470	0.640	0.248	0.230	16

Table 6.7: Within participant mean ± standard deviation for each shoe-surface condition horizontal active peak force from the acceleration task, and two-way ANOVA test results.

	Fibrelastic Nemeziz [N kg^{-1}]	Fibrelastic Predator [N kg^{-1}]	SISgrass Nemeziz [N kg^{-1}]	SISgrass Predator [N kg^{-1}]	Surface			Shoe			
					p	d	F	p	d	F	n
Pa01	5.15±1.3	5.43±1.3	6.07±0.7	5.38±1.2	0.455	0.274	0.592	0.002	1.936	14.557	16
Pa02	4.60±1.5	4.84±1.4	5.03±1.8	3.88±3.0	0.964	0.014	0.002	< 0.001	2.799	29.096	16
Pa04	4.46±1.6	7.84±2.9	5.42±1.9	4.22±1.5	0.252	0.465	1.438	0.007	1.577	10.264	16
Pa05	4.71±1.9	5.28±0.7	4.89±1.9	4.50±1.1	0.002	1.814	19.667	0.024	0.325	7.778	11
Pa06	5.42±0.9	3.90±2.1	4.50±1.1	4.82±1.6	0.087	0.631	3.418	0.001	1.908	17.082	16
Pa07	5.56±1.1	4.99±0.6	4.05±1.3	5.32±0.5	0.362	0.610	0.921	0.883	0.226	0.023	12
Pa08	5.53±1.8	5.94±0.8	5.94±1.0	6.08±2.0	0.061	0.821	4.197	0.011	1.337	8.783	16
Pa09	6.48±0.5	5.87±1.0	9.17±3.4	7.92±1.6	0.336	0.502	0.999	0.367	0.468	0.876	16
Pa11	5.57±1.2	4.83±0.3	5.94±3.0	6.32±2.6	0.033	1.180	5.730	0.259	0.511	1.396	16
Pa12	5.85±0.8	5.49±1.3	8.37±2.2	6.19±3.1	0.031	0.978	5.889	0.012	1.259	8.561	16
Pa13	7.32±1.8	6.46±1.2	4.61±2.9	6.29±1.3	0.668	0.228	0.193	0.880	0.079	0.024	16
Pa14	6.40±2.3	5.57±1.5	6.70±0.9	4.37±1.1	0.378	0.402	0.832	0.043	1.127	5.017	16
Pa15	5.30±0.9	4.56±1.8	5.95±1.1	5.51±1.0	0.361	0.316	0.897	< 0.001	2.159	18.514	16
Pa16	6.20±2.1	6.73±0.8	5.45±1.4	5.11±3.4	0.684	0.146	0.174	0.002	2.026	15.453	16
Pa17	4.19±1.0	4.63±0.7	5.31±0.9	4.30±0.4	0.895	0.055	0.018	0.014	1.480	8.145	16
Pa18	6.42±2.1	6.62±2.7	7.07±1.7	6.75±2.8	0.007	1.106	10.458	0.001	1.589	16.929	16
Pa19	7.53±1.8	9.21±1.4	8.01±1.8	8.02±3.5	0.195	0.572	1.869	0.020	1.281	6.970	16
Pa20	7.10±2.4	6.20±2.2	7.28±2.7	6.53±2.1	0.135	0.392	2.547	< 0.001	3.179	44.876	16

Table 6.8: Within participant mean ± standard deviation for each shoe-surface condition vertical impulse from the acceleration task, and two-way ANOVA test results.

	Fibrelastic Nemeziz [N s kg^{-1}]	Fibrelastic Predator [N s kg^{-1}]	SISgrass Nemeziz [N s kg^{-1}]	SISgrass Predator [N s kg^{-1}]	Surface			Shoe			
					p	d	F	p	d	F	n
Pa01	2.04±0.3	1.94±0.4	1.84±0.3	2.06±0.3	0.841	0.048	0.042	< 0.001	3.531	50.232	16
Pa02	2.34±0.2	2.46±0.1	2.15±0.2	2.36±0.2	0.789	0.147	0.075	0.690	0.220	0.167	16
Pa04	2.03±0.1	2.62±0.8	2.16±0.2	2.02±0.2	0.634	0.253	0.238	0.336	0.536	1.006	16
Pa05	2.32±0.2	2.17±0.2	2.21±0.1	2.43±0.3	0.468	0.288	0.562	0.007	1.634	10.478	16
Pa06	2.08±0.2	2.03±0.3	2.01±0.3	2.13±0.3	0.004	1.052	13.040	< 0.001	1.968	28.521	16
Pa07	2.09±0.2	2.17±0.4	2.04±0.3	2.15±0.4	< 0.001	3.744	60.270	0.405	0.187	0.746	16
Pa08	2.01±0.1	2.17±0.3	2.05±0.2	2.14±0.2	0.003	1.971	13.497	0.953	0.022	0.004	16
Pa09	2.09±0.2	2.27±0.2	2.14±0.3	2.57±0.3	0.696	0.211	0.161	0.574	0.306	0.335	16
Pa11	2.15±0.2	2.25±0.1	2.11±0.2	2.52±0.3	0.923	0.053	0.010	0.917	0.506	0.011	16
Pa12	2.23±0.2	2.31±0.3	2.63±0.6	2.22±0.3	0.164	0.666	2.198	0.039	1.147	5.341	16
Pa13	2.09±0.1	2.05±0.1	2.10±0.2	2.00±0.1	0.089	0.890	3.430	0.171	0.671	2.116	16
Pa14	2.05±0.2	1.99±0.3	2.19±0.7	2.05±0.3	0.125	0.493	2.713	0.001	1.673	18.589	16
Pa15	2.13±0.2	2.24±0.3	2.07±0.2	2.13±0.3	0.043	0.683	5.110	0.003	1.358	13.528	16
Pa16	2.42±0.2	2.32±0.3	2.07±0.3	2.19±0.2	0.212	0.505	1.740	0.011	1.372	8.961	16
Pa17	2.30±0.3	2.23±0.3	2.18±0.2	2.11±0.2	< 0.001	2.107	33.232	0.020	0.690	7.123	16
Pa18	1.89±0.2	2.14±0.3	2.07±0.2	1.89±0.2	0.051	0.959	4.697	0.213	0.539	1.733	16
Pa19	2.14±0.1	2.13±0.1	2.11±0.1	2.04±0.2	0.517	0.278	0.447	0.038	1.121	5.463	16
Pa20	2.09±0.2	1.97±0.1	2.11±0.1	2.05±0.1	0.115	0.883	2.895	0.387	0.433	0.808	16

Table 6.9: Within participant mean ± standard deviation for each shoe-surface condition horizontal impulse from the acceleration task, and two-way ANOVA test results.

	Fibrelastic Nemeziz [N s kg^{-1}]	Fibrelastic Predator [N s kg^{-1}]	SISgrass Nemeziz [N s kg^{-1}]	SISgrass Predator [N s kg^{-1}]	Surface			Shoe			
					p	d	F	p	d	F	n
Pa01	0.68±0.2	0.62±0.2	0.67±0.1	0.66±0.1	0.504	0.180	0.474	< 0.001	3.311	39.070	16
Pa02	0.66±0.2	0.66±0.2	0.69±0.3	0.51±0.3	0.725	0.096	0.130	< 0.001	1.977	26.270	16
Pa04	0.51±0.1	1.11±0.6	0.62±0.1	0.56±0.2	0.284	0.530	1.259	0.080	0.980	3.646	16
Pa05	0.62±0.3	0.78±0.1	0.66±0.3	0.54±0.2	0.001	1.690	19.186	0.159	0.442	2.255	16
Pa06	0.61±0.1	0.49±0.2	0.55±0.2	0.56±0.2	0.257	0.426	1.415	0.002	1.983	15.170	16
Pa07	0.52±0.3	0.71±0.2	0.66±0.2	0.81±0.2	0.437	0.427	0.646	0.760	0.163	0.098	16
Pa08	0.64±0.1	0.68±0.1	0.60±0.1	0.63±0.1	0.073	0.782	3.863	0.009	1.439	9.663	16
Pa09	0.76±0.1	0.72±0.1	1.03±0.3	0.87±0.1	0.592	0.288	0.304	0.420	0.443	0.697	16
Pa11	0.74±0.1	0.68±0.1	0.78±0.3	0.79±0.3	0.035	1.175	5.623	0.282	0.488	1.266	16
Pa12	0.64±0.1	0.64±0.1	1.17±0.5	0.64±0.4	0.058	0.924	4.390	0.053	0.952	4.609	16
Pa13	0.84±0.1	0.70±0.1	0.49±0.2	0.65±0.1	0.787	0.140	0.077	0.962	0.024	0.002	16
Pa14	0.61±0.0	0.61±0.0	0.79±0.1	0.54±0.1	0.740	0.183	0.116	0.968	0.022	0.002	16
Pa15	0.73±0.2	0.65±0.2	0.69±0.2	0.71±0.1	0.055	0.760	4.517	0.002	1.805	15.382	16
Pa16	0.87±0.2	0.77±0.2	0.63±0.2	0.62±0.4	0.198	0.542	1.857	0.012	1.435	8.869	16
Pa17	0.52±0.2	0.53±0.1	0.61±0.1	0.49±0.0	0.692	0.161	0.165	0.010	1.591	9.448	16
Pa18	0.76±0.2	0.75±0.2	0.77±0.1	0.82±0.2	0.048	0.812	4.826	0.003	1.682	13.602	16
Pa19	0.77±0.1	0.94±0.2	0.85±0.2	0.74±0.2	0.123	0.484	2.744	0.008	1.010	9.887	16
Pa20	0.76±0.1	0.61±0.2	0.81±0.2	0.71±0.2	0.500	0.225	0.483	0.001	2.005	18.133	16

Table 6.10: Within participant mean ± standard deviation for each shoe-surface condition contact time from the acceleration task, and two-way ANOVA test results.

	Fibrelastic Nemeziz [s]	Fibrelastic Predator [s]	SISgrass Nemeziz [s]	SISgrass Predator [s]	Surface			Shoe			
					p	d	F	p	d	F	n
Pa01	0.23±0.0	0.22±0.0	0.20±0.0	0.22±0.0	0.785	0.102	0.078	0.006	1.624	11.221	16
Pa02	0.24±0.0	0.24±0.0	0.23±0.0	0.23±0.0	0.324	0.471	1.059	0.062	1.047	4.235	16
Pa04	0.20±0.0	0.25±0.0	0.21±0.0	0.23±0.0	0.659	0.238	0.205	0.417	0.450	0.707	16
Pa05	0.24±0.0	0.24±0.0	0.25±0.0	0.24±0.0	0.014	0.883	8.170	0.001	1.560	18.383	16
Pa06	0.20±0.0	0.20±0.0	0.22±0.0	0.20±0.0	0.059	1.085	4.333	0.439	0.368	0.641	16
Pa07	0.22±0.0	0.21±0.0	0.22±0.0	0.23±0.0	< 0.001	3.268	85.339	0.007	0.594	10.385	16
Pa08	0.21±0.0	0.21±0.0	0.21±0.0	0.21±0.0	0.170	0.626	2.133	0.479	0.301	0.533	16
Pa09	0.20±0.0	0.23±0.0	0.22±0.0	0.21±0.0	0.245	0.597	1.494	0.452	0.369	0.605	16
Pa11	0.22±0.0	0.22±0.0	0.23±0.0	0.23±0.0	0.114	0.780	2.909	0.677	0.181	0.182	16
Pa12	0.21±0.0	0.21±0.0	0.26±0.1	0.20±0.0	0.812	0.125	0.059	0.554	0.316	0.370	16
Pa13	0.21±0.0	0.20±0.0	0.20±0.0	0.19±0.0	0.126	0.874	2.711	0.901	0.061	0.016	16
Pa14	0.22±0.0	0.22±0.0	0.22±0.0	0.22±0.0	0.018	1.444	7.469	0.888	0.060	0.021	16
Pa15	0.23±0.0	0.25±0.0	0.21±0.0	0.23±0.0	0.128	0.871	2.670	0.596	0.266	0.297	16
Pa16	0.25±0.0	0.23±0.0	0.23±0.0	0.25±0.0	0.855	0.081	0.035	0.120	0.796	2.809	16
Pa17	0.22±0.0	0.22±0.0	0.22±0.0	0.21±0.0	0.211	0.455	1.744	0.002	1.883	15.698	16
Pa18	0.20±0.0	0.22±0.0	0.21±0.0	0.22±0.0	0.834	0.064	0.046	0.002	1.612	16.662	16
Pa19	0.17±0.0	0.19±0.0	0.20±0.0	0.18±0.0	0.751	0.163	0.105	0.219	0.695	1.684	16
Pa20	0.19±0.0	0.19±0.0	0.21±0.0	0.21±0.0	0.644	0.253	0.224	0.817	0.126	0.056	16

6.4.2.3 Ground reaction force loading characteristics and contact time during the deceleration task

For each participant, the GRF loading characteristics and the contact time were calculated for each individual step, assigned to the deceleration task (green feet in Fig. 6.11). The between participants mean and standard deviation of each shoe-surface combination and variable are reported in table 6.12, with the results of the two-way ANOVA test. No significant differences were found either between shoes or surfaces.

Table 6.11: Between participants active peak force, impulse, and contact time mean ± standard deviation for each shoe-surface condition and variable for the deceleration task.

	Fibrelastic Nemeziz	Fibrelastic Predator	SISgrass Nemeziz	SISgrass Predator
Vertical active peak [N kg^{-1}]	18.64±4.60	19.12±4.30	18.51±4.76	18.83±4.83
Horizontal active peak [N kg^{-1}]	6.19±3.00	5.70±3.30	5.39±3.28	5.32±3.26
Vertical impulse [N s kg^{-1}]	1.94±0.50	2.03±0.55	1.89±0.52	1.96±0.52
Horizontal impulse [N s kg^{-1}]	0.61±0.36	0.55±0.25	0.50±0.24	0.57±0.30
Contact time [s]	0.17±0.03	0.18±0.04	0.17±0.04	0.17±0.03

Table 6.12: Between participants active peak force, impulse, and contact time two-way ANOVA test results for the deceleration task.

	Surfaces			Shoes			n
	p	*d*	*F*	*p*	*d*	*F*	
Vertical active peak	0.924	0.008	0.009	0.503	0.063	0.450	462
Horizontal active peak	0.485	0.058	0.488	0.282	0.102	1.161	419
Vertical impulse	0.722	0.034	0.127	0.492	0.062	0.474	488
Horizontal impulse	0.826	0.017	0.048	0.721	0.033	0.128	452
Contact time	0.902	0.012	0.015	0.536	0.055	0.383	503

In tables 6.13 to 6.17, mean ± standard deviation and within participant results for the two-way ANOVA test are reported for vertical and horizontal active peak force, vertical and horizontal impulse and contact time, respectively.

Table 6.13: Within participant mean ± standard deviation for each shoe-surface condition vertical active peak force from the deceleration task, and two-way ANOVA test results.

	Fibrelastic Nemeziz [N kg^{-1}]	Fibrelastic Predator [N kg^{-1}]	SISgrass Nemeziz [N kg^{-1}]	SISgrass Predator [N kg^{-1}]	Surface			Shoe			n
					p	*d*	*F*	*p*	*d*	*F*	
Pa01	17.56±2.2	17.16±2.7	17.95±5.7	18.15±4.1	0.178	0.528	1.926	0.617	0.187	0.257	28
Pa02	19.15±5.2	21.68±3.1	19.24±6.6	21.87±7.0	0.555	0.235	0.358	0.893	0.053	0.019	28
Pa04	15.97±5.2	18.76±2.7	18.16±4.9	20.24±5.7	0.307	0.406	1.095	0.811	0.097	0.059	26
Pa05	18.61±5.8	19.05±2.8	18.88±3.4	19.26±1.8	0.678	0.170	0.177	0.968	0.012	0.002	26
Pa06	20.15±3.1	19.66±4.4	18.61±3.8	19.98±5.0	0.743	0.129	0.110	0.664	0.172	0.194	28
Pa07	18.30±6.4	19.17±2.7	17.85±4.9	18.01±4.1	0.790	0.115	0.073	0.745	0.140	0.108	24
Pa08	19.33±5.4	21.93±4.6	20.19±5.2	18.00±6.1	0.568	0.242	0.336	0.891	0.075	0.019	26
Pa09	20.75±2.6	20.18±4.6	21.22±3.8	17.99±3.8	0.173	0.570	2.006	0.139	0.627	2.379	23
Pa11	18.25±5.0	19.36±4.6	15.46±4.3	15.54±5.1	0.763	0.120	0.093	0.856	0.072	0.034	28
Pa12	19.59±2.4	19.51±2.8	18.13±4.3	17.71±3.9	0.132	0.691	2.474	0.244	0.526	1.445	23
Pa13	16.55±2.0	20.07±4.9	17.96±3.7	21.35±3.7	0.232	0.562	1.545	0.820	0.101	0.054	20
Pa14	21.24±4.9	19.31±2.5	19.75±3.3	18.49±2.6	0.934	0.033	0.007	0.967	0.016	0.002	28
Pa15	16.63±3.7	19.10±6.3	17.85±6.1	20.33±4.2	0.797	0.111	0.068	0.836	0.089	0.044	24
Pa16	17.72±3.8	18.18±4.6	18.27±4.1	16.95±4.3	0.271	0.440	1.269	0.636	0.183	0.230	28
Pa17	17.44±4.4	17.58±3.8	17.83±3.5	17.43±3.9	0.621	0.195	0.251	0.599	0.208	0.284	28
Pa18	17.27±3.0	16.60±6.0	17.76±4.2	18.80±3.8	0.419	0.377	0.683	0.924	0.076	0.009	22
Pa19	21.11±3.1	18.35±2.6	21.15±4.3	18.16±4.2	0.166	0.598	2.063	0.425	0.328	0.493	24
Pa20	18.96±5.3	18.14±5.4	16.99±3.8	20.80±4.7	0.831	0.085	0.047	0.759	0.122	0.183	28

Table 6.14: Within participant mean ± standard deviation for each shoe-surface condition horizontal active peak force from the deceleration task, and two-way ANOVA test results.

	Fibrelastic Nemeziz [N kg^{-1}]	Fibrelastic Predator [N kg^{-1}]	SISgrass Nemeziz [N kg^{-1}]	SISgrass Predator [N kg^{-1}]	Surface			Shoe			
					p	d	F	p	d	F	n
Pa01	4.80±2.3	4.76±2.4	5.48±1.2	4.30±1.8	0.825	0.095	0.050	0.582	0.239	0.313	24
Pa02	4.59±2.2	4.76±2.3	4.94±1.9	3.79±1.4	0.370	0.316	0.837	0.190	0.496	1.828	27
Pa04	4.29±1.5	3.79±2.2	3.72±1.9	4.01±1.1	0.291	0.383	1.175	0.986	0.034	< 0.001	25
Pa05	6.04±2.1	4.47±2.8	4.97±1.3	9.14±4.0	0.667	0.204	0.192	0.822	0.085	0.052	21
Pa06	4.41±1.9	5.05±2.8	5.35±2.8	4.97±1.8	0.641	0.194	0.225	0.353	0.416	0.907	23
Pa07	8.98±2.6	6.51±4.8	8.90±6.5	6.20±1.7	0.770	0.108	0.089	0.825	0.070	0.051	19
Pa08	5.96±2.0	7.24±4.3	5.92±2.6	6.72±2.8	0.078	0.764	3.423	0.211	0.523	1.668	25
Pa09	5.97±1.8	7.06±2.7	5.38±4.0	6.10±2.7	0.507	0.279	0.458	0.321	0.441	1.042	22
Pa11	5.28±2.1	4.77±1.9	5.15±2.6	5.90±2.0	0.357	0.416	0.891	0.950	0.017	0.004	23
Pa12	5.12±3.9	8.40±2.4	4.41±1.7	4.90±3.5	0.238	0.507	1.482	0.306	0.434	1.105	24
Pa13	8.07±4.2	5.65±4.6	6.50±4.5	7.18±4.6	0.455	0.305	0.589	0.480	0.284	0.525	19
Pa14	5.89±2.9	5.36±2.3	6.02±4.0	5.75±1.6	0.986	0.002	< 0.001	0.971	0.006	0.001	27
Pa15	5.94±3.2	5.81±2.2	6.58±3.6	5.86±4.6	0.823	0.091	0.052	0.443	0.349	0.614	23
Pa16	7.91±3.1	6.73±4.3	3.83±1.7	7.85±6.2	0.631	0.197	0.237	0.909	0.056	0.014	27
Pa17	7.51±3.6	4.63±2.2	4.77±3.4	3.62±1.7	0.589	0.206	0.300	0.549	0.234	0.369	27
Pa18	7.01±2.2	6.31±3.9	7.06±4.0	3.62±1.3	0.494	0.305	0.488	0.483	0.312	0.515	21
Pa19	8.30±2.8	7.38±2.8	4.38±1.9	3.98±2.5	0.529	0.328	0.416	0.912	0.058	0.013	19
Pa20	6.89±2.1	4.56±1.7	5.13±2.5	4.49±1.5	0.224	0.530	1.578	0.588	0.227	0.303	23

Table 6.15: Within participant mean ± standard deviation for each shoe-surface condition vertical impulse from the deceleration task, and two-way ANOVA test results.

	Fibrelastic Nemeziz [N s kg^{-1}]	Fibrelastic Predator [N s kg^{-1}]	SISgrass Nemeziz [N s kg^{-1}]	SISgrass Predator [N s kg^{-1}]	Surface			Shoe			
					p	d	F	p	d	F	n
Pa01	1.90±0.3	1.64±0.2	1.60±0.4	1.61±0.3	0.270	0.437	1.273	0.951	0.024	0.004	28
Pa02	1.78±0.4	2.07±0.3	1.75±0.7	2.17±0.6	0.405	0.329	0.718	0.569	0.223	0.333	28
Pa04	1.33±0.3	1.81±0.4	1.65±0.5	1.76±0.4	0.335	0.383	0.971	0.500	0.272	0.470	26
Pa05	1.92±0.4	2.32±0.3	1.72±0.4	1.87±0.4	0.936	0.031	0.007	0.668	0.169	0.188	28
Pa06	2.02±0.3	2.65±0.9	1.71±0.3	1.92±0.3	0.459	0.287	0.565	0.405	0.325	0.718	28
Pa07	1.77±0.7	2.13±0.4	1.82±0.4	2.12±0.5	0.806	0.104	0.062	0.883	0.062	0.022	24
Pa08	1.83±0.4	1.71±0.5	2.02±0.8	1.55±0.5	0.493	0.296	0.486	0.673	0.194	0.184	26
Pa09	2.25±0.4	2.16±0.5	2.27±0.4	1.80±0.4	0.601	0.176	0.282	0.158	0.608	2.139	25
Pa11	2.00±0.5	2.17±0.4	1.89±0.5	1.93±0.5	0.884	0.057	0.022	0.737	0.133	0.116	28
Pa12	2.47±0.2	2.15±0.3	2.25±0.6	2.25±0.8	0.085	0.672	3.237	0.124	0.588	2.543	28
Pa13	2.07±0.5	2.06±0.7	2.04±0.3	2.20±0.4	0.009	1.059	8.106	0.229	0.412	1.526	28
Pa14	2.32±0.2	2.26±0.4	2.12±0.3	2.15±0.5	0.409	0.282	0.705	0.021	0.910	6.137	28
Pa15	1.82±0.5	1.82±0.2	1.71±0.3	2.05±0.5	0.353	0.355	0.895	0.392	0.326	0.760	28
Pa16	1.79±0.6	1.95±0.5	1.97±0.6	1.90±0.5	0.365	0.360	0.853	0.504	0.262	0.461	28
Pa17	1.82±0.7	2.25±0.6	1.90±0.5	2.07±0.4	0.385	0.351	0.788	0.317	0.397	1.051	25
Pa18	1.67±0.3	1.53±0.5	1.69±0.5	1.96±0.3	0.702	0.178	0.150	0.508	0.288	0.454	26
Pa19	1.95±0.3	2.12±0.4	2.04±0.5	1.68±0.5	0.404	0.328	0.721	0.627	0.188	0.242	28
Pa20	1.96±0.5	1.71±0.4	1.84±0.2	2.06±0.5	0.846	0.075	0.039	0.410	0.324	0.702	28

Table 6.16: Within participant mean ± standard deviation for each shoe-surface condition horizontal impulse from the deceleration task, and two-way ANOVA test results.

	Fibrelastic Nemeziz [N s kg^{-1}]	Fibrelastic Predator [N s kg^{-1}]	SISgrass Nemeziz [N s kg^{-1}]	SISgrass Predator [N s kg^{-1}]	Surface			Shoe			
					p	d	F	p	d	F	n
Pa01	0.54±0.3	0.41±0.2	0.45±0.1	0.43±0.2	0.151	0.609	2.226	0.643	0.164	0.221	25
Pa02	0.55±0.2	0.52±0.2	0.53±0.2	0.60±0.3	0.981	0.026	0.001	0.864	0.061	0.030	24
Pa04	0.42±0.1	0.41±0.1	0.36±0.1	0.47±0.1	0.729	0.143	0.124	0.831	0.084	0.047	25
Pa05	0.62±0.3	0.57±0.2	0.45±0.2	0.67±0.3	0.864	0.077	0.030	0.931	0.031	0.008	27
Pa06	0.49±0.1	0.59±0.2	0.43±0.1	0.47±0.1	0.659	0.199	0.201	0.731	0.145	0.121	26
Pa07	0.55±0.3	0.62±0.3	0.74±0.4	0.63±0.2	0.952	0.003	0.004	0.802	0.083	0.065	23
Pa08	0.53±0.1	0.55±0.2	0.52±0.1	0.56±0.2	0.683	0.287	0.173	0.714	0.139	0.139	23
Pa09	0.57±0.2	0.56±0.2	0.49±0.2	0.38±0.2	0.989	0.102	< 0.001	0.034	0.962	5.179	24
Pa11	0.57±0.1	0.50±0.2	0.48±0.2	0.64±0.1	0.773	0.078	0.085	0.900	0.054	0.016	24
Pa12	1.03±0.9	0.72±0.1	0.43±0.1	0.75±0.5	0.467	0.263	0.548	0.376	0.333	0.817	27
Pa13	0.84±0.5	0.55±0.4	0.64±0.4	0.66±0.4	0.984	0.026	< 0.001	0.547	0.245	0.374	26
Pa14	0.52±0.2	0.47±0.1	0.64±0.4	0.59±0.1	0.770	0.104	0.087	0.875	0.046	0.025	27
Pa15	0.50±0.1	0.52±0.2	0.48±0.2	0.54±0.2	0.696	0.151	0.156	0.184	0.556	1.880	27
Pa16	0.78±0.3	0.65±0.5	0.43±0.2	0.74±0.4	0.466	0.299	0.550	0.819	0.111	0.054	26
Pa17	0.67±0.4	0.58±0.2	0.51±0.3	0.47±0.3	0.897	0.062	0.017	0.334	0.448	0.984	23
Pa18	0.56±0.1	0.59±0.2	0.58±0.2	0.64±0.3	0.367	0.251	0.852	0.100	0.736	2.991	23
Pa19	0.55±0.3	0.63±0.3	0.40±0.2	0.46±0.3	0.286	0.471	1.197	0.213	0.544	1.644	26
Pa20	0.56±0.1	0.49±0.1	0.37±0.2	0.48±0.1	0.705	0.152	0.147	0.420	0.313	0.675	26

Table 6.17: Within participant mean ± standard deviation for each shoe-surface condition contact time from the deceleration task, and two-way ANOVA test results.

	Fibrelastic Nemeziz [s]	Fibrelastic Predator [s]	SISgrass Nemeziz [s]	SISgrass Predator [s]	Surface			Shoe			
					p	d	F	p	d	F	n
Pa01	0.18±0.0	0.16±0.0	0.14±0.0	0.15±0.0	0.391	0.340	0.762	0.474	0.282	0.529	28
Pa02	0.17±0.0	0.17±0.0	0.17±0.0	0.19±0.0	0.269	0.438	1.279	0.447	0.296	0.599	28
Pa04	0.11±0.1	0.16±0.0	0.13±0.1	0.17±0.0	0.757	0.116	0.098	0.084	0.707	3.247	28
Pa05	0.18±0.0	0.20±0.0	0.16±0.0	0.16±0.0	0.837	0.081	0.043	0.773	0.114	0.085	28
Pa06	0.17±0.0	0.24±0.1	0.16±0.0	0.16±0.0	0.321	0.387	1.029	0.293	0.412	1.157	28
Pa07	0.12±0.1	0.18±0.0	0.11±0.1	0.18±0.0	0.956	0.022	0.003	0.956	0.022	0.003	28
Pa08	0.15±0.0	0.13±0.0	0.16±0.0	0.09±0.1	0.969	0.015	0.002	0.906	0.044	0.014	28
Pa09	0.17±0.0	0.17±0.0	0.16±0.1	0.12±0.1	0.624	0.194	0.237	0.885	0.057	0.021	28
Pa11	0.19±0.0	0.19±0.0	0.18±0.0	0.18±0.0	0.769	0.116	0.089	0.769	0.116	0.089	28
Pa12	0.21±0.0	0.19±0.0	0.21±0.0	0.20±0.0	0.577	0.216	0.320	0.249	0.462	1.397	28
Pa13	0.18±0.0	0.17±0.0	0.19±0.0	0.15±0.0	0.190	0.512	1.820	0.190	0.512	1.820	28
Pa14	0.18±0.0	0.19±0.0	0.19±0.0	0.19±0.0	0.835	0.080	0.044	0.448	0.298	0.594	28
Pa15	0.17±0.0	0.16±0.0	0.15±0.0	0.16±0.0	0.250	0.425	1.389	0.816	0.083	0.056	28
Pa16	0.18±0.0	0.18±0.0	0.18±0.0	0.18±0.0	0.522	0.248	0.422	0.363	0.358	0.861	28
Pa17	0.14±0.1	0.20±0.0	0.15±0.1	0.16±0.1	0.891	0.053	0.019	0.267	0.446	1.292	28
Pa18	0.13±0.1	0.13±0.1	0.15±0.0	0.17±0.0	0.680	0.158	0.174	0.680	0.158	0.174	28
Pa19	0.14±0.0	0.18±0.0	0.16±0.0	0.15±0.0	0.052	0.802	4.163	0.900	0.046	0.016	28
Pa20	0.16±0.0	0.16±0.0	0.17±0.0	0.17±0.0	0.656	0.177	0.203	0.766	0.117	0.090	28

6.4.2.4 Ground reaction force loading characteristics and contact time during the change of direction task

For each participant, the GRF loading characteristics and the contact time were calculated for each individual step, assigned to the change of direction task (blue feet in Fig. 6.11). The between participants mean and standard deviation of each shoe-surface combination and variable are reported in table 6.19, with the results of the two-way ANOVA test. No significant differences were found either between shoes or surfaces.

Table 6.18: Between participants active peak force, impulse, and contact time mean ± standard deviation for each shoe-surface condition and variable for the change of direction task.

	Fibrelastic Nemeziz	Fibrelastic Predator	SISgrass Nemeziz	SISgrass Predator
Vertical active peak [N kg^{-1}]	19.98±2.74	20.06±2.72	19.56±3.46	19.29±2.93
Horizontal active peak [N kg^{-1}]	11.27±3.39	10.99±3.09	10.92±3.75	11.52±3.82
Vertical impulse [N s kg^{-1}]	11.27±3.39	10.99±3.09	10.92±3.75	11.52±3.82
Horizontal impulse [N s kg^{-1}]	4.18±1.14	4.24±1.07	4.06±1.10	4.07±1.19
Contact time [s]	0.32±0.09	0.33±0.09	0.33±0.09	0.33±0.09

Table 6.19: Between participants active peak force, impulse, and contact time two-way ANOVA test results for the change of direction task.

	Surfaces			Shoes			n
	p	*d*	*F*	*p*	*d*	*F*	
Vertical active peak	0.200	0.136	1.652	0.797	0.027	0.067	359
Horizontal active peak	0.925	0.010	0.009	0.946	0.007	0.005	356
Vertical impulse	0.706	0.040	0.143	0.475	0.076	0.510	360
Horizontal impulse	0.899	0.013	0.016	0.858	0.019	0.032	360
Contact time	0.798	0.027	0.066	0.637	0.050	0.223	360

In tables 6.20 to 6.24, mean ± standard deviation and within participant results for the two-way ANOVA test are reported for vertical and horizontal active peak force, vertical and horizontal impulse and contact time, respectively.

Table 6.20: Within participant mean ± standard deviation for each shoe-surface condition vertical active peak force from the change of direction task, and two-way ANOVA test results.

	Fibrelastic Nemeziz [N kg^{-1}]	Fibrelastic Predator [N kg^{-1}]	SISgrass Nemeziz [N kg^{-1}]	SISgrass Predator [N kg^{-1}]	Surface			Shoe			
					p	*d*	*F*	*p*	*d*	*F*	n
Pa01	21.19±1.3	19.75±2.6	22.98±3.1	21.34±2.1	0.853	0.084	0.036	0.446	0.351	0.610	20
Pa02	20.44±2.1	20.95±2.9	21.71±3.2	20.90±3.3	0.868	0.078	0.029	0.623	0.233	0.251	20
Pa04	20.91±4.1	21.96±2.6	20.70±4.3	17.04±1.6	0.572	0.270	0.332	0.548	0.288	0.376	20
Pa05	19.31±2.3	18.22±2.3	19.23±1.6	16.20±2.3	0.798	0.145	0.068	0.518	0.332	0.439	19
Pa06	18.94±1.5	18.77±1.5	17.99±1.4	17.92±1.0	0.124	0.763	2.630	0.755	0.139	0.101	20
Pa07	21.15±0.7	21.52±2.7	19.60±1.9	21.46±2.0	0.781	0.133	0.080	0.757	0.148	0.099	20
Pa08	21.15±3.9	21.15±3.1	20.52±3.1	19.75±2.7	0.922	0.047	0.010	0.980	0.012	0.001	20
Pa09	21.12±1.4	22.22±1.1	18.18±3.4	19.44±3.7	0.230	0.592	1.561	0.991	0.005	< 0.001	20
Pa11	20.02±1.8	19.39±1.2	17.40±1.9	17.15±1.7	0.317	0.483	1.068	0.881	0.069	0.023	20
Pa12	20.54±1.3	20.28±1.6	19.63±4.4	21.70±1.3	0.685	0.196	0.171	0.878	0.074	0.024	20
Pa13	18.12±3.0	19.02±2.3	17.79±4.2	18.49±3.1	0.697	0.185	0.157	0.452	0.364	0.594	20
Pa14	19.10±2.0	18.42±2.0	18.15±3.9	19.72±1.5	0.582	0.264	0.316	0.817	0.110	0.055	20
Pa15	18.49±1.8	19.29±2.0	19.96±2.6	20.31±4.0	0.515	0.314	0.443	0.911	0.053	0.013	20
Pa16	20.96±3.7	19.98±2.2	20.34±2.7	18.69±2.7	0.833	0.101	0.046	0.852	0.090	0.036	20
Pa17	18.69±1.6	20.89±1.9	19.25±0.7	19.84±0.7	0.872	0.074	0.027	0.308	0.496	1.109	20
Pa18	20.53±3.8	19.32±3.4	20.00±2.9	19.65±2.6	0.557	0.283	0.359	0.756	0.148	0.100	20
Pa19	20.60±1.4	20.91±1.7	19.88±2.8	19.42±1.9	0.772	0.140	0.087	0.920	0.048	0.010	20
Pa20	18.30±0.8	18.99±2.9	18.72±4.3	17.55±2.5	0.087	0.862	3.322	0.764	0.132	0.094	20

Table 6.21: Within participant mean ± standard deviation for each shoe-surface condition horizontal active peak force from the change of direction task, and two-way ANOVA test results.

	Fibrelastic Nemeziz [N kg^{-1}]	Fibrelastic Predator [N kg^{-1}]	SISgrass Nemeziz [N kg^{-1}]	SISgrass Predator [N kg^{-1}]	Surface			Shoe			
					p	*d*	*F*	*p*	*d*	*F*	n
Pa01	11.27±3.2	13.49±3.1	12.47±2.5	11.36±3.4	0.469	0.347	0.551	0.546	0.287	0.381	20
Pa02	10.97±2.0	10.22±1.8	10.95±0.8	10.99±1.3	0.635	0.205	0.235	0.193	0.599	1.847	20
Pa04	11.77±2.8	12.50±1.3	10.41±1.6	10.73±2.8	0.553	0.279	0.367	0.370	0.432	0.850	20
Pa05	10.58±2.7	10.80±2.3	10.49±3.3	8.29±3.1	0.871	0.068	0.027	0.647	0.253	0.218	19
Pa06	10.77±1.5	7.19±1.4	9.59±3.1	9.59±1.8	0.622	0.274	0.254	0.503	0.323	0.471	19
Pa07	11.01±4.1	8.94±1.7	9.11±1.6	11.06±3.9	0.743	0.170	0.111	0.701	0.207	0.154	19
Pa08	12.32±2.5	11.57±3.3	11.50±2.9	12.65±4.0	0.874	0.076	0.026	0.990	0.006	< 0.001	20
Pa09	11.77±2.0	10.87±3.0	9.89±5.3	8.17±1.3	0.837	0.097	0.044	0.501	0.323	0.475	20
Pa11	11.15±1.4	10.15±3.1	11.58±1.7	14.28±6.4	0.842	0.089	0.041	0.501	0.307	0.474	20
Pa12	11.46±4.6	9.22±3.1	10.09±1.6	12.31±5.5	0.774	0.121	0.085	0.752	0.234	0.104	20
Pa13	11.20±3.0	9.87±2.6	12.08±5.0	12.74±3.9	0.820	0.109	0.054	0.977	0.026	0.001	19
Pa14	11.68±3.3	11.84±3.8	12.09±5.8	12.80±3.0	0.929	0.043	0.008	0.971	0.017	0.001	20
Pa15	8.89±4.9	10.14±2.8	12.36±3.2	14.22±3.2	0.199	0.630	1.795	0.864	0.078	0.030	20
Pa16	10.64±4.8	11.66±1.9	10.85±4.5	11.35±3.9	0.933	0.040	0.007	0.663	0.210	0.197	20
Pa17	10.24±1.3	12.00±2.4	10.17±3.8	10.74±2.5	0.145	0.699	2.351	0.272	0.503	1.292	20
Pa18	14.97±4.9	12.53±3.4	11.42±3.2	12.34±3.6	0.345	0.453	0.948	0.690	0.185	0.165	20
Pa19	12.54±2.6	13.81±4.1	12.65±5.6	13.28±2.4	0.272	0.535	1.295	0.621	0.230	0.254	20
Pa20	9.51±3.0	10.24±1.6	9.18±4.9	9.82±2.7	0.691	0.182	0.164	0.310	0.483	1.099	20

Table 6.22: Within participant mean ± standard deviation for each shoe-surface condition vertical impulse from the change of direction task, and two-way ANOVA test results.

	Fibrelastic Nemeziz [N s kg^{-1}]	Fibrelastic Predator [N s kg^{-1}]	SISgrass Nemeziz [N s kg^{-1}]	SISgrass Predator [N s kg^{-1}]	Surface			Shoe			
					p	d	F	p	d	F	n
Pa01	4.49±1.0	4.75±0.4	4.54±0.7	4.51±0.9	0.954	0.028	0.004	0.937	0.038	0.006	20
Pa02	5.24±1.2	4.60±1.4	4.65±1.4	4.68±1.5	0.711	0.178	0.143	0.868	0.079	0.028	20
Pa04	4.22±0.9	4.40±0.7	3.46±1.8	4.08±2.0	0.890	0.066	0.020	0.709	0.180	0.144	20
Pa05	4.16±1.1	4.11±1.0	4.29±1.5	4.32±1.3	0.723	0.170	0.130	0.586	0.262	0.308	20
Pa06	3.72±0.5	3.50±0.9	3.89±0.3	3.57±0.9	0.545	0.285	0.383	0.327	0.474	1.023	20
Pa07	4.22±1.0	4.39±0.8	4.30±1.0	4.29±0.4	0.590	0.258	0.303	0.561	0.279	0.353	20
Pa08	4.42±0.6	4.39±0.7	4.41±0.6	4.18±1.0	0.909	0.053	0.014	0.262	0.551	1.354	20
Pa09	4.71±0.7	4.38±0.5	4.06±0.7	3.34±1.7	0.749	0.149	0.106	0.345	0.457	0.948	20
Pa11	3.95±0.5	4.26±1.3	3.87±0.4	3.53±0.7	0.481	0.337	0.520	0.489	0.331	0.502	20
Pa12	4.36±1.1	4.21±1.3	3.64±1.2	3.96±1.0	0.313	0.493	1.087	0.912	0.051	0.013	20
Pa13	3.94±0.3	4.15±0.6	4.21±0.2	3.98±0.3	0.553	0.282	0.368	0.719	0.169	0.134	20
Pa14	4.30±1.1	4.38±1.2	4.03±1.0	4.11±0.6	0.438	0.375	0.634	0.858	0.084	0.033	20
Pa15	3.12±0.7	3.11±0.9	3.75±0.8	3.73±0.7	0.858	0.086	0.033	0.970	0.018	0.002	20
Pa16	4.28±1.4	4.48±1.6	4.35±1.5	4.44±1.4	0.865	0.081	0.030	0.620	0.239	0.256	20
Pa17	3.27±1.5	3.99±0.6	3.56±1.1	3.26±1.0	0.510	0.302	0.454	0.224	0.586	1.599	20
Pa18	4.54±1.1	4.60±0.8	4.27±0.6	4.28±0.9	0.702	0.184	0.152	0.932	0.041	0.008	20
Pa19	3.44±0.6	3.94±0.4	3.68±0.8	4.08±0.8	0.587	0.262	0.308	0.794	0.125	0.071	20
Pa20	4.83±1.5	4.70±1.4	4.13±1.3	5.00±0.8	0.832	0.102	0.047	0.831	0.103	0.047	20

Table 6.23: Within participant mean ± standard deviation for each shoe-surface condition horizontal impulse from the change of direction task, and two-way ANOVA test results.

	Fibrelastic Nemeziz [N s kg^{-1}]	Fibrelastic Predator [N s kg^{-1}]	SISgrass Nemeziz [N s kg^{-1}]	SISgrass Predator [N s kg^{-1}]	Surface			Shoe			
					p	d	F	p	d	F	n
Pa01	2.85±1.2	3.44±1.1	3.26±1.5	2.79±1.1	0.887	0.069	0.021	0.928	0.043	0.008	20
Pa02	2.85±1.1	2.75±1.9	2.76±0.9	2.89±0.9	0.440	0.365	0.628	0.691	0.184	0.164	20
Pa04	2.86±1.2	2.72±0.8	2.44±1.5	2.39±1.2	0.986	0.008	< 0.001	0.618	0.341	0.258	20
Pa05	2.62±1.1	2.41±0.9	2.24±0.6	1.91±0.7	0.457	0.339	0.580	0.162	0.683	2.149	20
Pa06	2.01±0.4	1.15±0.7	1.97±0.4	2.01±0.5	0.224	0.593	1.597	0.589	0.350	0.035	20
Pa07	1.60±0.5	2.32±1.0	2.12±0.6	2.33±0.8	0.310	0.462	1.099	0.237	0.548	1.510	20
Pa08	2.77±1.0	2.51±0.8	2.43±0.8	2.59±0.4	0.643	0.222	0.223	0.579	0.267	0.321	20
Pa09	2.61±1.3	2.30±1.0	2.42±1.1	1.59±1.0	0.697	0.187	0.157	0.949	0.031	0.004	20
Pa11	2.31±0.4	2.47±1.3	2.36±0.5	2.22±0.6	0.502	0.300	0.473	0.292	0.484	1.186	20
Pa12	2.28±0.8	2.09±1.2	2.07±0.8	2.11±0.7	0.589	0.253	0.304	0.938	0.036	0.006	20
Pa13	2.35±0.3	2.12±0.6	2.53±0.8	2.59±0.5	0.815	0.113	0.057	0.850	0.091	0.037	20
Pa14	2.40±0.8	2.48±0.8	2.63±1.3	2.27±0.4	0.867	0.080	0.029	0.844	0.094	0.040	20
Pa15	1.69±0.9	1.77±0.6	2.40±0.9	2.41±0.4	0.720	0.173	0.133	0.871	0.078	0.027	20
Pa16	2.34±1.6	2.80±1.7	2.43±1.4	2.71±1.5	0.941	0.036	0.006	0.840	0.097	0.042	20
Pa17	1.73±0.9	2.18±0.3	2.17±1.4	1.87±0.6	0.289	0.497	1.203	0.396	0.391	0.761	20
Pa18	3.01±1.2	3.06±1.2	2.66±0.7	2.69±1.2	0.484	0.339	0.513	0.803	0.119	0.065	20
Pa19	2.14±0.6	2.65±0.7	2.24±0.6	2.96±0.9	0.474	0.336	0.538	0.399	0.400	0.752	20
Pa20	2.62±0.9	2.54±0.9	2.06±0.7	2.52±0.6	0.799	0.120	0.067	0.868	0.078	0.029	20

Table 6.24: Within participant mean ± standard deviation for each shoe-surface condition contact time from the change of direction task, and two-way ANOVA test results.

	Fibrelastic Nemeziz [s]	Fibrelastic Predator [s]	SISgrass Nemeziz [s]	SISgrass Predator [s]	Surface p	Surface d	Surface F	Shoe p	Shoe d	Shoe F	n
Pa01	0.34±0.1	0.36±0.1	0.34±0.1	0.35±0.1	0.702	0.183	0.152	0.662	0.210	0.198	20
Pa02	0.41±0.1	0.37±0.1	0.36±0.1	0.37±0.1	0.726	0.166	0.127	0.777	0.134	0.083	20
Pa04	0.32±0.1	0.30±0.1	0.27±0.1	0.34±0.1	0.857	0.086	0.033	0.765	0.144	0.093	20
Pa05	0.34±0.1	0.35±0.1	0.37±0.1	0.36±0.1	0.728	0.165	0.125	0.513	0.315	0.448	20
Pa06	0.30±0.0	0.28±0.1	0.32±0.0	0.31±0.1	0.369	0.427	0.856	0.369	0.427	0.856	20
Pa07	0.32±0.1	0.34±0.1	0.33±0.1	0.31±0.0	0.689	0.191	0.166	0.595	0.255	0.295	20
Pa08	0.31±0.1	0.32±0.0	0.32±0.1	0.31±0.1	0.836	0.097	0.044	0.341	0.464	0.961	20
Pa09	0.31±0.0	0.29±0.0	0.33±0.0	0.31±0.1	0.374	0.425	0.836	0.492	0.324	0.495	20
Pa11	0.30±0.0	0.35±0.1	0.32±0.0	0.29±0.0	0.437	0.372	0.635	0.507	0.325	0.461	20
Pa12	0.32±0.1	0.33±0.1	0.31±0.1	0.28±0.1	0.546	0.292	0.381	0.950	0.050	0.004	20
Pa13	0.33±0.1	0.33±0.0	0.36±0.1	0.33±0.1	0.751	0.151	0.104	0.551	0.287	0.372	20
Pa14	0.34±0.1	0.35±0.1	0.34±0.1	0.31±0.1	0.615	0.242	0.263	0.776	0.136	0.084	20
Pa15	0.26±0.1	0.27±0.1	0.29±0.0	0.28±0.1	0.863	0.083	0.031	0.654	0.216	0.208	20
Pa16	0.33±0.1	0.35±0.1	0.34±0.1	0.36±0.1	0.834	0.101	0.045	0.864	0.082	0.030	20
Pa17	0.27±0.1	0.30±0.1	0.30±0.1	0.27±0.1	0.457	0.335	0.581	0.215	0.584	1.664	20
Pa18	0.31±0.1	0.34±0.1	0.32±0.0	0.35±0.1	0.898	0.062	0.017	0.778	0.136	0.082	20
Pa19	0.28±0.1	0.29±0.0	0.29±0.1	0.33±0.1	0.592	0.259	0.299	0.932	0.041	0.008	20
Pa20	0.40±0.1	0.38±0.1	0.35±0.1	0.41±0.1	0.918	0.050	0.011	1.000	< 0.001	< 0.001	20

6.4.3 Subjective-sensory data tests

The between participants mean ± standard deviation answers to the subjective-sensory data test are reported in table 6.25, and the results of the two-way ANOVA test in table 6.26. A statistical significant difference, indicated with darker green colour, between participants was present only for the perceived pitch hardness between surfaces ($p = 0.046$, $d = 0.470$, $F = 4.122$).

Table 6.25: Questionnaire results reported as mean ± standard deviations.

	Fibrelastic Nemeziz	Fibrelastic Predator	SISgrass Nemeziz	SISgrass Predator
Perceived pitch hardness	3.87 ± 2.0	4.42 ± 1.9	5.00 ± 1.9	5.05 ± 1.5
Perceived shock absorption	5.21 ± 2.1	4.88 ± 1.8	5.22 ± 1.4	4.89 ± 1.4
Fatigue on muscle and tendons	3.59 ± 2.4	3.75 ± 2.1	3.47 ± 2.0	3.40 ± 2.2
Overall foot control	7.21 ± 1.9	6.78 ± 1.9	6.05 ± 2.1	7.19 ± 1.5
Perceived traction on straight acceleration	5.49 ± 1.0	5.61 ± 1.1	5.10 ± 0.5	5.73 ± 1.0
Perceived traction on cutting movements	5.45 ± 0.9	5.32 ± 1.3	4.56 ± 1.3	5.48 ± 1.1
Perceived traction on turning movements	5.32 ± 1.3	5.26 ± 1.4	4.96 ± 1.3	5.45 ± 0.9
Overall traction performance	6.95 ± 1.6	6.95 ± 1.8	6.03 ± 1.8	7.25 ± 1.1
Perceived performance time	6.38 ± 1.3	6.11 ± 1.2	5.93 ± 1.6	6.13 ± 1.6

Table 6.26: Questionnaire two-way ANOVA *p*-values results and Cohen's *d* effect sizes (n=76).

	Surfaces			Shoes		
	p	*d*	*F*	*p*	*d*	*F*
Perceived pitch hardness	0.046	0.470	4.122	0.493	0.156	0.475
Perceived shock absorption	0.978	0.004	0.001	0.417	0.191	0.666
Fatigue on muscle and tendons	0.648	0.107	0.210	0.930	0.020	0.008
Overall foot control	0.399	0.192	0.721	0.419	0.184	0.661
Perceived traction on straight acceleration	0.526	0.144	0.406	0.086	0.400	3.025
Perceived traction on cutting movements	0.174	0.306	1.881	0.146	0.329	2.161
Perceived traction on turning movements	0.779	0.065	0.080	0.464	0.170	0.543
Overall traction performance	0.418	0.183	0.664	0.109	0.369	2.632
Perceived performance time	0.537	0.144	0.386	0.921	0.023	0.010

6.4.4 Relationship between biomechanical and subjective-sensory data

In order to evaluate the relationship between performance time and perception of time or overall traction between shoe-surface conditions, Spearman's rank correlation coefficient was calculated, and the results are reported in table 6.27 for each participant. Since, faster performance times correspond to lower values, whereas faster time and higher traction perceptions to higher scores, coefficients representing a high or

Table 6.27: Spearman's rank correlation coefficient between performance time and traction perception or time perception for each participant. High and very high negative correlation (darker green colour) represents the preferable condition, since faster performance times correspond to lower values, whereas faster time and higher traction perceptions to higher scores.

	Performance time vs Perceived time	Performance time vs Perceived traction
Pa01	0.00	0.40
Pa02	0.20	0.40
Pa03	0.40	0.32
Pa04	0.11	0.40
Pa05	0.80	0.60
Pa06	0.00	0.00
Pa07	0.80	1.00
Pa08	−0.40	0.20
Pa09	0.20	0.63
Pa10	−0.60	−0.40
Pa11	0.40	−0.32
Pa12	−0.32	−0.40
Pa13	0.00	0.11
Pa14	−0.80	0.40
Pa15	−0.40	−0.32
Pa16	0.32	0.20
Pa17	0.82	0.32
Pa18	−0.20	−0.40
Pa19	−1.00	0.40

very high negative correlation (< -0.70) are of interest. Only two participants (Pa14 and Pa19) perceived the time with good accuracy between shoe-surface conditions, whereas the perceived traction ranking has no correspondence with the performance time for any of the participants.

In tables 6.28 to 6.32, Spearman's rank correlation coefficient between GRF loading characteristics and contact time with traction perception, specific to each individual task, are reported. Positive high and very high correlations between traction perception and GRF loading characteristics, and negative high or very high correlations between traction perception and contact times are of interest. No values are reported for participants Pa05 and Pa15 in the evaluation of straight acceleration, because they did not perceive differences between shoe-surface conditions during this task; thus, a ranking was not possible. For the same reason, participant Pa19 was excluded, perceiving no differences in traction during all the movements analysed.

Table 6.28: Spearman's rank correlation coefficient between estimated vertical active peak force and traction perception for the first step of acceleration and change of direction manoeuvres.

	Acceleration	Unpredicted 45° cut	Anticipated 45° cut	Left leg 90° cut	Right leg 90° cut	Turn
Pa01	−0.80	−0.40	0.60	0.20	−0.40	0.40
Pa02	0.80	0.11	−0.32	−0.95	−0.32	0.40
Pa04	−0.32	−0.40	−0.80	−0.40	−0.20	0.40
Pa05		−1.00	−1.00	−0.40	−0.40	−1.00
Pa06	−0.77	−0.77	0.26	0.26	0.77	0.77
Pa07	−1.00	−0.80	−0.20	−0.80	−0.20	0.40
Pa08	−0.26	0.77	0.26	0.77	−0.77	0.32
Pa09	−0.40	0.80	0.40	1.00	1.00	0.80
Pa11	0.80	0.60	0.80	0.60	0.20	−0.11
Pa12	0.20	−0.80	−0.40	−0.80	0.40	−1.00
Pa13	0.40	−0.80	0.40	0.20	0.40	0.80
Pa14	0.40	0.95	−0.63	0.21	0.63	0.20
Pa15		1.00	0.40	−0.20	0.20	−0.26
Pa16	−0.80	0.95	−0.74	−0.21	−0.74	−0.40
Pa17	0.40	−0.40	−0.80	−0.20	−0.20	−0.40
Pa18	−0.32	0.21	−0.11	0.63	−0.21	0.95

Table 6.29: Spearman's rank correlation coefficient between estimated horizontal active peak force and traction perception for the first step of acceleration and change of direction manoeuvres.

	Acceleration	Unpredicted 45° cut	Anticipated 45° cut	Left leg 90° cut	Right leg 90° cut	Turn
Pa01	−1.00	0.80	0.40	0.20	0.00	0.80
Pa02	−0.80	−0.95	0.11	0.21	0.32	0.40
Pa04	−0.32	0.80	−0.40	0.80	1.00	−0.40
Pa05		0.20	−0.80	−0.40	−0.40	−1.00
Pa06	0.26	0.77	−0.26	0.77	0.77	0.87
Pa07	−0.80	0.80	−0.20	0.00	−0.80	−1.00
Pa08	0.77	−0.26	0.26	−0.77	0.77	0.11
Pa09	0.60	0.20	0.80	0.40	−0.20	0.60
Pa11	0.80	−0.40	0.00	1.00	−0.40	−0.21
Pa12	−0.20	−1.00	−0.80	0.40	0.00	0.40
Pa13	0.40	0.80	−0.20	0.40	−0.80	0.50
Pa14	−0.20	−0.21	0.74	0.63	−0.95	0.20
Pa15		0.40	0.40	0.60	0.80	0.26
Pa16	0.60	0.95	−0.95	0.21	0.21	1.00
Pa17	0.80	0.80	−0.40	−0.40	0.00	−0.40
Pa18	−0.21	−0.74	0.74	−0.11	−0.11	−0.21

Table 6.30: Spearman's rank correlation coefficient between estimated vertical impulse and traction perception for the first step of acceleration and change of direction manoeuvres.

	Acceleration	Unpredicted 45° cut	Anticipated 45° cut	Left leg 90° cut	Right leg 90° cut	Turn
Pa01	−0.40	0.80	0.80	−0.20	−0.40	0.40
Pa02	1.00	−0.63	−0.21	−0.21	−0.21	−0.40
Pa04	−0.95	−0.20	−0.20	0.80	0.40	0.20
Pa05		0.80	−0.40	0.20	0.20	0.40
Pa06	−0.26	0.26	0.77	−0.77	−0.77	−0.26
Pa07	−0.80	0.20	−0.20	0.20	0.80	−0.40
Pa08	0.77	0.26	0.26	−0.77	−0.26	−0.21
Pa09	−0.20	−0.20	0.40	0.60	0.60	0.40
Pa11	0.80	0.00	−0.20	−0.80	−0.20	0.21
Pa12	0.00	0.40	−0.40	−0.60	−0.80	0.20
Pa13	0.80	−0.40	−0.80	0.40	−0.40	−0.60
Pa14	−0.80	−0.21	−0.11	0.63	0.32	−0.20
Pa15		0.80	−0.20	0.40	0.40	0.77
Pa16	−0.20	0.95	−0.95	−0.32	0.32	0.40
Pa17	0.40	−1.00	0.20	0.60	−0.80	0.60
Pa18	−0.74	−0.21	−0.11	0.74	−0.95	0.21

Table 6.31: Spearman's rank correlation coefficient between estimated horizontal impulse and traction perception for the first step of acceleration and change of direction manoeuvres.

	Acceleration	Unpredicted 45° cut	Anticipated 45° cut	Left leg 90° cut	Right leg 90° cut	Turn
Pa01	−0.20	0.80	0.40	0.80	0.00	0.20
Pa02	−0.40	−0.63	−0.11	−0.95	0.32	0.40
Pa04	−0.32	0.40	−0.40	0.80	0.80	−0.80
Pa05		0.80	−0.40	0.20	0.20	0.40
Pa06	−0.77	0.77	0.77	0.77	−0.26	−0.26
Pa07	−0.40	0.40	−0.40	0.20	0.00	0.40
Pa08	0.77	−0.77	0.77	−0.26	−0.26	−0.21
Pa09	−0.60	0.80	0.80	−0.40	−0.40	0.60
Pa11	0.40	−0.40	0.00	1.00	0.00	0.74
Pa12	0.40	−1.00	−0.80	−0.20	−0.80	0.40
Pa13	−0.40	1.00	−0.20	0.60	−0.80	0.40
Pa14	−0.40	−0.21	0.21	0.32	−0.95	−0.80
Pa15		0.40	−0.20	0.40	0.40	0.26
Pa16	−0.20	0.95	−0.74	−0.32	0.95	0.80
Pa17	−0.40	−0.20	−0.40	0.60	−1.00	0.60
Pa18	−0.63	−0.74	−0.11	−0.11	−0.11	−0.95

Table 6.32: Spearman's rank correlation coefficient between estimated contact time and traction perception for the first step of acceleration and change of direction manoeuvres.

	Acceleration	Unpredicted 45° cut	Anticipated 45° cut	Left leg 90° cut	Right leg 90° cut	Turn
Pa01	0.20	0.20	0.21	−0.20	0.20	−0.63
Pa02	0.40	0.21	−0.21	−0.21	0.32	−0.95
Pa04	0.74	0.63	−0.21	0.32	0.63	0.40
Pa05		0.32	−0.32	0.20	0.20	0.95
Pa06	0.00	0.26	0.77	−0.77	−0.77	−0.77
Pa07	0.63	0.40	−0.32	0.20	0.80	−0.40
Pa08	−0.77	0.54	0.82	−0.77	0.00	−0.21
Pa09	−0.20	−0.32	−0.80	−1.00	0.60	−0.80
Pa11	−0.32	0.26	−0.32	0.21	0.11	0.50
Pa12	0.00	0.80	0.40	−0.60	−0.80	0.32
Pa13	−0.32	0.45	−0.95	0.40	−0.40	−1.00
Pa14	0.63	−0.83	0.63	0.11	−1.00	−0.40
Pa15		−0.20	−0.40	0.63	0.00	0.77
Pa16	0.63	0.95	−0.83	−0.32	0.63	1.00
Pa17	0.40	−0.95	0.40	0.63	−0.80	0.11
Pa18	−0.50	−0.21	−0.74	0.21	−0.32	−0.95

6.5 Discussion

In this chapter, the method validated previously to estimate 3D GRFs was applied in-field with the aim of evaluating the interaction between hybrid turf surface systems (Fibrelastic vs SISgrass) and shoes (Nemeziz vs Predator), and their relationship with performance, perception and surfaces' mechanical properties. These interactions were evaluated for acceleration, deceleration and change of direction tasks separately. The findings will be discussed in the following sections: surface mechanical tests (Sec. 6.5.1), biomechanical tests (Sec. 6.5.2), subjective-sensory data tests (Sec. 6.5.3) and the relationship between mechanical, biomechanical and subjective-sensory data (Sec. 6.5.4).

6.5.1 Surface mechanical tests

Hybrid turfs are the dominant surfaces for the major football professional leagues. Labosport, as part of their ScorePlay^{TM} testing system, tested 68 different hybrid pitches (33 stitched-based, 13 carpet-based and 22 reinforce rootzone systems), of which the 94.1% are venues for elite level teams (33 stitched-based, 12 carpet-based and 19 reinforced rootzone) placed in different countries in the world. In chapter 3, a statistical analysis was performed to compare the mechanical properties of the different hybrid turf surface construction systems and, since they have an artificial component, their mechanical properties were compared with FIFA artificial turf requirements as well. In order to satisfy quality, performance and safety standards, shock absorption, vertical deformation and rotational traction must fall inside the following bands: $60-70\%$, $4-10$ mm, and $30-45$ Nm, respectively [122]. It was concluded that the majority of the hybrid turf surfaces tested, which are representative of the surfaces where professional teams train and play, satisfies FIFA quality, performance and safety requirements; different hybrid turf constructions have similar compliance, whereas, even if not significantly different, higher rotational traction values were found between the stitched-based system and the other two types of hybrid turfs, with the 35.7% of stitched-based surfaces exceeding the upper FIFA band limit.

A stitched-based (SISgrass) and a reinforced rootzone (Fibrelastic) hybrid turf surface were available for testing. In order to identify where the mechanical properties of these surfaces sit, if they are representative of the average hybrid turfs, and respect FIFA artificial turf pitches standards; their mechanical properties were assessed with the AA and rotational traction test devices. The mechanical test results showed that both surfaces do not achieve FIFA artificial turf requirements, reporting very low values for shock absorption and vertical deformation (37.0% and 41.7%, and 3.7 mm and 3.3 mm, respectively for Fibrelastic and SISgrass), and very high values for rotational

traction (48.8 Nm and 57.3 Nm respectively for Fibrelastic and SISgrass) compared to the surfaces tested by Labosport (Fig. 6.13). The very low values measured for shock absorption and vertical deformation could result in higher deceleration and impact forces when athletes land on them, with consequent higher risk of injury (Sec. 2.2.1). Whereas, the high values found for the rotational traction could cause foot fixation, with consequent higher risk of ligament injury to the knee and ankle joints, since the shoe can not move freely during change of direction manoeuvres, while the structures above the foot continue to rotate [34–38] (Sec. 2.2.2). These large differences in the mechanical properties between the hybrid turf surfaces available for testing and Labosport data means that the surfaces were not representative of the pitches used in match play. The difference could be due to the age, level of usage and maintenance, which is assumed lower compared to professional teams' pitches since research surfaces are used only periodically.

Between the surfaces (Table 6.1), higher rotational traction was measured on the SISgrass surface through the rotational traction test device, which suggests a higher risk of foot fixation on this surface. This is in agreement with what reported in chapter 3, where 35.7% of stitched-based hybrid pitches exceeded the rotational traction upper limit specified in the FIFA requirement and a higher median value was found in comparison to the other hybrid turf constructions, suggesting a higher risk of foot fixation when athletes change direction on stitched-based hybrid pitches. Whereas, higher impact forces were measured on the Fibrelastic surface through the AA device, which results in lower values of shock absorption. In section 2.2.1, it was reported that shock absorption is influenced by the amount of surface vertical deformation, thus, also a lower vertical deformation would be expected on the Fibrelastic surface. However, this is not the case and suggests that mechanical tests are not able to report the full picture of the complexity of playing surfaces and their visco-elastic properties.

Smeets et al. [44] showed that rotational traction on dry stitched-based hybrid turf and natural grass is similar, but when tested in a wet scenario only the former surface was almost not influenced, whereas the latter presented a decrease in rotational traction (Sec. 2.3.1.3). This would result in loss of grass cover, tears and, therefore, a decrease in surface playability. No studies were found in the literature comparing the moisture content between different hybrid turf surface construction systems. From Labosport ScorePlay™ dataset (Ch. 3), a significant difference and smaller variability were found in the moisture content data for stitched-based hybrid turfs compared to reinforced rootzone ones (19.1% vs 30.4%), suggesting that the stitched-based system is the hybrid turf type less influenced by the weather conditions. In this study, the same mean values of moisture content between testing days were obtained for the Fibrelastic and SISgrass surfaces (20.0% vs 20.0%), with similar measurements be-

tween the two surfaces on different testing days, regardless of the weather conditions and amount of rain fallen; thus, no differences in consistency were found. From these results, it can be concluded that the mechanical properties are not influenced by the moisture content and the differences between the two surfaces were consistent during the whole period of testing, regardless of the weather.

6.5.2 Biomechanical tests

In section 6.3.2.5, it was reported that the agility course was designed in order to be representative of purposeful movements recorded during match play, by including accelerations, decelerations, anticipated and unpredicted changes of direction, and be completed in less than 13.1 s, the mean duration recorded during match play for high intensity actions [23]. The latter aspect was satisfied, since a mean performance time of 8.93±0.58 s, ranging from 7.98 s to 10.52 s between participants and shoe-surface conditions, was recorded in this study.

The results obtained from the statistical analyses (Tables 6.2 and 6.3) showed that the performance time is not influenced by shoes or surfaces; however, the analysis of the performance times reported in table 6.3 suggests that they could be influenced by the specific shoe-surface interaction for individual participants. For example, the SISgrass-Nemeziz combination shows big differences compared to the other conditions for participants Pa12 (10.52 s vs 9.00 s, 9.44 s and 9.57 s) and Pa14 (8.91 s vs 9.24 s, 9.30 s and 9.37 s), or the Fibrelastic-Predator interaction for participant Pa17 (9.39 s vs 9.12 s, 9.12 s and 9.17 s). Therefore, it is believed that the performance time is influenced by specific participant-shoe-surface interactions and could not be attributed to only shoe or surface characteristics.

The movement tasks in the agility course were classified as acceleration, deceleration and change of direction tasks (Fig. 6.11). Differences were found during the acceleration task between shoe conditions in the horizontal active peak force ($p < 0.001$, $d = 0.997$, $F = 69.225$), vertical ($p < 0.001$, $d = 0.459$, $F = 16.176$) and horizontal impulses ($p < 0.001$, $d = 0.831$, $F = 50.353$) in the inter-participant analysis (Table 6.5). Such differences were observed also in the within participant analysis for the majority of participants (78%, 50% and 56%, respectively for the same GRF loading characteristics; Tables 6.7 to 6.9). Differences were found between participants (Table 6.5) also in the contact time analysis between surface and shoe conditions ($p = 0.005$, $d = 0.318$, $F = 7.844$ and $p < 0.001$, $d = 0.493$, $F = 18.232$, respectively) and between surface conditions for the vertical impulse ($p < 0.001$, $d = 0.517$, $F = 20.183$). However, a smaller percentage of participants showed differences for within participant analyses for these parameters (17%, 28% and 22% participants, respectively;

Tables 6.10 and 6.8).

No significant differences were found during deceleration or change of direction tasks either between shoes or surfaces between participants (Tables 6.12 and 6.19), and only for three participants in different parameters during deceleration steps; Pa13 for vertical impulse between surfaces ($p = 0.009$, $d = 1.059$, $F = 8.106$), Pa14 for vertical impulse between shoes ($p = 0.021$, $d = 0.910$, $F = 6.137$), and Pa09 for horizontal impulse between shoes ($p = 0.034$, $d = 0.962$, $F = 5.179$). A reason for these results could be sought in differences on the forefoot region of the shoe outsole. Deceleration and change of direction tasks are characterised by heel-toe footfall patterns, as evidenced inspecting the video recordings, and the highest traction demands are exerted by the players on the surface during the impact peak phase, corresponding to heel and foot-flat contact. Whereas, during acceleration tasks, athletes contact the surface only with the forefoot, thus higher mechanically available traction on this region of the outsole allows them to better accelerate away from the surface without slipping, which would result in a loss of performance.

Hamill [141] reported that differences in the midsole shoe hardness influence the impact peak, time to impact peak and loading rate; whereas, the magnitude of the active peak force is not generally affected by footwear construction. Nemeziz and Predator shoes differ in the ankle support, studs' shape, rigidity of the outsole and heel structure. The data analysis shows that during the acceleration task the Nemeziz shoe allows the application of higher horizontal force, especially when interacting with the SISgrass surface, suggesting that the cylindrical studs allow players to utilise more traction during this task compared to the Predator's prismatic studs. The effect of the Predator's more rigid outsole in the midsole and heel regions could not be investigated during the impact peaks, since the beginning of stance phase could not be accurately predicted, due to accelerometer range and sample frequency limitations highlighted in the previous chapter (Ch. 5). However, when comparing the effect of shoes' traction properties, differences should be restricted to the outsole design, since athletes may be more inclined to perform better, consciously or unconsciously, in a shoe design that is visually appealing or more comfortable [124].

Previous works by Schrier et al. [25] and Sterzing et al. [66] found no differences in utilised traction during sprint acceleration, whereas a significant increase in translational and rotational utilised traction was observed during change of direction tasks or a slalom course. Therefore, the authors concluded that traction has a significant effect on turning movements, whereas compliance appears to improve performance where traction does not have a significant effect, such as during sprint acceleration (Sec. 2.3.2.3). Conclusions on the effect of compliance can not be drawn from this study,

since the two surfaces, where the agility course was performed, present similar values. Whereas, the effect of traction can be analysed, and the results of this study suggest that traction may have a significant effect not only during change of direction tasks but also during sprint acceleration, which is in disagreement with previous research. Schrier et al. [25] compared the interaction of indoor shoe and firm ground football boot on artificial turf, and Sterzing et al. [66] of shoes with elliptic and bladed studs on artificial turf, neither of which is specifically designed for artificial turf surfaces and, as a result, could have provided undesired levels of traction. Both too low or too high traction conditions was shown by Müller et al. [81] to result in movement adaptations when players perform changes of direction tasks, as well as, during straight acceleration (Sec. 2.3.2.3). Therefore, traction could have a significant effect also during straight acceleration, as shown in this study; with previous research conclusions limited by the comparison between shoe-surface interaction conditions offering an unsuitable amount of traction.

Differences in traction should be analysed during the most demanding phase of foot contact of the specific movement analysed, however the initial contact was not used for comparison, due to the low accuracy of its estimation. Therefore, the use of the active peak force may explain the absence of significant differences during deceleration and change of direction tasks in this study. However, the method allowed to analyse the phase with the highest forces during straight acceleration, during which differences were found.

Due to the impact of COVID-19 on the data collection presented in the previous chapter (Ch. 5), it was not possible to evaluate the reliability and sensitivity of the developed method, however, its validity in the estimation of 3D GRF was evaluated for different movements and for a wide range of forces by comparison with force platforms' measurements. The reliability of a method developed from IMU recording might be affected by factors such as sensor calibration and subject preparation in terms of sensor attachment [142], however, the sensors used in this study were factory calibrated and raw measurements were used to estimate GRFs, which should decrease the day-to-day variability. Moreover, the same researcher attached the sensors on specific locations using the same bandaging technique for all the participants, reducing the inter-subject variability. In order to evaluate if the developed method is as sensitive as laboratory measurements to differentiate between different shoe and surface conditions, it would have been informative to compare the GRF estimation with the force platform measurements while altering the coefficient of traction between shoe and surface. This could have been obtained by attaching different materials to the shoe outsole or applying various amounts of wax to the floor, as different authors [63, 76, 77] did to evaluate the relationship between mechanically available and utilised traction (Sec.

2.3.2.3). Although reliability and sensitivity of the new method were not evaluated, both group and individual differences were found between shoes for the straight acceleration task, suggesting that these differences are not a consequence of day-to-day or trial-to-trial variability in measurements from the system, but they are related to the difference in studs' shape. In the literature review (Sec. 2.3.1.2), differences in studs' penetration and effective cross sectional area were found to affect translational traction, therefore, in future studies it would be beneficial to include a measurement of stud penetration to the biomechanical tests, as well as the perimeter and cross sectional area values for the studs considered in order to provide a better understanding of the differences found.

6.5.3 Subjective-sensory data tests

The subjective-sensory data test results (Table 6.25 and 6.26) revealed that between participants a difference was perceived only for the pitch hardness between surfaces ($p = 0.046$, $d = 0.470$, $F = 4.122$). SISgrass was felt as significantly harder compared to Fibrelastic (5.02 ± 1.7 and 4.15 ± 2.0, respectively), suggesting that the perception of this surface characteristic is more affected by the surface vertical deformation, rather than by shock absorption (Table 6.1). Even if not statistically significant, higher shock absorption was perceived wearing Nemeziz (5.22 ± 1.8) compared to Predator (4.88 ± 1.6), suggesting an influence due to the cushioning properties of the shoes.

In the literature review (Sec. 2.2.1), it was reported that high foot instability and fatigue are associated with high values of shock absorption and vertical deformation [25, 27]. In this study, the participants reported a good overall foot control (6.81 ± 1.9), and low values of fatigue perceived on muscles and tendons (3.55 ± 2.2), which is in accordance with the measured low surface compliance. Moreover, lower values of fatigue on muscles and tendons were perceived on average on SISgrass than on Fibrelastic (3.43 ± 2.1 and 3.67 ± 2.3, respectively), suggesting that fatigue, as well as the perception of pitch hardness, is more related to the surface vertical deformation than to shock absorption.

The highest traction was perceived between participants (Table 6.25) for the SISgrass-Predator interaction during acceleration, cutting and turning tasks (6.72 ± 1.6, 5.73 ± 1.0, 5.48 ± 1.1, respectively) and the lowest values for the SISgrass-Nemeziz condition (5.10 ± 0.5, 4.56 ± 1.3, 4.96 ± 1.3, respectively), whereas smaller differences were perceived on the Fibrelastic surface regardless the shoes worn (5.49 ± 1.0, 5.45 ± 0.9, 5.32 ± 1.3, and 5.61 ± 1.1, 5.32 ± 1.3, 5.26 ± 1.4, for Nemeziz and Predator respectively); showing that participants perceived bigger differences between shoes on the SISgrass surface. Between tasks, higher traction for each shoe-surface interaction is

perceived during straight acceleration, especially on the SISgrass surface. The same trend found for the individual tasks is present for the overall traction perception as well (7.25 ± 1.1, 6.03 ± 1.8, 6.95 ± 1.6 and 6.95 ± 1.8 for SISgrass-Predator, SISgrass-Nemeziz, Fibrelastic-Nemeziz and Fibrelastic-Predator, respectively). This perception is judged with a higher score compared to what is perceived during the single tasks investigated. This, together with the highest GRF values recorded during the impact peak of the deceleration steps (Fig. 6.10), suggests that very high traction might have been perceived during the steps approaching the changes of direction, which were not investigated in the subjective-sensory test. The investigation of deceleration steps could provide useful information in future work.

In addition to the lowest values of perceived traction, the interaction SISgrass-Nemeziz reported also the lowest score for overall foot control (6.05 ± 2.1) and the slowest perceived performance time (5.93 ± 1.6); whereas, the fastest times were perceived for the Fibrelastic-Nemeziz interaction (6.38 ± 1.3). In the literature review (Sec. 2.2.2), it was highlighted that traction should lie in an optimum range that provides adequate slip resistance for dynamic movements without leading to foot fixation, thus, both too low or too high traction would result in a loss of performance. The results from this study show a relationship between the perceptions of traction and time to complete the agility course when the lowest traction is perceived; whereas, the highest traction sensed (SISgrass-Predator) is not related to the perception of the fastest time, suggesting that the desired level of traction could have been exceeded. It is not thought that this is influenced by the surface hardness, since the SISgrass surface, even if perceived as significantly harder, was judged with a score very close to the fair line mark (5.02 ± 1.7).

6.5.4 Relationship between mechanical, biomechanical and subjective-sensory data

The relationships between GRF loading characteristics, contact time and performance time with the participants' perception of traction were evaluated through Spearman's rank correlation coefficient. The purpose of this was to highlight if the perception of traction ranking corresponds to that of the measured variables. Participants were asked to judge the traction perceived during straight acceleration, cutting and turning manoeuvres, whereas no information were asked regarding the deceleration steps. The relationship was evaluated for each change of direction manoeuvre individually, and the results of each comparison were reported in tables 6.28 to 6.32. In the previous chapter (Ch. 5, Table 5.8), it was concluded that it is possible to rank different shoe-surface conditions both in the vertical and horizontal direction. The impulse

should be used to rank changes of direction, regardless the angle of the manoeuvre, owing to high correlations coefficients (> 0.70) found in chapter 5. Whereas, to rank the acceleration task with the same accuracy, the active peak force estimated during the first step of acceleration should be evaluated. Very high accuracy (correlation coefficient of 0.97) was shown for all the movements when analysed with the contact time (Ch. 5). The majority of the relationships (81%) between perception and loading characteristics did not present high correlation (Tables 6.28 to 6.32). Only three participants (Pa08, Pa11 and Pa17) ranked the traction during straight acceleration in accordance with the estimated horizontal active peak force value; and one or more changes of direction horizontal impulses were ranked with high to very high correlation with the traction perception for a total of eight participants. In the latter case, the relationship was associated with the leg pushing off from the cut (left leg for Pa01 and Pa06, right leg for Pa16), with the angle of the manoeuvre (90° cut for Pa04 and 45° cut for Pa09 and Pa06), or showed no connections (90° and 180° changes of direction performed with different legs for Pa11). Even if contact time is a measure of performance, with shorter times associated with quicker changes of direction, a consistent relationship with the perceived traction was not found. These low correlations may be related to participants' movement adjustments due to undesired traction conditions, which, as suggested by Hamill [141], results in an alteration of the GRF loading characteristics.

In the literature review (Sec. 2.3.2.2), two studies [27, 72] comparing performance time and surfaces' mechanical properties were reported. Faster performance times were associated with surfaces having rotational traction values inside the FIFA artificial turf required band [27]; whereas conflicting results were found for shock absorption. One study [27] found the performance time affected only if the surface is excessively rigid, by recording slower times; and another study [72] found that higher shock absorption is related to slower performance times. In this study, slightly faster times were recorded on average on the Fibrelastic surface, which presents lower rotational traction and lower shock absorption compared to the SISgrass surface. However, these mechanical properties, as previously reported, are higher and lower than the required band, respectively, suggesting that worse performances compared to the average hybrid turf surfaces are obtained.

Spearman's rank correlation coefficient was used also to assess the relationship between the time taken to complete the agility course with the perception of this time and of the overall traction. Only two participants (Pa14 and Pa19) perceived the time with high correlation between shoe-surface conditions, whereas the perceived traction ranking has no correspondence with the performance time for any of the participants. This is in disagreement with the results of previous research [64, 66, 79], which found

an association between running time performance with players' perceptions of faster times (Sec. 2.3.3). However, it is important to note, that the average score given to the perception of the time to complete the course was 6.14, highlighting that the participants did not feel able to complete the agility course at the best of their possibilities. This highlights limitations in the shoe-surface interaction and in the course design, due to the presence of obstacles, which may have altered players' movements. Obstacles might have reduced the possibility of trunk leaning during the 90° cut, and the area available for the manoeuvres; however, this was necessary to enforce participant movement around the course, to analyse changes of direction tasks of the desired angles and to be comparable between legs, shoe-surface conditions and participants. This highlights how shoe-surface interaction research should either focus on courses that allow participants to achieve best performance times through movement adaptation, or design courses to elicit maximal traction to understand the limits of shoe-surface interaction performance.

6.5.5 Summary of the findings

The hybrid turf surfaces where this study was carried out were not representative of the pitches used by elite level teams, since comparatively low compliance and high rotational traction were measured. This suggests that athletes on these surfaces are slower and subjected to higher decelerations and impact peak forces, especially on the SISgrass surface. These differences could be due to the age, level of usage and maintenance of these surfaces, which is assumed lower compared to professional teams' pitches since research surfaces are used only periodically. Moreover, the pool of participants taking part to this study were recreational players or competed at lower level on natural or artificial grass surfaces. Therefore, the results of this study are specific to these available surfaces; whereas, in order to have a representative evaluation of shoe-surface interaction on hybrid football fields, future work should be conducted on an average sample of the football hybrid turf surfaces used in match play and involve high level players, familiar with these fields.

The shoes worn by participants were both firm ground boots, but differed for studs' shape, outsole rigidity, heel construction and ankle support, whereas the difference in mass could be considered as negligible. Firm ground footwear are designed for natural grass surfaces in good and dry condition, thus they were suitable for this study, since it was reported that hybrid turf surfaces have similar properties to natural grass in case of dry conditions, and their characteristics are almost not influenced by the weather [44]. However, the evaluation of these shoes interaction with natural grass surfaces, for which they are specifically designed, in comparison to their interaction with hybrid turf surfaces is difficult, due to the challenges in ensuring similar moisture

content levels between surfaces, and avoiding wear on natural grass, which would affect player movement when completing more trials of an agility course on the same area.

To evaluate shoe-surface interaction, the phase of stance during which the highest GRFs are measured should be analysed. During deceleration and change of direction steps, this corresponds to the impact peak phase, and to the push-off phase during acceleration tasks, both for vertical and horizontal force components. Therefore, shoe-surface interaction could not be accurately evaluated for the most demanding tasks, due to the high errors in the estimation of impact peak forces obtained in the previous chapter (Ch. 5); this represents a limitation in this study. Whereas, the prediction of the active peak force allowed the comparison between shoe-surface conditions during straight acceleration, with the results showing that Nemeziz's cylindrical studs allowed the application of higher horizontal force, especially on the SISgrass surface. However, athletes may be more inclined to perform better, consciously or unconsciously, in a shoe design that is visually appealing or more comfortable [124], therefore, this study presents a limitation when comparing the effect of shoes' traction properties, and the differences should be restricted to the outsole design.

Previous research [82, 84, 85] showed how the application of higher vertical force in the steps preceding a change of direction and not decelerating predominantly on the penultimate step could result in longer ground contact times and slower change of direction performance. A decrease in performance was shown also during unanticipated conditions compared to preplanned manoeuvres, due to the lower amount of time that athletes have to implement appropriate postural adjustment strategies as a response to a sudden stimulus [86]. Therefore, another limitation in this study related to the low accuracy in the measurement of the impact peak force, is that a comparison between the change of direction steps and the preceding ones is not possible, as well as a comparison between the unpredicted and anticipated change of direction manoeuvres.

A significant difference in the subjective-sensory test was found only for the pitch hardness, property that seems to be affected by the surface vertical deformation, rather than by shock absorption. Higher shock absorption was felt by the participants when wearing Nemeziz compared to Predator, which suggests an influence due to the cushioning properties of the shoes. Differences in traction perception were associated to specific shoe-surface condition rather than to individual shoes or surfaces, with the highest traction felt between participants for the SISgrass-Predator interaction, however, this is not related to the perception of the fastest time.

For the majority of the movements and participants there was not a high or very high

correlation between traction perception and GRF loading characteristics or contact time. This suggests that participants' perceptions of traction were not related only to the GRF components, but it was affected by other variables, such as shoe cushioning and comfort, or movements of the foot inside the shoe. Moreover, some subjects might have adjusted their kinematics in response to undesired traction conditions or to avoid the obstacles present in the agility course, resulting in an alteration of the GRF loading characteristics [141]. This could have led to an inaccurate interpretation of the between participants data, where the group mean does not reflect the subject's specific adaptation. Therefore, future work should investigate the estimation of athletes' kinematics in relation to their kinetics. Moreover, when player movement is evaluated while completing an agility course, future work should focus on course designs that either allow athletes to achieve fastest performance times, removing the use of obstacles that may limit their movements, or lead to the application of maximal GRF which allows to evaluate the limits of shoe-surface interaction.

To conclude, the results of this study showed that performance and GRF loading characteristics are not consistent between participants, shoes or surfaces; and traction between shoe and surface should lie in an optimum range, which is specific to each individual. Therefore, shoe-surface interaction can not be explained only by the shoe or surface characteristics, but it is a complex interaction between surface, shoe, participant, task and environment, that needs to be considered together. The evaluation of this complex interaction highlighted group and individual differences between shoes for the straight acceleration task.

6.6 Conclusion

In this chapter, the method previously validated to estimate 3D GRFs using eight IMUs was applied in the field. The aim was to evaluate the effect of two hybrid turf surfaces of different construction, a stitched-based (SISgrass) and a reinforced rootzone (Fibrelastic), and two shoes (Nemeziz vs Predator) on players' performance and traction perception.

Lower vertical deformation and higher rotational traction were found on the SISgrass surface compared to the Fibrelastic, which could result in performance reduction and increase of injury risk during change of direction tasks. Moreover, SISgrass was perceived as significantly harder, and bigger differences in traction between shoes were perceived when completing the agility course on it. However, the mechanical tests data suggest that these results are specific to the surfaces were the tests where carried out, and do not represent average hybrid turf surface samples.

Even if specific to the surfaces where the tests were carried out, this study allowed a first comparison between hybrid turf systems and their effect on players' performance and traction perception. In fact, to the best of the author's knowledge, performance and perception have been widely analysed on natural grass and artificial turf, whereas differences on hybrid turf surfaces were not investigated before, even if these are the main surfaces used by elite players. Moreover, the analysis of kinetics was previously limited to the laboratory environment; whereas the method used in this study allowed the evaluation of shoe-surface interaction in the field, with the possibility of measuring movements more closely related to those recorded in a real game environment, in a larger testing area and to record consecutive steps.

Finally, the results of this study showed that players' movements can not be explained only by the effect of different surfaces or shoes conditions, but they are the result of a complex interaction between five main parameters acting individually and together to achieve the best performance: surface, shoe, participant, task and environment. The evaluation of this complex interaction highlighted group and individual differences between shoes for the straight acceleration task, with Nemeziz's cylindrical studs allowing the application of higher horizontal force, especially on the SISgrass surface, compared to Predator's prismatic studs.

Chapter 7

Conclusion

7.1 Summary of the research

The aim of this programme of research was to evaluate the effect of football hybrid turfs on player movement. Nowadays, the majority of elite level football teams around the world play and train on hybrid turf surfaces, especially in the UEFA regions. However, despite their popularity in the professional game, the literature review (Ch. 2) highlighted a lack of knowledge regarding their mechanical characteristics and their relationship with performance and injury risk.

A secondary analysis of Labosport ScorePlay^{TM} dataset (Ch. 3) filled this gap of knowledge by identifying the mechanical properties' ranges of hybrid turfs used in match play and comparing them with those of natural grass surfaces. Higher values of shock absorption and vertical deformation were measured on natural grass surfaces, which suggest a higher possibility of energy being lost and, as a consequence, performance reduction compared to hybrid turfs. Between hybrid turf surface systems, the stitched-based construction was found to be the most consistent. It is less affected by weather and usage, and its performance could be more consistent during a season. However, the higher values measured for rotational traction on stitched-based systems compared to the other hybrid turf constructions, suggest a higher risk of foot fixation, with consequent possibility of performance reduction and increase of injury risk, during change of direction tasks.

The evaluation of shoe-surface interaction is fundamental in order to increase athletic performance and minimise the risk of injury. However, this evaluation is typically performed through biomechanical measurements in the laboratory, which is not representative of a real game environment. To understand and interpret the results of biomechanical testing, these should be supported by mechanical and subjective-sensory data. In the literature review (Ch. 2), it was highlighted that changes in

magnitude and direction of the external forces and player's lower limb kinematics are the result of player's adaptation to differences in shoe-surface conditions, which may be related to the mechanical properties of the surface and player's traction perception.

This programme of research led to the development of a method to assess shoe-surface interaction in the field through a body-worn measurement system, based on the recordings of eight IMUs. A first development of this method was presented and validated during a football-relevant movement in chapter 4. 3D GRFs were estimated from the accelerations recorded on eight body segments, representing a LLT model, through the application of Newton's second Law of Motion and the use of cut-off frequencies individually selected for each sensor and axis. The results obtained from this study highlight the improvements associated with a multiple-sensor approach in the evaluation of the horizontal GRF component during high-intensity movements, compared to the use of a single sensor attached on the sacral region, as was considered in previous studies [107, 108].

In the study presented in chapter 5, some improvements in the method design were implemented in order to provide a more accurate representation of segmental accelerations, reduce the amount of oscillations and their variability between individuals and segments. The sensors were placed in correspondence of each segment CoM, and the attachment technique was defined specifically for each location. Despite these improvements, the use of Newtonian mechanics presented a series of limitations when used to evaluate football-specific movements. Therefore, a modification and extension to the work described by Clark et al. [112, 113] was used to develop a new method to estimate instantaneous force components and GRF loading characteristics from two mechanical phenomena: the collision of the lower limb with the surface and the motion of the remainder of the body mass throughout the stance phase.

A validation study (Ch. 5) was conducted in a laboratory environment, therefore, each sensor orientation was estimated from the trajectories of four markers fixed on sensor mount frames, designed to address the magnetic interference problem; whereas in the field, where magnetic interferences should not be present, the method considers a sensor fusion algorithm to estimate the sensor orientation from the accelerometer, gyroscope and magnetometer's measurements. Different levels of accuracy were obtained between tasks, with the errors increasing with the movement intensity. The results show the validity of the method in the estimation of the GRF curve profile and impulses during change of direction tasks of different angles. Contact time was predicted for a variety of high-intensity movements with RMSE of 14 ms, giving the possibility of directly evaluating performance in field-based research. In addition, the

reliable estimation of the active peak force for the majority of the movement considered provides the possibility of comparing utilised traction with traction perception. Therefore, this method represents an improvement compared to current state of the art GRF estimation and can be used in the field to evaluate shoe-surface interaction and its relationship with performance and traction perception during football-specific movements.

The method was applied in the field to evaluate the effect of two hybrid turf surfaces of different construction, a stitched-based (SISgrass) and a reinforced rootzone (Fibrelastic), on player movement, while completing an agility course. Two pairs of shoes were worn in turn by participants in order to evaluate the effect of different footwear conditions as well. Shoe-surface interaction differences were evaluated in relationship with surfaces' mechanical properties and players' perceptions (Ch. 6).

The mechanical tests results suggest that the surfaces where the study was carried out are not representative of the hybrid turf surfaces used by professional teams. However, as for the elite level teams' pitches, higher rotational traction was found on the stitched-based surface, which could result in performance reduction and increase of injury risk during change of direction tasks. Moreover, this type of surface compared to the reinforced rootzone turf had also lower vertical deformation, was perceived as significantly harder, and bigger differences in traction between shoes were perceived when completing the agility course on it. The results highlight how differences in traction perception were associated to specific shoe-surface condition rather than to individual shoes or surfaces. The prediction of in-field GRF allowed the comparison between shoe-surface conditions relatively to specific tasks. In particular, the estimation of the active peak force highlights differences between shoes during straight acceleration, with the results showing that Nemeziz's cylindrical studs provide higher traction, especially on the SISgrass surface. The results of this study highlight also the implications for the course design in shoe-surface interaction and perception research. Studies evaluating player movement while completing an agility course should focus on course designs that either allow athletes to achieve fastest performance times, removing the use of obstacles that may limit their movements, or lead to the application of maximal GRF which allows to evaluate the limits of shoe-surface interaction.

The results of this in-field based study confirmed that mechanical, biomechanical and subjective-sensory tests should always be conducted together to provide a full picture of the shoe-surface interaction. Players' movements can not be explained only by the effect of different surfaces or shoes conditions, but they are the result of a complex interaction between five main parameters: surface, shoe, participant, task and environment.

To conclude, to the best of the author's knowledge, this thesis represents the first collection of data on hybrid turf surfaces' mechanical properties and the evaluation of hybrid turfs' effect on player movement in the field. Moreover, this programme of research led to the development of an IMU-based method, which gives the possibility of estimating 3D GRFs and contact times in the field during high-intensity movements representative of a real game scenario. With this method, data can be collected in a large testing area without the need for participants to adjust their movements to target a specific area, and it provides the possibility of analysing consecutive steps, which represents a great benefit in the evaluation of performance. Therefore, this method represents a great advantage compared to laboratory studies and could be used to characterise different shoes or surfaces in a variety of field-based sport activities, which may provide useful information in the design of new surface-specific footwear and more representative mechanical test devices.

7.2 Limitations of the research

The main limitations in this programme of research are related to the IMU sensors used, with their accelerometer range and sample frequency limited to ±16 g and 100 Hz, respectively. These limitations mainly affect the estimation of the impact peak, which represents the phase of stance during which the highest GRFs are measured during deceleration and change of direction steps. This denies the possibility to evaluate shoe-surface interaction for the most demanding tasks, compare the change of direction stance phases with the preceding ones, and compare the unpredicted and anticipated change of direction manoeuvres. Moreover, the low accuracy obtained in the prediction of the impact peak force has an effect also in the estimation of the instantaneous GRF.

Other limitations related to the method are the use of average segment inertia parameters, based on generic anthropometric tables found in the literature, and the method definition based on the movements recorded on only three subjects. The former is used to assign a percentage of body weight to each segment based on an average population sample, therefore, it could introduce uncertainty being not subject specific. The latter could have led to subject-specific definitions, not valid for a wider population sample.

Despite the perfect repeatability in the manual selection of the stance phases, this is time consuming, as well as the analysis of the video recordings to identify the stance phases corresponding to the change of direction tasks. Therefore, the use of this method outside a research environment may be unpractical.

The in-field study was carried out on surfaces not representative of the pitches used by elite level teams, and the pool of participants were recreational players or competed at lower level on natural grass or artificial turf surfaces, therefore, not familiar with hybrid turfs. Moreover, participants wore in turn two pairs of footwear to compare the effect of shoes' traction properties. Differences should be restricted to the outsole design, since athletes may be more inclined to perform better, consciously or unconsciously, in a shoe design that is visually appealing or more comfortable [124].

7.3 Future work

Future work should be conducted to develop the method using new generation IMUs, able to record accelerations with a minimum range of ±60 g and a minimum sample frequency of 500 Hz, to improve the estimation of GRFs during the first 30% of the stance phase. In addition, the method should include the estimation of players' kinematics, which might explain alterations of the GRF loading characteristics, since participants might adjust their movements in response to undesired traction conditions or to avoid obstacles present in the agility course. The kinematics evaluation can be performed from the orientation in the global coordinate system of the same IMU sensors used to estimate kinetics. An automatic approach in the identification of stance phase events and tasks should be investigated to make the method more accessible to a wider community and less trained personnel. This would allow the analysis of players' movement during normal training sessions on a daily basis. Finally, the method should be validated with a bigger pool of participants to avoid any subject-specific definition and check the reliability on a higher number of movement techniques.

With regard to the in-field study, in order to evaluate the effect of representative hybrid turf surfaces on players' movement, future work should be conducted on an average sample of football hybrid turf surfaces used during match-play and involve high level players, familiar with these fields. In addition, an improved course design should be investigated, in order to find a compromise between allowing participants to achieve their best time and ensuring that specific tasks are performed without movement alterations, resulting in a valid perception measurement.

References

[1] E. M. Hennig and T. Sterzing, "The influence of soccer shoe design on playing performance: A series of biomechanical studies," *Footwear Science*, vol. 2, no. 1, pp. 3–11, 2010.

[2] FIFA, "FIFA Big Count 2006," 2007.

[3] M. P. Hilgers and M. Walther, "Evolution of soccer shoe design," *International Journal of Athletic Therapy and Training*, vol. 16, no. 3, pp. 1–4, 2011.

[4] J. J. Henderson, J. R. Crum, T. F. Wolff, and J. N. Rogers, "Athletic field root zone mixes: what is the best mix for your field?," in *Proceedings of the 71st Annual Michigan Turfgrass Conference*, (East Lansing, Michigan, USA), pp. 96–99, 2001.

[5] B. Barry and P. Milburn, "Tribology, friction and traction: understanding shoe-surface interaction," *Footwear Science*, vol. 5, no. 3, pp. 137–145, 2013.

[6] I. T. James, "Advancing natural turf to meet tomorrow's challenges," *Proceedings of the Institution of Mechanical Engineers, Part P: Journal of Sports Engineering and Technology*, vol. 225, no. 3, pp. 115–129, 2011.

[7] A. Kowalewski, G. Stahnke, T. Cook, and R. Goss, "Best management practices for construction of sand-based, natural grass athletic fields for football and soccer," 2015.

[8] F. D. Anderson, P. R. Fleming, P. J. Sherratt, and K. Severn, "Novel field equipment for assessing the stability of natural and hybrid turfs," *Sports Engineering*, vol. 21, no. 4, pp. 321–331, 2018.

[9] F. D. Anderson, P. Fleming, P. Sherratt, and K. Severn, "Investigating shear stability of Rugby Union natural turf pitches," *Procedia Engineering*, vol. 112, pp. 273–278, 2015.

[10] S. Williams, P. A. Hume, and S. Kara, "A review of football injuries on third and fourth generation artificial turfs compared with natural turf," *Sports Medicine*, vol. 41, no. 11, pp. 903–923, 2011.

[11] H. Andersson, B. Ekblom, and P. Krustrup, “Elite football on artificial turf versus natural grass: Movement patterns, technical standards, and player impressions,” *Journal of Sports Sciences*, vol. 26, no. 2, pp. 113–122, 2008.

[12] A. Agrawal, S. Kishor, D. Sagar, and K. Rani, “Techno, Economic, Feasibility Review of Artificial Turf in India,” *Journal of civil engineering and environmental technology*, vol. 1, no. 5, pp. 24–28, 2014.

[13] W. Potthast, R. Verhelst, M. Hughes, K. Stone, and D. De Clercq, “Football-specific evaluation of player-surface interaction on different football turf systems,” *Sports Technology*, vol. 3, no. 1, pp. 5–12, 2010.

[14] W. Winterbottom, *Artificial grass surfaces for Association Football: report and recommendations*. [London]: Sports Council, 1985.

[15] T. Sterzing, “Soccer boots and playing surfaces,” in *Soccer science* (T. Strudwick, ed.), pp. 179–202, Human Kinetics, Champaign, IL, USA, 1 ed., 2016.

[16] F. Lulli, M. Volterrani, S. Magni, and R. Armeni, “An innovative hybrid natural-artificial sports pitch construction system,” *Proceedings of the Institution of Mechanical Engineers, Part P: Journal of Sports Engineering and Technology*, vol. 225, no. 3, pp. 171–175, 2011.

[17] C. Andrews, “Hybrid football pitches: why the grass is always greener,” *Engineering and Technology*, vol. 11, no. 10, 2017.

[18] FIFA, “FIFA Quality Programme for Football Turf,” Tech. Rep. October, FIFA, 2015.

[19] “https://www.centpapiers.com/euro-2016-les-gazons-maudits-une-magouille-de-recidiviste/ [Accessed on 6th October 2020].”

[20] A. Thomson, “Evolution of natural grass playing surfaces for elite football,” *Sports medicine journal*, vol. 5, no. 2, pp. 322–327, 2016.

[21] “Xtreme Grass: The Hybrid Method, https://www.actglobal.com/blog/xtreme-grass-hybrid-method/ [Accessed on 6th October 2020].”

[22] J. Bloomfield, R. Polman, and P. O’Donoghue, “The ’Bloomfield Movement Classification’: Motion Analysis of Individual Players in Dynamic Movement Sports,” *International Journal of Performance Analysis in Sport*, vol. 4, no. 2, pp. 20–31, 2004.

[23] J. Bloomfield, R. Polman, and P. O'Donoghue, "Physical demands of different positions in FA Premier League soccer," *Journal of Sports Science and Medicine*, vol. 6, no. 1, pp. 63–70, 2007.

[24] T. Little and A. G. Williams, "Specificity of Acceleration, Maximum Speed, and Agility in Professional Soccer Players," *The Journal of Strength and Conditioning Research*, vol. 19, no. 1, pp. 76–78, 2005.

[25] N. M. Schrier, J. W. Wannop, R. T. Lewinson, J. Worobets, and D. Stefanyshyn, "Shoe traction and surface compliance affect performance of soccer-related movements," *Footwear Science*, vol. 6, no. 2, pp. 69–80, 2014.

[26] D. J. Stefanyshyn and B. M. Nigg, "Energy and Performance Aspects in Sport Surfaces," in *Proceedings of the International Association for Sports Surface Sciences 3rd Symposium on Sports Surfaces, August 2003, Calgary*, pp. 31–46, 2003.

[27] J. Sánchez-Sánchez, J. García-Unanue, P. Jiménez-Reyes, A. Gallardo, P. Burillo, J. L. Felipe, and L. Gallardo, "Influence of the mechanical properties of third-generation artificial turf systems on soccer players' physiological and physical performance and their perceptions," *PLoS ONE*, vol. 9, no. 10, pp. 27–32, 2014.

[28] P. W. Cawley, R. S. Heidt, P. E. Scranton, G. M. Losse, and M. E. Howard, "Physiologic Axial Load, Frictional Resistance, and the Football Shoe-Surface Interface," *Foot & ankle internation*, vol. 24, no. 7, pp. 551–556, 2003.

[29] M. Shorten, B. Hudson, and J. Himmelsbach, "Shoe-Surface Traction of Conventional and In-Field Synthetic Turf Football Surfaces," in *Proceedings XIX International Congress of Biomechanics (Ed P. Milburn et al.), University of Otago, Dunedin, New Zealand*, 2003.

[30] E. C. Frederick, "Optimal Frictional Properties for Sport Shoes and Sport Surfaces," *11th International Symposium on Biomechanics in Sports*, pp. 15–22, 1993.

[31] R. Kent, J. Forman, D. Leddley, and J. Crandall, "Characterization of Athletic Shoe-Surface Mechanics in situ at Loads and Rates Relevant to Game Situations," in *Ircobi Conference*, pp. 40–50, 2011.

[32] B. M. Nigg, "The validity and relevance of tests used for the assessment of sports surfaces," *Medicine and science in sports and exercise*, vol. 22, no. 1, pp. 131–139, 1990.

[33] B. M. Nigg and M. R. Yeadon, "Biomechanical aspects of playing surfaces," *Journal of Sports Sciences*, vol. 5, no. 2, pp. 117–145, 1987.

[34] J. W. Wannop and D. J. Stefanyshyn, “The effect of translational and rotational traction on lower extremity joint loading,” *Journal of Sports Sciences*, vol. 34, no. 7, pp. 613–620, 2016.

[35] J. S. Torg, T. C. Quedenfeld, and S. Landau, “The shoe-surface interface and its relationship to football knee injuries,” *The American Journal of Sports Medicine*, vol. 2, no. 5, pp. 261–269, 1974.

[36] B. M. Cameron and O. Davis, “The swivel football shoe: a controlled study,” *The Journal of sports medicine*, vol. 1, no. 2, pp. 16–27, 1973.

[37] J. W. Wannop, J. T. Worobets, and D. J. Stefanyshyn, “Footwear Traction and Lower Extremity Joint Loading,” *The American Journal of Sports Medicine*, vol. 38, no. 6, pp. 1221–1228, 2010.

[38] R. B. Lambson, B. S. Barnhill, and R. W. Higgins, “Football cleat design and its effect on anterior cruciate ligament injuries: A three-year prospective study,” *American Journal of Sports Medicine*, vol. 24, no. 2, pp. 155–159, 1996.

[39] D. C. Silva, R. Santos, J. P. Vilas-Boas, R. Macedo, A. M. Montes, and A. S. Sousa, “Influence of Cleats-Surface Interaction on the Performance and Risk of Injury in Soccer: A Systematic Review,” *Applied Bionics and Biomechanics*, vol. 2017, 2017.

[40] E. Hennig and T. Milani, “Testmethoden zur Beurteilung von Laufschuhen,” *dynamed: Zeitschrift für Technik in Medizin und Sport*, vol. 1, no. 1, pp. S. 33–35, 1996.

[41] B. Keshvari, J. Mitternacht, and V. Senner, “Competitive study of stud characteristics on the penetrability,” *Footwear Science*, vol. 9, no. sup1, pp. S60–S61, 2017.

[42] R. Dé and D. James, “The effect of stud shape on penetration characteristics through synthesized natural turf in football,” in *Procedia Engineering*, pp. 648–653, 2014.

[43] R. F. Kirk, I. S. G. Noble, T. Mitchell, C. Rolf, S. J. Haake, and M. J. Carré, “High-speed observations of football-boot-surface interactions of players in their natural environment,” *Sports Engineering*, vol. 10, no. 3, pp. 129–144, 2007.

[44] K. Smeets, P. Jacobs, R. Hertogs, J.-P. Luyckx, B. Innocenti, K. Corten, J. Ekstrand, and J. Bellemans, “Torsional injuries of the lower limb: an analysis of the frictional torque between different types of football turf and the shoe outsole,” *British Journal of Sports Medicine*, vol. 46, no. 15, pp. 1078–1083, 2012.

[45] J. D. Clarke and M. J. Carré, "Improving the performance of soccer boots on artificial and natural soccer surfaces," in *Procedia Engineering*, pp. 2775–2781, 2010.

[46] A. Thomson, R. Whiteley, M. Wilson, and C. Bleakley, "Six different football shoes, one playing surface and the weather; Assessing variation in shoe-surface traction over one season of elite football," *PLoS ONE*, vol. 14, no. 4, pp. 1–13, 2019.

[47] C. Webb, S. Forrester, and P. Fleming, "Rotational traction behaviour of artificial turf," in *Procedia Engineering*, vol. 72, pp. 853–858, Elsevier B.V., 2014.

[48] M. J. Hall and P. Riou, "Football blades: A cause for concern," *British Journal of Sports Medicine*, vol. 38, no. 5, p. 642, 2004.

[49] F. Galbusera, D. Z. Tornese, F. Anasetti, S. Bersini, P. Volpi, L. La Barbera, and T. Villa, "Does soccer cleat design influence the rotational interaction with the playing surface?," *Sports Biomechanics*, vol. 12, no. 3, pp. 293–301, 2013.

[50] M. R. Villwock, E. G. Meyer, J. W. Powell, A. J. Fouty, and R. C. Haut, "Football Playing Surface and Shoe Design Affect Rotational Traction," *The American Journal of Sports Medicine*, vol. 37, no. 3, pp. 518–525, 2009.

[51] T. Grund, V. Senner, and K. Grube, "Development of a test device for testing soccer boots under gamerelevant highrisk loading conditions," *Sports Engineering*, vol. 10, no. 1, pp. 55–63, 2007.

[52] D. J. Stefanyshyn, J. S. Lee, and S. K. Park, "The influence of soccer cleat design on resultant joint moments," *Footwear Science*, vol. 2, no. 1, pp. 13–19, 2010.

[53] J. W. Wannop, G. Luo, and D. J. Stefanyshyn, "Footwear traction at different areas on artificial and natural grass fields," *Sports Engineering*, vol. 15, no. 2, pp. 111–116, 2012.

[54] M. Caple, I. James, and M. Bartlett, "Mechanical behaviour of natural turf sports pitches across a season," *Sports Engineering*, vol. 15, no. 3, pp. 129–141, 2012.

[55] N. Smith, R. Dyson, and L. Janaway, "Ground reaction force measures when running in soccer boots and soccer training shoes on a natural turf surface," *Sports Engineering*, vol. 7, no. 3, pp. 159–167, 2004.

[56] H. Driscoll, J. Kelley, B. Kirk, H. Koerger, and S. Haake, "Measurement of studded shoe-surface interaction metrics during in situ performance analysis," *Sports Engineering*, vol. 18, no. 2, pp. 105–113, 2015.

[57] H. F. Driscoll, *Understanding shoe-surface interactions in football*. PhD thesis, Sheffield Hallam University, 2012.

[58] D. McGhie and G. Ettema, "On the 'trench effect' theory: A biomechanical analysis of the relationship between traction and shoe orientation on third-generation artificial turf," *Footwear Science*, vol. 6, no. 1, pp. 41–50, 2014.

[59] R. Grönqvist, W.-r. Chang, T. K. Courtney, T. B. Leamon, M. S. Redfern, and L. Strandberg, "Measurement of slipperiness: fundamental concepts and definitions," *Ergonomics*, vol. 44, no. 13, pp. 1102–1117, 2001.

[60] R. El Kati, *Effect of mechanical behaviour of artificial turf on player-surface interaction in soccer*. PhD thesis, Loughborough University, 2012.

[61] G. A. Livesay, D. R. Reda, and E. A. Nauman, "Peak torque and rotational stiffness developed at the shoe-surface interface: The effect of shoe type and playing surface," *American Journal of Sports Medicine*, vol. 34, no. 3, pp. 415–422, 2006.

[62] M. G. Hughes, L. Birdsey, R. Meyers, D. Newcombe, J. L. Oliver, P. M. Smith, M. Stembridge, K. Stone, and D. G. Kerwin, "Effects of playing surface on physiological responses and performance variables in a controlled football simulation," *Journal of Sports Sciences*, vol. 31, no. 8, pp. 878–886, 2013.

[63] J. Worobets and J. W. Wannop, "Influence of basketball shoe mass, outsole traction, and forefoot bending stiffness on three athletic movements," *Sports Biomechanics*, vol. 14, no. 3, pp. 351–360, 2015.

[64] C. Müller, T. Sterzing, J. Lange, and T. L. Milani, "Comprehensive evaluation of player-surface interaction on artificial soccer turf," *Sports Biomechanics*, vol. 9, no. 3, pp. 193–205, 2010.

[65] D. De Clercq, G. Debuyck, J. Gerlo, S. Rambour, V. Segers, and I. Van Caekenberghe, "Cutting performance wearing different studded soccer shoes on dry and wet artificial turf," *Footwear Science*, vol. 6, no. 2, pp. 81–87, 2014.

[66] T. Sterzing, C. Müller, E. M. Hennig, and T. L. Milani, "Actual and perceived running performance in soccer shoes: A series of eight studies," *Footwear Science*, vol. 1, no. 1, pp. 5–17, 2009.

[67] J. T. Fuller, C. R. Bellenger, D. Thewlis, M. D. Tsiros, and J. D. Buckley, "The Effect of Footwear on Running Performance and Running Economy in Distance Runners," *Sports Medicine*, vol. 45, no. 3, pp. 411–422, 2015.

[68] J. R. Gdovin, C. C. Williams, S. J. Wilson, V. L. Cazas-Moreno, L. A. Luginsland, C. R. Allen, H. Chander, C. Wade, and J. C. I. Garner, "Influences of Athletic Footwear on Ground Reaction Forces During A Sidestep Cutting Maneuver on Artificial Turf," *International Journal of Kinesiology and Sports Science*, vol. 6, no. 2, p. 30, 2018.

[69] E. Brock, S. Zhang, C. Milner, X. Liu, J. T. Brosnan, and J. C. Sorochan, "Effects of two football stud configurations on biomechanical characteristics of single-leg landing and cutting movements on infilled synthetic turf," *Sports Biomechanics*, vol. 13, no. 4, pp. 362–379, 2014.

[70] G. L. Gains, A. N. Swedenhjelm, J. L. Mayhew, H. M. Bird, and J. J. Houser, "Comparison of speed and agility performance of college football players on field turf and natural grass," *Journal of Strength and Conditioning Research*, vol. 24, no. 10, pp. 2613–2617, 2010.

[71] S. M. Choi, K. W. R. Sum, and F. L. E. Leung, "Comparison between Natural Turf and Artificial Turf on Agility Performance of Rugby Union Players," *Advances in Physical Education*, vol. 05, no. 04, pp. 273–281, 2015.

[72] H. Nunome, T. Iga, and H. Suito, "Comparison of zig-zag run performance, surface hardness and foot motion," *Footwear Science*, vol. 9, no. sup1, pp. S141–S143, 2017.

[73] P. Rouch, X. Drevelle, L. Benouaich, and P. Thoreux, "Influence of Playing Surface on Knee Loads During Running, Sidestep Cutting and Drop Jumping," *33rd International Conference on Biomechanics in Sports, Poitiers, France*, pp. 458–461, 2015.

[74] T. Sterzing, C. Müller, S. Schwanitz, S. Odenwald, and T. L. Milani, "Discrepancies between mechanical an biomechanical measurements of soccer shoe traction on artificial turf," in *26th Symposium of the International Society of Biomechanics in Sports*, pp. 339–342, 2008.

[75] D. T. P. Fong, Y. Hong, and J. X. Li, "Human walks carefully when the ground dynamic coefficient of friction drops below 0.41," *Safety Science*, vol. 47, no. 10, pp. 1429–1433, 2009.

[76] G. Luo and D. Stefanyshyn, "Identification of critical traction values for maximum athletic performance," *Footwear Science*, vol. 3, no. 3, pp. 127–138, 2011.

[77] A. Pedroza, S. Fernandez, R. Heidt, and C. Kaeding, "Evaluation of the shoe-surface interaction using an agility maneuver," *Medicine and Science in Sports and Exercise*, vol. 42, no. 9, pp. 1754–1759, 2010.

[78] G. Luo and D. Stefanyshyn, “Identification of critical traction values for maximum athletic performance,” *Footwear Science*, vol. 3, no. 3, pp. 127–138, 2011.

[79] T. Sterzing, C. Müller, and T. L. Milani, “Traction on artificial turf: Development of a soccer shoe outsole,” *Footwear Science*, vol. 2, no. 1, pp. 37–49, 2010.

[80] A. V. Dowling, S. Corazza, A. M. W. Chaudhari, and T. P. Andriacchi, “Shoe-Surface Friction Influences Movement Strategies During a Sidestep Cutting Task,” *The American Journal of Sports Medicine*, vol. 38, no. 3, pp. 478–485, 2010.

[81] C. Müller, T. Sterzing, M. Lake, and T. L. Milani, “Different stud configurations cause movement adaptations during a soccer turning movement,” *Footwear Science*, vol. 2, no. 1, pp. 21–28, 2010.

[82] T. Dos’Santos, C. Thomas, P. A. Jones, and P. Comfort, “Mechanical determinants of faster change of direction speed performance in male athletes,” *The Journal of Strength and Conditioning Research*, vol. 31, no. 3, pp. 696–705, 2016.

[83] K. L. Havens and S. M. Sigward, “Cutting mechanics: Relation to performance and anterior cruciate ligament injury risk,” *Medicine and Science in Sports and Exercise*, vol. 47, no. 4, pp. 818–824, 2015.

[84] K. L. Havens and S. M. Sigward, “Whole body mechanics differ among running and cutting maneuvers in skilled athletes,” *Gait and Posture*, vol. 42, no. 3, pp. 240–245, 2015.

[85] N. J. Nedergaard, U. Kersting, and M. Lake, “Using accelerometry to quantify deceleration during a high-intensity soccer turning manoeuvre,” *Journal of Sports Sciences*, vol. 32, no. 20, pp. 1897–1905, 2014.

[86] T. F. Besier, D. G. Lloyd, T. R. Ackland, and J. L. Cochrane, “Anticipatory effects on knee joint loading during running and cutting maneuvers.,” *Medicine and science in sports and exercise*, vol. 33, no. 3, pp. 1176–1181, 2001.

[87] S. T. Jamison, X. Pan, and A. M. W. Chaudhari, “Knee moments during run-to-cut maneuvers are associated with lateral trunk positioning,” *Journal of Biomechanics*, vol. 45, no. 11, pp. 1881–1885, 2012.

[88] J. Roberts, P. Osei-Owusu, A. Harland, A. Owen, and A. Smith, “Elite football players’ perceptions of football turf and natural grass surface properties,” in *Procedia Engineering*, vol. 72, pp. 907–912, 2014.

[89] C. Y. M. Morio, L. Sissler, and N. Guéguen, "Static vs. dynamic friction coefficients, which one to use in sports footwear research?," *Footwear Science*, vol. 7, no. Supp1, pp. 63–64, 2015.

[90] C. Morio, A. Bourrelly, L. Sissler, and N. Gueguen, "Perceiving slipperiness and grip: A meaningful relationship of the shoe-ground interface," *Gait and Posture*, vol. 51, no. 1, pp. 58–63, 2017.

[91] E. Bergamini, G. Ligorio, A. Summa, G. Vannozzi, A. Cappozzo, and A. M. Sabatini, "Estimating orientation using magnetic and inertial sensors and different sensor fusion approaches: Accuracy assessment in manual and locomotion tasks," *Sensors*, vol. 14, no. 10, pp. 18625–18649, 2014.

[92] A. Cavallo, A. Cirillo, P. Cirillo, G. De Maria, P. Falco, C. Natale, and S. Pirozzi, "Experimental Comparison of Sensor Fusion Algorithms for Attitude Estimation," *IFAC World Congress*, vol. 19, no. 1, pp. 7585–7591, 2014.

[93] A. I. Cuesta-Vargas, A. Galán-Mercant, and J. M. Williams, "The use of inertial sensors system for human motion analysis," *Physical Therapy Reviews*, vol. 15, no. 6, pp. 462–473, 2010.

[94] G. S. Faber, C. C. Chang, I. Kingma, J. T. Dennerlein, and J. H. van Dieën, "Estimating 3D L5/S1 moments and ground reaction forces during trunk bending using a full-body ambulatory inertial motion capture system," *Journal of Biomechanics*, vol. 49, no. 6, pp. 904–912, 2016.

[95] J. Kodama and T. Watanabe, "Examination of inertial sensor-based estimation methods of lower limb joint moments and ground reaction force: Results for squat and sit-to-stand movements in the sagittal plane," *Sensors (Switzerland)*, vol. 16, no. 8, 2016.

[96] S. Min and J. Kim, "Inertial sensor based inverse dynamics analysis of human motions," in *IEEE/ASME International Conference on Advanced Intelligent Mechatronics, AIM*, pp. 177–182, IEEE, 2015.

[97] N. G. Elvin, A. A. Elvin, and S. P. Arnoczky, "Correlation between ground reaction force and tibial acceleration in vertical jumping," *Journal of Applied Biomechanics*, vol. 23, no. 3, pp. 180–189, 2007.

[98] R. Howard, R. Conway, and A. J. Harrison, "Estimation of force during vertical jumps using body fixed accelerometers," in *25th IET Irish Signals & Systems Conference*, pp. 102–107, 2014.

[99] A. Pouliot-Laforte, L. N. Veilleux, F. Rauch, and M. Lemay, "Validity of an accelerometer as a vertical ground reaction force measuring device in healthy children and adolescents and in children and adolescents with osteogenesis imperfecta type I," *Journal of Musculoskeletal Neuronal Interactions*, vol. 14, no. 2, pp. 155–161, 2014.

[100] I. Setuain, J. Martinikorena, M. Gonzalez-Izal, A. Martinez-Ramirez, M. Gómez, J. Alfaro-Adrián, and M. Izquierdo, "Vertical jumping biomechanical evaluation through the use of an inertial sensor-based technology," *Journal of Sports Sciences*, vol. 34, no. 9, pp. 843–851, 2016.

[101] U. Meyer, D. Ernst, S. Schott, C. Riera, J. Hattendorf, J. Romkes, U. Granacher, B. Göpfert, and S. Kriemler, "Validation of two accelerometers to determine mechanical loading of physical activities in children," *Journal of Sports Sciences*, vol. 33, no. 16, pp. 1702–1709, 2015.

[102] Y. Ohtaki, K. Sagawa, and H. Inooka, "A method for gait analysis in a daily living environment by body-mounted instruments," *JSME International Journal Series C*, vol. 44, no. 4, pp. 1125–1132, 2001.

[103] A. Karatsidis, G. Bellusci, H. M. Schepers, M. de Zee, M. S. Andersen, and P. H. Veltink, "Estimation of ground reaction forces and moments during gait using only inertial motion capture," *Sensors (Switzerland)*, vol. 17, no. 1, p. 75, 2017.

[104] J. M. Neugebauer, K. H. Collins, and D. A. Hawkins, "Ground reaction force estimates from ActiGraph GT3X+ hip accelerations," *PLoS ONE*, vol. 9, no. 6, 2014.

[105] E. Charry, W. Hu, M. Umer, A. Ronchi, and S. Taylor, "Study on estimation of peak Ground Reaction Forces using tibial accelerations in running," *Proceedings of the 2013 IEEE 8th International Conference on Intelligent Sensors, Sensor Networks and Information Processing: Sensing the Future, ISSNIP 2013*, vol. 1, pp. 288–293, 2013.

[106] D. P. Raper, J. Witchalls, E. J. Philips, E. Knight, M. K. Drew, and G. Waddington, "Use of a tibial accelerometer to measure ground reaction force in running: A reliability and validity comparison with force plates," *Journal of Science and Medicine in Sport*, vol. 21, no. 1, pp. 84–88, 2018.

[107] I. Setuain, P. Lecumberri, J. P. Ahtiainen, A. A. Mero, K. Häkkinen, and M. Izquierdo, "Sprint mechanics evaluation using inertial sensor-Âbased technology: A laboratory validation study," *Scandinavian Journal of Medicine and Science in Sports*, vol. 28, no. 2, pp. 463–472, 2018.

[108] R. D. Gurchiek, R. S. McGinnis, A. R. Needle, J. M. McBride, and H. van Werkhoven, "The use of a single inertial sensor to estimate 3-dimensional ground reaction force during accelerative running tasks," *Journal of Biomechanics*, vol. 61, pp. 263–268, 2017.

[109] D. W. Wundersitz, K. J. Netto, B. Aisbett, and P. B. Gastin, "Validity of an upper-body-mounted accelerometer to measure peak vertical and resultant force during running and change-of-direction tasks," 2013.

[110] G. Logar and M. Munih, "Estimation of joint forces and moments for the in-run and take-off in ski jumping based on measurements with wearable inertial sensors," *Sensors (Switzerland)*, vol. 15, no. 5, pp. 11258–11276, 2015.

[111] J. Verheul, W. Gregson, P. Lisboa, J. Vanrenterghem, and M. A. Robinson, "Whole-body biomechanical load in running-based sports: The validity of estimating ground reaction forces from segmental accelerations," *Journal of Science and Medicine in Sport*, vol. 22, no. 6, pp. 716–722, 2019.

[112] K. P. Clark, L. J. Ryan, and P. G. Weyand, "Foot speed, foot-strike and footwear: Linking gait mechanics and running ground reaction forces," *Journal of Experimental Biology*, vol. 217, no. 12, pp. 2037–2040, 2014.

[113] K. P. Clark, L. J. Ryan, and P. G. Weyand, "A general relationship links gait mechanics and running ground reaction forces," *Journal of Experimental Biology*, vol. 220, no. 2, pp. 247–258, 2017.

[114] Y. Guo, F. Storm, Y. Zhao, S. A. Billings, A. Pavic, C. Mazzà, and L. Z. Guo, "A new proxy measurement algorithm with application to the estimation of vertical ground reaction forces using wearable sensors," *Sensors (Switzerland)*, vol. 17, no. 10, pp. 1–14, 2017.

[115] A. C. Miller, M. Aljohani, H. Kim, and K. Kipp, "Neural network method to predicting stance-phase ground reaction force in distance runners," in *37th Internation Society of Biomechanics in Sport Conference*, pp. 399–402, 2019.

[116] F. J. Wouda, M. Giuberti, G. Bellusci, E. Maartens, J. Reenalda, B. J. F. van Beijnum, and P. H. Veltink, "Estimation of vertical ground reaction forces and sagittal knee kinematics during running using three inertial sensors," *Frontiers in Physiology*, vol. 9, no. MAR, pp. 1–14, 2018.

[117] G. Leporace, L. A. Batista, L. Metsavaht, and J. Nadal, "Residual analysis of ground reaction forces simulation during gait using neural networks with different configurations," *Proceedings of the Annual International Conference of the IEEE Engineering in Medicine and Biology Society, EMBS*, pp. 2812–2815, 2015.

[118] FIFA, "Handbook of Test Methods," tech. rep., FIFA, 2015.

[119] Labosport ScorePlay, "https://labosport.com/services/labosport-scoreplay."

[120] FIFA, "Handbook of Test Methods for Football Turf," tech. rep., FIFA, 2006.

[121] K. A. Severn, P. R. Fleming, J. D. Clarke, and M. J. Carre, "Science of synthetic turf surfaces: investigating traction behaviour," *Proceedings of the Institution of Mechanical Engineers, Part P: Journal of Sports Engineering and Technology*, vol. 225, no. 3, pp. 147–158, 2011.

[122] FIFA, "Handbook of Requirements," tech. rep., FIFA, 2015.

[123] R. Kent, J. Crandall, J. Forman, D. Lessley, A. Lau, and C. Garson, "Development and assessment of a device and method for studying the mechanical interactions between shoes and playing surfaces in situ at loads and rates generated by elite athletes," *Sports Biomechanics*, vol. 11, no. 3, pp. 414–429, 2012.

[124] M. K. Pryhoda, R. J. Wathen, J. Dicharry, K. B. Shelburne, D. Feeney, K. Harrison, and B. S. Davidson, "Alternative upper configurations during agility-based movements: part 1, biomechanical performance," *Footwear Science*, vol. 13, no. 1, pp. 91–103, 2021.

[125] P. de Leva, "Adjustments to Zatsiorsky-Seluyanov's segment inertia parameters," *Journal of Biomechanics*, vol. 29, no. 9, pp. 1223–1230, 1996.

[126] NOAA, "Magnetic Field Calculators."

[127] V. Ahlstrom and K. Longo, "Human factors design standard (HFDS)," tech. rep., Atlantic City International Airport, NJ: Federal Aviation Administration William J. Hughes Technical Center, 2003.

[128] J. Røislien, L. Rennie, and I. Skaaret, "Functional limits of agreement: A method for assessing agreement between measurements of gait curves," *Gait and Posture*, vol. 36, no. 3, pp. 495–499, 2012.

[129] K. Gruber, H. Ruder, J. Denoth, and K. Schneider, "A comparative study of impact dynamics," *Journal of Biomechanics*, vol. 31, no. 5, pp. 439–444, 1998.

[130] C. Bélaise, Y. Blache, A. Thouzé, T. Monnet, and M. Begon, "Effect of wobbling mass modeling on joint dynamics during human movements with impacts," *Multibody System Dynamics*, vol. 38, no. 4, pp. 345–366, 2016.

[131] J. C. Ziegert and J. L. Lewis, "The effect of soft tissue on measurements of vibrational bone motion by skin-mounted accelerometers," *Journal of Biomechanical Engineering*, vol. 101, pp. 218–220, 1979.

[132] A. Forner-Cordero, M. Mateu-Arce, I. Forner-Cordero, E. Alcántara, J. C. Moreno, and J. L. Pons, "Study of the motion artefacts of skin-mounted inertial sensors under different attachment conditions," *Physiological Measurement*, vol. 29, no. 4, pp. N21–N31, 2008.

[133] M. T. Pain and J. H. Challis, "The influence of soft tissue movement on ground reaction forces, joint torques and joint reaction forces in drop landings," *Journal of Biomechanics*, vol. 39, no. 1, pp. 119–124, 2006.

[134] L. Nokes, J. A. Fairclough, W. J. Mintowt-Czyz, I. Mackie, and J. Williams, "Vibration analysis of human tibia: The effect of soft tissue on the output from skin-mounted accelerometers," *Journal of Biomedical Engineering*, vol. 6, no. 3, pp. 223–226, 1984.

[135] M. A. Lafortune, E. Henning, and G. A. Valiant, "Tibial shock measured with bone and skin mounted transducers," *Journal of Biomechanics*, vol. 28, no. 8, pp. 989–993, 1995.

[136] D. McGhie and G. Ettema, "Biomechanical analysis of traction at the shoe-surface interface on third-generation artificial turf," *Sports Engineering*, vol. 16, no. 2, pp. 71–80, 2013.

[137] P. O. Riley, R. W. Kent, T. A. Dierks, W. B. Lievers, R. E. Frimenko, and J. R. Crandall, "Foot kinematics and loading of professional athletes in American football-specific tasks," *Gait and Posture*, vol. 38, pp. 563–569, 2013.

[138] E. Colino, J. Sánchez-Sánchez, J. García-Unanue, E. Ubago-Guisado, P. Haxaire, A. Le Blan, and L. Gallardo, "Validity and reliability of two standard test devices in assessing mechanical properties of different sport surfaces," *Polymer Testing*, vol. 62, no. October, pp. 61–67, 2017.

[139] J. Cohen, *Statistical power analysis fot the behavioral sciences*. Erlbaum Associates Lawrence, second ed., 1998.

[140] D. E. Hinkle, W. Wiersma, and S. G. Jurs, *Applied Statistics for the Behavioral Sciences*. Wadsworth Publishing Co Inc, 2002.

[141] J. Hamill, "Evaluating sport shoes using ground reaction force data," in *Conference proceedings of the 14th International Symposium on Biomechanics in Sports.*, pp. 111–119, 1996.

[142] I. Poitras, F. Dupuis, M. Bielmann, A. Campeau-Lecours, C. Mercier, L. J. Bouyer, and J. S. Roy, "Validity and reliability of wearable sensors for joint angle esti-

mation: A systematic review," *Sensors (Switzerland)*, vol. 19, no. 7, pp. 1–17, 2019.

Appendix A

Sensor selection

The following four IMU sensors were available and analysed in order to select the most appropriate to collect the data of interest:

STT-IWS iSen (STT System, Spain)
Size: 56 x 38 x 18 mm
Weight: 46 g
Integrated devices: three-axis accelerometer, gyroscope and magnetometer, operating between ± 2000°s^{-1}, ± 16 g and ± 1300 µT, respectively.
Maximum sample frequency: 100 Hz

MetaMotionR (mbientlab, California, USA)
Size: 27 x 27 x 4 mm
Weight: 5.67 g
Integrated devices: three-axis accelerometer, gyroscope and magnetometer, operating between ± 2000°s^{-1}, ± 16 g and ± 1300 µT (x, y-axis)/± 2500µT (z-axis), respectively.
Maximum sample frequency: 800 Hz (accelerometer and gyroscope), 25 Hz (magnetometer)

RunScribes (Scribe Labs, California, USA)
Size: 35 x 25 x 7.5 mm
Weight: 9 g
Integrated devices: three-axis accelerometer, gyroscope and magnetometer, operating between ± 2000°s^{-1}, ± 16 g and ± 1300 µT, respectively.
Maximum sample frequency: 500 Hz

Aktos-T (myon AG, Switzerland)
Size: 32.7 x 25.5 x 7.8 mm
Weight: 5.3 g

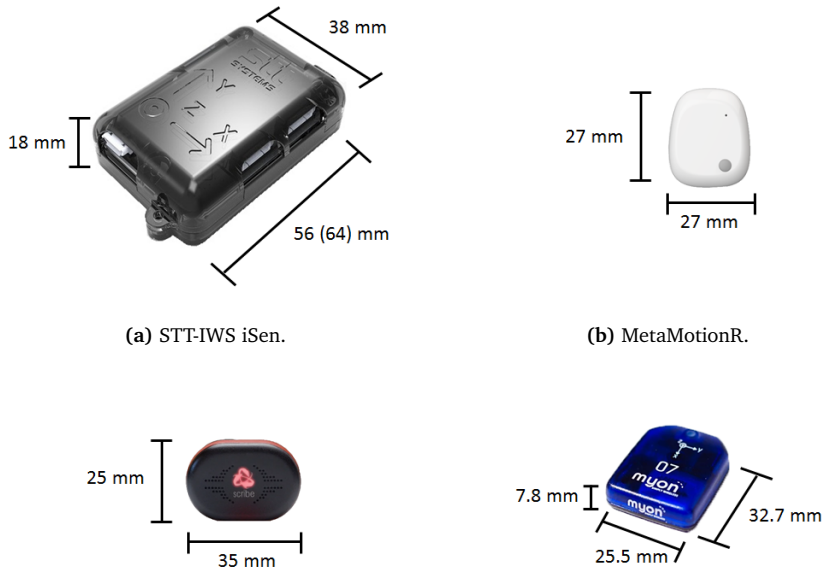

(a) STT-IWS iSen.

(b) MetaMotionR.

(c) RunScribes.

(d) Aktos-t.

Figure A.1: IMU analysed.

Integrated devices: three-axis accelerometer, gyroscope and magnetometer, operating between ± 2000°s^{-1}, ± 16 g and ± 1 mT, respectively.
Maximum sample frequency: 286 Hz

In order to identify the best sensor to use in the GRF estimation, a series of characteristics were taken into account:

- *Dimension and weight:* The iSen sensors dimension are bigger and more than 5 times heavier compared to the other devices, leading to more oscillations and mass added to athletes' body segments with the risk to alter their movements.
- *Connection:* All the devices analysed are wireless IMUs, either using bluetooth or Wi-Fi connection. The former is used by MetamotionR and was found unstable when more than three devices were connected simultaneously, with consequent loss of data; whereas the latter connection type did not show stability problems during recording.
- *Measurement range:* In section 2.4.1.1, a limitation found in some studies was reported as the accelerometer range, which was not able to capture the peak acceleration at very high impact loadings [101], however, all the sensors available are characterised by a ± 16 g range.
- *Sample frequency:* The peak impact force during a 90° change of direction task is reported to occur after 0.02 - 0.03 s [136, 137], therefore sensors with higher sample frequency would provide the possibility of capturing this peak with higher accuracy.

- *Magnetometers calibration:* The iSen sensors were the only devices considered which included magnetometers factory calibrated; the runscribe sensors available did not allow to download magnetometers data; whereas MetaMotionR and myon Aktos-T did not allow magnetometers calibration through their software, but required a self-written code and a calibration procedure to be repeated over time.

From the considerations above, it was concluded that each one of the sensor analysed presents advantages and disadvantages compared to the others. A minimum of eight sensors was necessary for this research application and the problem of bluetooth connection stability excluded the choice of using MetaMotionR. The lowest sample frequency available for the iSen sensors represents a limitation in the determination of the impact peak force, however these sensors compared to the others have the advantage of magnetometers factory calibrated and ready to use. Gyroscope integration to estimate the sensors' orientations could be used to exclude magnetometers' readings, however this technique would produce higher estimation errors over time due to gyroscope bias drift, especially for fast movements involving impacts [91], as the football-related manoeuvres analysed in this work are (Sec. 2.4). These considerations brought to select the iSen as the sensors of choice, other disadvantages of these sensors are their higher weight and bigger dimensions, which effects could be reduced. An appropriate attachment method technique could reduce the higher amount of oscillations produced and the added mass is considered not able to alter athletes' movements during the fast and short tasks analysed, but it could be a limit on the foot segment when the onset of fatigue comes into play, such as during a 90 minute match, as suggested by previous research [63, 66] (Sec. 2.3.2.1).

Appendix B

A pilot study to define the sensor attachment method

B.1 Introduction

In chapter 4, a method developed to estimate 3D GRFs using eight IMU sensors was described and validated during a LSJ movement. The results showed the improvements of this approach compared to previous studies [107,108], however some limitations were highlighted, such as the presence of different oscillatory responses between sensors and participants, dependent on different locations, attachment methods and amount of tissue artefacts. In order to improve the attachment methods a pilot study was conducted and will be presented in this appendix.

B.2 Aim and objectives

The aim of this study is to identify the appropriate technique to attach the IMUs to each body segment of interest, in order to limit the undesired noises and reduce the differences in oscillatory responses between locations.

To achieve this, the following objectives have been identified:

1. identify different methods to attach the sensors;
2. compare the oscillatory responses associated with the identified IMUs' attachment methods.

B.3 Methods

B.3.1 Participants

A single participant (age: 28 years; mass: 72.7 kg; stature: 1.72 m) volunteered to take part in the study.

B.3.2 Experimental setup

The same sensors described in section 4.3.2 were utilised. Different methods to attach the IMUs to each body segment and limit the undesired noises due to sensors' oscillations after impact were identified. The fixation of the IMUs was performed through different equipments, such as velcro elastic bands, adhesive velcro, medical tape, a heart rate monitor, thermoplastic plates and a 75 mm large elastic auto-adhesive bandage. The compared techniques are described in the next sections.

B.3.2.1 HAT segment

Three different attachment methods were considered:

- *attachment 1:* the sensor was placed on the back and secured with tape, as shown in figure B.1a;
- *attachment 2:* the sensor was placed on the back and secured with tape and a 75 mm wide elastic auto-adhesive bandage wrap around the subject's torso;
- *attachment 3:* the sensor was placed on the front, attached to a heart rate monitor strap through adhesive velcro and further secured with a 75 mm wide elastic auto-adhesive bandage wrap around the subject's torso, as shown in figure B.1b;

(a) Attachment 1. **(b)** Attachment 3.

Figure B.1: Trunk attachment methods.

B.3.2.2 LPT segment

Two different attachment methods were considered:

- *attachment 1:* the sensor was placed over the midPSIS and secured with tape, as shown in figure B.2a;
- *attachment 2:* the sensor was placed over the midPSIS and secured with tape and a 75 mm wide elastic auto-adhesive bandage wrap around the subject's waist, as shown in figure B.2b.

(a) Attachment 1. **(b)** Attachment 2.

Figure B.2: LPT attachment methods.

B.3.2.3 Thigh segment

Six different attachment methods were considered:

- *attachment 1:* the sensor was placed on the lateral aspect of the thigh and attached to an elastic velcro band, as shown in figure B.3c;
- *attachment 2:* the sensor was attached over the rectus femoris through adhesive velcro and secured with tape and a 75 mm wide elastic auto-adhesive bandage wrap around the subject's thigh, as shown in figure B.3d;
- *attachment 3:* the sensor was fixed, through adhesive velcro, to a 40 x 70 mm thermoplastic plate (Fig. B.3a), which was attached to the subject's rectus femoris through double sided tape, and secured with medical tape and a 75 mm wide elastic auto-adhesive bandage wrap around the subject's thigh, as shown in figure B.3d;
- *attachment 4:* the sensor was fixed, through adhesive velcro, to a 40 x 70 mm thermoplastic plate (Fig. B.3a), which was attached to the subject's fascia lata through double sided tape, and secured with medical tape and a 75 mm wide elastic auto-adhesive bandage wrap around the subject's thigh, as shown in figure B.3e;
- *attachment 5:* the sensor was fixed, through adhesive velcro, to a 50 x 100 mm thermoplastic plate (Fig. B.3b), which was attached to the subject's rectus femoris through double sided tape, and secured with medical tape and a 75 mm wide elastic auto-adhesive bandage wrap around the subject's thigh, as shown in figure B.3d;
- *attachment 6:* the sensor was fixed, through adhesive velcro, to a 50 x 100 mm thermoplastic plate (Fig. B.3b), which was attached to the subject's fascia lata through double sided tape, and secured with medical tape and a 75 mm wide elastic auto-adhesive bandage wrap around the subject's thigh, as shown

in figure B.3e.

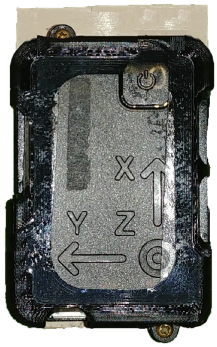

(a) Small thermoplastic.

(b) Big thermoplastic.

(c) Attachment 1.

(d) Attachment 2, 3 and 5.

(e) Attachment 4 and 6.

Figure B.3: Thigh attachment methods.

B.3.2.4 Shank segment

Two different attachment methods were considered:

- *attachment 1:* the sensor was placed on the lateral aspect of the shank and attached to an elastic velcro band, as shown in figure B.4a;
- *attachment 2:* the sensor was attached over the tibia bone through adhesive velcro, and secured with tape and a 75 mm wide elastic auto-adhesive bandage wrap around the subject's shank, as shown in figure B.4b.

(a) Attachment 1. **(b)** Attachment 2.

Figure B.4: Shank attachment methods.

B.3.2.5 Foot segment

Three different attachment methods were considered:

- *attachment 1:* the sensor was attached over the laces through adhesive velcro and further secured with medical tape, as shown in figure B.5a;
- *attachment 2:* the sensor was attached over the laces through adhesive velcro and further secured with medical tape and a 75 mm wide elastic auto-adhesive bandage wrap around the subject's foot, as shown in figure B.5b;
- *attachment 3:* the sensor was fixed, through adhesive velcro, to a 40 x 70 mm thermoplastic plate (Fig. B.3a), which was attached to the subject's shoe over the laces through double sided tape, and secured with medical tape and a 75 mm wide elastic auto-adhesive bandage wrap around the subject's foot, as shown in figure B.5b.

(a) Attachment 1. **(b)** Attachment 2 and 3.

Figure B.5: Foot attachment methods.

B.3.3 Protocol

The participant performed an agility course, including acceleration, 90° and 180° change of directions on a natural grass surface wearing football studded shoes.

B.3.4 Data processing

For each IMU, the discrete Fourier transform of the raw acceleration measured along each sensor local axis was calculated, using the *fft* custom-build function in Matlab. From this, the PSD for each axis and sensor was calculated through the following formulas:

$$PSD_{x_i} = \frac{\left|fft(a_{x_i})\right|^2}{N} \tag{B.1}$$

$$PSD_{y_i} = \frac{\left|fft(a_{y_i})\right|^2}{N} \tag{B.2}$$

$$PSD_{z_i} = \frac{\left|fft(a_{z_i})\right|^2}{N} \tag{B.3}$$

where a_{x_i}, a_{y_i}, a_{z_i} are the accelerations measured by sensor i along the x, y and z axis, respectively, and N is the number of samples.

Matlab R2019a (Mathworks, Natick, MA, USA) was used to precess the data.

B.4 Results

B.4.1 HAT segment

In figure B.6 is reported, for each anatomical axis of the body, the PSD comparison between the different attachment methods described in section B.3.2.1.

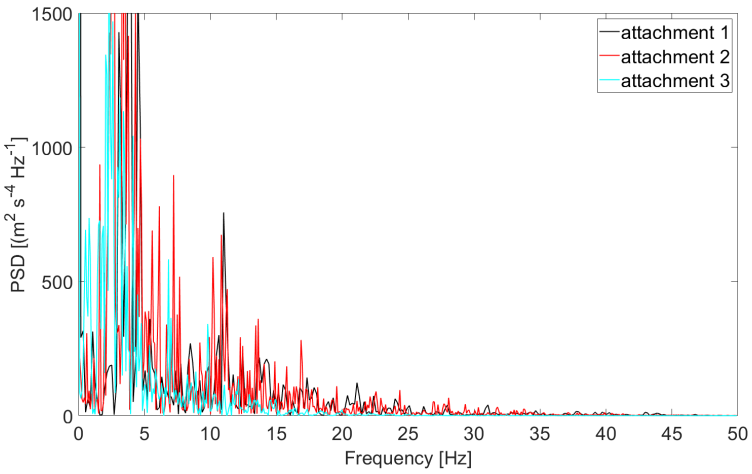

(a) Vertical axis.

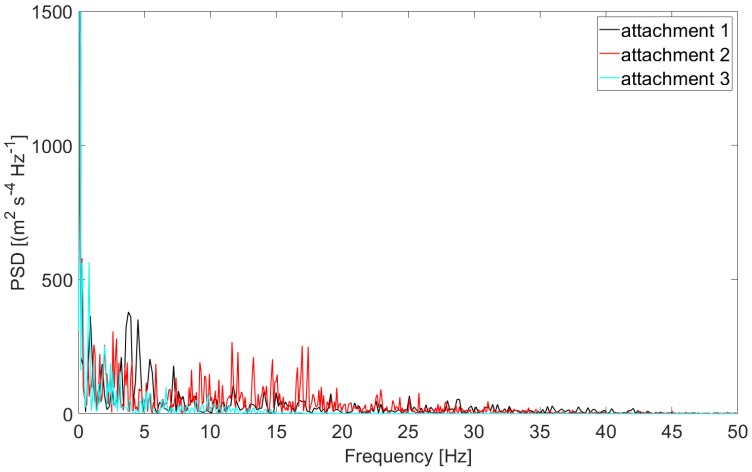

(b) Antero-posterior axis.

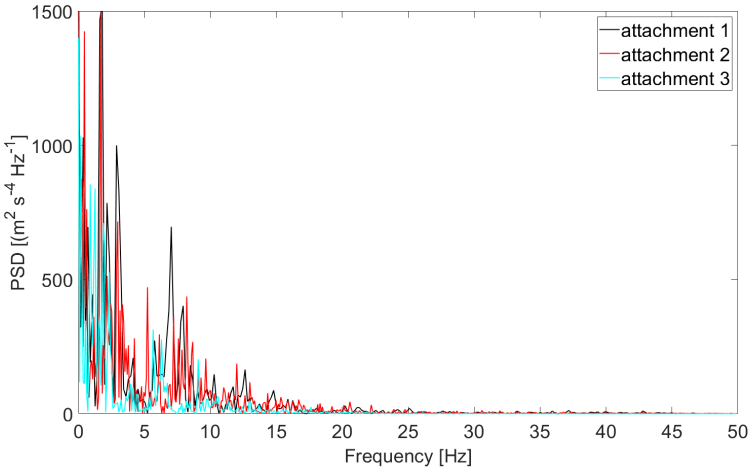

(c) Medio-lateral axis.

Figure B.6: HAT attachment method comparison.

B.4.2 LPT segment

In figure B.7 is reported, for each anatomical axis of the body, the PSD comparison between the different attachment methods described in section B.3.2.2.

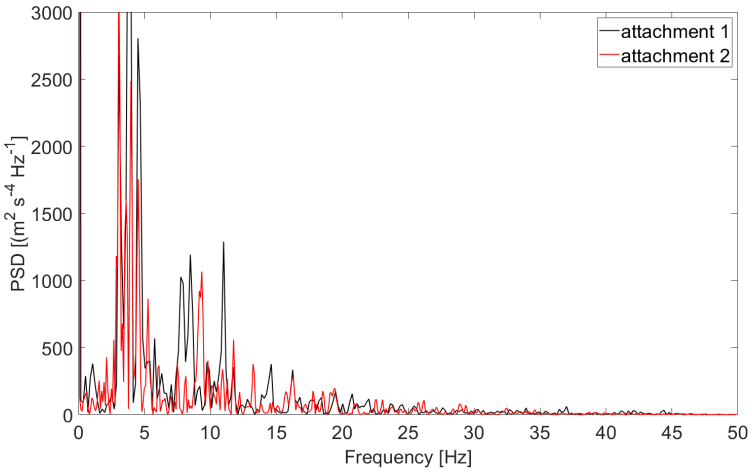

(a) Vertical axis.

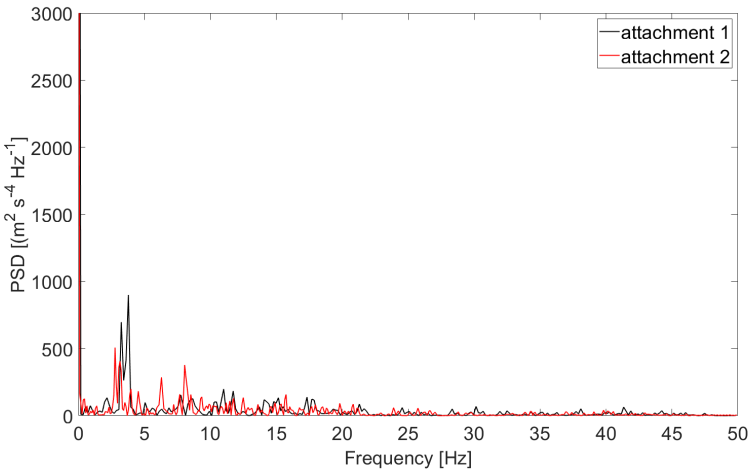

(b) Antero-posterior axis.

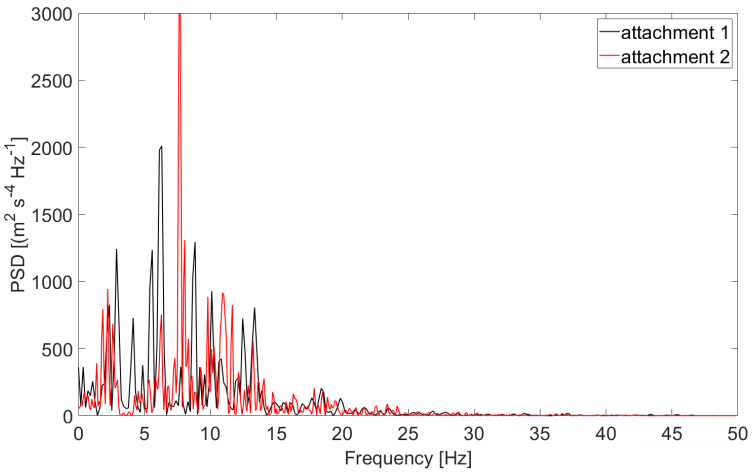

(c) Medio-lateral axis.

Figure B.7: LPT attachment method comparison.

B.4.3 Thigh segment

In figures B.8 to B.11 are reported, for each anatomical axis of the body, the PSD comparison between the different attachment methods described in section B.3.2.3.

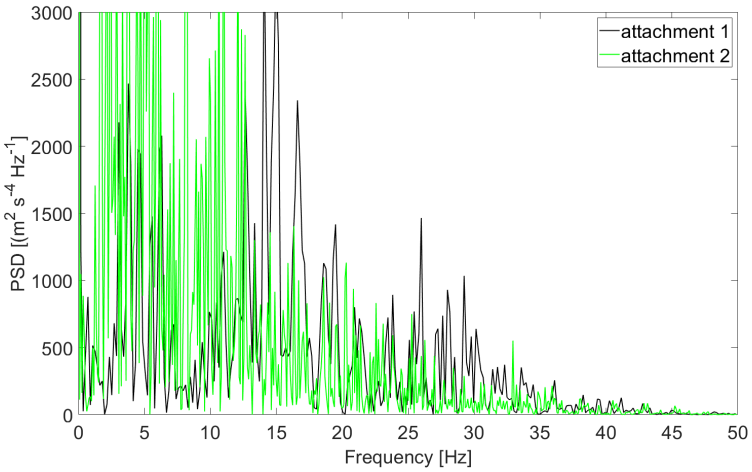

(a) Vertical axis.

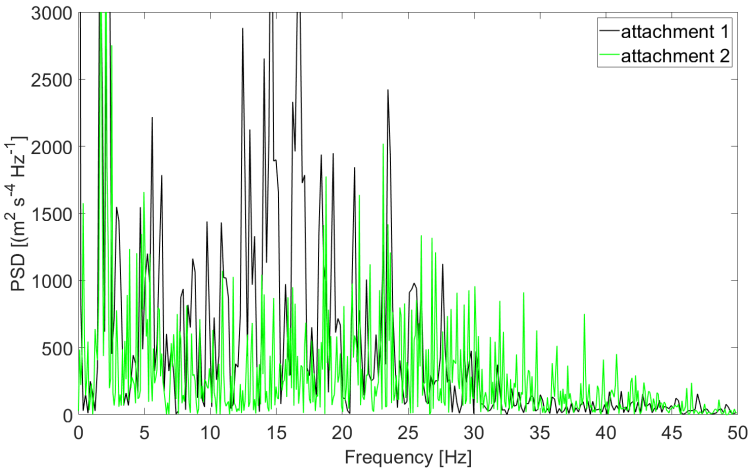

(b) Antero-posterior axis.

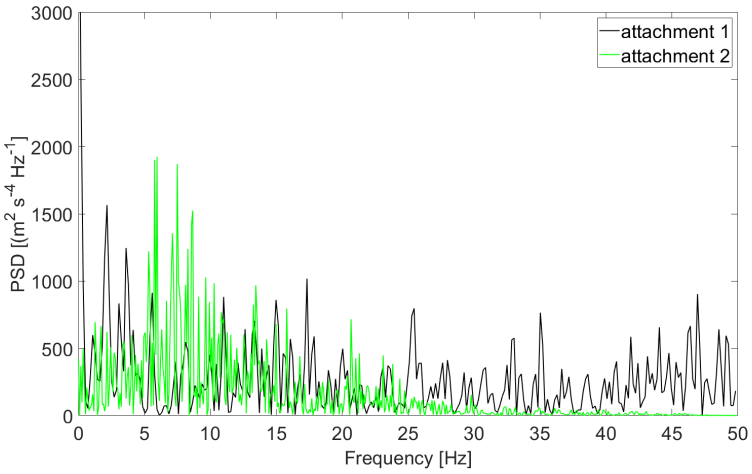

(c) Medio-lateral axis.

Figure B.8: Thigh attachment method 1 and 2 comparison.

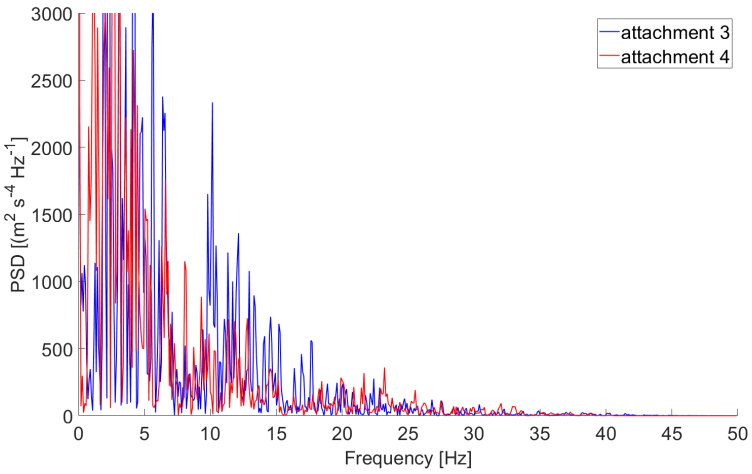

(a) Vertical axis.

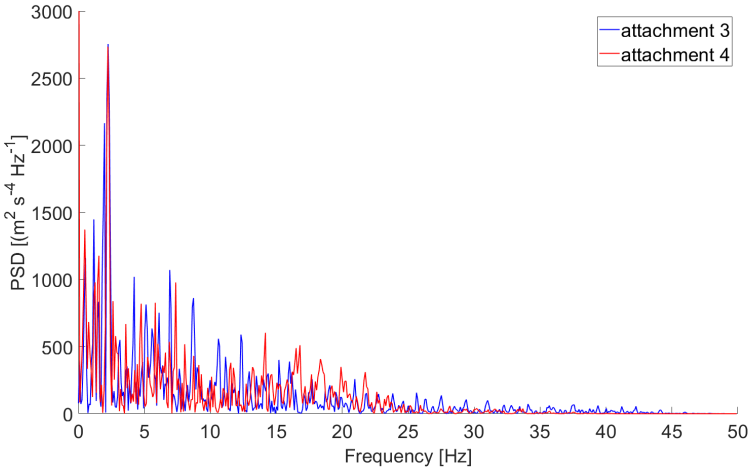

(b) Antero-posterior axis.

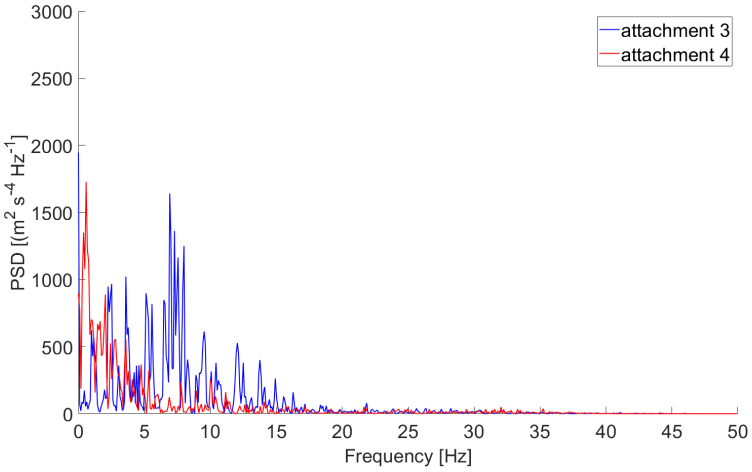

(c) Medio-lateral axis.

Figure B.9: Thigh attachment method 3 and 4 comparison.

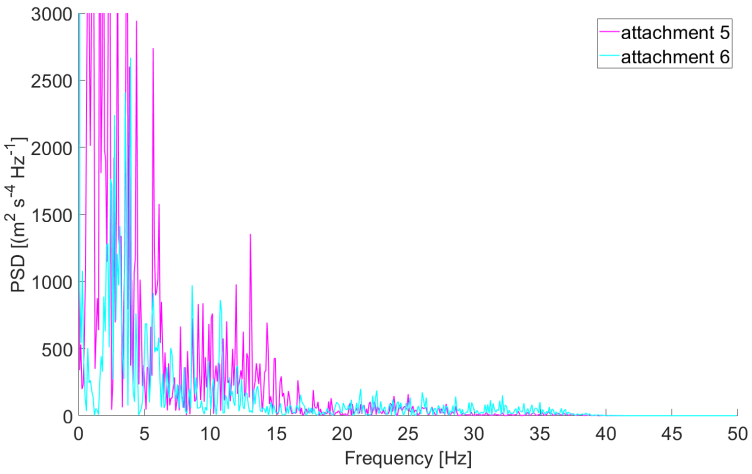

(a) Vertical axis.

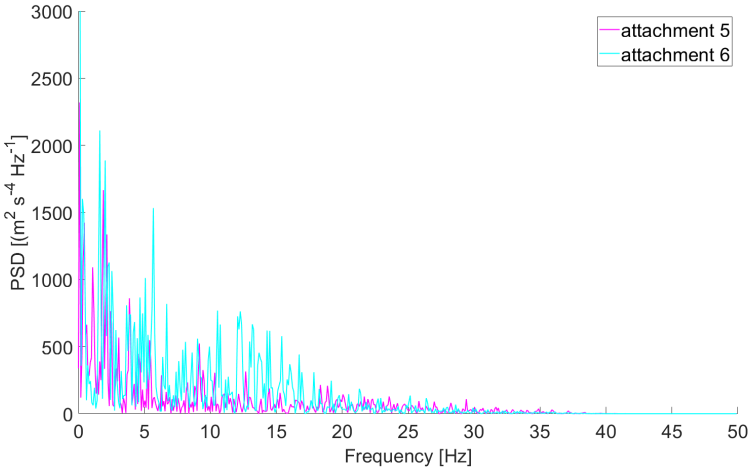

(b) Antero-posterior axis.

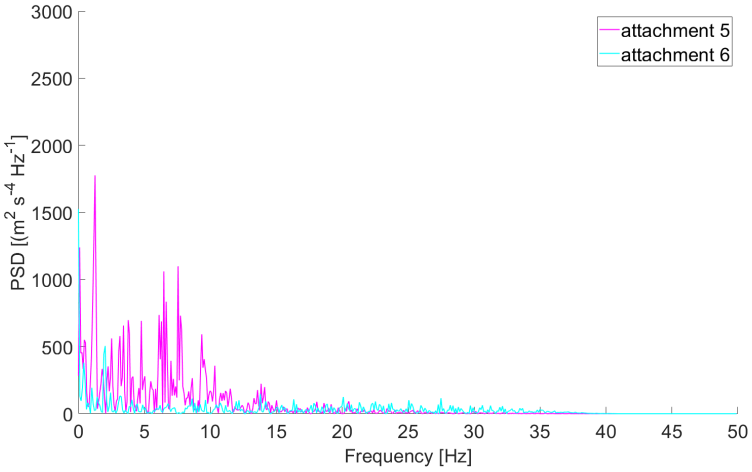

(c) Medio-lateral axis.

Figure B.10: Thigh attachment method 5 and 6 comparison.

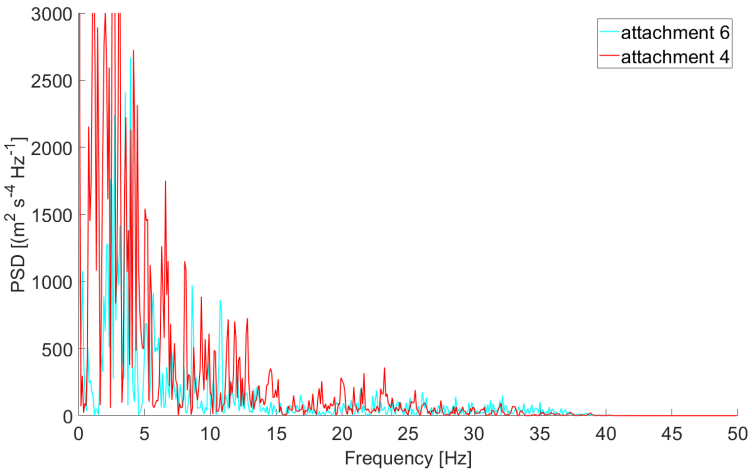

(a) Vertical axis.

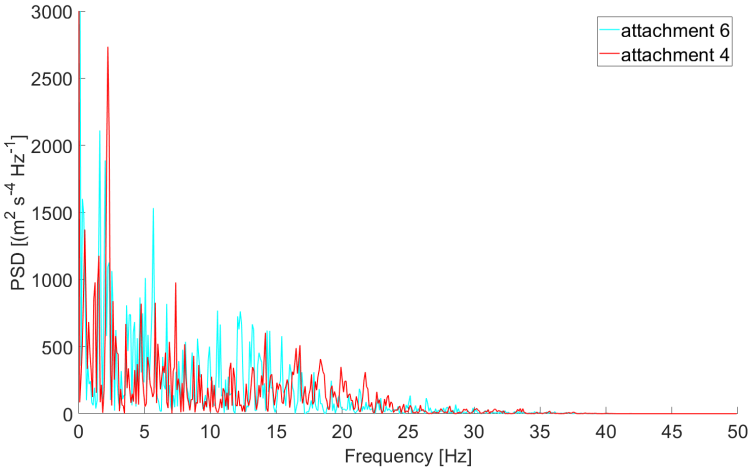

(b) Antero-posterior axis.

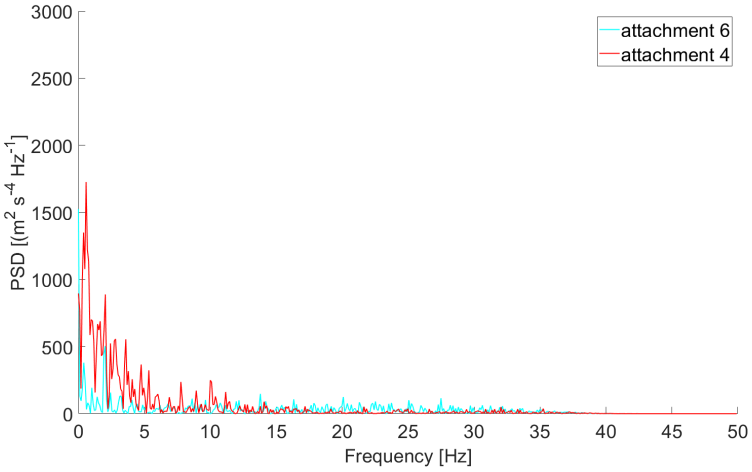

(c) Medio-lateral axis.

Figure B.11: Thigh attachment method 4 and 6 comparison.

B.4.4 Shank segment

In figure B.12 is reported, for each anatomical axis of the body, the PSD comparison between the different attachment methods described in section B.3.2.4.

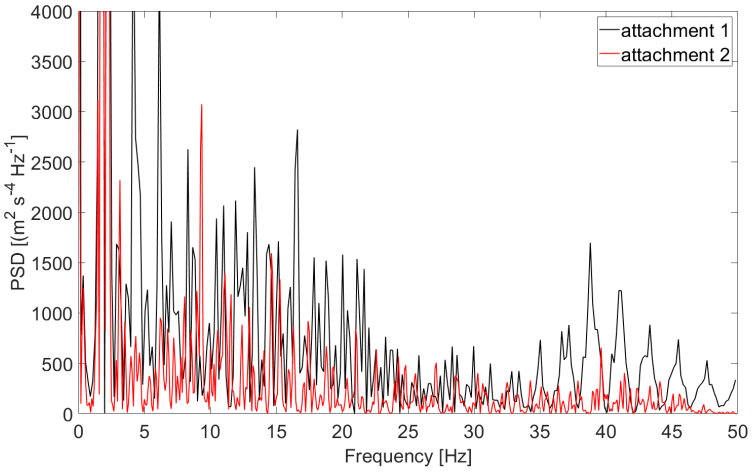

(a) Vertical axis.

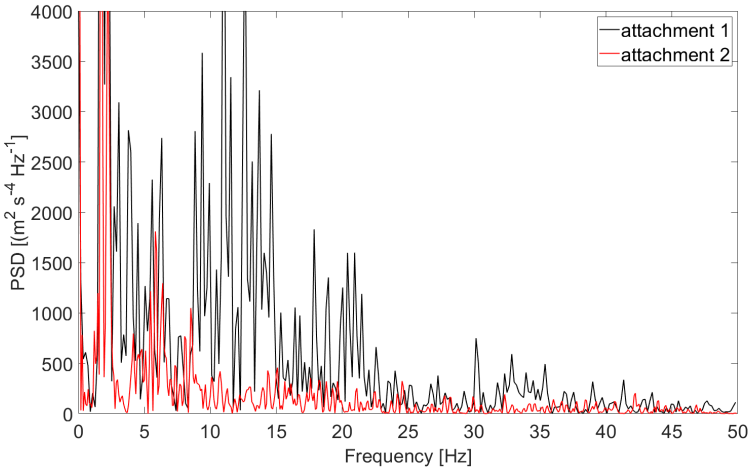

(b) Antero-posterior axis.

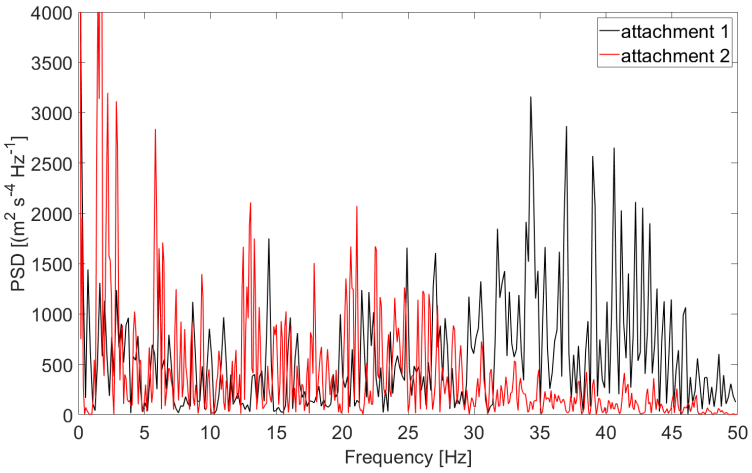

(c) Medio-lateral axis.

Figure B.12: Shank attachment method comparison.

B.4.5 Foot segment

In figure B.13 is reported, for each anatomical axis of the body, the PSD comparison between the different attachment methods described in section B.3.2.5.

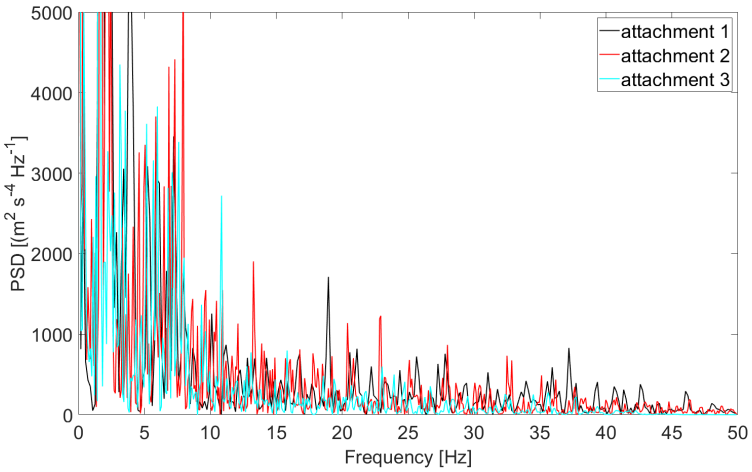

(a) Vertical axis.

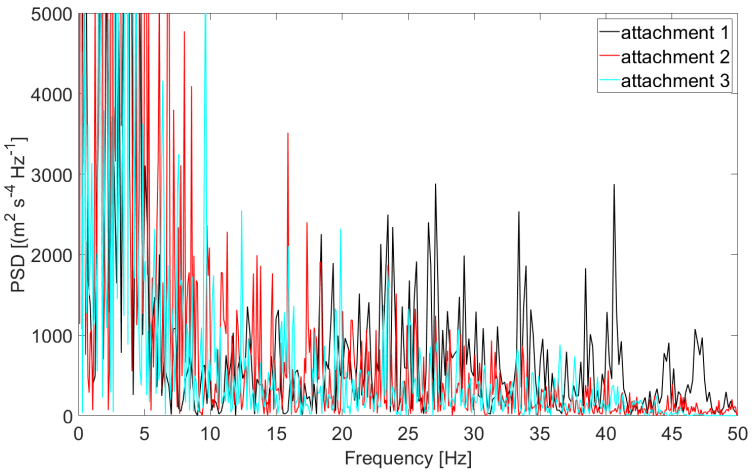

(b) Antero-posterior axis.

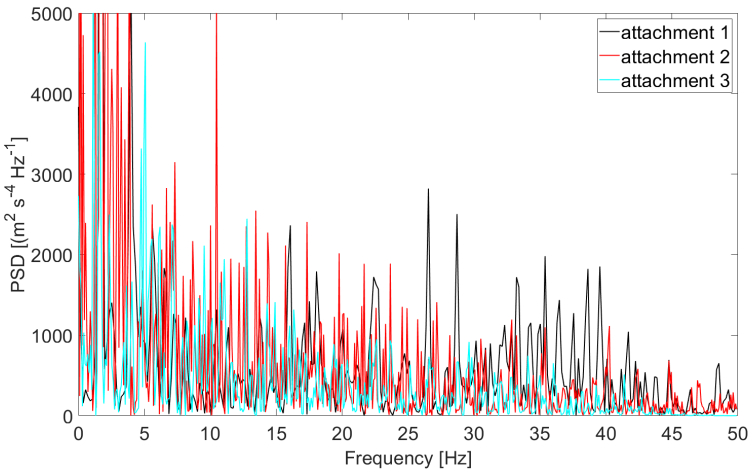

(c) Medio-lateral axis.

Figure B.13: Foot attachment method comparison.

B.5 Discussion

B.5.1 HAT segment

The graphical comparison between the different attachment techniques used for the HAT segment (Fig. B.6) allows to conclude that the placement of the sensor over the sternum through the use of a heart rate monitor reduces the amount of oscillations compared to the placement of the sensor over the spinal column, since lower PSD at the higher frequencies is observed. This was also confirmed by the participant, who perceived the placement on the sternum as more stable, since on the back, the location corresponds to a point in between the scapulae, which movement affected the sensor stability. The use of a heart rate monitor and the elastic auto-adhesive bandage helped to keep the sensor on the desired location and to reduce the noise.

B.5.2 LPT segment

The LPT attachment methods differ for the use of the elastic auto-adhesive bandage, which, as can be seen from figure B.7, do not influence the noise presence. However, the second attachment method was selected, since it helps to keep the sensor in place when the glue on the medical tape and the velcro loses its adhesiveness during longer testing sessions.

B.5.3 Thigh segment

The attachment methods used for the thigh segment are compared two by two, in order to better analyse their effect. As it can be seen from figures B.8 to B.11, the sensor attachment on velcro straps band, technique used in chapter 4, presents higher values at the higher frequency components. This noise is mainly reduced by the application of the elastic auto-adhesive band around the subject's thigh, which prevent the sensor to move on top of the strap, limiting the effect of the oscillations to the tissue artefacts.

The use of a thermoplastic plate was analysed in order to understand if this could further limit the oscillations. Two different thermoplastic plate dimensions were selected in order to cover the size of the sensor and fit over a single muscle. Moreover, the difference in the sensor attachment over the rectus femoris or the fascia lata was compared. As it can be seen from figures B.9 and B.10, the sensor placement over the fascia lata reduces the oscillations on the vertical and medio-lateral axes for both the thermoplastic plate dimensions considered; on the antero-posterior axis more oscillations were observed for the bigger plate on the fascia lata compared to the rectus femoris, whereas no differences between the locations were present for the smaller plate. Since

the attachment on the lateral aspect of the thigh presents less oscillation compared to the frontal attachment with the exception of the medio-lateral axis with the use of the smaller thermoplastic plate, it was chosen as the thigh attachment location. The direct comparison of the two thermoplastic plates attachment on the fascia lata are reported in figure B.11. As it can be seen, the use of a bigger plate reduces the amount of noise along the vertical and medio-lateral anatomical axes, which are aligned with the directions of the main force contributions during acceleration, deceleration and changes of direction task, such as 180° turn. For this reasons, the attachment method 6 was selected.

B.5.4 Shank segment

For the shank segment, two attachment methods were considered, the first was used in chapter 4 and the second required to apply the sensor through adhesive velcro directly to the tibia bone and further secure it through medical tape and elastic auto-adhesive bandage. The use of a thermoplastic plate was not considered because the sensor, differently from the thigh segment, could be applied directly on a bone, which provides a flat and rigid surface on which the sensor size could fit, and the tissue artefacts are considerably reduced compared to the attachment over a muscle. Figure B.12 shows better results for the second attachment method.

B.5.5 Foot segment

Figure B.13 reports the PSD comparison between the different attachment methods evaluated for the feet. The participant was wearing football studded shoes, for this reason, the auto-adhesive bandage was wrapped around the shoe through the mid-foot area of the outsole, where no studs are present. The bandage thickness do not interfere with the participant's foot contact, traction performance and perception. A small thermoplastic plate was considered in order to provide a rigid platform for the sensor to be attached to, and its size was chosen to fit over the subject's foot. As can be seen from the figure, the use of bandage around the shoe results in reduced PSD, further decreased by adding the use of a thermoplastic plate.

B.6 Conclusion

In chapter 4, the need for an improvement in the attachment method in order to reduce the oscillatory responses was highlighted. In this study, different attachment techniques were considered for each body segment. Improved methods were found by using an elastic auto-adhesive bandage, to minimise the oscillations of the sensors

compared to the body segment, and by directly applying the sensors on bones or rigid thermoplastic plates to reduce the tissue artefacts.

To summarise, the following attachment methods were selected:

- *HAT segment:* sensor placed over the sternum, attached to a heart rate monitor strap through adhesive velcro, and further secured with a 75 mm wide elastic auto-adhesive bandage wrap around the subject's torso, as shown in figure B.1b;
- *LPT segment:* sensor attached over the midPSIS through adhesive velcro, and secured with tape and a 75 mm wide elastic auto-adhesive bandage wrap around the subject's waist, as shown in figure B.2b;
- *Thigh segment:* sensor fixed, through adhesive velcro, to a 50 x 100 mm thermoplastic plate (Fig. B.3b), which was attached to the subject's fascia lata through double sided tape, and secured with medical tape and a 75 mm wide elastic auto-adhesive bandage wrap around the subject's thigh, as shown in figure B.3e;
- *Shank segment:* sensor attached over the tibia bone through adhesive velcro, and secured with tape and a 75 mm wide elastic auto-adhesive bandage wrap around the subject's shank, as shown in figure B.4b;
- *Foot segment:* sensor fixed, through adhesive velcro, to a 40 x 70 mm thermoplastic plate (Fig. B.3a), which was attached to the subject's shoe over the laces through double sided tape, and secured with medical tape and a 75 mm wide elastic auto-adhesive bandage wrap around the subject's foot, as shown in figure B.5b.

These attachment methods will be used in chapter 5 and 6.